UNINTERRUPTIBLE POWER SUPPLY SYSTEM USING A DUAL CONVERTER IN QUASI-RESONANT MODE

A thesis submitted for the degree of doctor of philosophy

by

Uwe Schmidt

Department of Electrical and Electronic Engineering, Brunel University

September 1995

Acknowledgement:

This thesis is the result of a collaborative project between the BRUNEL UNIVERSITY WEST LONDON, U.K. and the FACHHOCHSCHULE FÜR TECHNIK ESSLINGEN, GERMANY.

Therefore, I like to thank both my supervisors, in the U.K and in Germany, for their guidance and support. At Brunel University this is Dr. Pratap Mehta and at the Fachhochschule Esslingen this is Prof. Fritz Seutter. Through Dr. Mehta's connections to industry especially to Malcom Goodman (then: STC company) practical and industrial experience was added to the thesis. Malcom Goodman supplied several magnetic components.

Furthermore, special thanks to Thomatronik, Rosenheim and there especially to Dr. Lu (Engineer at Thomatronik Herbert M.Müller GmbH, Rosenheim) has to be given. His company enabled the author to use a very sophisticated electromagnetic simulation program.

A special thanks has to be given to Claus M. Habiger (Dept. E.E. & E.) for introducing me into the British University system and all other areas which were of interest. Also his colleague Holger Kumm supported me, especially during the difficult periods of the project, and therefore I like to thank him as well.

I wish to pay my tribute to Anthony J. Morton for reading the thesis several times through and criticising it in a very constructive way.

ABSTRACTS

Uninterruptible Power Supply (UPS) systems have become a standard to protect electronic devices such as servers and host computers. Also, the energy supply of whole buildings is linked with large UPS systems to ensure a steady power flow. Two system configurations are widely used which differ in price and their ability to protect very sensitive load. This thesis illustrate an analytical examination of all existing systems and concludes with the finding of new configurations with increased efficiency and reduced costs.

A *dual converter* is proposed as the heart of the new UPS system. This converter links the necessary two sources of the UPS through a common transformer. The transformer operates at a high frequency which is enabled due to the resonant switching technique used.

The results of this paper were achieved using mathematical analysis, electrical and electro-magnetic simulation as well as by experiments carried out on the self designed circuit boards in the laboratory. These boards were built in a modular way to enable series testing and thereby optimise the dimensioning of the system.

Table of contents:

List of Figures:

List of Tables:

List of symbols and definitions

symbol	*unit*	specification
Φ	$Wb=Vs$	flux
ρ	$\frac{\Omega \cdot mm^2}{m}$	specific resistance
μ_o	$\frac{Wb}{A \cdot m}$	natural field constant
μ_R	1	relative permeability
D	mm	penetration depth
a	mm	distance between the windings
A_{vrim}	mm^2	primary area
A_e	mm^2	magnetic area
A_n	mm^2	cross area of the magnetic core
A_{sec}	mm^2	secondary area
B	$\frac{Wb}{m^2}$	magnetic flux density
b	mm	winding breath
B_m	$\frac{Wb}{m^2}$	flux density with matter
B_o	$\frac{Wb}{m^2}$	flux density without matter
C_f	F	filter capacitor
C_o	F	output capacitor
C_{oss}	F	internal parasitic capacitance of a MOSFET
C_r	F	resonant capacitor
D	1	duty ratio
$D_1 D_2$	-	output diode referring to a dual converter
D_o	-	output diode
EMI	-	electromagnetic interference
f	Hz	frequency
H	A/m	magnetic field strength
h_w	mm	winding high
I_{ds}	A	drain source current
I_O	A	load current
$IGBT$	-	insulated gate bipolar transistors
k	1	coupling factor
L_f	$\frac{V \cdot s}{A}$	filter inductance
l_{gap}	mm	length of airgap
l_c	mm	length of magnetic path in the core
l_{fe}	mm	length of magnetic path
L_{leak}	$\frac{V \cdot s}{A}$	leakage inductance
L_r	$\frac{V \cdot s}{A}$	resonant inductance

M	$\frac{V \cdot s}{A}$	mutual inductance
MOS_x	-	power switches referring to a dual converter
$MOSF$	-	metal-oxide-semiconductor field effect transistor
ET		
MTL	mm	mean turns length
N	1	number of turns; turns ratio N_p/N_s
n	-	windows number
N_1	$turns$	number of primary
N_p	$turns$	primary turns
N_s	$turns$	secondary turns
P	W	power
P_{loss}	W	power dissipated during on-period
PWM	-	pulse width modulation
R_{fe}	W	ferrite resistance
R_{Load}	W	resistance of the load
R_{on}	W	on-state resistance
S, s	mm	spacing
SOA	-	safe operation area
T_S	s	switching time
$V_1 V_2$	V	input voltage referring to a dual converter
V_d	V	input voltage
V_{ds}	V	drain source voltage
V_i	V	input voltage
V_{ind}	V	voltage inductance into the core
V_o	V	output voltage
VCO	-	voltage controlled oscillator
$VLSI$	-	very large scale integrated
W_W	mm	window width
x	mm	distance between wall of a coil former and the flux
X	$\frac{V \cdot s}{A}$	(leakage) inductance in a transformer model
Z_O	V/A	resonance Impedance

resonant impedance : $Z_R = \sqrt{\frac{L_R}{C_R}}$

resonant frequency: $\omega^2 = \frac{1}{L_R \cdot C_R}$

resonant impedance : $L_R = \frac{Z_R}{w}$

ratio of turns: $N = \frac{N_p}{N_s}$

CHAPTER 1

INTRODUCTION

Uninterruptible Power Supply (UPS) systems are used to protect critical loads against power outages and power line overvoltage as well as undervoltage conditions. Also they suppress incoming line transient and harmonic voltage disturbances. These disturbances can have various sources. Starting a large engine or an atmospheric disturbance like lightning bolts in the vicinity of a critical load can cause severe damage to it. Even a loose plug can be the reason for major problems in operating very sensitive loads.

The rapid increase of electronic equipment in almost every field of industry, medicine and the private and domestic sector has led to an increasing dependency on them. This becomes obvious if one imagines a power outage in a modern operating theatre. The damage caused by a break down of for example a server or a host computer in a computer network can not easily be quantified. These are just a few examples that underline the increasing importance of UPS systems. Furthermore, there is a trend towards installation of large UPS systems capable of protecting a complete building [Nek93].

Whilst the pace of development in computer and associated technologies has quickened in recent years, there has not been a similar rate of progress in power supply systems. In particular there is considerable demand for smaller and more efficient UPS systems capable of fast response.

To obtain a new UPS system with all the mentioned features a systematic investigation of the existing systems was carried out. On-line systems ensure very good load protection on the expense of rather high losses during normal operation. On the other hand off-line systems supply power directly to the load, hence are more efficient, but their response time is rather poor. After looking at this general differences the existing UPS systems were divided into functional sections. The resulting block structures were the subject of further

inspection. In a next step the single blocks, especially the DC-DC converter unit (due to its high loss delivery) were carefully examined.

By introducing a novel concept called the *dual converter* or to be more precise the dual input quasi-resonant converter several advantages could be achieved when applied to a UPS system.

This novel concept is introduced in Chapter 3. The most significant aspect of this converter is the use of a single transformer combining the two power sources in parallel rather than in series as in on-line systems. This transformer is operated at frequencies significantly higher than existing UPS systems. Since the most obvious method of operating such systems at high frequency is to use soft switching or resonant techniques, existing switching methods are surveyed and a suitable approach is specified. To employ the parasitic leakage inductance of the transformer windings as part of the resonant circuits a detailed study of transformer core types and material and the winding configuration was carried out to design a transformer for operating at above 500kHz.

The two operation modes of the *dual converter* were examined separately. The result of this analysis was a voltage frequency relation for each part of the *dual converter*. Additionally, different simulations of the circuit were carried out. Therefore, a similar procedure was chosen. The two input parts were simulated separately and the results were compared to those of the mathematical analysis. Thereafter the change-over period of the *dual converter* from one source to the other was simulated. The determination of the resonant frequency was critically examined, mathematically proven and confirmed by simulation in Chapter 4.

The aim of the practical work was to verify the concept of the *dual converter.* Such a converter was build and tested. A modular set-up of the circuit was achieved by using interface circuit boards onto which the different transformers were mounted. These boards were then screwed onto the main board rather than being soldered. The drawbacks of screwed connections are compensated by the achieved flexibility. The determination of the components of the circuit was supported by a special program that was developed by the author.

Every design of a converter represents a compromise. As a result of the increase of the switching frequency and the related decrease in size, the winding and magnetic losses increase. In this work another compromise had to be made. The increase of the airgap of the magnetic core ensures a smoother change-over due its ability to store power. The drawback is that the magnetic stray field increases, which results in further losses. This effect is visualised with help of the coloured prints attached to section 4.2.2.

The voltage and power levels of the produced *dual converter* were limited to 50 volts and 50 watts respectively due to the easy availability of the appropriated facilities at both Brunel University and at Fachhochschule für Technik Esslingen. Problems that occur with higher and maybe more realistic voltage levels would basically not jeopardise the concept of the *dual converter.*

The authors main contribution is the finding of this new UPS system that allows good load protection combined with highly efficient operation in normal mode. The above mentioned design program can be used to easily dimension a quasi-resonant converter and is therefore a further step to reduce the uncertainties related to resonant techniques.

CHAPTER 2

THE NEED FOR UNINTERRUTIBLE POWER SUPPLY SYSTEMS

2.1 General

The rapid growth in the demand for Uninterrutible Power Supply (UPS) systems has been due to two main causes. Firstly, the increased use of electronic equipment requires integrity of power supply to the equipment, to protect itself from damaging parts within the equipment and corruption of data, which can also occur due to total failure of power supply. Secondly, the equipment itself could be a source of interference e.g. harmonic currents generated by for example thyristor regulators. Further, there is a trend towards reducing the operating voltage level in digital systems from 5 Volts to 3.3 Volts ((Motorola reduced the voltage level to 3.6V in its new RISC[1]-Processor [MCP93]) to lower the energy consumption. This of course results in an even greater sensitivity to interference in power supply systems.

An example of the effect of a power supply interruption was clearly reported on the 9th of October 1993 [Stu93] by a German newspaper.

"Yesterday at lunch time a short circuit in a step-down station of Technical Works Stuttgart (TWS) led to a power outage in Feuerbach and Zuffenhausen (suburbs of Stuttgart). This caused a voltage drop in the whole city. City-trains and tubes temporarily stopped, a lot of computers broke down. ... The outage[2] lasted for three minutes. As a result of the short circuit the transformer which supplies the step-down station with power turned off. This short outage in the 110 000V-net led to a blackout which had effects in the whole city area. According to the head of department of the power distribution of the TWS, Willibald Banschbach, the voltage dropped for 0.2 seconds.

[1]Reduced instruction set computing
[2]An explanation is given later in this Chapter

Banschbach: 'This was enough to take effect on some consumers'. ... Also traffic control systems and other computers failed for a short period. ... Yesterday Willibald Banschbach of the TWS said: 'The consumer always have to take under voltage conditions into account.'..."

Just three days later on the 12th of October the same newspaper reported about another outage [Stt93].

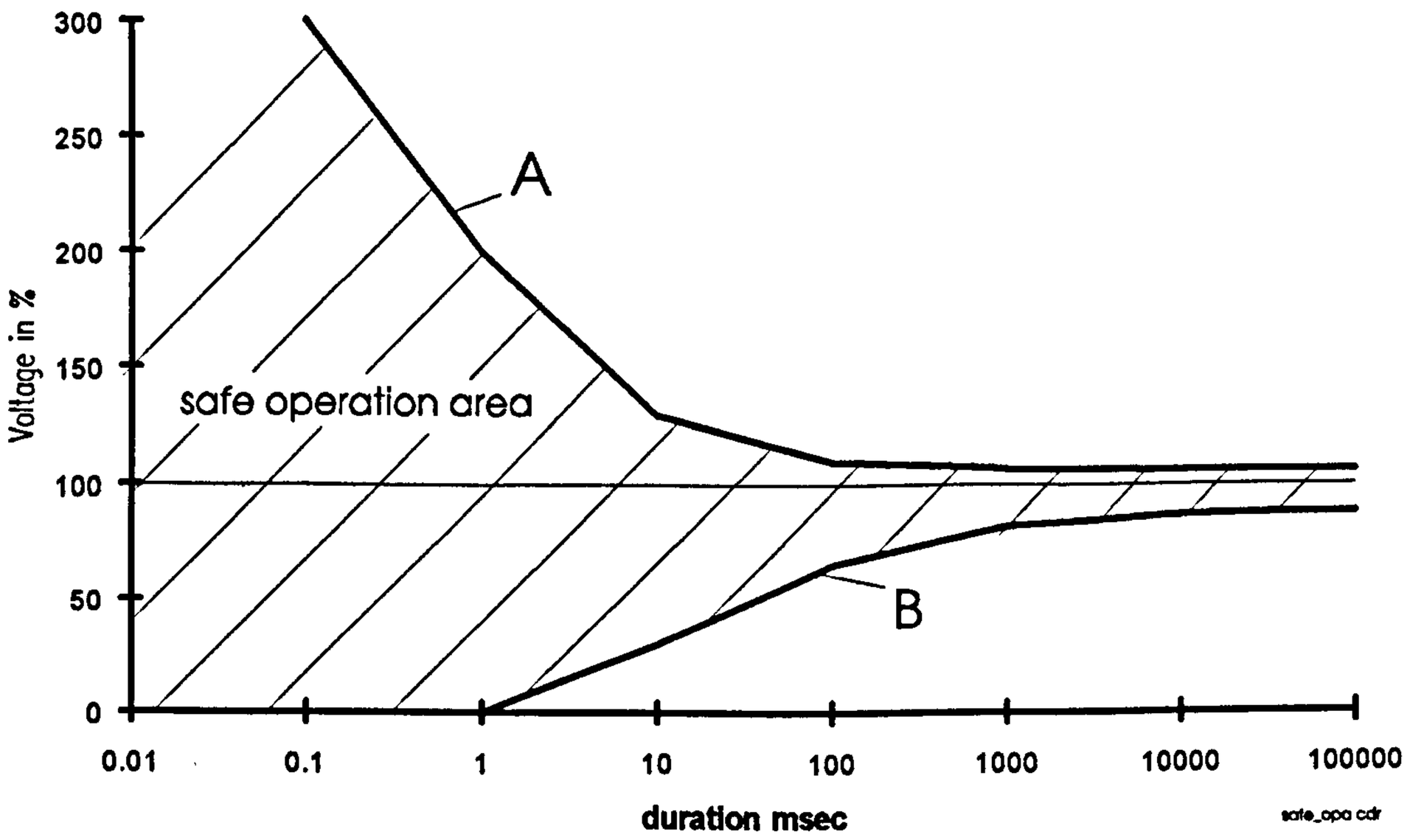

Figure 2.1 ***save operation area of a computer system [Was90]***

Figure 2.1 shows the sensitivity of electronic devices (such as computer systems) to the voltage levels and the duration of the over or under voltage conditions. This of course limits the operation of the equipment within the safe operating area. The area above curve *A* represents the conditions under which the device could be destroyed because of an overvoltage condition over too

long a period. Under curve *B* data could be lost, or the general functions of the device are not guaranteed.

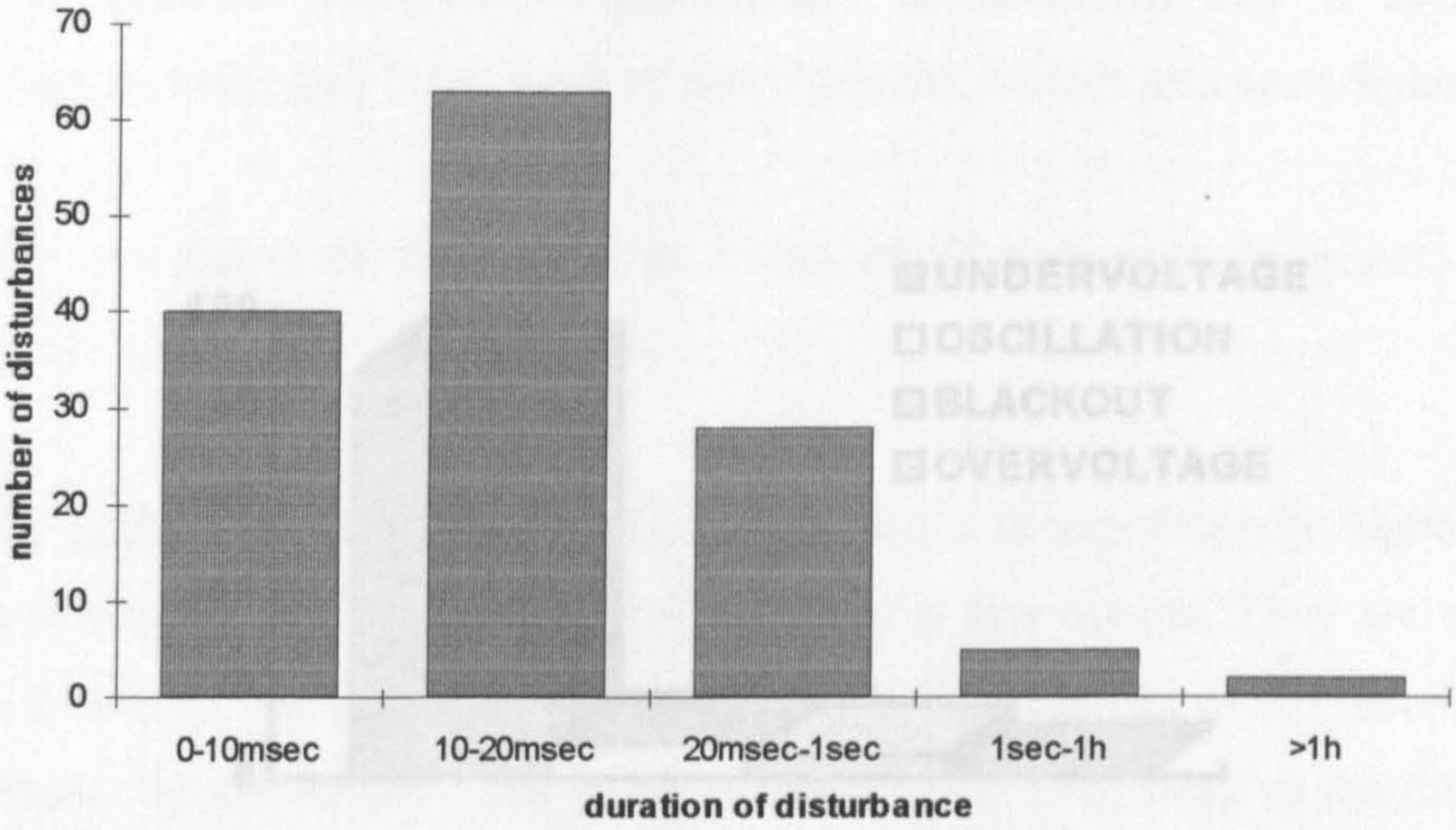

Figure 2.2 Average number of disturbances p.a. in respect to their duration

Figure 2.2 shows the results of a survey carried out at 68 locations in Germany in 1983 [Gil93].

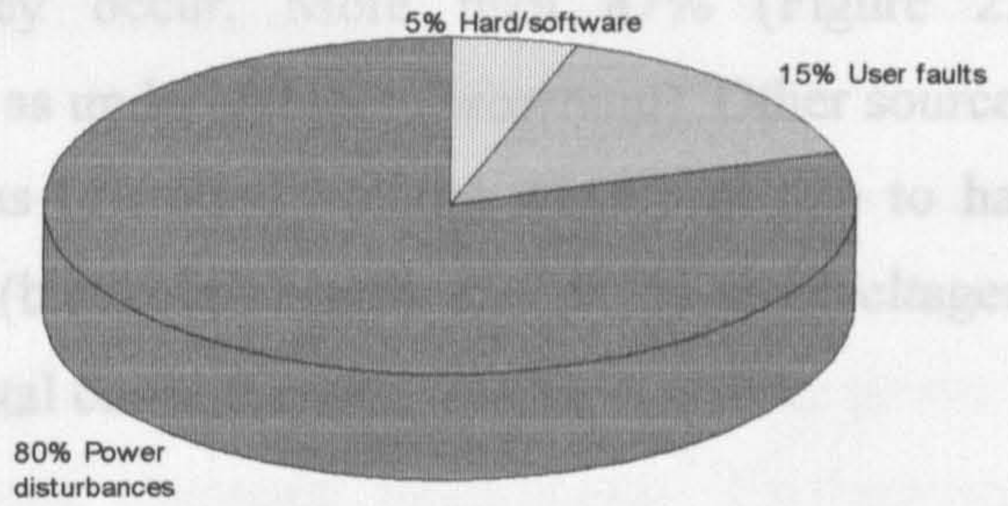

Figure 2.3 Reasons for computer breakdowns

This was also confirmed by a study carried out by AT&T and IBM in the laboratories of Bell where 80% of breakdowns were related to voltage irregularities as illustrated in Figure 2.3.

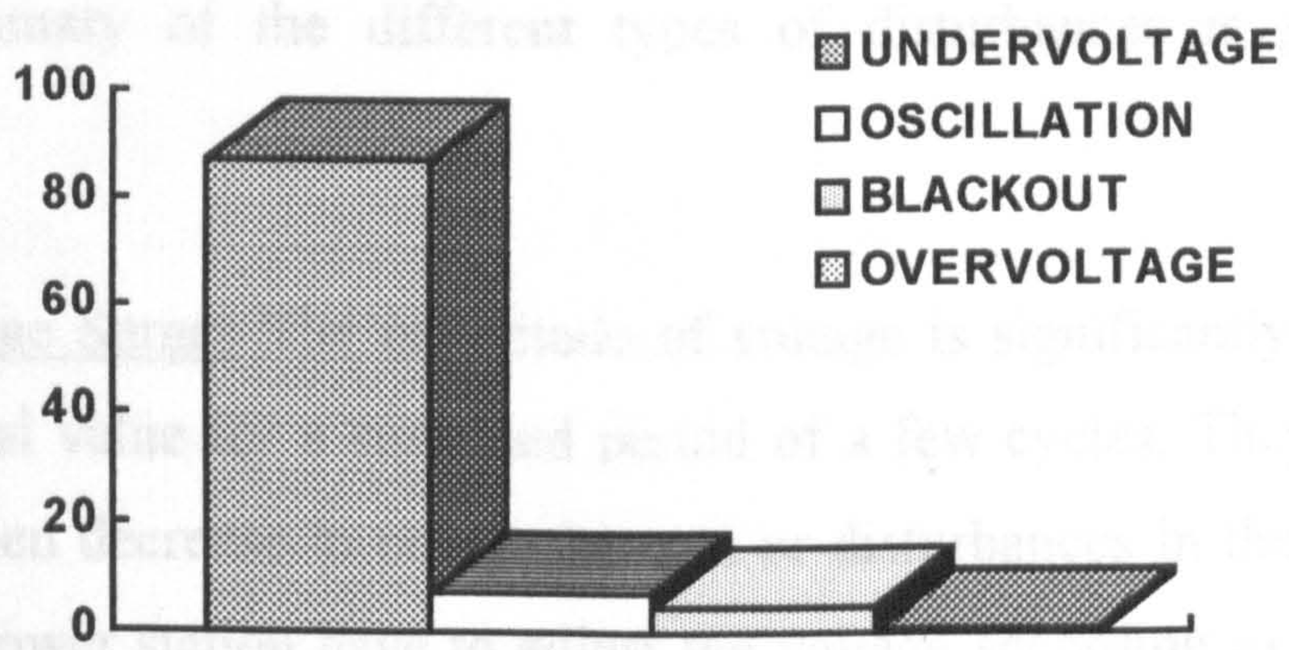

Figure 2.4 Types of power disturbances in the United States

Beside the loss of data a quarter of power failures result in damage to hardware including hard disks.

Figure 2.4 shows which types of power disturbances occur in the U.S.A and how frequently they occur. More than 87% (Figure 2.4) of voltage-irregularities appear as undervoltages (brownout). Other sources of disturbance are 7.4% oscillations (distorted voltage waveform due to harmonics), 4.7% total break downs (blackout/outage) and 0.7% overvoltages. Nevertheless, overvoltages have fatal consequences.

It is important to recognise that there are other causes of power disturbance not directly related to total power supply systems interruptions. Typically short

circuits, incorrectly dimensioned fuses and electromagnetic interference (EMI) cause voltage irregularities. Electromagnetic interference could also be transmitted through transformers, air, through an organism or via the power line. The sources of these disturbance could be electrostatic discharges, radio systems, portable telephones, atmospheric disturbances like a stroke of lightning, or inductive loads such as transformers, motors and neon lights.

A brief summary of the different types of disturbances is given below [Moh89].

- Overvoltage Surges The magnitude of voltage is significantly higher than its nominal value for a sustained period of a few cycles. They are caused by a sudden decrease in power demand or disturbances in the distribution system. Power station have to adjust the voltage according to the demand. This process is rather slow and therefore there is a time lag between the reaction and changes in demand. Furthermore, surges could occur due to short circuits in the vicinity of a sensitive load. After a short breakdown, the voltage peaks up to double or even three times the nominal voltage for a period of 100μsec to 1msec. A 15% overvoltage is tolerable, above this damage may occur and the equipment life may be shortened.

- Undervoltage (Brownout/Sag). The voltage is substantially lower than its nominal value for a few cycles. This kind of fault is the most frequent one. Undervoltage conditions occur due to the sudden increase in power demand in the vicinity of the electronic systems, or as often happens because of the reduction of the mains voltage at the power stations. This is done due to peak demands in industry. Furthermore, huge power consumers can produce overload in the network. For example, the starting

current of a lift can be a reason for under voltage in a building[3], hence in a computer system or network. The state of the art machines are able to handle about 20% of undervoltage conditions. Higher undervoltages lead to a breakdown of such systems.

- Outage (Blackout). This type of disturbance occurs 5,000 to 6,000 times a year[4]. Many computer systems of the new generation are able to overcome outages of 20mses or even more, others are less tolerant. Most of statistically not registered failures lie between 20msec and 100msec. Nevertheless, these failure can be as damaging as the longer outages. Moreover, user generated outages are added to the powerline failures, e.g. the removal of fuses.

- Voltage Spikes. These are superimposed on the normal 50Hz (60Hz) waveforms and occur occasionally (not on a repetitive basis). The reason for such spikes can be lightning strikes (voltage impulses up to several thousands volts) with a duration between a few milliseconds and some 100msec. The pulses get transmitted through the network and force their way into the sensitive parts of electronic devices. On account of these spikes many motherboards and hard disks may sustain severe damage.

- Chopped Voltage Waveform. This refers to a repetitive chopped waveforms of the supply voltage such as those associated with thyristor voltage regulators.

---

[3]Special examinations on this issue are carried out in the "Intelligent buildings" group at Brunel University West London

[4]This number is valid for Germany; according to [Gil93]

- Harmonics. A distorted voltage waveform that contains components at harmonic frequencies exist on a sustained basis (usually low-order multiples of the line frequency).

- EMI. This refers to high-frequency noise, which may be conducted through the power lines or radiated from its source (e.g. switch mode power supplies).

- Mechanical switching of large loads. This often causes bouncing of the circuit breaker contacts leading to oscillations (400Hz to 5kHz). Such disturbances are reflected into the power lines and can easily travel long distances.

2.2 Applications and Configurations

2.2.1 Applications

The importance of research in the field of UPS systems are signified by the statement made by K. Neumann of the "Technische Universität Berlin":

> *"The demand of UPS devices will rapidly increase in the next decade. Areas of growth are office-automation, host and local computers, medical apparatus and sensitive controlling units in industry and in power stations"* [Neu92].

The applications for UPS systems range from small power such as electronic access control systems, emergency and stand-by lighting, lifts and other vital

equipment and services. Loss of data in an access control system even in a medium size company could mean a serious loss of information requiring a great deal of manual work to reinstall the system. Generally stand-by batteries or diesel generators are provided for security.

2.2.2 Configurations

The various fields in which UPS systems are used demand different configurations. The parameters of the load such as

- power demand
- load variation
- sensivity

lead to specific demands on UPS systems. As a result of this load classification, UPS systems can be categorised in respect of

- power handling capability
- response time.

Additional factors which have to be taken into account at the design stage are the availability of space and weight.

Figure 2.5 shows various types of UPS systems generally in use. The internal (built in the equipment) arrangement is normally used in small and/or portable equipment. For the external arrangement (the UPS system is connected to the equipment as a separate unit) a number of alternative schemes are available as discussed below.

Firstly, a brief overview of the most common UPS systems (external) is given to show the main differences as well as the elements which they have in

common. Secondly, two internal configurations are derived from a classical (on-line) system. Finally, the proposed UPS system is set into this context.

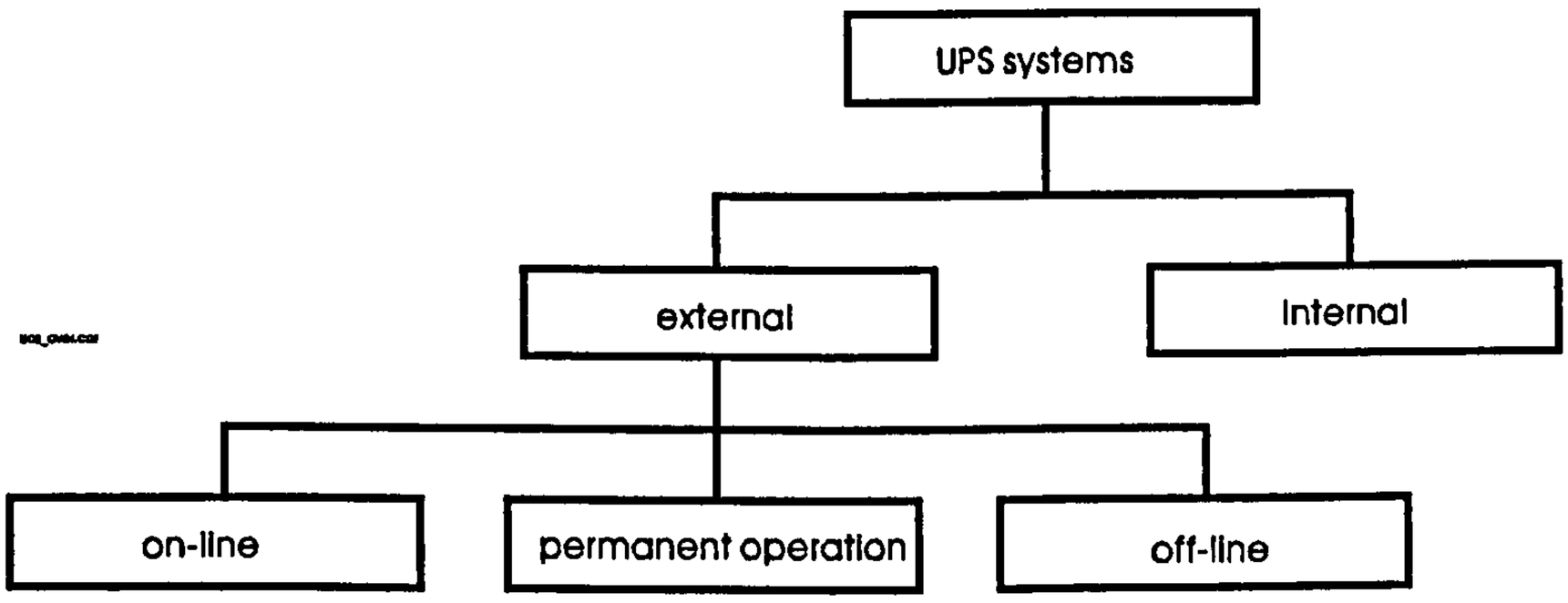

Figure 2.5 Classification of UPS systems

External Systems

(i) On-line systems:

Wherever a very sensitive load has to be protected, on-line arrangements are used as shown in Figure 2.6. The load is permanently supplied via the UPS systems providing an excellent protection. An emergency bypass is included to take-over in case of any system failure or sudden high power demand. The stand-by battery is trickle charged via a DC-DC converter which could be made optional if the battery arrangement can supply the required voltage level. This will be described in more depth in section 2.3.

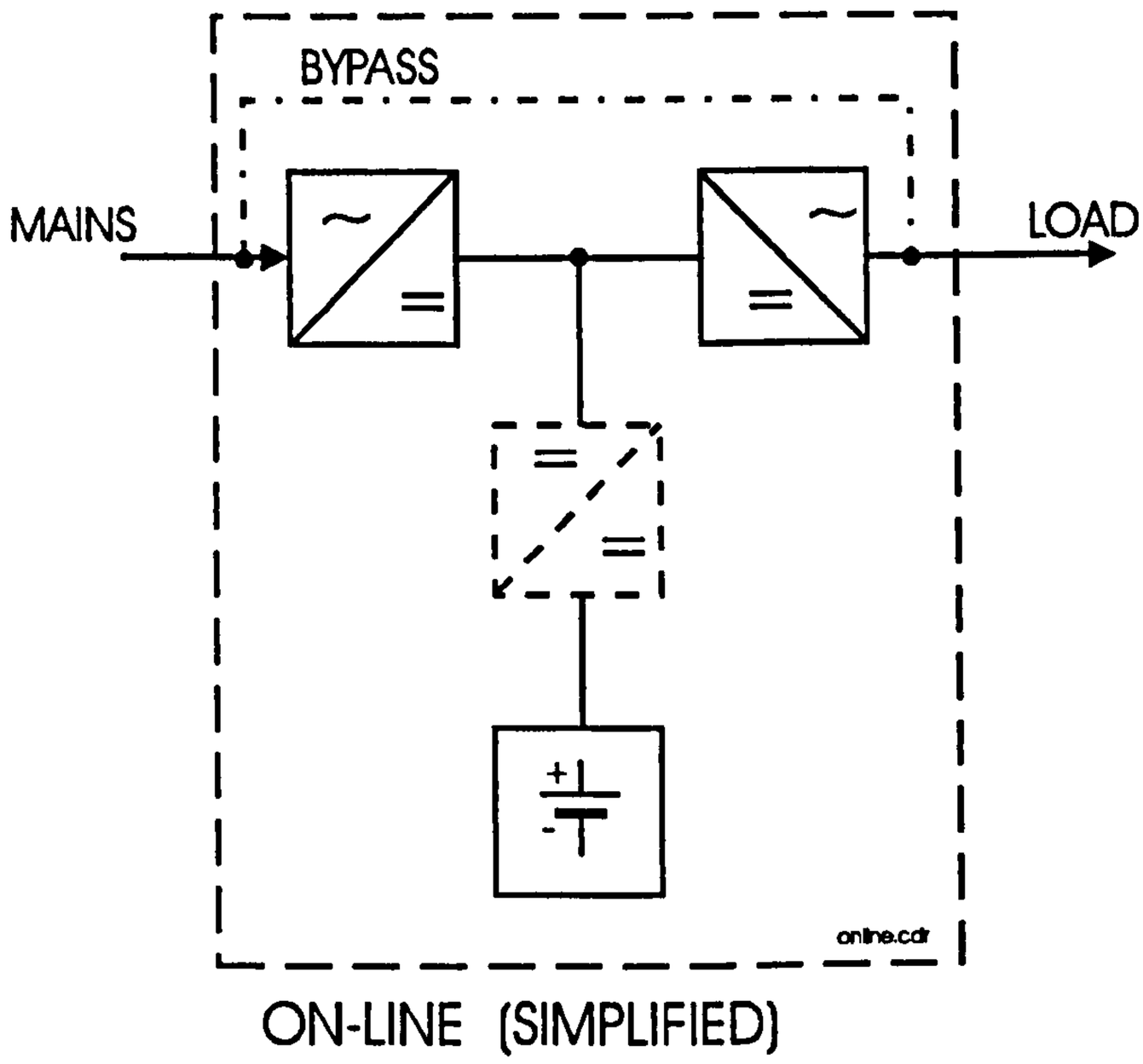

Figure 2.6 On-line UPS

(ii) UPS system with uninterrupted battery take-over:

For higher power ratings and relatively short duration of emergency the load is also permanently connected to the rectifier system as can be seen in Figure 2.7. However, to increase overall efficiency of the system the battery is charged through a separate unit and takes over in case of power failure within one millisecond or thereabouts. The transition from one source to another is uninterrupted; during the transition both the power sources may supply the load simultaneously. A buffer capacitor may be included in the main line to cater for short interruptions.

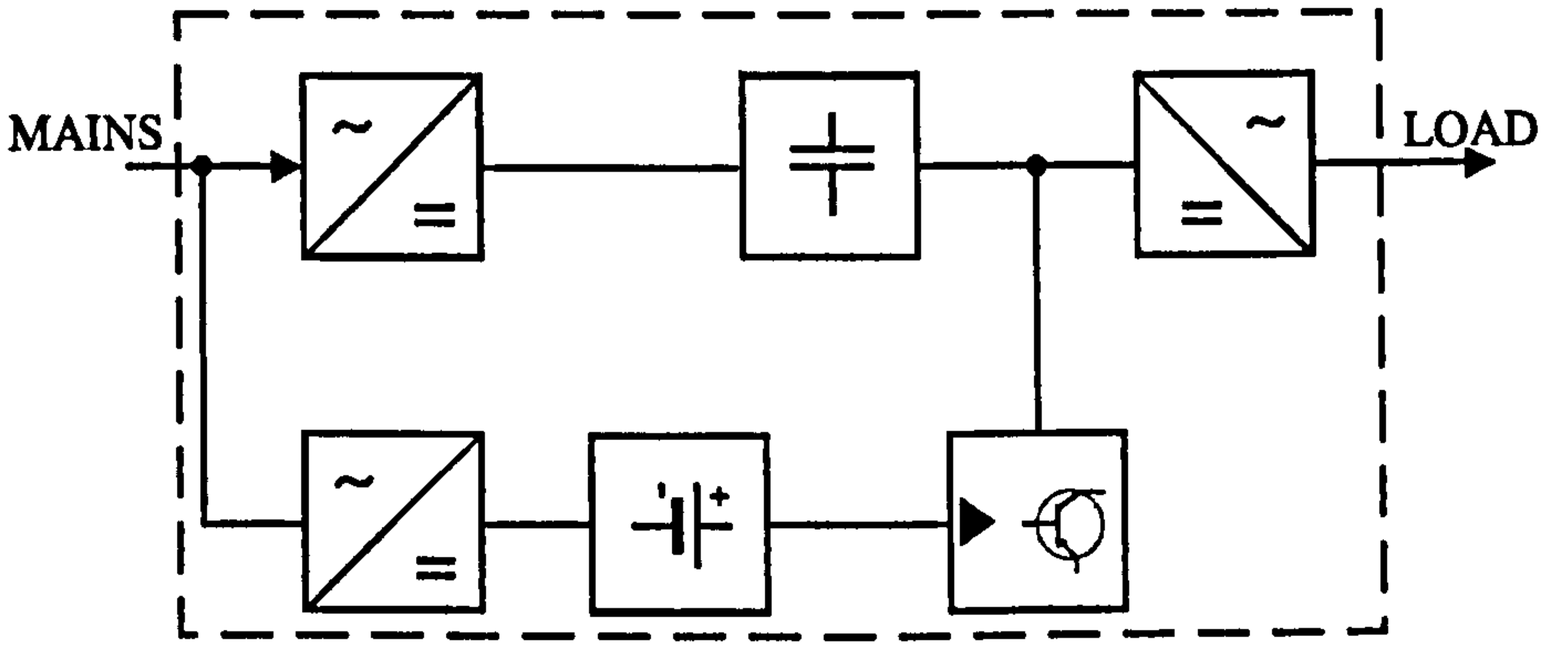

Figure 2.7 UPS system with uninterrupted battery take-over

(iii) Bypass or off-line systems:

In the arrangement shown in Figure 2.8 the load is directly supplied from the mains during normal operation. A suitable filter (not shown) may be included to surpress harmonic disturbances. The charger, the battery and the associated inverter are inactive during normal operation except for charging the battery.

During power failure the load is automatically supplied from the emergency source. In contrast to *(ii)* above the charger handles only the power for the battery. If power failure of duration of more than 100msec is acceptable the unit can be operated in a stand-by mode, hence the inverter is switched on only during power failures. The power rating for this arrangement depends mainly on the switching time of the relay which is approximately inversely proportional to the power that can be handled by the switch. Off-line systems can include a power generator which takes over after an additional delay time.

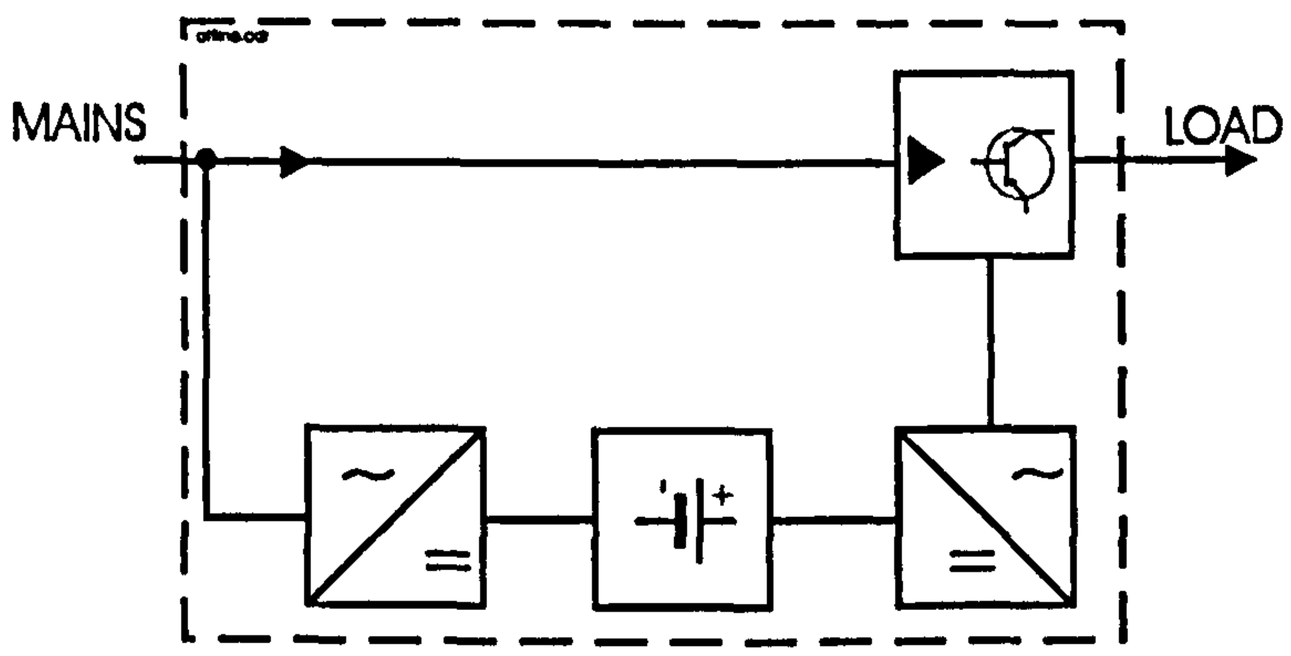

Figure 2.8 Off-line UPS

Internal systems:

Further configurations to improve efficiency:

In an external on-line system such as that shown in Figure 2.9 the UPS is linked between the mains and the load so that all power is transmitted through it. A battery bank is required to achieve a voltage level equivalent to the output voltage of the rectifier. The bank consists of several batteries which are connected in series. The investigation of such battery banks shows that the imbalance in the characteristics of individual cells leads to premature failures of the whole battery bank [Sch93]. Herein lies a major problem of UPS systems which operate with such a bank. Another drawback of such on-line systems is that power is converted several times before it is supplied to the load.

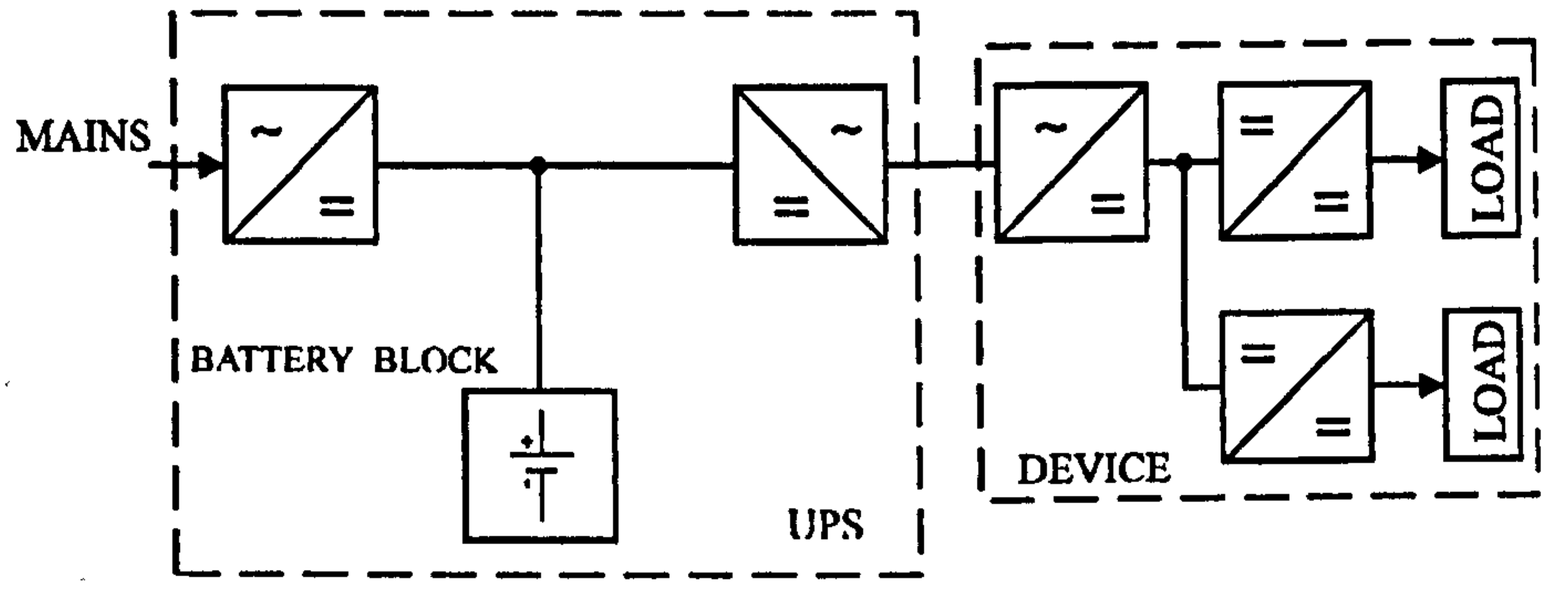

Figure 2.9 device backed up by standard on-line UPS

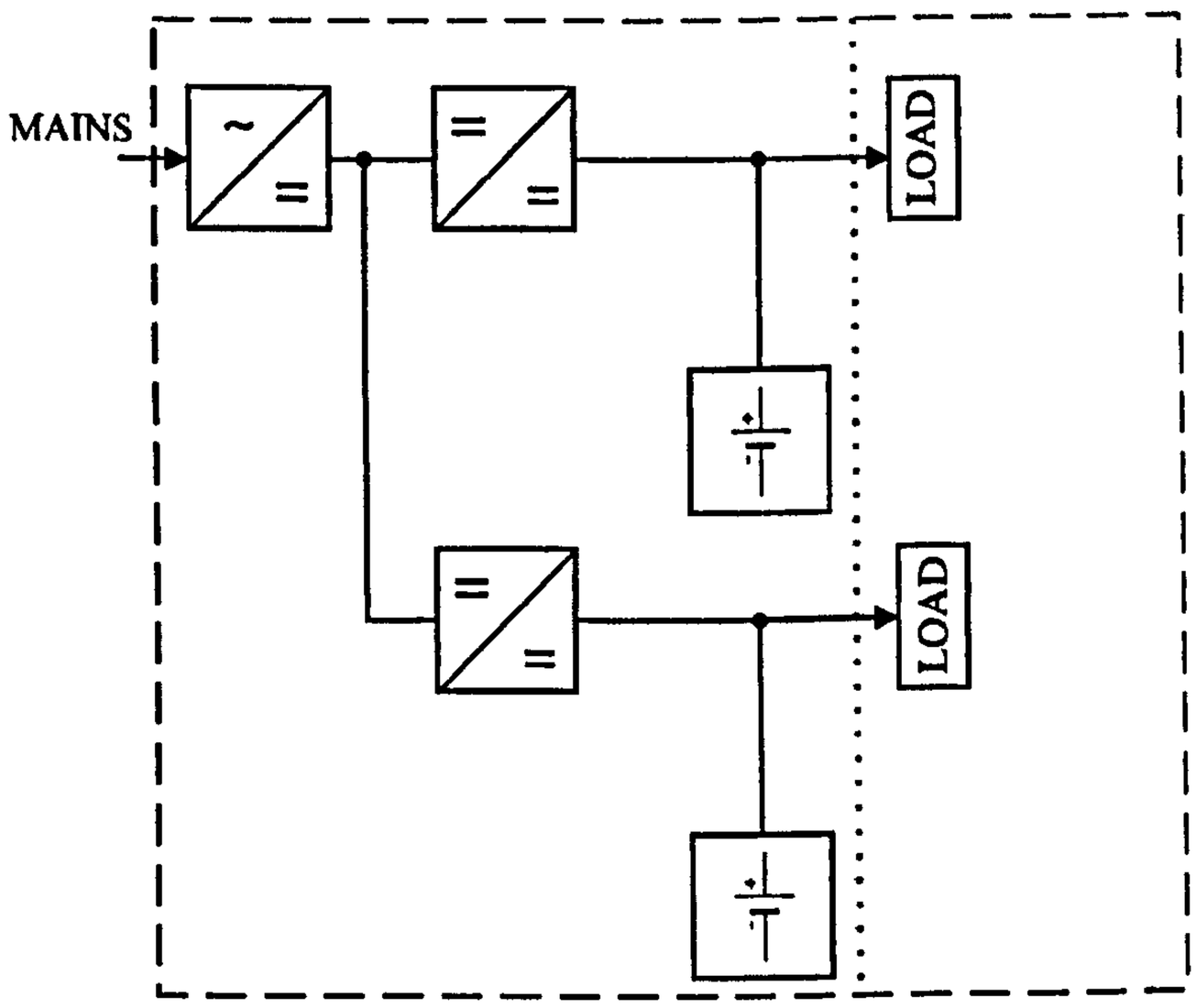

Figure 2.10 Inbuilt on-line UPS version 1

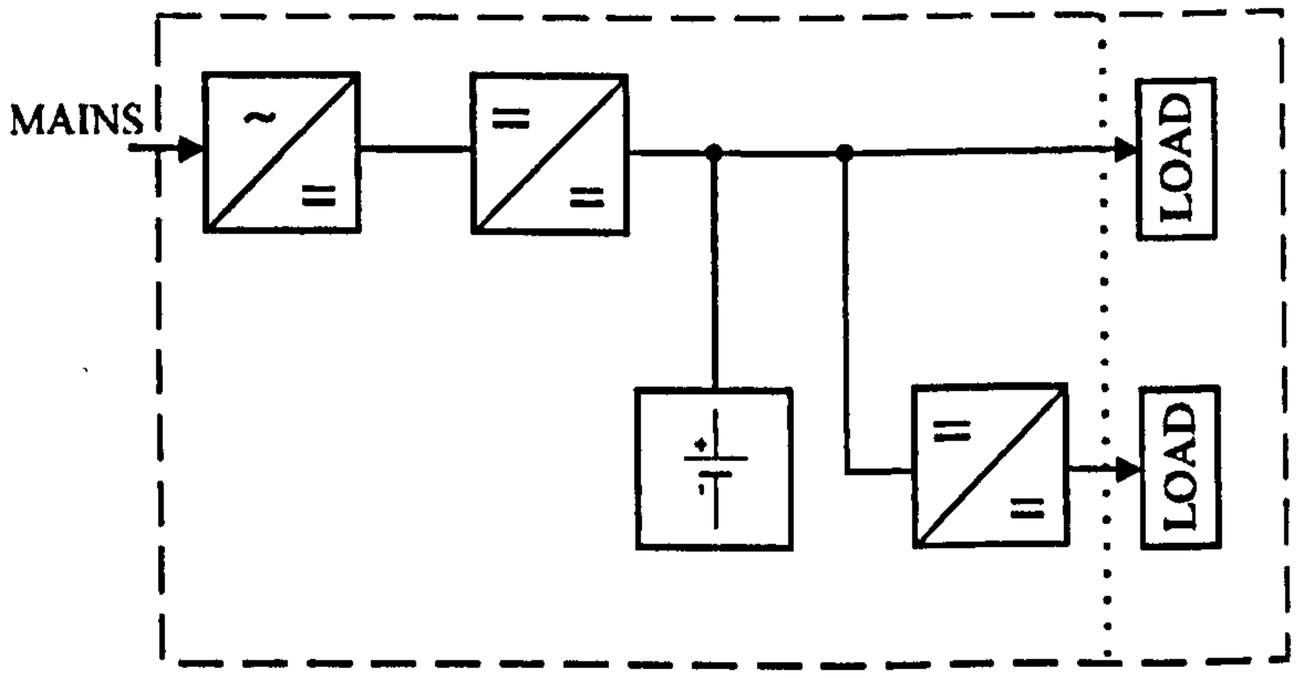

Figure 2.11 Inbuilt on-line UPS version 2

Internal UPS systems are included within the equipment to be protected. The incoming AC voltage is converted to a DC level and then directly supplied to the load. Hence, the number of power conversion stages is reduced. Additionally the battery voltage can be chosen according to the voltage required by the load making a battery bank redundant. Figures 2.10 and 2.11 show modifications to that shown in Figure 2.9 suitable for internal use and making them more efficient because they have a reduced number of conversion stages. All three arrangements provide two output levels.

The rectified voltage in *Version 1* shown in Figure 2.10 is supplied to two DC-DC converters and supported by one battery each, resulting in two different output voltage levels. *Version 2* which is shown in Figure 2.11 embodies only one battery. The second voltage level is achieved by a converter which is linked to the load via a battery. Both systems are more efficient than the above standard version. A justification is given by simply summing up the number of conversion stages in each version:

On-line standard:	*Version 1:*	*Version 2:*
4 conversions	2 conversions for load 1 2 conversions for load 2	2 conversions for load 1 3 conversions for load 2

Table 2.1 comparison of number of conversions

Furthermore, in the two built in versions the batteries do not have to be formed as a bank if the voltage level, required by the loads, is 24 Volts or less.

2.3 Components of a UPS System

An examination of a UPS system in order to clarify its basic functions is given below:

I. The AC input voltage has to be converted into a low level DC voltage (eventually two levels e.g. 12V/5V). Almost every application such as computers, electronic apparatuses and small drives need only DC voltages.

II. The battery or any other power-storage device must be charged by the mains. Therefore, most certainly at least one conversion stage is required to produce the necessary DC voltage.

III. The power-storage device has to supply the voltage to the load in case of a power failure.

IV. Power disturbances other than brownouts (87%) have to be compensated or filtered.

The function of each block in a UPS system is explained and the way it contributes to the system is examined. According to these functions the overview is displayed in table 2.2.

The most significant blocks are discussed in more detail below and where possible alternatives to the standard set-up are given.

block	*function*
AC-AC converter	voltage reduction to battery level / intermediate circuit level
Rectifier (AC-DC)	voltage rectification to supply / transfer through battery
Filter	noise reduction
Charger	supply battery due to discharge in an emergency case
DC/DC converter	reduction to load level produce voltage level to fit intermediate circuit for high frequency transformation
Inverter (DC-AC)	produce AC voltage as required for the device to be protected
by-pass	to circumvent the UPS in case of system defects or high current requests.
battery	storage of energy that has to be delivered to the load in case of power failure.

Table 2.2 components of a UPS system and their function

AC-AC converters:

To reduce the incoming voltage of the mains to the required intermediate voltage level many UPS systems use AC-AC converters. Simply by putting two windings on a common transformer with the appropriate turns ratio the voltage transformation is achieved. Due to the low transformation frequency (50/60Hz ≡ work-frequency) these components use up large amounts of space and are responsible for high losses in the form of emitted heat.

(by-pass) switch:

This element varies with the type of UPS system. It is a static switch in the off-line systems. The permanent operation mode UPS type embodies a switch that allows parallel operation of both sources, the mains and the battery. In the on-line systems a by-pass switch is used to circumvent the UPS in case of system defects or high current demand. The switch in an *(ii)* above connects the battery to the load in case of undervoltage in the mains hence allowing a parallel operation. In an off-line system a static switch is used, therefore only one source at time can be linked to the load.

Battery:

According to VDE (Verein deutscher Elektroingenieure)[5] emergency lightning may only be backed up by lead (Pb) or nickel-cadmium (NiCd) batteries. NiCd-batteries are mostly used where high charge currents linked with short delay times are frequently occurring. Criteria to select the right battery for a UPS are listed in the table 2.3.

A major factor for lifetime of rechargeable systems is determined by how many cycles it can be operated. Due to latest reports[6] VIDOR battery company in the U.K. has developed are-usable alkali battery. Unfortunately, it is not yet clear which possibilities there are to use them in UPS systems, especially for low power application. One drawback could be that they can not be recharged as often as their counterparts.

---

[5]VDE (unification of electrical engineer in Germany)
[6]Financial Times: "Charged up for battle"; 2th of December 1993

parameter	lead	NiCd
capacity [Ah]	1 - 63	10^{-2} - 15
energy density [Wh/l]	10 - 100	30 - 80
voltage in each cell [V]	25 - 35	15 - 45
possible current [A]	2	1,2
charge / discharge cycles	500 - 1,500	up to 8,000

Table 2.3 secondary batteries (or accumulators) for use in UPS systems [Her86] p.248

alternatives to a battery:

Power storage is of major concern not only in UPS systems but also in the automotive industry and in the field of portable electronic equipment such as drilling machines and mobile telephones. Hence, a significant amount of research is carried out by scientists and engineers from different backgrounds into this topic. Two realistic examples are mentioned below which could help to overcome the limits of power storage capabilities of the existing systems.

- mechanical inertia system coupled to a engine / generator[7]:

  In UPS systems batteries could be substituted by kinetic energy storage systems. At the Argonne National Laboratory (US state Illinois) researchers developed an kinetic energy storage system incorporating super conducting magnetic bearings [Spi94]. These systems operate with virtually no losses and hence excel existing batteries. Such systems would not require a

[7]Mechanical inertia systems have been used for years e.g. in Switzerland, where buses store energy from downhill drives onto a large rotating disk to reuse it for the uphill drive

permanent recharging of the buffer. Therefore, it would not be necessary to include a steady link between the energy storage device and the power system. Additionally such systems would not wear out due to the very low friction coefficient because they operate without friction. Using batteries as storage medium has another severe drawback that can be overcome using the described kinetic energy storage systems: batteries have to be checked and replaced after a defined period. This causes additional costs in the long run of such systems.

- organic polymers:

  According to a report in the Financial Times at the 16th of February 1995 scientists in Japan [Tok95] have developed a composite organic cathode that can be used in a rechargeable lithium battery. The resulting system possesses high energy-storage capability combined with low weight and good mechanical strength.

DC/DC converter:

Some UPS systems do possess a DC-DC converter[8], nevertheless some arrangement do not require them. DC-DC converters are of course required if the incoming AC current shall not be transformed with 50 Hz but with high frequency and a single battery shall be used. This reduces the space occupied by this functional block. Additionally, the drawbacks (as explained in Chapter 2.1) linked with the use of battery banks can be overcome.

[8]As described in Chapter 2.1 in some on-line system the incoming AC-voltage is rectified and then reduced to the battery-level, by a DC-DC converter (step-down). Another DC-DC converter (step-up) is used to boost the voltage up again, hence it can be inverted to AC-voltage.

2.3.1 Resonant Technique in UPS Systems

The most significant items which contribute to the overall weight and volume of UPS systems are magnetic and capacitive components and stand-by batteries. Therefore, to improve the power to weight ratio it is necessary to a) reduce the volume, the weight and the size of the magnetic and capacitive components and b) to select converter configurations with high efficiency.

It can be shown that for a given flux density the core area is inversely proportional to the frequency of operation.

$$A_n = \frac{1}{f} \cdot \frac{V_{ind}}{B \cdot N} \tag{2.1}$$

For example, a 20kHz transformer would in theory require a core area 400 times smaller than a 50Hz transformer for the same power as illustrated in Figure 2.12.

However it is not possible to reduce the cross area section A_n of the magnetic core for a given air gap indefinitely. With the decreasing cross sectional area of a transformer the leakage flux increases. Hence, the magnetic coupling factor and the transmitted voltage decrease. Additionally the resistance of the inductive elements also increases [See92].

Nevertheless, there has been a trend in recent years to increase the switching frequency in order to achieve lighter and more compact power supplies. Standard pulse-width modulation technique hereby limit the switching frequency to some hundreds of kilohertz.

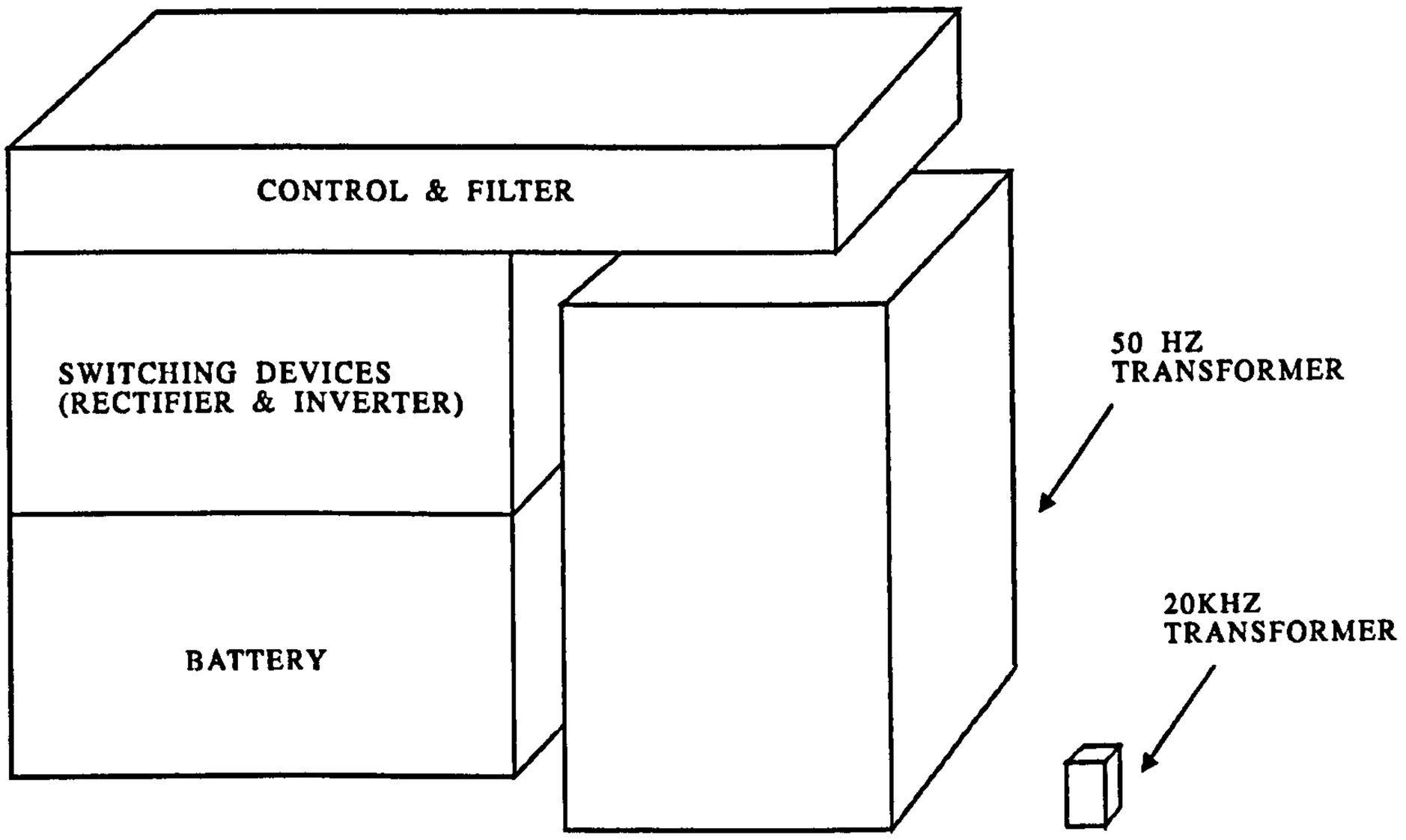

Figure 2.12 Component volume distribution in a conventional 50 Hz UPS [Meh90]

Resonant techniques could help to overcome this limit and would therefore enable designers to use significant smaller core areas for the transformers. Detailed research has been carried out by several groups in the last decade[9]. There are many conferences and papers on resonant mode techniques. The introduction to one such article begins:

> *"Resonant technology of energy conversion is rapidly progressing due to its advantage such as small size, low weight, fast dynamic response, and low EMI"* [Ngo87].

[9]e.g. Virginia Power Electronics Center; Kobe University; Institute for Power Electronics and Electrical Drives University Paderborn

This quotation accurately sums up the basic advantages of the resonant technology.

By looking at the available UPS systems it appears that no company has yet introduced resonant techniques into their products. The question arises as to why such a carefully researched technique is not applied to commercial products. Even in the DC-DC market this technique is, until now, only used by one company [Vic91][10], while some prototype converters were used e.g. for space applications [Wei88].

A possible reason could be that it is possible to increase power densities with standard PWM converters because of the development in the semiconductor devices especially MOSFETs (as well as the IGBTs for higher loads) which are used as power switches. These MOSFETs are much faster, with turn on and turn off times shorter than 50 nsec compared with the bipolar transistors. Also devices rated at higher voltages (up to 1200 V) and current levels are now available.

Another explanation may be that resonant converters are more sensitive to load variations and more difficult to control. Therefore the lack of know-how in industry in this field and the complexity of a resonant converter may discourage designers from adapting resonant techniques.

To use high frequency switching techniques it is necessary to modify the configuration of the UPS systems commonly used. This is illustrated in Figure 2.13, where the upper circuit shows the standard configuration of an on-line UPS system. The required reduction of the incoming voltage to the battery level is achieved by using an ac/ac transformer. In the modified version, for

[10]Vicor, 23 Fromtage Road, Andover, MA 01810 USA. They introduced Zero-Current switching in 1985/6 into a DC-DC converter.

high frequency use, the functional blocks are swapped. The ac/dc conversion precedes the voltage reduction stage, a dc/dc converter. This conversion stage is a key element in the high frequency system.

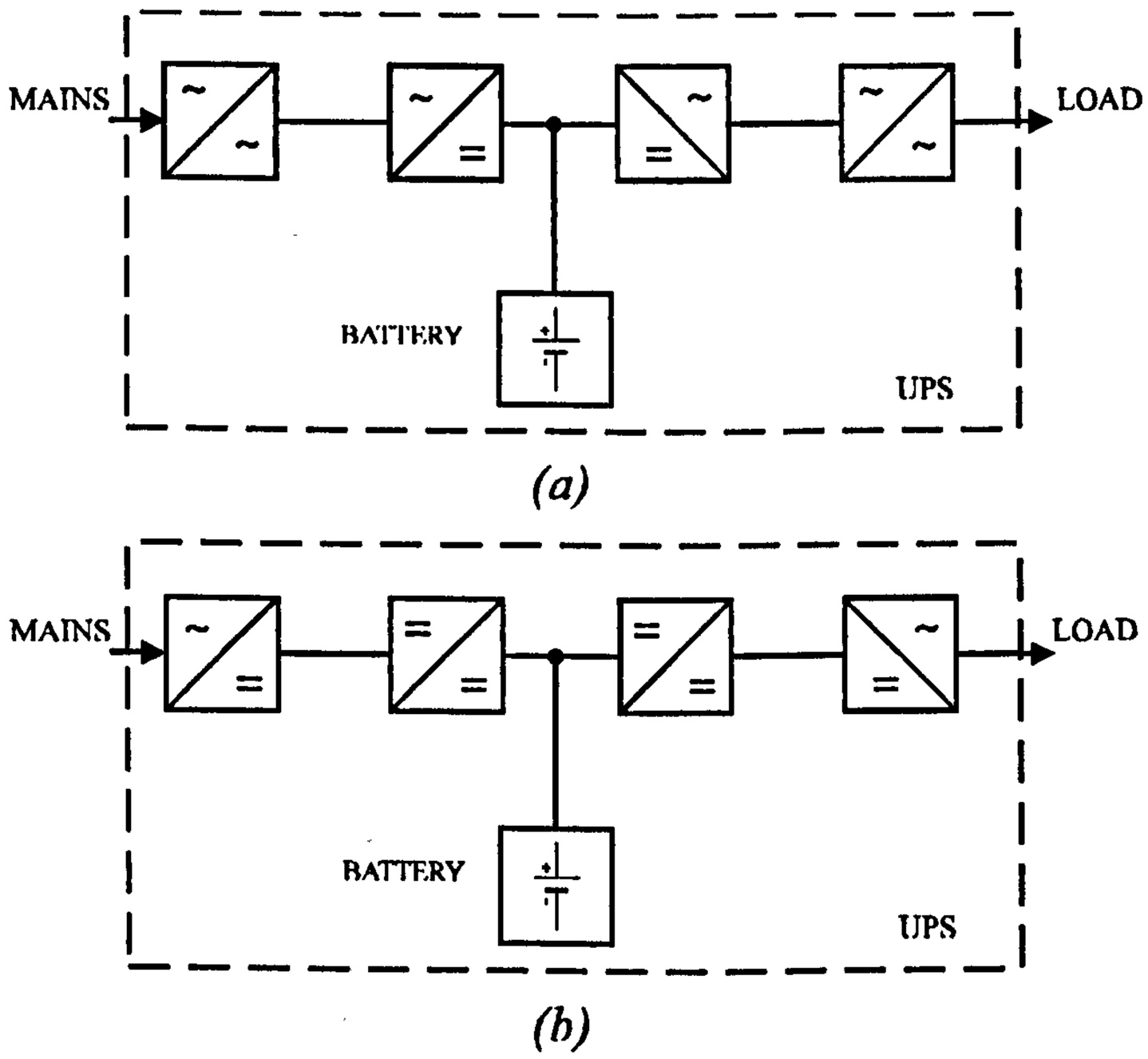

Figure 2.13 ***on-line UPS with 50Hz converters (a) respectively high-frequency conversion (b)***

2.3.2 Converter types

In Figure 2.14 the modern DC-DC converter technology is reviewed. It is the authors perception that a large class of converters fall within such classification. Level 1 in the scheme divides the converters into the well established "hard-switching" PWM converters and the "soft-switching" modern resonant converters respectively, as well as the more recently

introduced PWM zero-voltage / zero-current mode converters[11]. The latter combines resonant switching and pulse width modulated power transfer. This technology suits mostly high power levels where the complexity is not a significant penalty. Therefore, it will not be investigated here any further.

Level 2 divides the resonant converters into three sub groups [Lee89]. Starting from the right, the conventional resonant converters are the first group, often referred to as series resonant converters and parallel-resonant converters and their derivatives. Resonant converters are generally controlled using the frequency modulation technique as opposed to the pulse width modulation technique used in PWM converters. If the parallel or the series resonant converters are operated below resonant frequency, all power switches can be operated with natural commutation (zero-current switching). If they are operated below one-half of the resonant frequency the power switches are also turned on under zero-current conditions. However, if operated above the resonant frequency all power switches are turned on under zero-voltage condition but not turned off under zero-current condition. More recently control techniques have been proposed to operate parallel and series resonant converters at fixed frequencies. These circuits although given different names such as phase-controlled, duty-cycle controlled or clamped mode resonant converters operate essentially under the same principle.

Quasi-resonant circuits (QRC) can be regarded as hybrids of PWM converters and resonant converters. While the underlying power conversion principle[12] of the quasi-resonant circuits is the same as PWM converters, a resonant network is employed to shape the current in the switch or voltage across it so that the

---

[11]This group of converters is widely covered by the work of Ionel Dan Jitaru of ITT Powersystems Corporation.
[12]QRCs are frequency controlled, hence do not operate at a constant frequency.

Overview.cdr

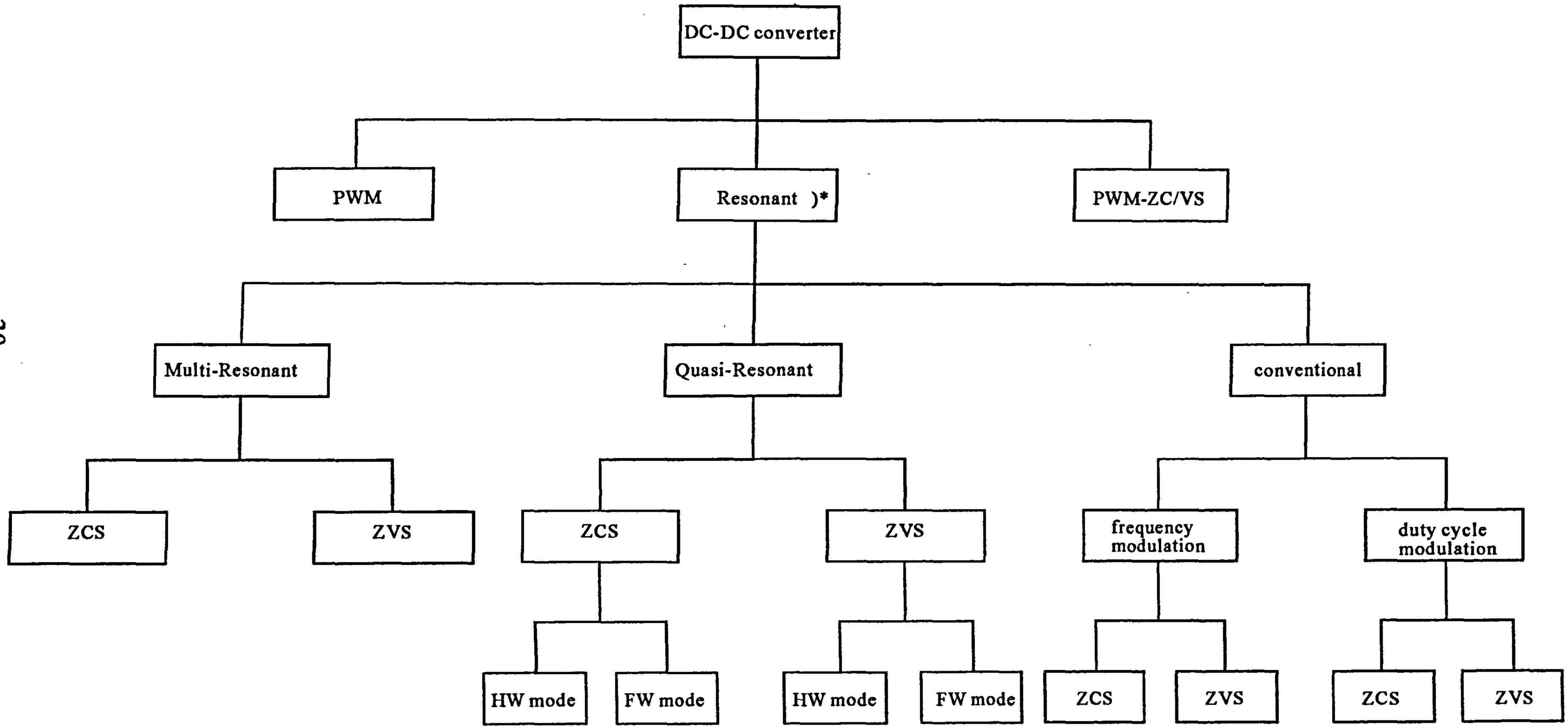

)* Source of this branch: Fred C.LEE: "High-Frequncy Resonant, Quasi-Resonant, and Multi-Resonant converters

Figure 2.14 overview of DC-DC converters

power switches operate either under zero-current switching (ZCS) or zero-voltage switching (ZVS) condition. Both ZCS and ZVS can operate in half-wave or full-wave mode. The quasi-resonant converters in half-wave mode of operation are rather load sensitive while the QRCs become load insensitive in full-wave mode of operation. Half-wave ZCS-QRCs usual operate at higher efficiencies than the full-wave version due to additional circulating current in the full-wave configuration. The full-wave operation of the ZVS-QRCs is less practical because the energy stored in the output capacitor of the power FET is trapped and hence dissipated in the switch during turn on, thus defeating the purpose of ZVS. ZVS-QRCs in half-wave operation have a limited load range but this can be extended at the expense of imposing high voltage stress on the power switch.

In Level 3 within the multi-resonant category employing the ZVS technique, all semiconductor components in the circuit can be operated under ZVS condition. Transformer leakage inductance, magnetising inductance and other important parasitic elements can form part of the circuit. Multi-resonant converters are suitable for very high-frequency operation and can operate from no-load to full-load. A major drawback is that when multi-resonant converters are operated under a wide input voltage variation their efficiency deteriorates rapidly.

CHAPTER 3

THE DUAL CONVERTER

This Chapter presents the main contribution of this thesis - the development and the implementation of the concept of the *dual converter* in a UPS system. As will be described in more detail in this Chapter two voltage sources are linked via a multi-winding transformer. Hence, the load can be powered alternatively or simultaneously from one of the input sources. As illustrated in Figure 3.1 there are three main aspects: the circuit configuration and its operating principle, the applied switching technique and the multi-winding transformer. These aspects are examined individually in detail and the overall structure of the UPS is studied.

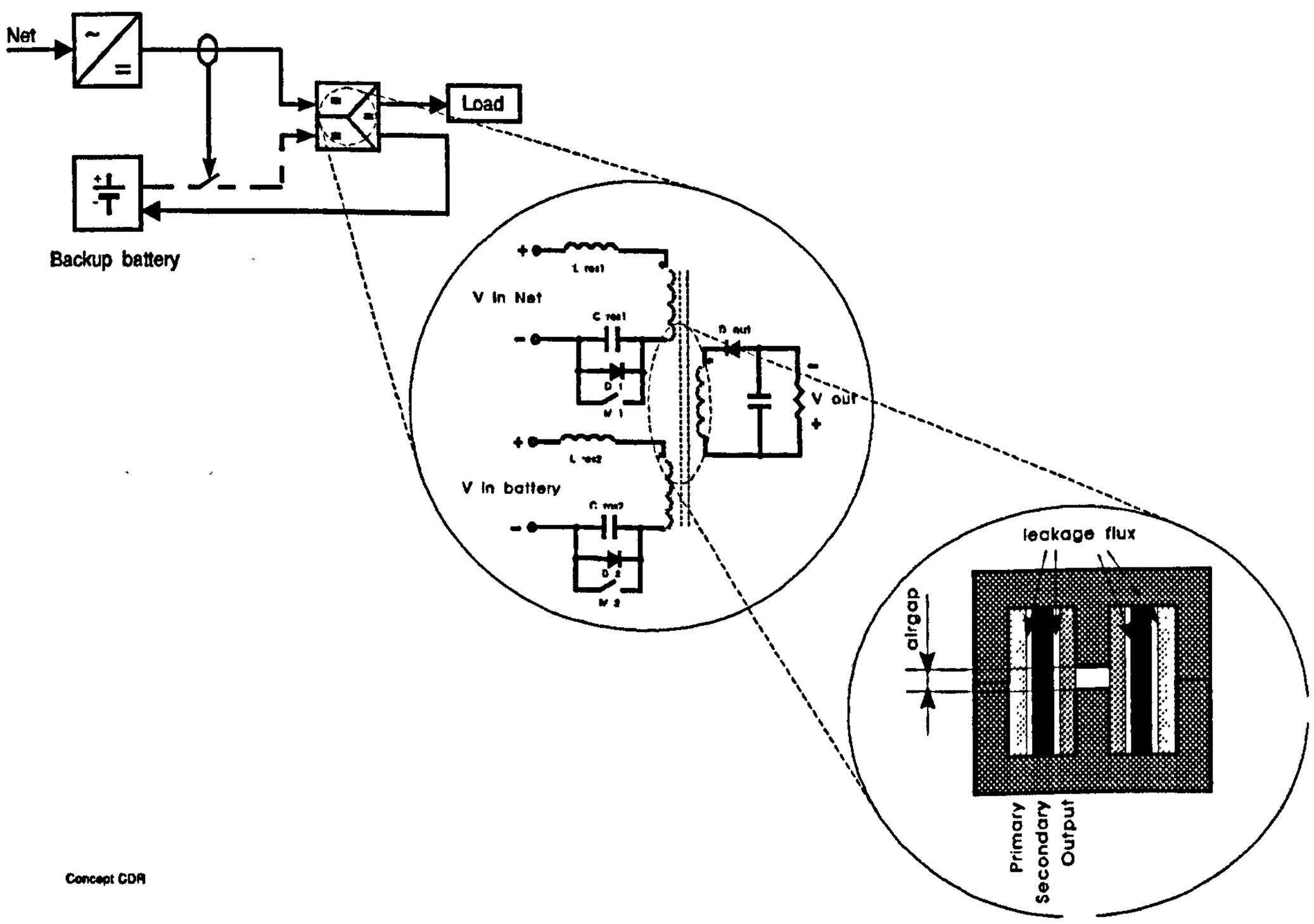

Figure 3.1 The concept of the dual converter

3.1 The principle of the dual input system

Figure 3.2 shows the block diagram of the proposed system in which the multi-winding transformer is fed from the mains as well as from the stand-by battery via a flyback resonant converter. The secondary winding of the transformer supplies the load via a rectifier and a filter.

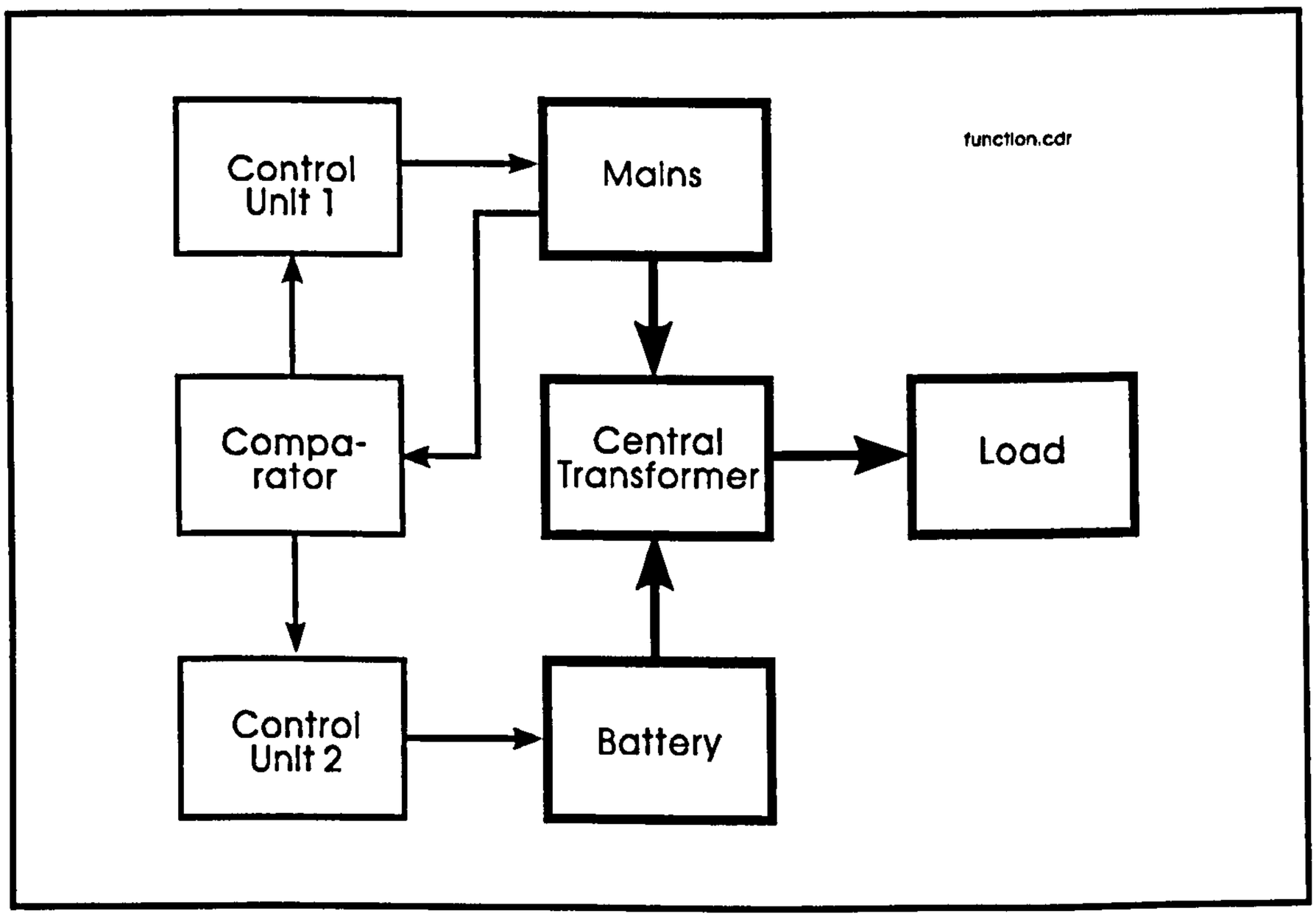

Figure 3.2 Functional scheme

The comparator, which monitors the mains voltage in combination with control units 1 and 2 is used to activate the appropriate power source. In a UPS system it is essential that the change over from the mains to the stand-by batteries is smooth. In the proposed system this is achieved by the storage of sufficient energy in the magnetic core of the transformer, whereas the conventional approach in a UPS would be to provide an additional capacitor for this purpose.

As will be explained in section 3.2.1 for a conventional flyback converter, the energy is stored during each half cycle of operation in the airgap of the transformer and is delivered to the output during the other half cycle. The energy storage capacity of the transformer is designed to be sufficient to cater for abnormal load conditions. As a result a reduced number of components are required for the proposed system.

3.2 Elements of the *dual converter*

High frequency converters and in particular resonant converters call for appropriate devices to suit special demands. All components contribute to the overall efficiency of the system and the importance of each single element can not be overestimated. Especially, the design and determination of the power handling components have great influence on the converters. The proposed multi winding transformer, which is discussed in section 3.2.3, adds to the complexity of the system. Therefore an even more careful choice of the components used has to be made.

3.2.1 The derivation of the *dual converter*

The proposed *dual converter* combines two modified versions of a conventional flyback converter via a multi winding transformer, operating either in a step-up or a step-down mode. Each converter operates in a quasi-resonant mode to reduce switching losses and hence permits higher switching frequencies and therefore smaller capacitive and inductive components. Using a zero-voltage mode allows the circuit to run at frequencies higher than those

possible in zero-current mode. Hence, a zero-voltage (half-wave) mode was chosen for the *dual converter.* This new converter should be named "*zero-voltage half-wave dual quasi-resonant flyback converter*". As this seemed to be a rather cumbersome name the author decided to use a simpler name - *dual converter.*

Conventional flyback converter:

With a buck-boost converter the incoming voltage level can either be boosted or be reduced. Flyback converters are directly derived from buck-boost converters. In other words a flyback converter is the isolated version of a buck-boost converter. The electrical isolation can be achieved by placing a second winding on the inductor of a buck-boost converter, which isolates the input from the output of the converter.

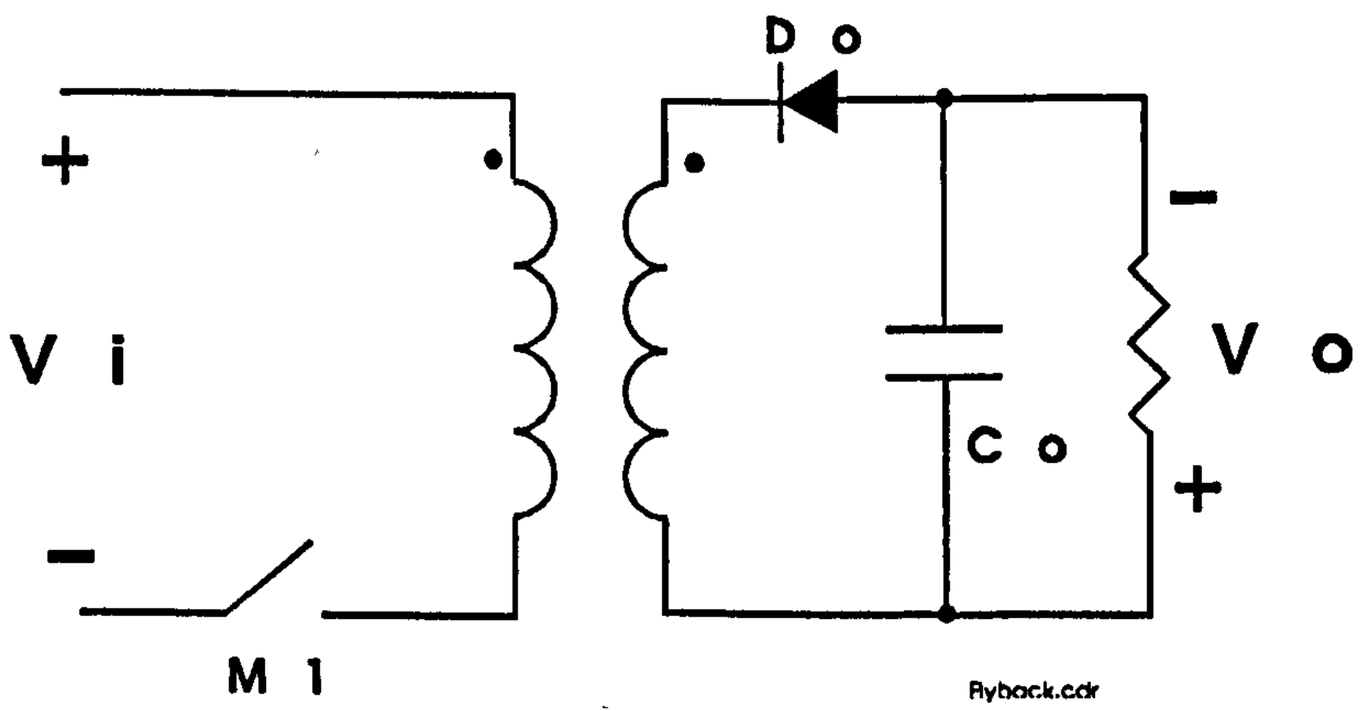

Figure 3.3 Conventional flyback converter

In Figure 3.3 a conventional flyback converter is shown and its operating function is described below.

During the "on-period" of the switch, M_1 , the current flows through the primary winding and thereby stores energy in the magnetic core of the transformer. This energy is then, during the "off-period" of the switch, released from the core of the transformer and supplied to the load[13]. Thus, the transformer can be regarded as a two-winding inductor. The output voltage of the transformer needs to be rectified and smoothed to provide a proper DC voltage for the load, which is done by the output diode D_o and the capacitor C_o.

A great benefit of the flyback converter is that several output-voltage levels can be achieved by simply placing additional secondary windings onto the transformer. Thus depending on the number of turns in the windings the required level of output voltage can be achieved.

Dual flyback converter:

By combining two primary parts of such a flyback converter, a "dual flyback converter" can be achieved. The two input parts are linked through the central transformer, enabling that the output can be powered from source V_1 or V_2. Figure 3.4 shows a simplified drawing of such a converter.

The two sources can also be operated simultaneously, allowing power sharing between the sources.

---

[13]Due to the law of Lenz the introduced voltage is opposing its cause. This is the explanation for the voltage inversion.

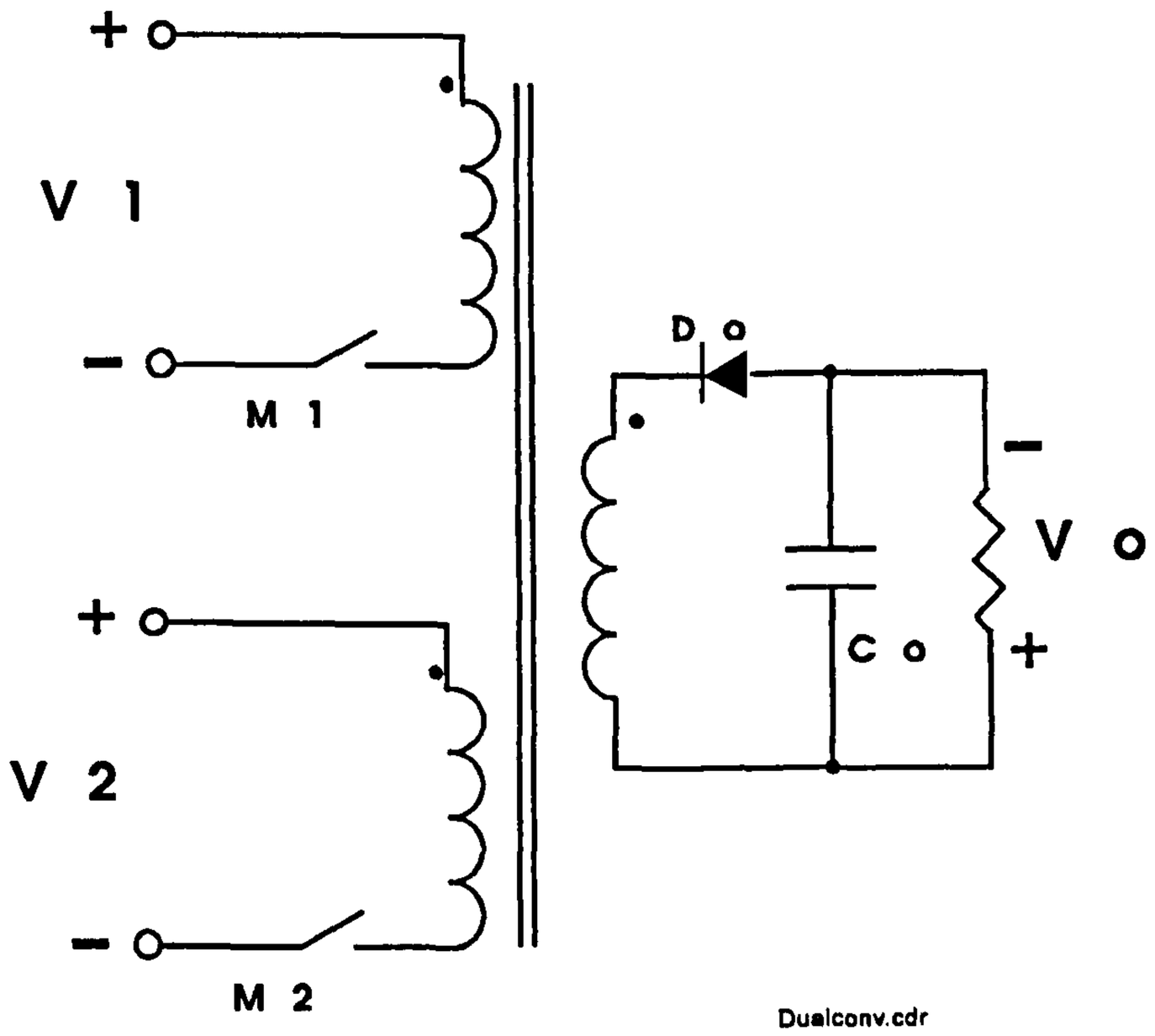

Figure 3.4 dual flyback converter

*The proposed **dual converter***
or zero-voltage half-wave quasi-resonant dual flyback converter:

The quasi-resonant switching technique will be explained in section 3.2.2. This advanced technique was applied to the aforementioned dual flyback converter, leading to a circuit set-up which is shown in Figure 3.5. The switches M_1 and M_2 of the dual flyback converter were replaced by quasi-resonant switches to obtain resonant switching conditions. C_{r1} and L_{r1} C_{r2} and L_{r2} form resonant tanks that enables the circuit to operate under zero-voltage conditions.

The anti-parallel diodes D_1 and D_2 cut off the negative voltage swing, which is produced by the resonant tank, facilitating half-wave operation.

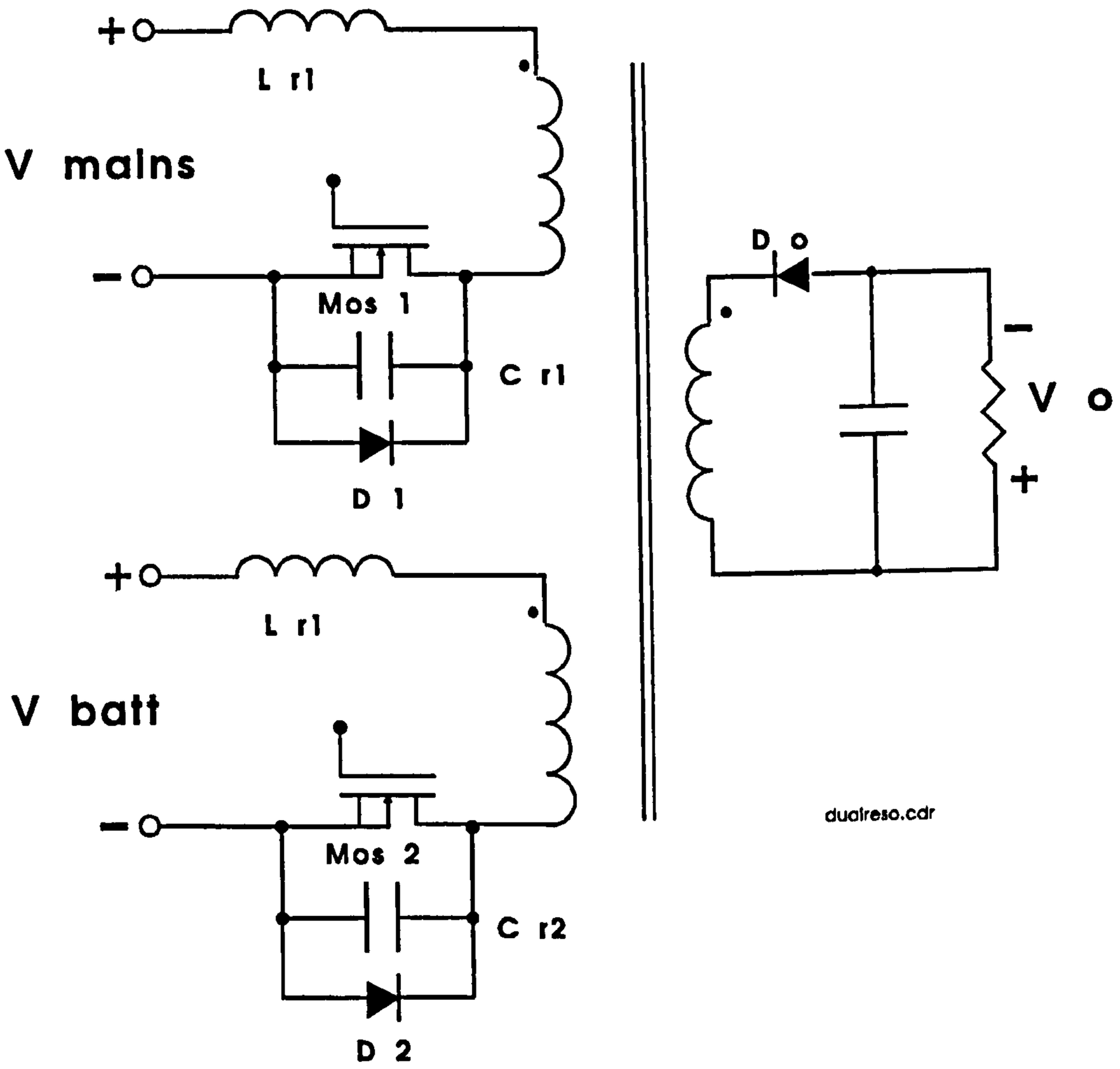

Figure 3.5 ***The proposed*** **dual converter**

A great advantage of this circuit is that the parasitic elements of a conventional flyback converter, such as the capacitor C_{oss} (equivalent to C_{r1} and C_{r2}) of the MOSFET Mos_1 and Mos_2 and the leakage inductance L_{leak} of the transformer can be used as parts of the resonant elements. This will be demonstrated in Chapter 3.2.3.2 for the leakage inductance.

On the output side the diode D_o rectifies the voltage across the secondary side of the transformer. The scheme in Figure 3.5 does not include the snubber circuit that was placed across this output diode to reduce voltage spikes and the ringing due to this diode.

3.2.2 Switches and Switching techniques

The switches used in the *dual converter* can be divided into active and passive switching elements. Nevertheless, it should be kept in mind that it would have been possible to use a controllable (active) switch instead of the output-rectifying diode, which would also allow bi-directional power conversion[14]. For the special purpose that was aspired with the *dual converter* this possibility was not required. However, the variations that has been outlined in Chapter 2.3 as alternatives for a battery, could require a bi-directional operation of the *dual converter* and would hence call for a controllable switch.

Rectifying diodes:

To reduce switching losses in the rectifying elements either fast or very fast recovery or Schottky diodes should be chosen.

Fast and very fast recovery diodes have moderate to high forward voltage drops, ranging anywhere from 0.8 to 1.2 Volts. Because of this and because of their high blocking voltage capabilities these diodes are particularly suited for low-power auxiliary voltage rectification for outputs above 12 volts. To allow

[14]One example for such a converter is given in the work of Biswajit Ray [Ray92], see also Chapter 2.3.1

operation at high frequency (>20kHz) fast and very fast recovery diodes offer reduced reverse recovery times in the nanosecond region for some types [Chr89].

Schottky barrier diodes have an extremely low forward voltage drop of about 0.5 Volts even at high forward currents. This makes the Schottky rectifier particularly effective for low voltage outputs, such as 5 volts, since in general these outputs deliver high load currents. The reverse recovery time in a Schottky rectifier is negligible because this device is a majority carrier semiconductor and therefore there is no minority carrier storage to be removed during switching.

Therefore the decision was made to use the Schottky barrier device with regard to the rather low output voltage that is demanded for the chosen applications of the *dual converter*. The problem associated with these diodes is that they have a reverse blocking capability of only approximately 100 volts which can be accepted for this application. Also Schottky diodes tend to cause ringing problems, especially at high frequencies. During the laboratory tests this effect occurred very often. It will be demonstrated in Chapter 5 how this problem can be dealt with by appropriate design of the snubber circuit.

Power-switches:

The development of semiconductor switching devices during the last two decades has created a totally different situation in the design of converters, power supplies and UPS systems. Bipolar transistors were replaced by MOSFETs or IGBTs. Linked with this change in switches is the introduction of new driving circuits. Less power is needed to drive these new switches because they are voltage controlled rather than current controlled. This leads

to a further reduction of power losses. Additionally, the great advantage of MOSFETs over bipolar transistor is that they allow a switching frequency that can be at least ten times higher, even with conventional switching techniques. As mentioned in section 2.3.1 this can lead to a reduction in the size by almost the same factor. Furthermore, MOSFETs require a less complex drive circuit. A power-MOSFET offers the designer a high-speed, high-power, high-voltage device with high gain with almost no storage time, and no thermal runaway [Her86].

For high power applications IGBTs can be used. Unfortunately, it is not possible to switch them as fast as MOSFETs. Nevertheless, soft-switching techniques are becoming very popular here as well.

MCT (MOS controlled tyhristors) are a new class of power semiconductor devices that may be the trend setter for high power application.

> *"A new device technology has been introduced by the Harris Power Semiconductor Division, which offers significant advantages over existing power devices such as IGBTs conventional thyristors, and FETs at current up to 120 amperes and voltages up to 1200 volts"* [Tem93].

For the proposed *dual converter* and a power rating of less than 100 watts MOSFETs are the best choice. MOSFETs are nowadays able to withstand a voltage level of above 1200 volts. This limit is important because of the overvoltage caused by the zero-voltage switching technique which will be explained later in this Chapter. The peak voltage can be ten times the nominal input voltage value. Nevertheless, the on-state resistance of a MOSFET

increases with its ability to withstand high voltages. The losses due to this "on-resistance" R_{on} of the switches can be given by:

$$P_{losson} = R_{on} \cdot I_{switch} \tag{3.1}$$

MOSFET	max. voltage stress	on-state resistance R_{on}	max. dissipated power
IFR540	100V	0.085Ω	125W
IRF740	400V	0.55Ω	125W
BUZ357	1000V	2.0Ω	125W

Table 3.1 Selection of significant MOSFET data

Hence, for the selection of the appropriate MOSFET this issue must be taken into account. The important data of some representative switches are given in table 3.1.

Switching techniques:

Pulse width modulation (PWM) techniques are nowadays mainly used in DC-DC converters. The controllable switches are operated in a switch-mode where they have to turn on and off the entire load current during each switching action. This is why these converters output is typically square wave voltage. As a result the switches are subjected to high switching stresses as well as high switching power losses which increase linearly with the switching frequency. The diagram below shows the overlapping of the voltage V_{ds} across the switch and the current I_{ds} through it and the related power P_v during one cycle of

operation. Whenever this voltage and this current occur simultaneously losses are the result. These losses can hence be expressed as:

$$P_{loss} = V_{ds} \cdot I_d \qquad (3.2)$$

The effects of two developments in recent years can be explained with the aid of Figure 3.6. Firstly, the increase of the switching frequency to reduce the size of magnetic and capacitive elements result in higher switching losses. This is because the periods during which losses occur are relatively large in relation to one switching cycle. Secondly, the development in semiconductors led to a reduction of the real switching time, hence reduced losses.

The term "switching time" here means the period during which the current through the switch builds up and the voltage across it drops at turn-on of the switch and vice versa at turn-off. MOSFETs have switching times as low as a few tens of nanoseconds, resulting in a present switching frequency limit of approximately 500kHz using conventional switching techniques.

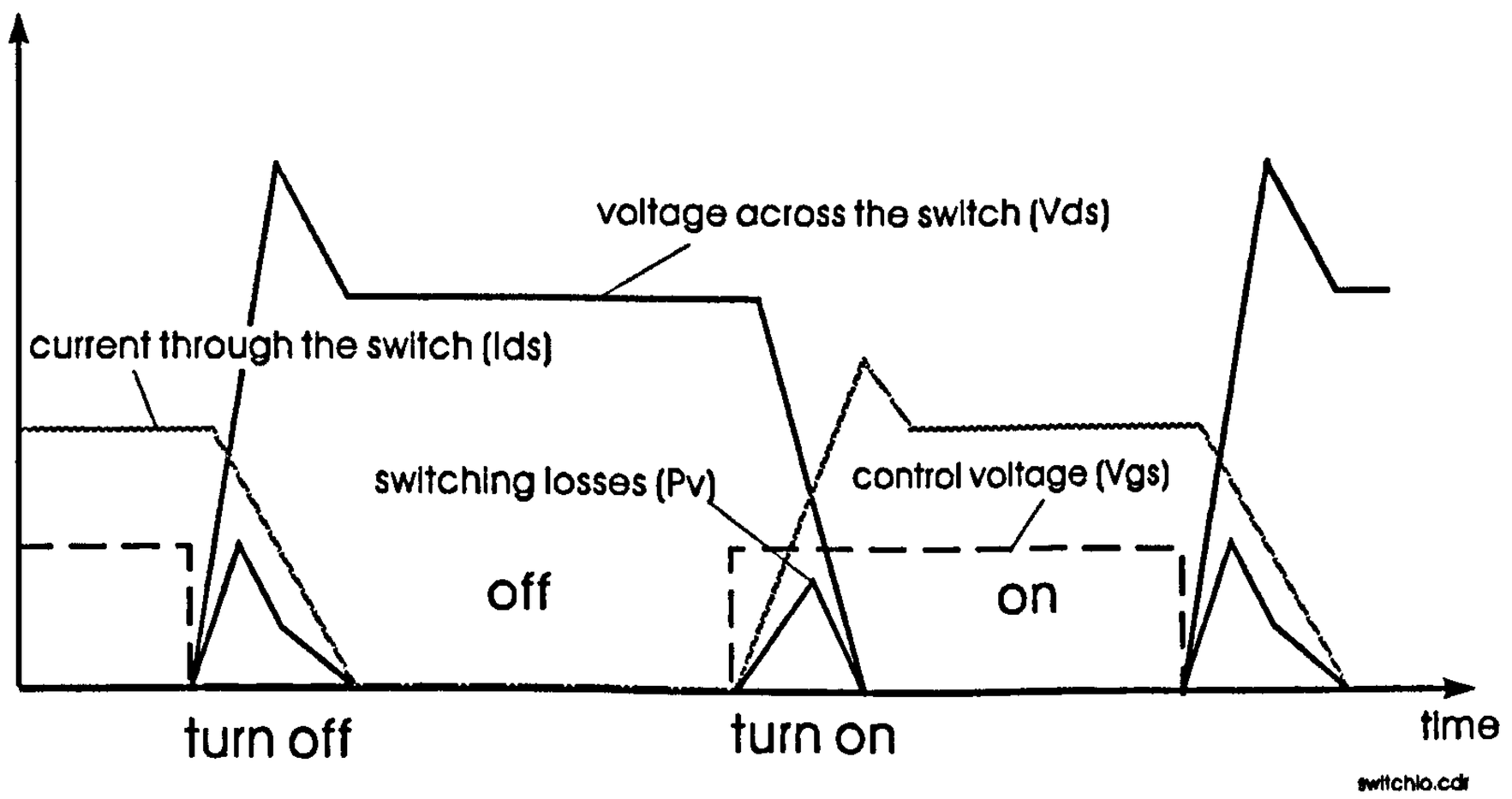

Figure 3.6 Switching losses with PWM (not to scale)

Associated with equation 3.2 is a popular fallacy: the current I_{ds} that is responsible for switching-losses is only the current through the drain-source path of the MOSFET as indicated in Figure 3.7. In practice, it is difficult to measure this current, due to the internal parasitic capacitor C_{oss} in parallel with the drain-source connection inside the MOSFET. The current into the capacitor is not dissipated, but released back into the circuit. Hence, it has to be carefully examined which current is multiplied by the voltage across the switch, to obtain realistic results.

Another significant drawback of the PWM switch-mode operation is the ElectroMagnetic Interference (EMI) which is produced due to the large *di/dt* and *dv/dt* caused by the above mentioned fast switching time.

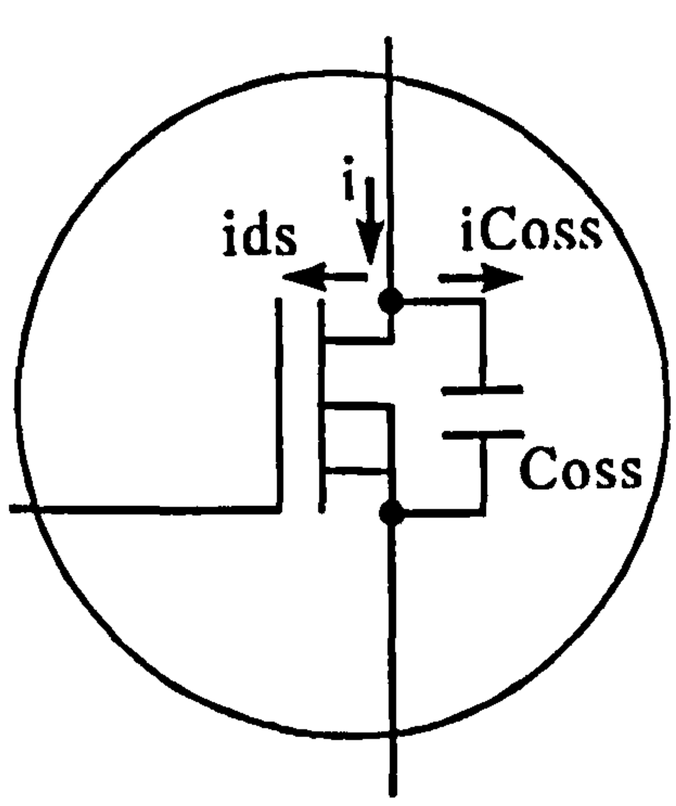

Figure 3.7 Currents in a MOSFET due to parasitic capacitance C_{oss}

The dotted paths in Figure 3.8 show a typical trajectory for inductive switching with conventional forced turn-off. The paths traverse through a

high-stress region where the switch is subjected to high voltage and high current simultaneously.

The trajectory for inductive switching with a resonant switch moves mostly along either the voltage axis or the current axis both at turn-on and turn-off, as shown in the diagram.

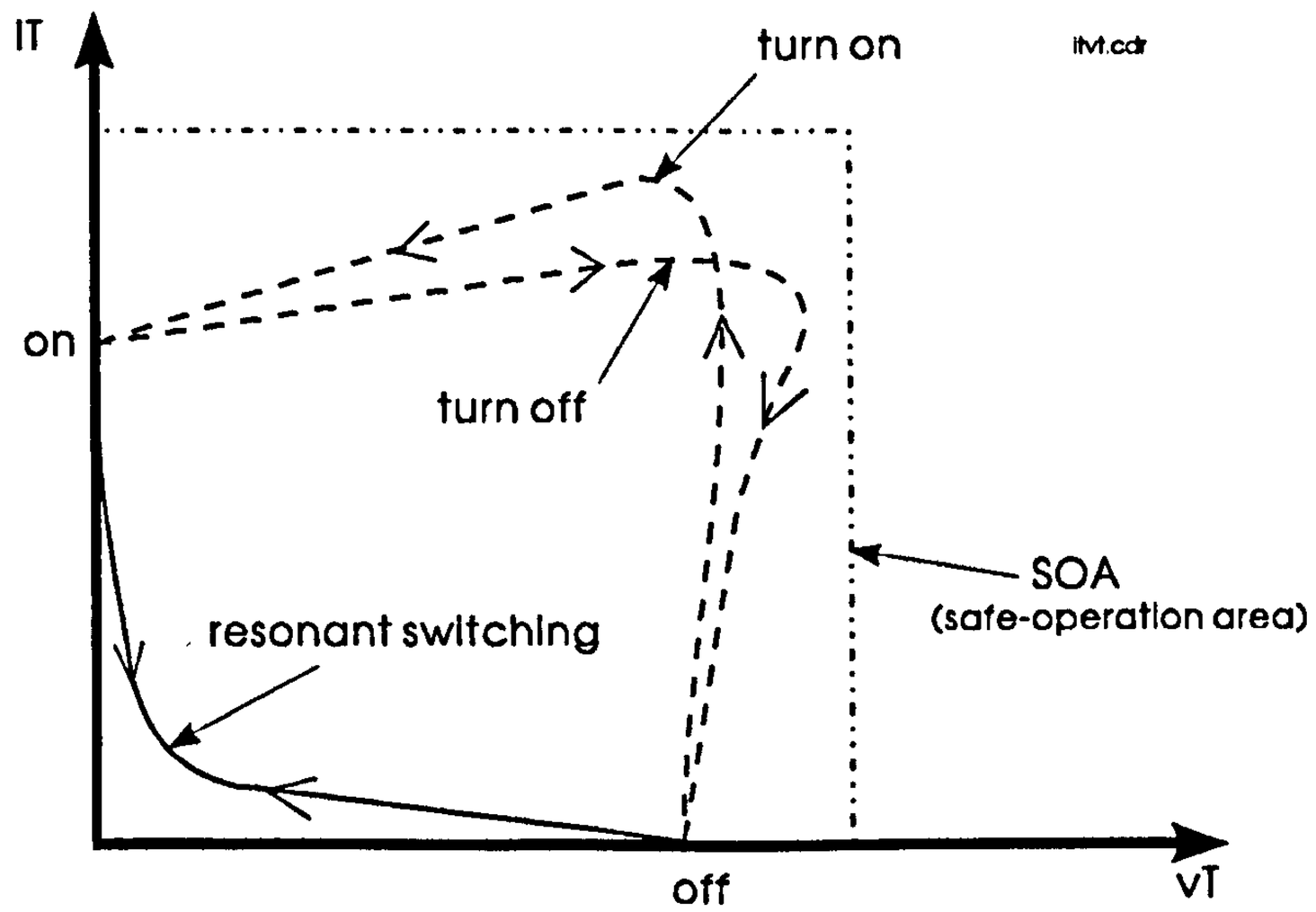

Figure 3.8 Switch-mode inductive current switching PWM and quasi-resonant mode

Design compromises are therefore necessary when using PWM techniques such as over dimensioning of the switch and other components. To overcome these drawbacks designers can use modern resonant switching technology instead of the established PWM technology.

Quasi-resonant switching:

According to equation 3.2 the product of current through a switch and voltage across it is equivalent to the power dissipated during one switching period. Setting one factor to zero would theoretically reduce losses to zero, hence enable a lossless switching operation.

Zero-voltage and zero-current switching modes were introduced in order to fulfil this demand [Vin83], [Liu86]. The application of these techniques results in either zero turn-on or zero turn-off losses which is demonstrated in Figure 3.9 and 3.10.

Ideally, a resonant circuit would be one with both zero turn-on and zero turn-off switching losses. However, in practice this is not possible for any circuit composed of a switch and a network of linear passive components, as has been shown mathematically by B. Molnar [Mol84], [Row90].

The different ways in which a standard switch can be transformed into a resonant switch are shown in Figure 3.11. The concept of the resonant switch was conceived through the following observation. When energy is injected into an LC-tank circuit, it is exchanged between the inductor and the capacitor in a sinusoidal fashion. Because of its ability to sustain a sinusoidal oscillation an LC-tank circuit can be used as a lossless (or low-loss) wave form-shaping device.

When it is desired to shape the current wave form, the inductor in the resonant tank is connected in series with the switching device. The resulting subcircuit with the capacitor in parallel with the switch / inductor combination is called current-mode resonant switch. There are two types of current-resonant switch

configurations: L-type and M-type. In both cases resonance occurs during the major portion of the on-time of the switch.

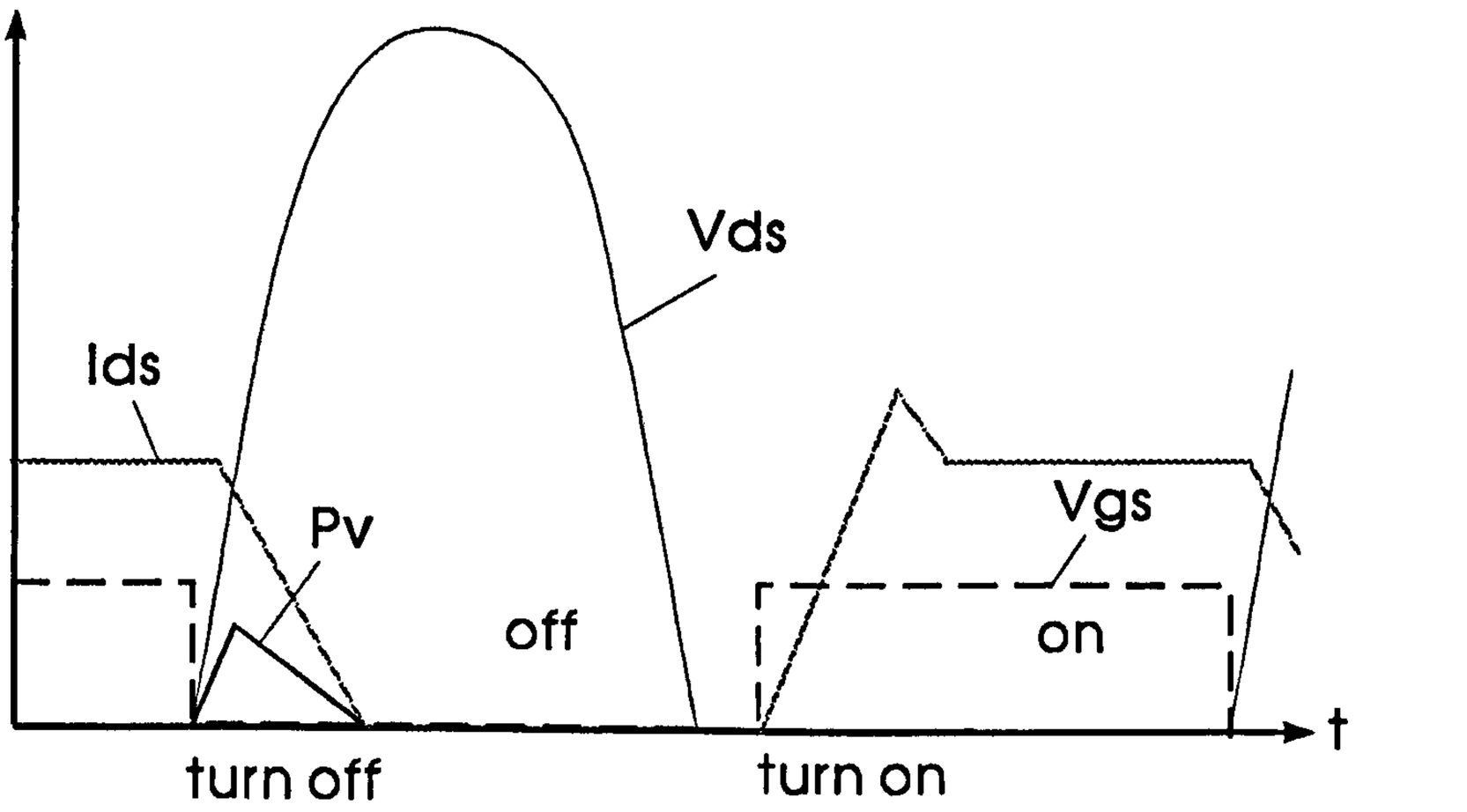

Figure 3.9 Switching losses with zero voltage-mode

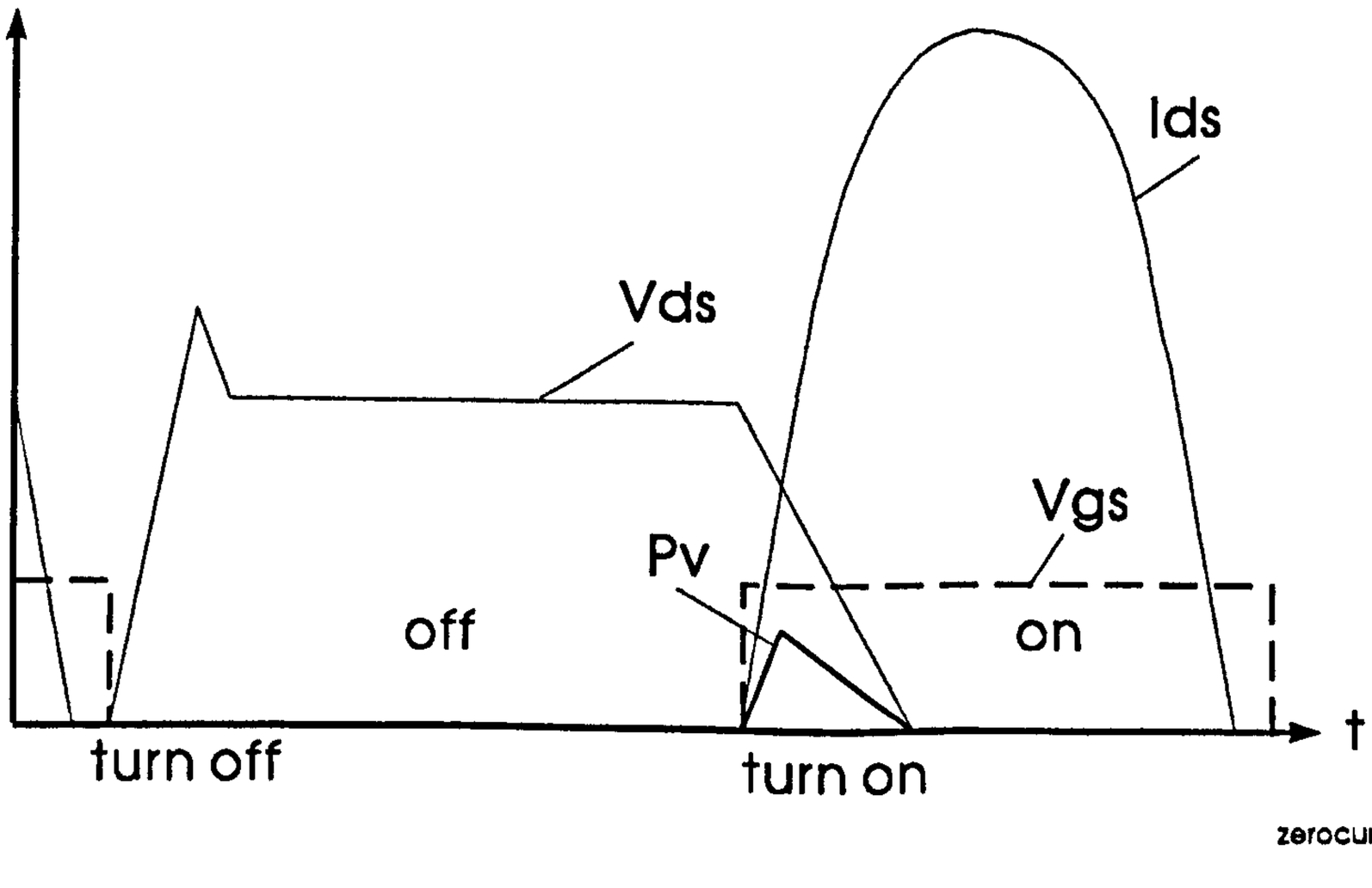

Figure 3.10 Switching losses with zero current-mode

When it is desired to shape the voltage wave form the capacitor in the resonant tank is connected in parallel with the switch. The two resulting voltage-mode resonant switches are also shown in Figure 3.11 (types (c) and (d)). Here the resonant period is located during the major portion of the off-time of the switch.

The task of the designer is to choose between the two options. As shown in the Figures 3.9 and 3.10 zero-voltage mode converters result in high voltage stresses during the off-time of the switching cycle and zero-current mode converters are exposed to high current stresses over the switch during the on-time. Hence, this is going to be an important aspect for consideration for designing a resonant converter.

A major difference between the quasi-resonant converter compared to the PWM converter is the controllability of the output voltage: The output voltage of PWM converters is controlled by modulating the on-period at a constant switching frequency. Quasi-resonant converters operate at a variable switching frequency, hence their control is called pulse density control.

The two variations of quasi-resonant converters are explained below. For simplicity and to aid understanding the author has limited this discussion to the half-wave modes for each version. This means the resonant period can not exceed a half cycle. More detailed information can be found in several publications, e.g. [Moh89], [Syk89].

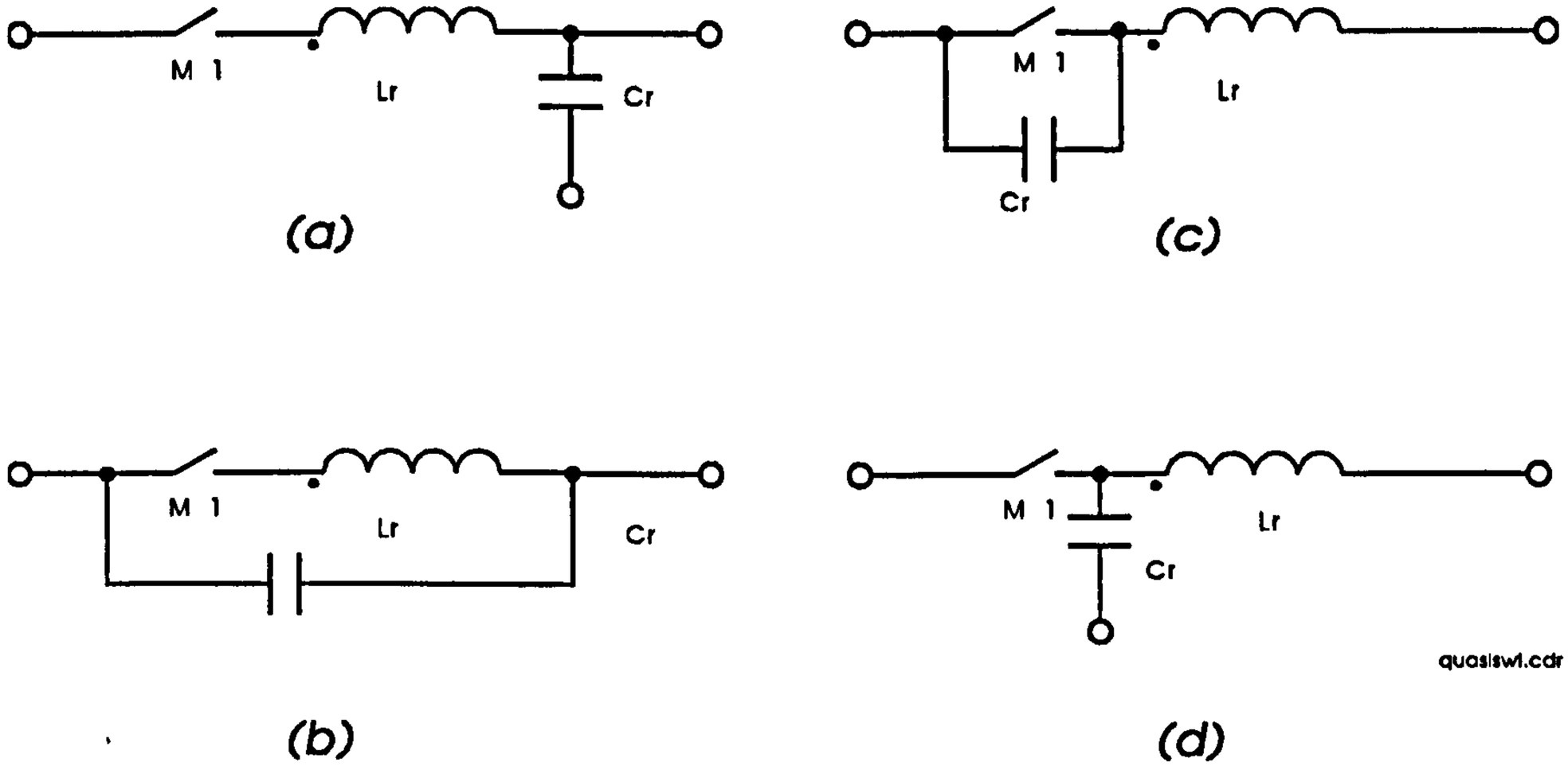

Figure 3.11 ***resonant switch configurations***[15]

(a) current mode L-type

(b) current mode M-type

(c) voltage mode L-type

(d) voltage mode M-type

Both techniques require a resonant tank across the switch in order to shape the voltage / current wave form. The two major categories can be derived from this:

Zero-current mode:

The zero-current mode is the original version of the two and was patented in the U.S.A. in 1983 [Vin83]. Typically, the switch turns off at zero current. The peak resonant current flows through the switch whereas the voltage across the switch remains the same as in the PWM counterpart. To show the operation of such a circuit a modified version of the buck converter is discussed.

---

[15]according to the definitions made by Kwang-Hwa Liu [Liu86]

The diagram gives the wave forms of the current through the switch and the voltage across the resonant capacitor C_r. A typical operating cycle is divided in four time intervals. For each interval the corresponding circuit is drawn to help understand the operation of the converter.

At time t_0, the switch is turned on. The current in the switch builds up linearly until it becomes equal to I_o at time t_1. Beyond this time the current resonates to peak at

$$I_{peak} = I_o + \frac{V_d}{Z_o} \tag{3.3}$$

The current in the switch eventually drops to zero at t_2. A 'reverse' diode in series with the switch stops the current from reversing. An additional delay period ensure lossless turn-on of the switch. The voltage across the capacitor, C_r , shows also the typical resonant wave form, but phase shifted (90° in advance of the current I_r in relation to I_o). Beyond t_3, the load current just freewheels through the diode until a time t_4, when the switch is turned on and the next cycle begins.

The combined periods between time t_0 and t_2 is determined by C_r and L_r and is therefore constant, whereas the time interval t_3 to t_4 is variable and is used to control the output voltage (off-time pulse density control).

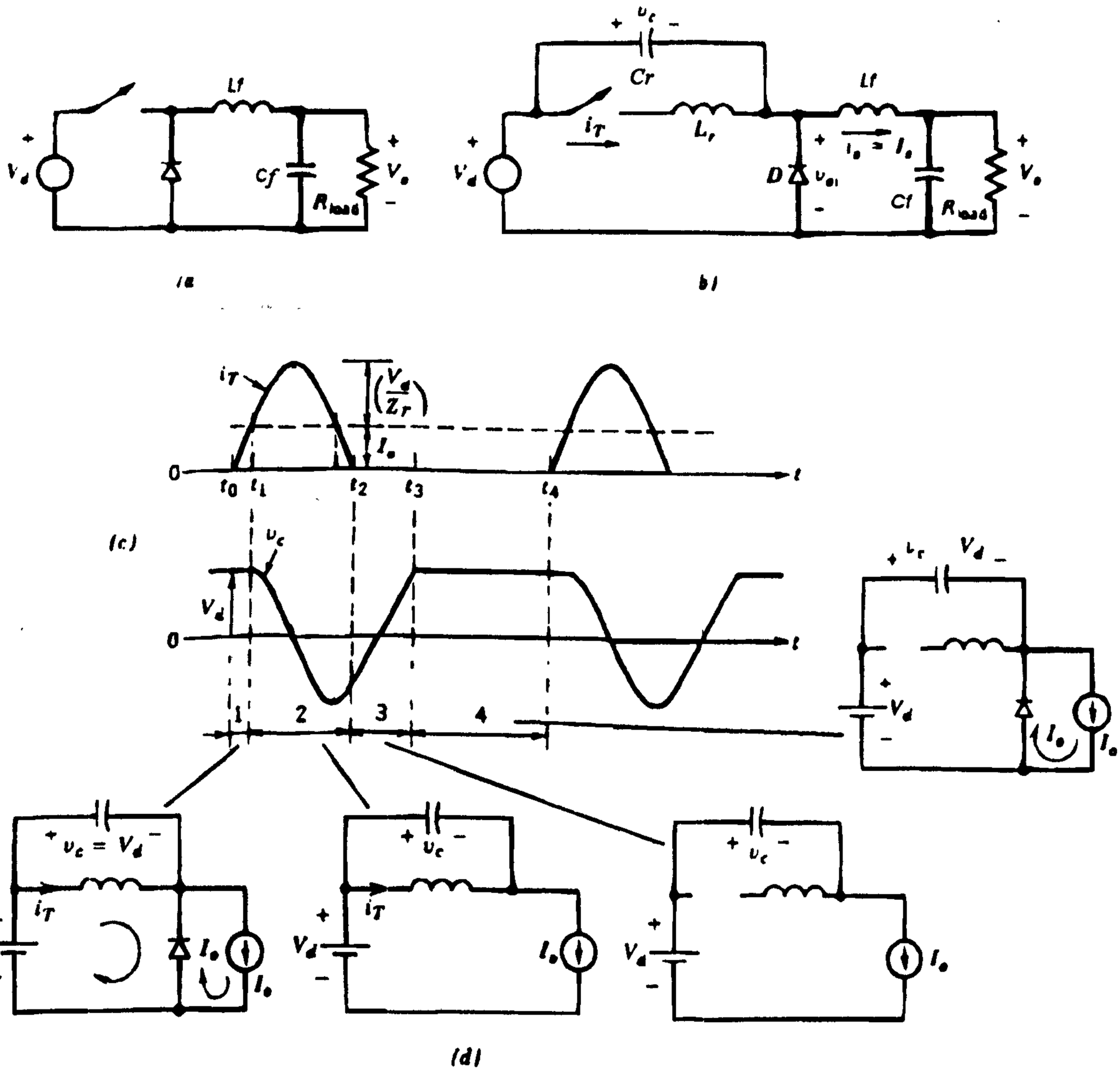

Figure 3.12 Zero-current resonant mode buck converter [Moh89]

(a) ... standard buck converter

(b) ... zero-current quasi-resonant buck converter

(c) ... Wave forms

(d) ... temporary valid circuits

Zero-voltage mode:

The zero-voltage mode is defined as a topology where the switch action occurs at zero voltage. The peak voltage appears across the switch and unfortunately

it can be up to ten times higher than the input voltage due to the resonant swing.

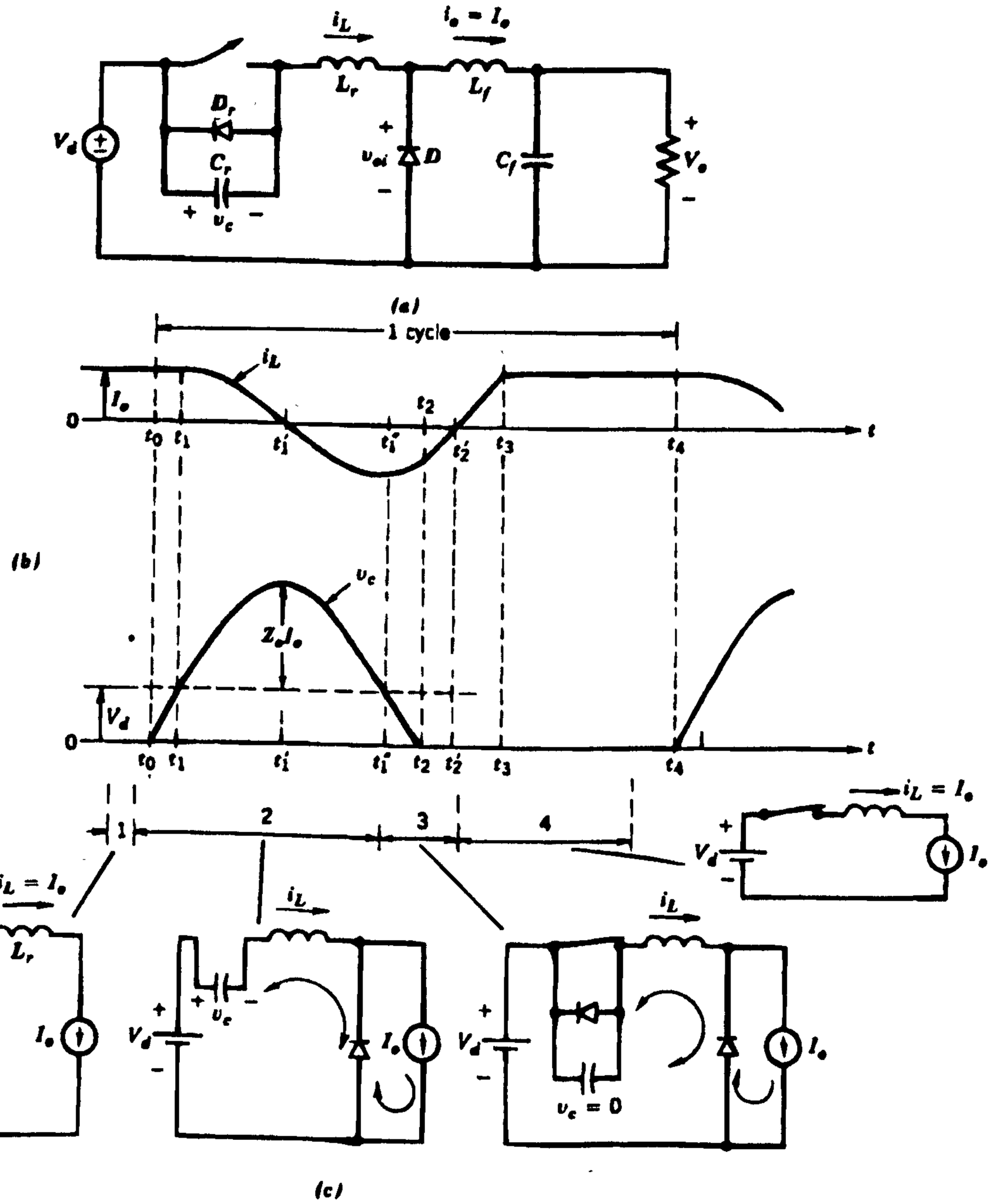

Figure 3.13 Zero-voltage resonant mode buck converter [Moh89]

The peak resonant current remains approximately the same as in the PWM version of the converter. At time t_0, the switch is turned off. The voltage across

the resonant capacitor builds up in approximately linearly. Beyond t_1, the diode D becomes forward biased, and C_r and L_r resonate, to peak at

$$V_{peak} = Z_o \cdot I_o + V_o \tag{3.4}$$

At t_2, the capacitor voltage reaches zero and cannot reverse due to the built in reverse blocking diode of MOSFETs. Beyond t_2 the switch can be turned on at zero voltage, hence without losses. The current I_L increases linearly until t_3. Once I_L reaches I_o, the freewheeling diode D turns off. The switch conducts I_o as long as it is kept on until t_4. Again the time interval t_3 to t_4 is used to control the output voltage (on-time pulse density control). With zero-voltage switching it is the off-time of the switch operation that has to be constant and the on-time is varied to achieve different voltage levels.

Comparison of zero-current mode and zero-voltage mode:

A comparison is given to justify the choice of the author, even though he is aware of the fact that with the relatively low switching frequency (of about 700kHz) used for this thesis the benefits are relatively small. In the zero-current version the load current I_o must not exceed $\frac{V_d}{Z_o}$ for natural turn off at zero current. Therefore there is a limit on how low the load resistance can be tolerated. By placing a diode in anti-parallel with the switch the output voltage can be made insensitive to load variations (fullwave operation mode) [Lee86].

Criterion	Zero-current mode	Zero-voltage mode
maximum frequency	1 Mhz	> 10 Mhz
Voltage stress	less than double V_{in}	at least double V_{in}
Current stress	higher than with PWM	equal to PWM
Transformer flux reset	not required	not required
Switching losses	low	very low
Energy transfer	during switch "on"	during switch "off"
Load/Frequency relation	f_s increases with load	f_s decreases with load
least efficient	under light load	under high load

Table 3.2 Compare zero-current mode with zero-voltage mode applied to a flyback converter [Syk89]

In the zero-voltage mode topology discussed here, the switch needs to withstand a forward voltage (during the off-period) that is higher than V_d. Therefore, if the output load current I_o varies within a wide range, the switch experiences very high voltage (refer to analysis in Chapter 4). In general, zero-voltage mode is preferable over zero-current mode at high switching frequencies (above 1Mhz). Operating a converter at high frequency is of course desirable to minimise the size of the components (see equation 2.1). Using zero-current mode with the switch turned on at a finite voltage, the energy in the internal capacitor, C_{oss}, is dissipated in the switch. By operating in zero-voltage mode to a converter, this capacitor can be used as part of the resonant capacitor. This will be discussed later in more detail. The table 3.2 summarises the characteristics of the two modes of switching.

Further quasi resonant topologies:

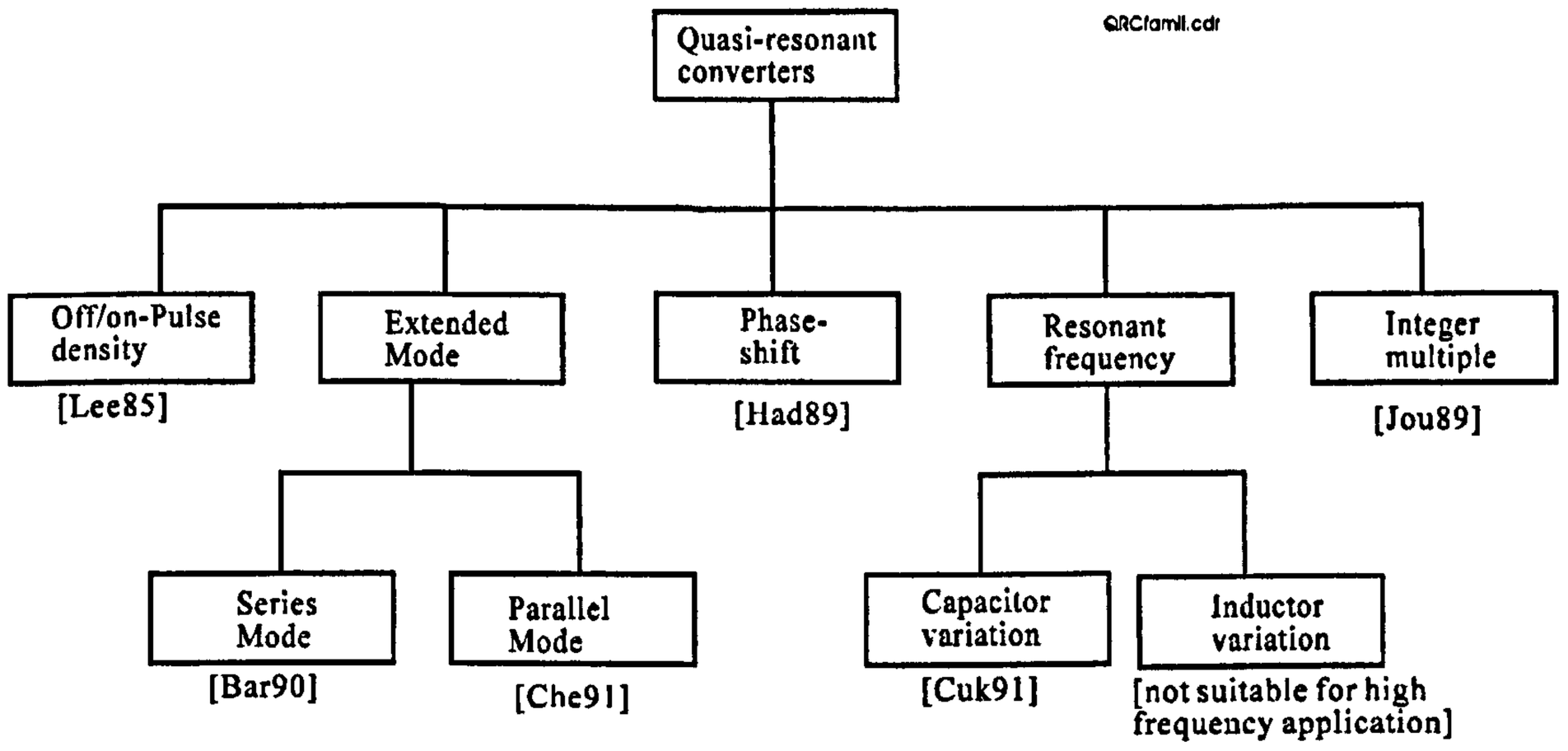

Figure 3.14 Quasi-resonant converters

The application of quasi-resonant switching techniques has led to a new family of converters which is given in Figure 3.14. They can be divided into subgroups; the modulation method for each topology is used as a classification criteria.

The branch on the left hand side includes the original version of the quasi-resonant converter, the patented zero-current converter of P.Viniarelli. The switching frequency in pulse density controlled converters can vary significantly over the load range. Hence, the variation of the load should be kept in certain limits, or in other words, the use of pulse density controlled converters is limited to applications with constant load.

To overcome this restriction, modificated versions of this original quasi-resonant converters have been developed over the last decade. Most of them aim for constant frequency operation in order to deal with load variation. This

can be achieved by applying resonant frequency converters. Instead of changing the switching frequency, the resonant frequency is changed by either varying the resonant capacitor or the resonant inductor.

3.2.3 Transformer design

The design of high-performance transformers and inductors is normally one of the most exacting and demanding aspects in the implementation of high-frequency resonant converters because magnetic components have the most significant effect on the efficiency and on the size of converters. It is particularly important in this work because a single multi-winding transformer is used to combine the two power sources. That means all energy is transferred via this central element.

Equation 2.1 in section 2.3.1 implies that a considerable improvement in power to volume ratio can be obtain by increasing the switching frequency. However, any increase in switching frequency is a matter of compromise because low loss material that has to be used, saturates at lower flux density [Row90]. Hence, the selection of the most suitable material is a very important issue. Additionally, winding losses also increase with the switching frequency.

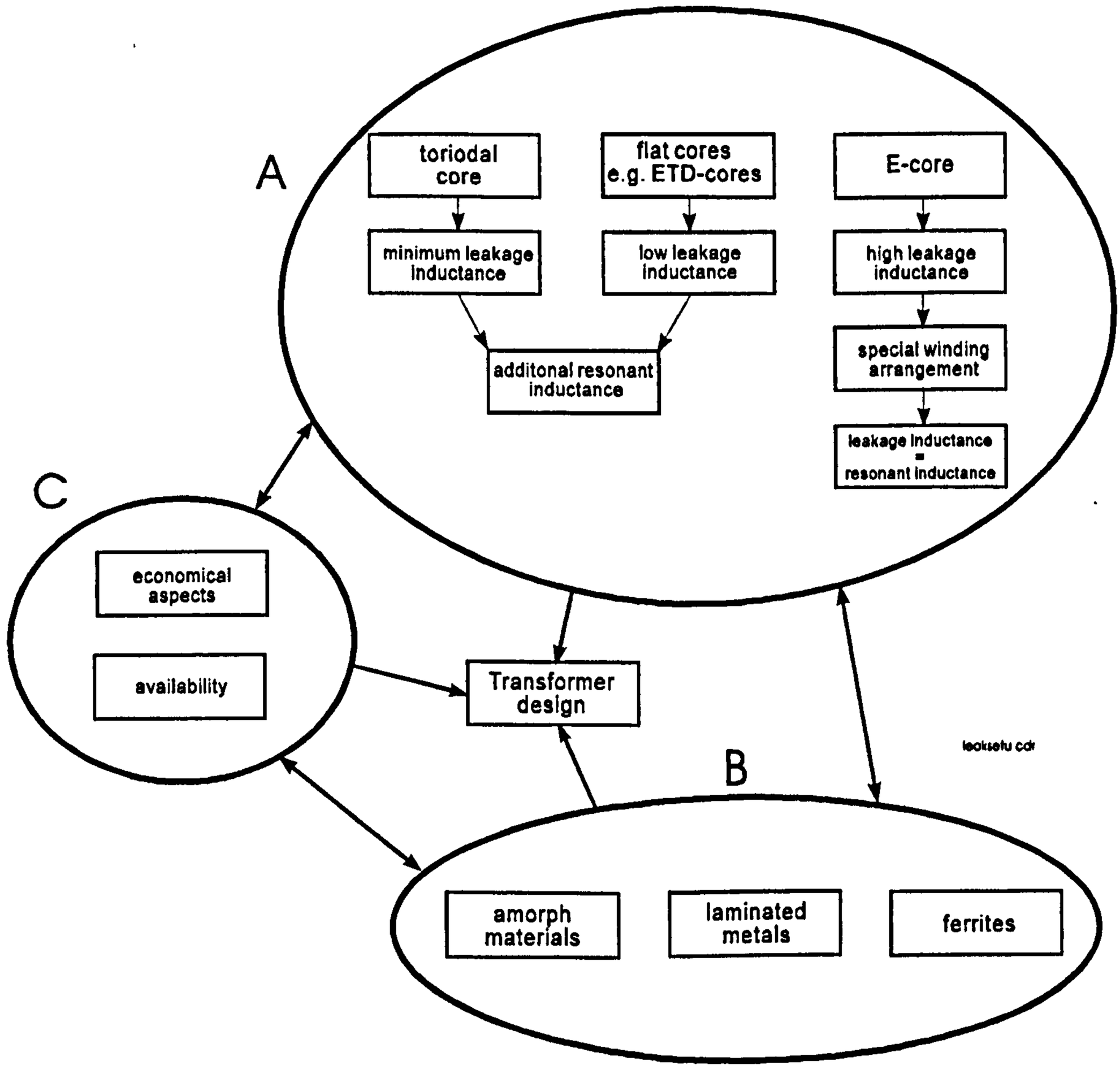

Figure 3.15 relation between the various design issues of a resonant power transformer

Another limiting factor in increasing the switching frequency of power converters is the leakage inductance of power transformers. To alleviate this problem it is necessary to place all windings as close as possible to one another. The restriction set by the safety regulations, make it practically difficult to reduce the leakage inductance sufficiently in off-line power supplies, where one winding is directly connected to the mains, while the other

is connected to the DC output[16].

The design process of a power transformer is very complex with several interrelated parameters and issues to be taken into account. To demonstrate the complexity and the relation between the most important points of the design Figure 3.15 is given.

Three main groups represented by three circles (A,B,C) in the figure can be clearly identified: the core design including the winding arrangement (A), the core material (B) and the economic aspects (C). Group (A), the selection of the appropriate core type was partly influenced by the availability and the costs (group (C)) of the different applicants. Also the core material (group (B)) influenced the choice of the core type due to the fact that not all shapes of cores are available in all materials as can be seen in table 3.6 later in this Chapter.

Basically, three possible core types are worth mentioning. These different core types can be distinguished according to their ability to reduce the leakage inductance within themselves. This criteria is used as a classification in circle A.

- Use of a *toroidal core* shape reduces the leakage flux to a minimum but makes automatic winding virtually impossible.

- In the last few years several manufacturers have developed special *flat cores* for high-frequency power transformers in order to reduce the leakage

---

[16]the safety standard for business machines in Germany (VDE-0806) is based on IEC's recommendation IEC 380, and it is by far the most stringent electrical safety standard for power supplies [Chr89]

inductance and to achieve very flat transformers which can be built in computers on printed circuit boards.

- The rather high leakage inductance of conventional *E-cores* can be used as resonant inductance which eliminates the necessity of using an additional inductor for the resonant tank.

3.2.3.1 Selection of core and material

The final designed of the transformer adapted for this project consisted of a ferrite E-core (Siemens E42/15 material: N87). The two input windings and the output winding have been arranged in such a way that the resulting parasitic leakage inductance could be used as part of the resonant tank.

In Figure 3.16 some core shapes and the possible materials are compared. The selection of a suitable material can only be achieved by the selection of the appropriate material, e.g. amorphous material is virtually only available in a toroidal core shape.

Producers of amorphous metals emphasise the advantages of such materials over ferrite materials. This applies to cores for wide band transformers as well as to cores for power transformers. Apart from their electrical resistance, ferrites have, at best, equal properties in some areas. The saturation flux density of amorphous materials is far better than that of ferrites. Even the drawback of the lower electrical resistance can be avoided by using cores constructed using thin layers. Such a method efficiently reduces eddy currents. In the manufacturing process of amorphous metals such layers are commonly used and indeed they enable converters to be operated with lower losses, even

at high frequencies. Even if the characteristics of ferrites improve in the future, they will not reach the efficiency level of amorphous metals (and laminated metals) because a further reduction of the layer thickness is possible.

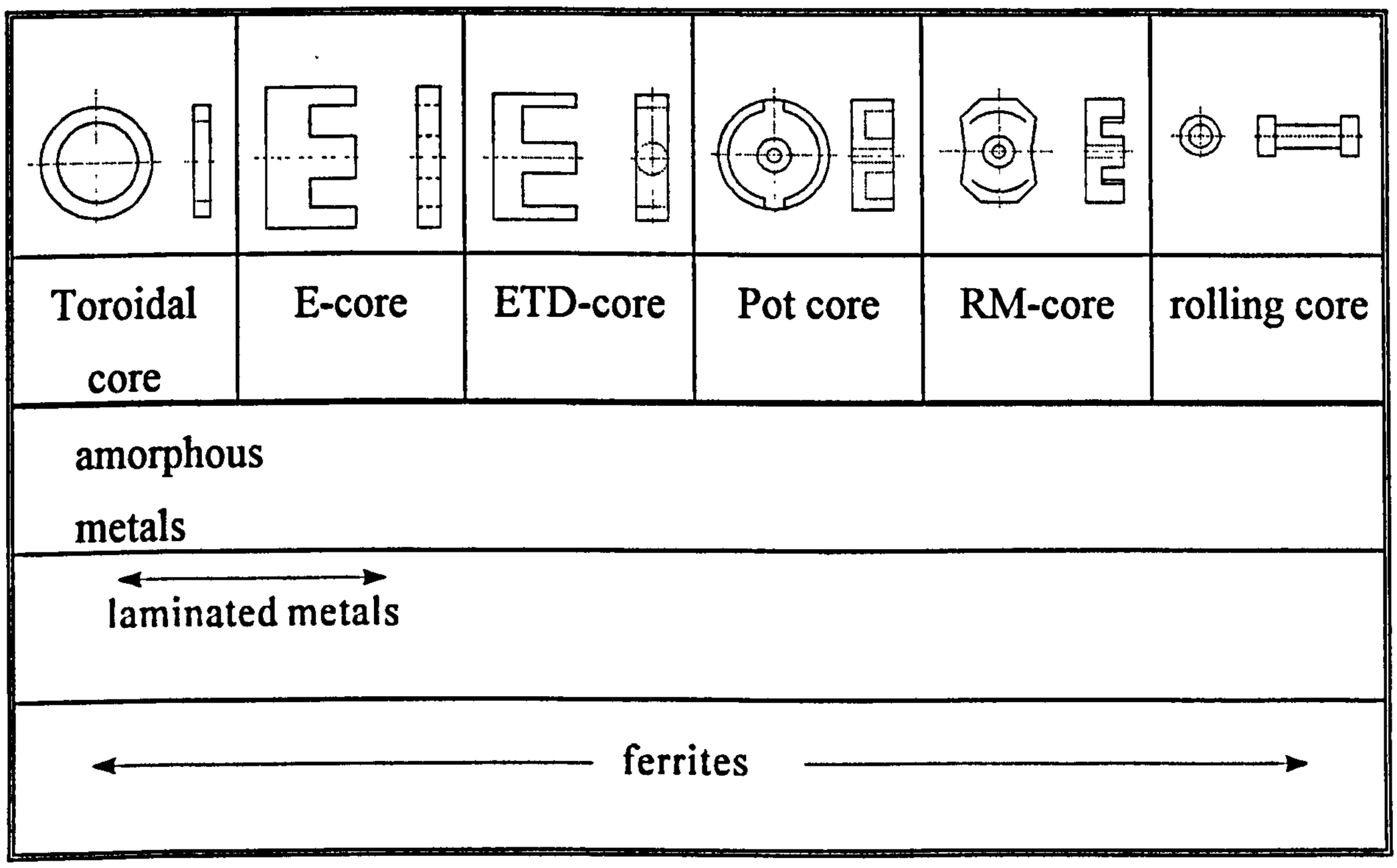

Figure 3.16 different core shapes and materials used [Rößß90]

The reason why ferrite transformers are the most preferred choice in almost every application in the field of wide band and power transformers can be seen in Figure 3.16. They are available in a huge variety of shapes and hence can be perfectly adapted to the different applications. This is due to the manufacturing process of ferrite transformers. For amorphous metals on the other hand toroidal cores are the only cost-efficient solution. Sheet metals or laminated cores can be produced in E-core shapes. In this shape they are used for some special applications. However, the great area of the combined cores, which provide a large automation potential and therefore low cost production, is restricted to ferrites.

Latest research in MID (moulded interconnect devices) has shown a way to use the ideal core shape i.e. the toroid for high-frequency converters. The obvious, above mentioned drawback of low automation potential is overcome through this technique. Additionally the leakage inductance of transformers using toroid cores are 3 to 10 times lower compared to standard transformers [Bog92]. Unfortunately no such converter is as yet commercially available. The MID technique is derived from the three dimensional printed circuit board design.

In the field of ferrite transformers research was carried out into the field of special high-frequency cores such as ETD-cores, which have been issued during the last years. Unfortunately the size of cores with such a shape is still restricted, hence it was not possible to use them for the *dual converter* at the temporary power rating.

Ferrites

Ferrites are magnetic materials which have a permeability $\left(\mu_r = \frac{B_m}{B_o}\right)$ greater than one, where B_m is the flux density with matter and B_o is the flux density without matter.

Incomplete *inner* electron shells, as in transition metals (Fe, Ni, Co, Gd, Er), lead to parallel spin momentum of the atomic electrons. Whole crystal areas of the size of 10 μm^2 to 1 mm^2 are magnetised equally (Weiss' domains) [Wei65]. In an unmagnetised condition they are placed without order so that the material seems unmagnetised. Through an external field these areas are increasingly directed according to the field lines. Ferrites are of great technical importance either as soft magnetic material or as permanent magnetics. They

are not metals but ionic crystals and therefore they show a high specific resistance ($1<\rho<10^3\ \Omega m$) in relation to metals ($\rho\cong10^{-7}\Omega m$). For that reason hardly any eddy current is measurable, this makes them perfectly suitable for high-frequency applications (e.g. cores for operation frequencies of up to 5 MHz). Ferrites belong to the group of polycrystalline ceramics, so-called black ceramics. They are produced by the usual techniques found in the ceramics industry.

The crystal structure is determined by the distribution of the different ions in the different lattice sites as well as by the appearance of vacancies and associated distribution of the valences in the presence of ions of changing valency, like iron, manganese or nickel.

The microstructure must differ according to the requirements that the ferrites has to satisfy. Of the characteristics of the microstructure, the mean particle size, the porosity, the separation at the grain boundaries as well as the distribution of grain sizes and pores have the greatest influence on magnetic properties of ferrites [Mer93]. Its mechanical strength also depends on the microstructure.

Generally, two main groups of high-permeability ferrite materials can be differentiated:

- MnZn ferrites (mixed crystals of Fe_2O_3, MnO and ZnO) for applications up to a few MHz, and
- NiZn ferrites (mixed crystals of Fe_2O_3, NiO and ZnO) for applications up to a few 100 MHz.

It can be seen that for the *dual converter* the MnZn-ferrites fully satisfy the demands.

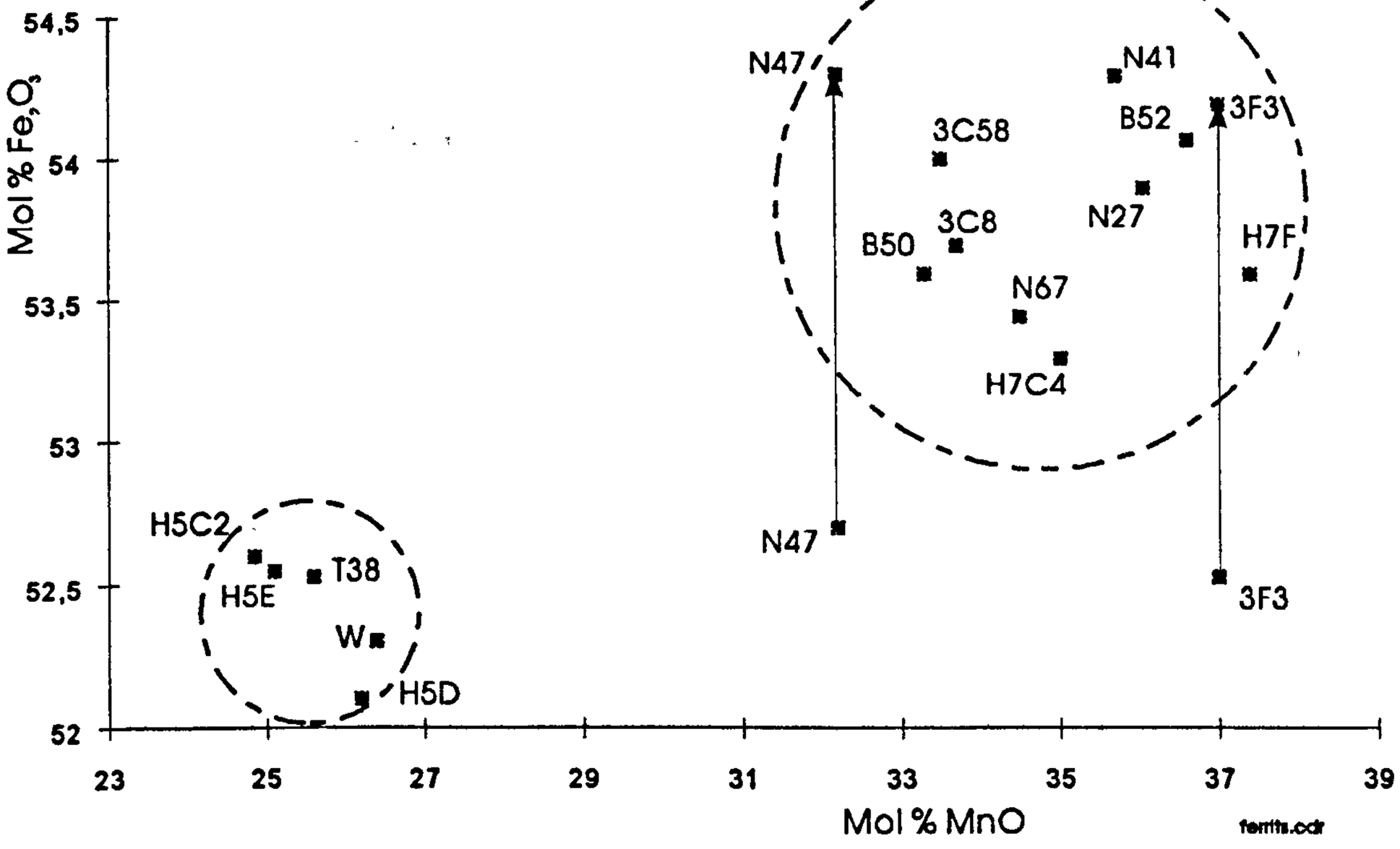

Figure 3.17 Composition of MnZn-ferrites [Rõß90]

In the Figure 3.17 the different ferrite materials are listed and compared. Here the iron oxide content versus the manganese content is shown (with the zinc content represented as the difference to 100%). The chart contains a number of popular wide band ferrites and ferrites used for power conversion by various producers. A concentration is observable in two areas of the diagram which are marked by the dotted circles: the group of the power transfer ferrites on the upper right hand side and the wide band ferrites on the left respectively. Two exceptions are the materials N47 (Siemens) and 3F3 (TDK). These two materials are primarily designed for high frequency power applications of some 100 kHz or so. These two materials contain between 1 and 2 Mol % of zincoxide and/or titanium oxide, which helps to increase the specific resistance and which have, in some respects, the same influence as an increase of iron.

Adding the zincoxide and titaniumoxide to the iron oxide contents move them into the group of the power transformers where they belong to.

For the *dual converter* N87 from Siemens was used. This material was only recently launched on the market (therefore it is not listed in the chart above). It is especially suited for high-frequency applications up to several hundred kHz.

3.2.3.2 Windings and leakage inductance

Winding material:

Even though, hundreds of different types of wires are available on the market, basically four types of wires can be identified with respect to high frequency applications and the accompanying effects. These wire types are:

- single wire
- twisted wire
- litzwire
- foil

The most important effect that influences the choice of the winding material is the skin effect. Therefore, a brief explanation of it follows.

Skin effect:

A straight, isolated, round wire carrying alternating current (ac) generates a concentric, circular magnetic field: both in the wire itself and in the surrounding space[17]. This field induces eddy currents that oppose its

[17]Isolated in this context means that there are neither other conductors nor magnetic fields in the vicinity of the wire.

penetration, enhancing the current flow near the surface and reducing it near the centre of the wire as shown in Figure 3.18

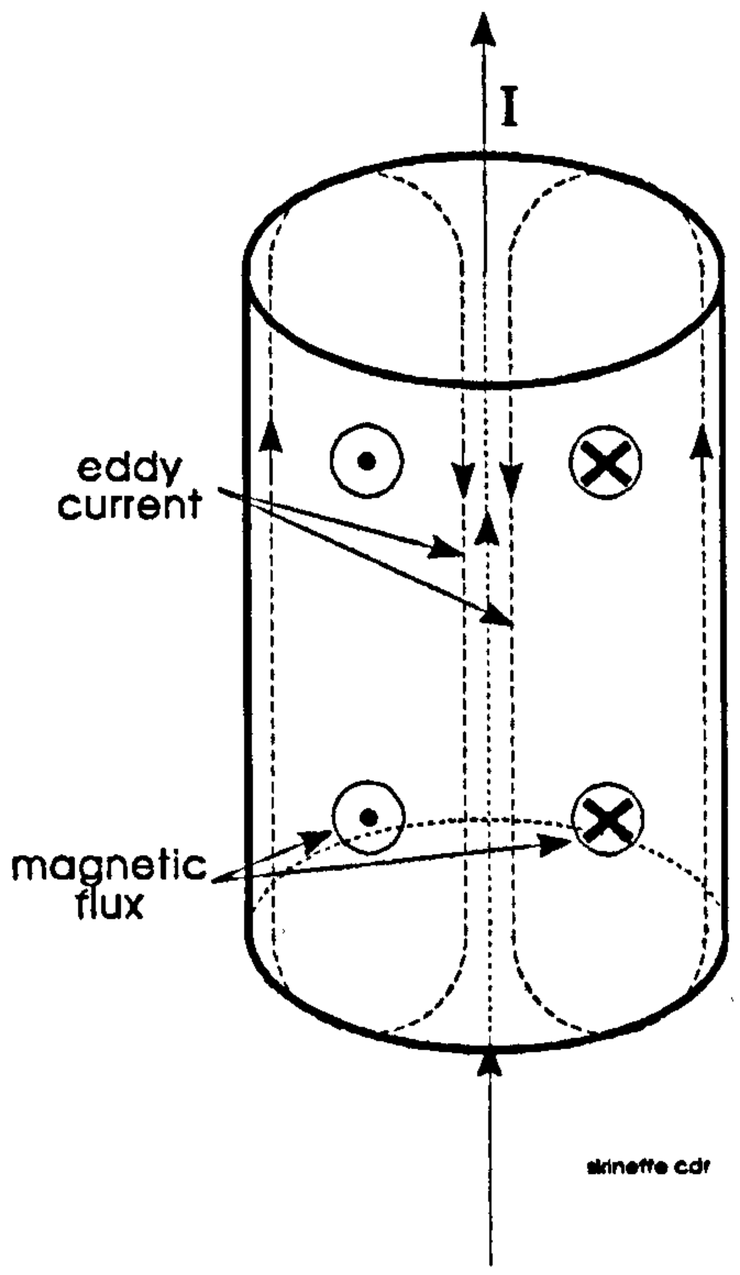

Figure 3.18 Skin effect

There is a tendency for the current to flow only at the surface of the wire: the skin effect. This current distribution results in the ac resistance of the wire being greater than its dc resistance. If the wire is replaced by a tube of the same material and diameter, such that the tube has the same dc resistance as the wire for ac, its wall thickness will be equal to Δ. For this reason Δ is known as the skin thickness[18].

[18]The term penetration depth is often used for Δ, but some authorities prefer this term for the wavelength ($2\pi\Delta$)

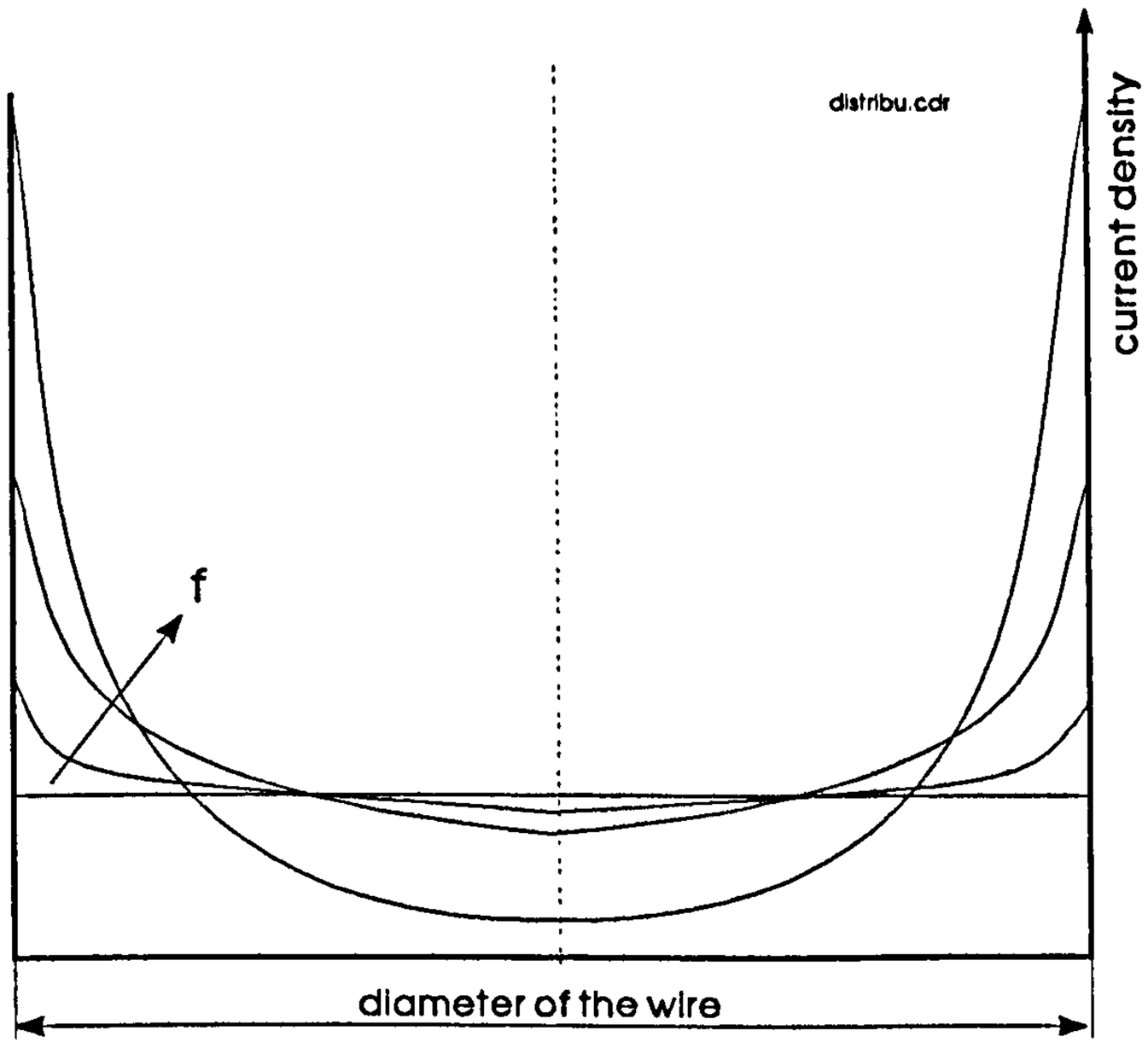

Figure 3.19 ***Current distribution in a wire carrying constant ac at various frequencies***

Figure 3.19 shows that with the increase of the frequency the current is forced to the outer sections (skin) of the wire. The skin effect is magnified exponentially as the numbers of layers are increased (proximity effect).

By using twisted or litz wire material the skin effect can be reduced, because the current is forced to the inner part of the lead. This is achieved because the wires are interweaved in such a manner that each wire moves within the group to successively occupy each level within the field. A drawback of these wires is their reduced space (copper) factor which is illustrated in the table below.

Number of wires	4	5	6
Utilisation factor	0.686	0.685	0.667

Table 3.3 ***Utilisation of single strands [Uni90a]***

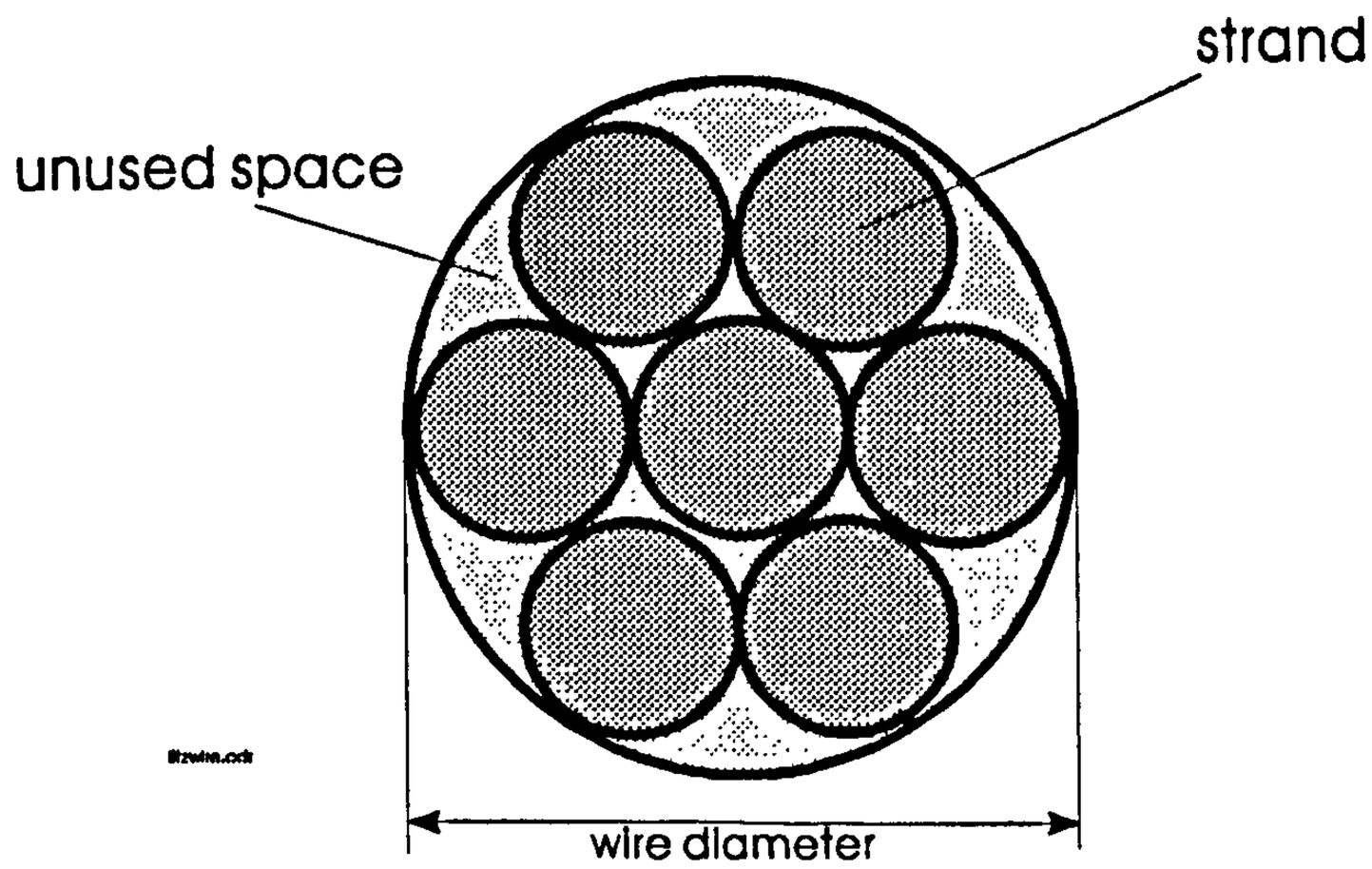

Figure 3.20 copper utilisation in a litz wire

Figure 3.20 additionally clarifies this effect. The space between the single strands of a litz wire increases with the number of used strands.

An alternative to twisted wires are thin strip windings (foil), especially for low voltage, high current windings with few turns and large conductor area. Each turn is a layer and each turn must be insulated from the others. Strips cannot be subdivided into several parallel thin strips unless the individual strips are in different winding sections, otherwise unequal induced voltages will cause large eddy currents to circulate from one strip to another and losses will be high.

Winding arrangement and leakage inductance

The location of the different windings is of importance and influences the behaviour of the transformer, as will be clarified in the course of this section. An explanation of the term "leakage inductance" follows below.

The main flux that couples primary and secondary windings of a transformer is core bound. Flux also crosses the winding space. This flux is not common to all windings and not even all turns in the same winding, and is therefore known as leakage flux. Its appearance can be regarded as a measurement of the coupling. The leakage flux density is maximum at the interface between primary and secondary.

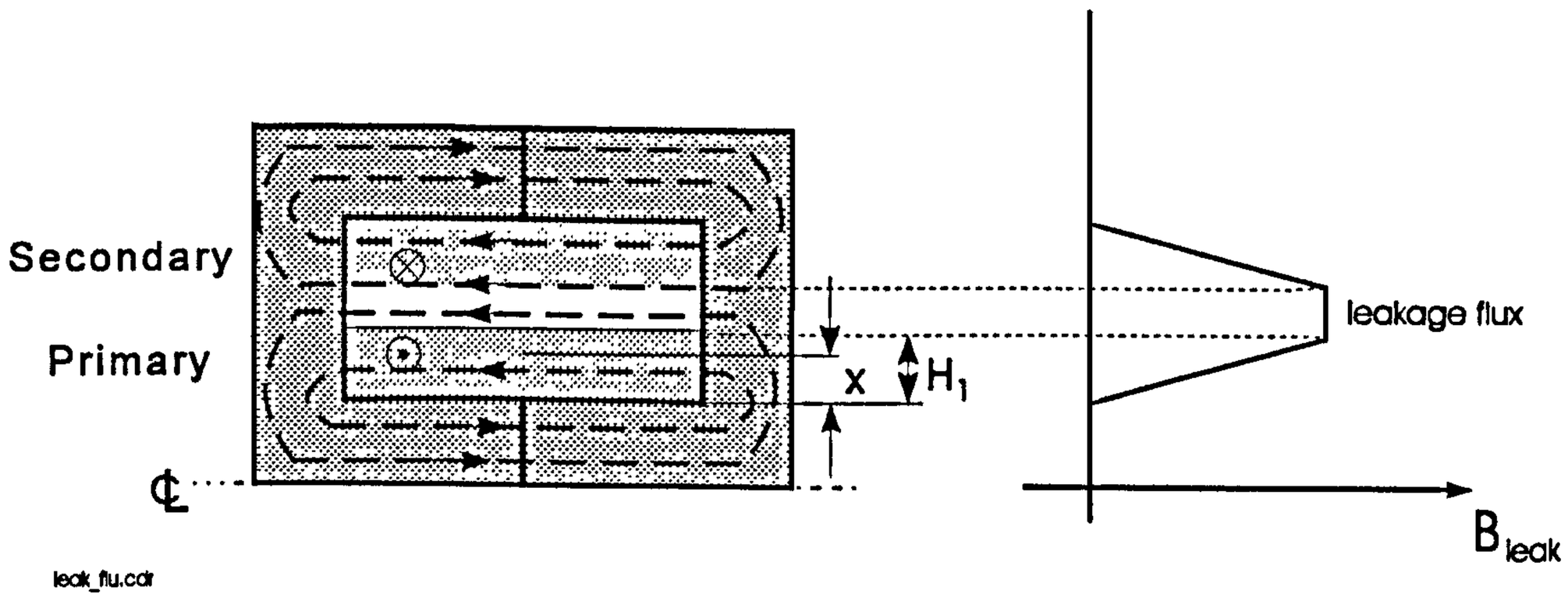

Figure 3.21 Leakage flux density distribution

Figure 3.21 demonstrates this. On both sides of this maximum, the flux density falls approximately linearly to zero over the height of the winding.

$$\int \frac{B}{m_o} \cdot ds = N \cdot I \cdot \frac{x}{H_1} \qquad (3.5)$$

Here a flux path crossing the winding window at a distance x from the wall of the coil former is considered and the current density over the height of the primary is assumed to be constant. The distance along the flux path is labelled s, and the number of ampere-turns enclosed is named NIx/H_1. Hence the leakage flux density can be expressed by:

$$B = m_o \cdot \frac{N}{b} \cdot I \cdot \frac{x}{H_1} \qquad (3.6)$$

where b is the flux path length outside core material. The leakage flux is not due to imperfect core material but is an intrinsic property of a winding. The leakage flux through the windings gives rise to eddy-currents in the conductors. The average leakage flux density and thus the eddy-current losses can be reduced by suitable mixing of primary and secondary windings. To achieve this designers may either split the primary and secondary in two half or arrange them in a sandwich mode. The splitting and sandwiching process could, of course, be repeated to further reduce eddy-current loss. However, this quickly becomes unpractical: each interface between primary and secondary portions requires extra insulation, usually including screens to reduce radio-frequency interference. Their presence reduces the space (copper) factor attainable in the winding window, eventually to such a degree that any improvement is either lost or not worth the extra complication.

Calculation of the leakage inductance:

Normally, in high frequency magnetics design, considerable effort is expanded to minimise leakage inductance and eddy current losses in the windings. Modern cores designed for switching power supplies have window areas that are long and narrow to minimise the number of winding layers and minimise the magnetic field strength between the windings by stretching it out across a wide window. However, in this application, there is no desire to minimise leakage inductance but instead to utilise it for a specific purpose.

If the same flux is common to both (all) windings the voltages must be proportional to the number of turns [Leh73]. Therefore, for an ideal transformer

$$v_1/v_2 = N_1/N_2 \qquad (3.7)$$

Also, the maximum mutual inductance can be calculated:

$$M_{max} = \sqrt{L_1 \cdot L_2} \tag{3.8}$$

The coupling of the windings in a transformer are expressed by the factor *k*. Hence, *k* indicates how close to ideal a transformer is.

$$k = \frac{M}{\sqrt{L_1 \cdot L_2}} \tag{3.9}$$

The leakage inductance is given by

$$L_{\sigma 1} = L_1 - \frac{N_1}{N_2} \cdot M \tag{3.10}$$

$$L_{\sigma 2} = L_2 - \frac{N_2}{N_1} \cdot M \tag{3.11}$$

for the primary and the secondary winding, respectively.

Different publications recommend different methods to calculate the leakage inductance according to physical properties of a transformer. Hence, a prediction of the leakage inductance would be possible knowing the winding arrangement. It is important to note that some methods suit only particular winding and transformer set-ups.

An approximation for the leakage inductance of a planar transformer regarding small distances between the winding discs and ETD 34 cores is provided in the following equation [Scl93]:

$$L_s = \left(\frac{\mu_0 \cdot A_e}{l_{fe}^2} - \frac{A_{prim}^2 \cdot A_{sec}^2}{\mu_a \cdot 4 \cdot A_e \cdot a^6 \cdot \pi^2} \right) \cdot a \cdot \mu_0 \cdot N_{sec}^2 \cdot N_{prim} \cdot \sqrt{N_{prim} + 4} \tag{3.12}$$

Another source derives an equation for the leakage inductance as the sum of all the leakage energy in every window of the core of a transformer [Che92]. All secondary windings are short-circuited. This makes the magnetising field

intensity along the core close to zero. By evaluating the integration of the individual magnetic fields throughout the volume of each window, the total leakage inductance is given by:

$$L_{total} = \frac{\mu_0 \cdot n \cdot N_1^2 \cdot b \cdot MTL}{3 \cdot h_w} \tag{3.13}$$

The third and the last source that is worth mentioning gives a further equation to calculate the leakage inductance [Dix93]. This method was applied for this project.

$$L_{Leak} = \frac{\mu_0 \cdot \mu_r \cdot N^2 \cdot (MTL \cdot S)}{W_W} \tag{3.14}$$

Using the reluctance modelling and duality to translate the physical structure of a magnetic device into its equivalent inductance values and their locations it was possible to determine the leakage inductors for the proposed *dual converter.*

As it can be observed in Figure 3.22 the flux lines in one core-half are reflected by the reluctances and the flux sources in the centre of the graph. To achieve a dual equivalent of the existing circuit a node (A, B, C, D) has to be placed into every mesh of the original circuit and an additional node (E) for the outer mesh has to be set. Thereafter the received nodes are linked in such a way that each path of the new circuit crosses a path of the existing circuit, resulting in the new meshes (1, 2, 3, 4, 5). Additionally, the flux sources ($\Phi t/dt$) are transferred into voltage sources (volts/turn).

The aim of the procedure was to adjust the leakage inductance so that it equals the required resonant inductance value $L_{Leak} \equiv L_r$, hence making an additional physical element unnecessary. This avoids the voltage divider effect between

the discrete resonant inductance and the resonant transformer which would reduce the efficiency. It is therefore only the inductance of the transformer which acts as resonant inductance.

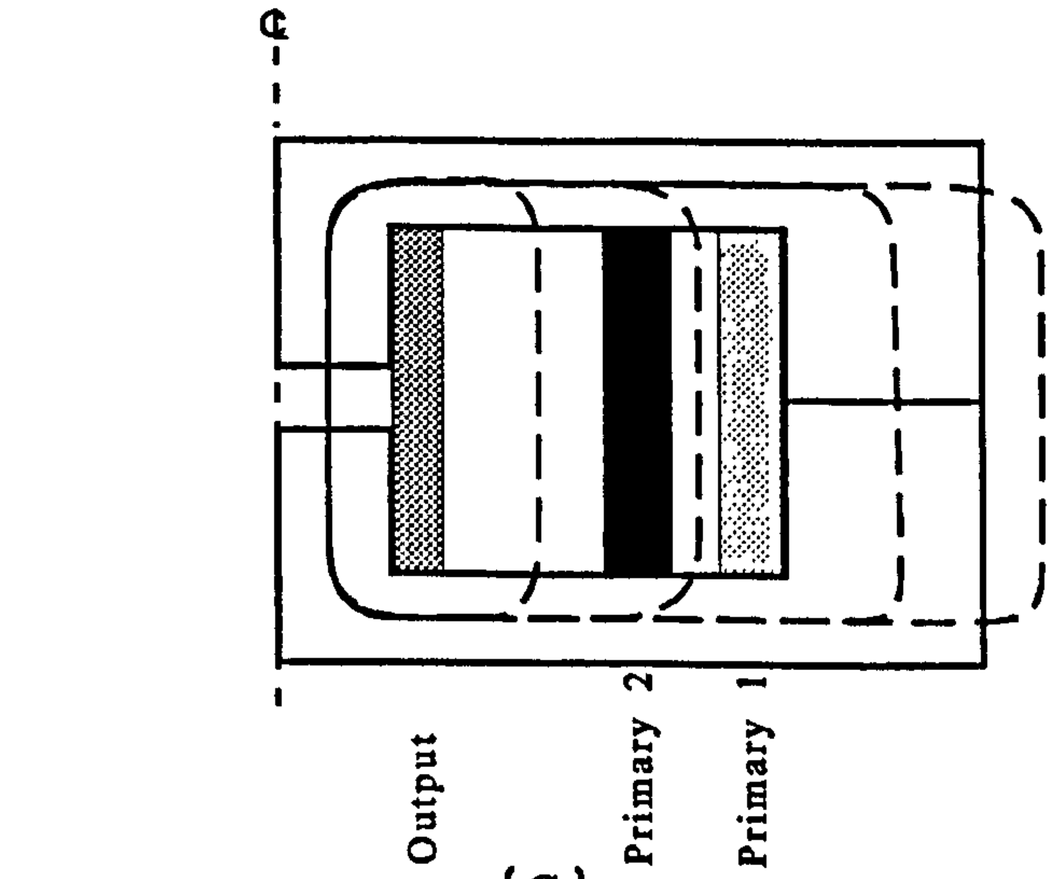

(a)

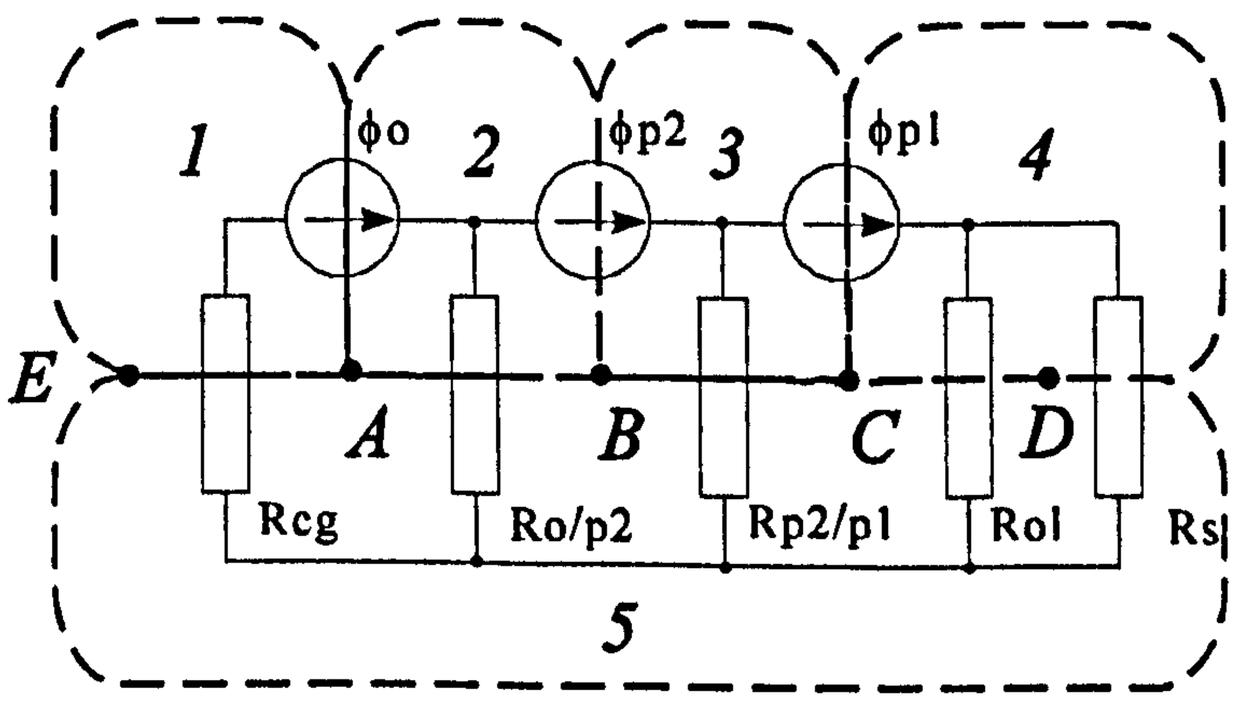

reluctan.cdr

(b)

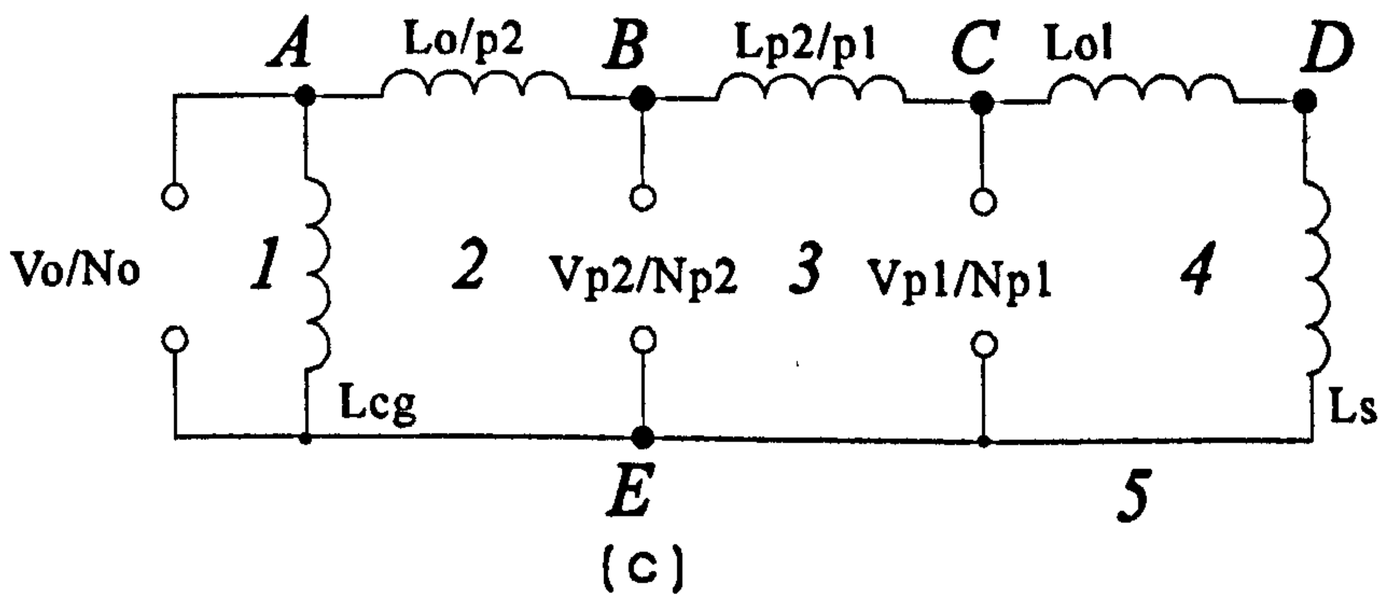

(c)

Figure 3.22 (a)transformer winding arrangement
(b)Reluctance model of the coupled inductors
(c) Electrical equivalent circuit of the coupled inductors

The application of this technique can be found in section 5.1.1. There the necessary distance between the windings is calculated in order to achieve the required resonant inductance. It can be observed that the leakage inductance of the primary winding 2 (battery source) could be adjusted to the desired value. Therefore, this inductance was used as resonant inductance L_{r2} for the secondary input of the *dual converter.* The necessary resonant inductance L_{r1} of mains input was too large to be achieved only with the leakage inductance of the transformer. A larger core would have been necessary and hence the effect of saving space would have been lost.

3.2.4 Control

A time profile of the change over period in case of a power failure of the mains is given in Figure 3.23

At a pre-set voltage level which can be adjusted according to the requirement of any application, the stand-by battery is switched on. There is a certain delay time before the actual change over takes place. This is due to a special set-up that is explained in section 5.1.3. The arrows on the left in Figure 3.23 indicate the instant when the stand-by source is activated and the mains is deactivated. The same applies to the arrows on the left hand side, but in reverse.

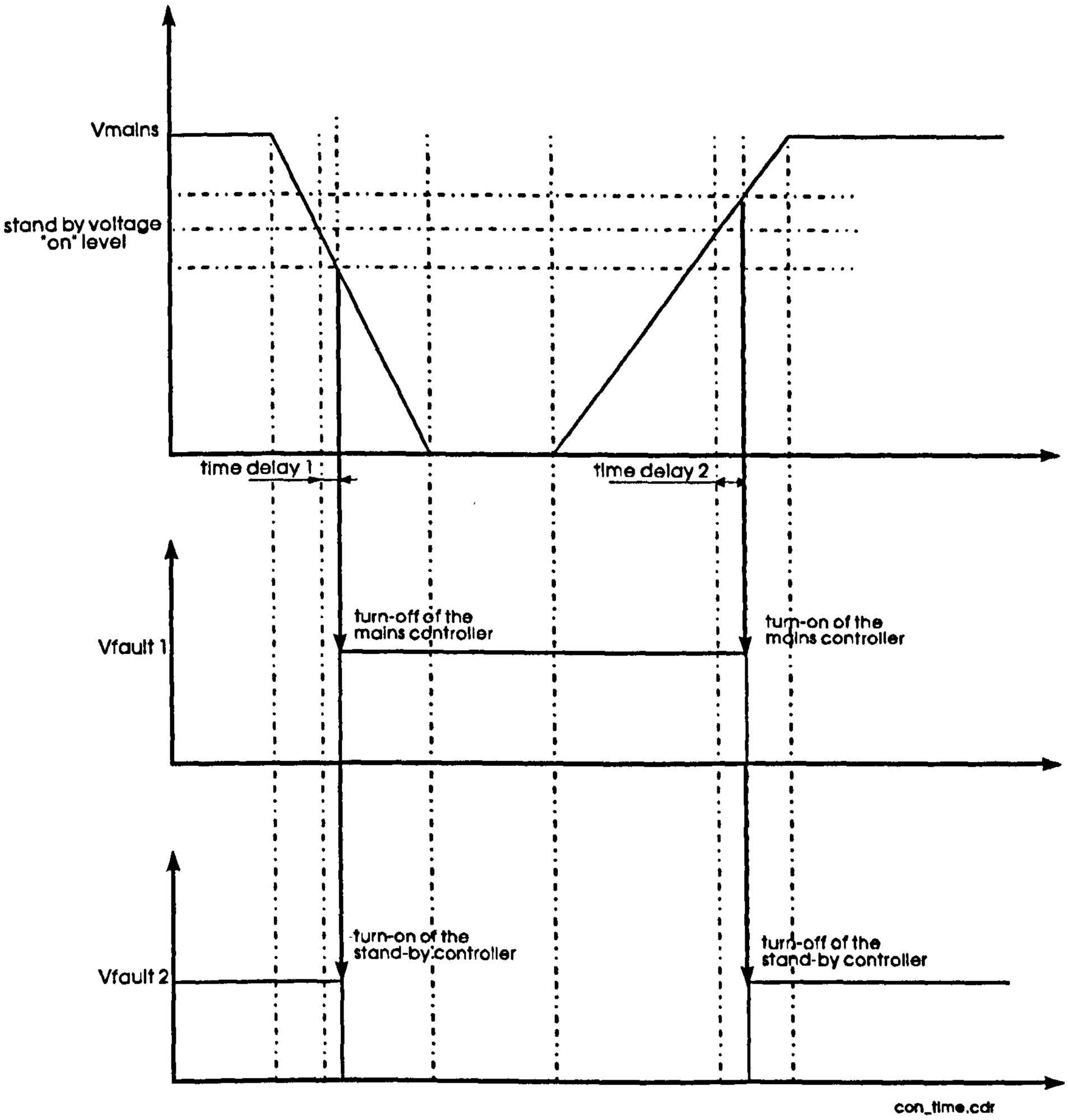

Figure 3.23 change over from the mains to the stand-by and vice versa for the UPS

CHAPTER 4

ANALYSIS AND SIMULATION OF THE *DUAL CONVERTER*

Analyses of resonant converters have been presented in many publications in recent years. At the Virginia Power Electronics Centre a group of specialists has provided a large amount of mathematical work on resonant techniques and published a large number of papers on converters operating in resonant mode. However, the publications from this group have not covered all aspects of resonant techniques. By providing only extracts of the work that was carried out, these papers did little to increase the understanding in the field. Hence, this Chapter was necessary and essential to the project because it is the basis for the dimensioning of the *dual converter* as well as for the clear understanding of how the circuit operates. The influence of the various components in the circuit can be directly examined with support of the following analysis. The best basis for such an examination was found to be a mathematical description of a quasi-resonant buck-boost converter [Liu86].

Using simulation to examine complex technical processes is becoming more common due to the availability of fast and powerful computers on the one hand and because of the recently developed appropriated software packages on the other. However, it is essential to fully understand a system in order to set up a model for a computer aided simulation of it.

4.1 Analysis of a quasi-resonant flyback converter

This Chapter gives a mathematical description of the *dual converter.* A relation between the input and output voltage with respect to the switching frequency is presented. This is essential because the switching frequency is the control parameter for the circuit, whereas the resonant frequency is fixed due to the physical dimensions of the resonant elements[19].

[19]Attempts were made by several engineers to control the resonant frequency, rather than the switching frequency. This was achieved by using switched capacitors or a capacitor matrix [Chu91].

The proposed *dual converter* introduced in Chapter 3.1 shows that two quasi-resonant flyback converters incorporate in conjunction with a multi-winding transformer. Except during the change-over period which is examined in section 4.2.1 and on the practical circuit, only one such converter operates at a time. Therefore analyses were carried out on a quasi-resonant flyback converters as illustrated in Figure 4.1. The switch and the passive components are assumed to be ideal.

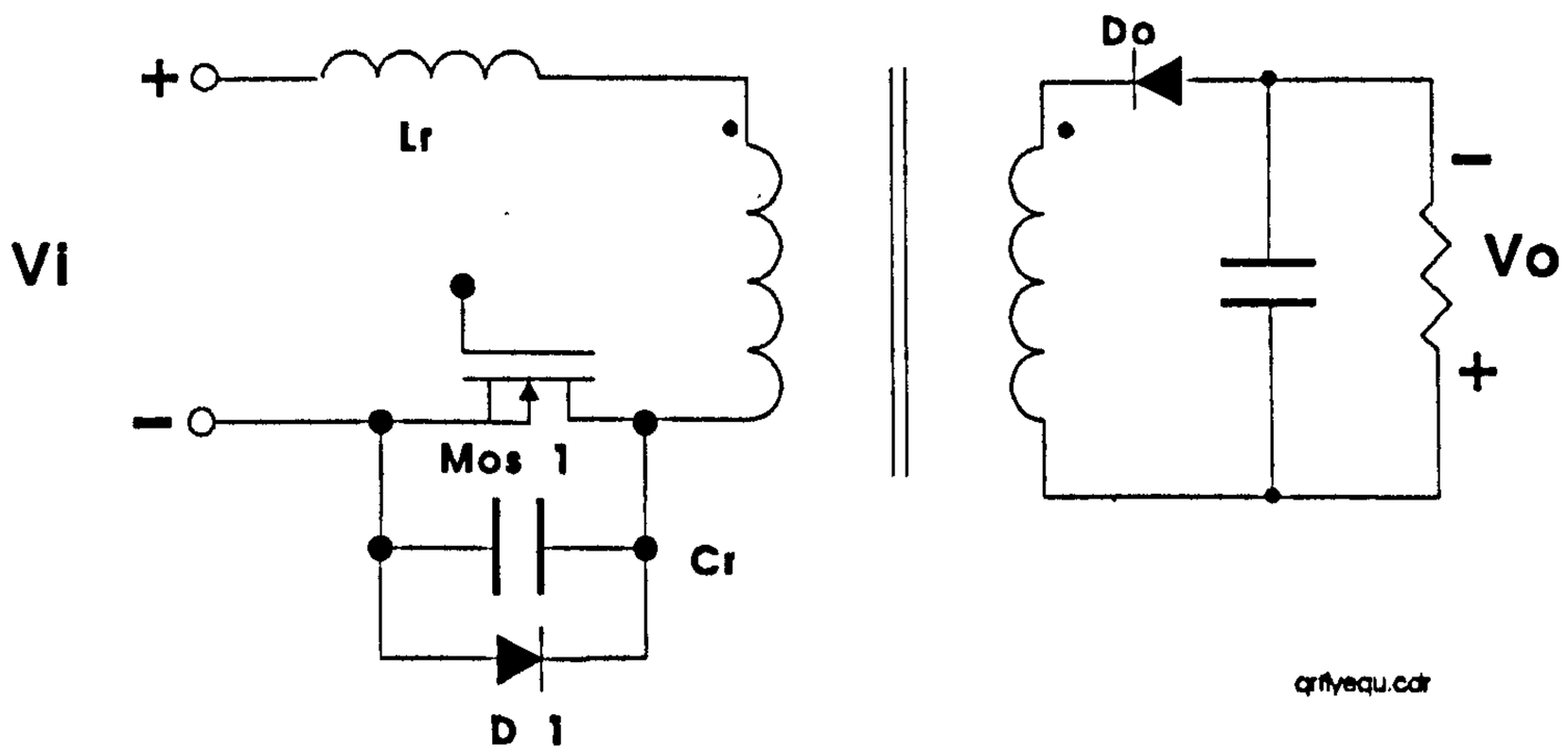

Figure 4.1 Quasi-resonant flyback converter

The transformer was replaced by a one winding equivalent model.

Transformer model:

The applied model enabled the transformation of the flyback converter into its buck/boost counterpart [Füh82]. Several devices had to be transferred:

Referred components magnitude:

$$R_2' = N^2 \cdot R_2 \tag{4.1}$$

$$X_2' = N^2 \cdot X_2 \tag{4.2}$$

$$Z' = N^2 \cdot Z \tag{4.3}$$

$$V_2' = N \cdot V_2 \tag{4.4}$$

$$I_2' = \frac{I_2}{N} \tag{4.5}$$

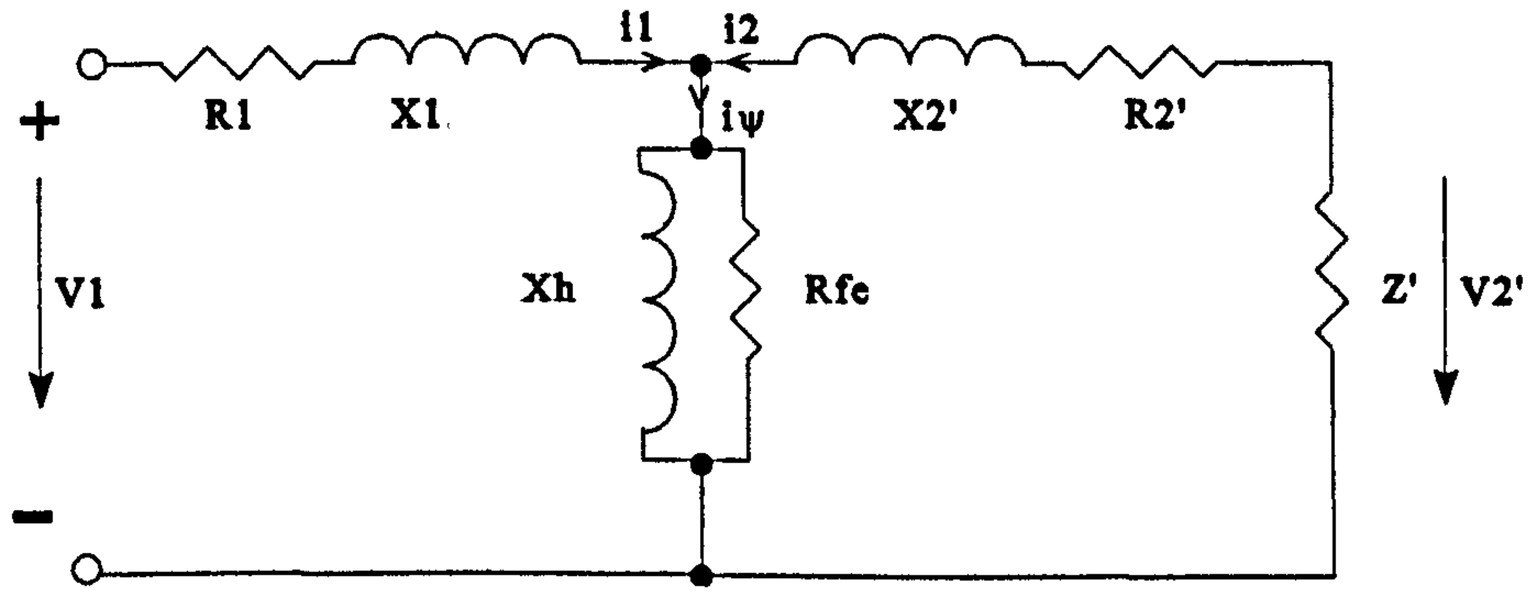

Figure 4.2 Transformer model

The transformer in Figure 4.2 represents a realistic model taking into account most of the parasitic components. To make the analysis manageable some simplifications are made by setting R_1, R_2, R_{fe}, and X_2' to zero. The leakage inductance X_l is included as a part of the resonant inductor. Figure 4.3 shows the modified circuit including the transformer model.

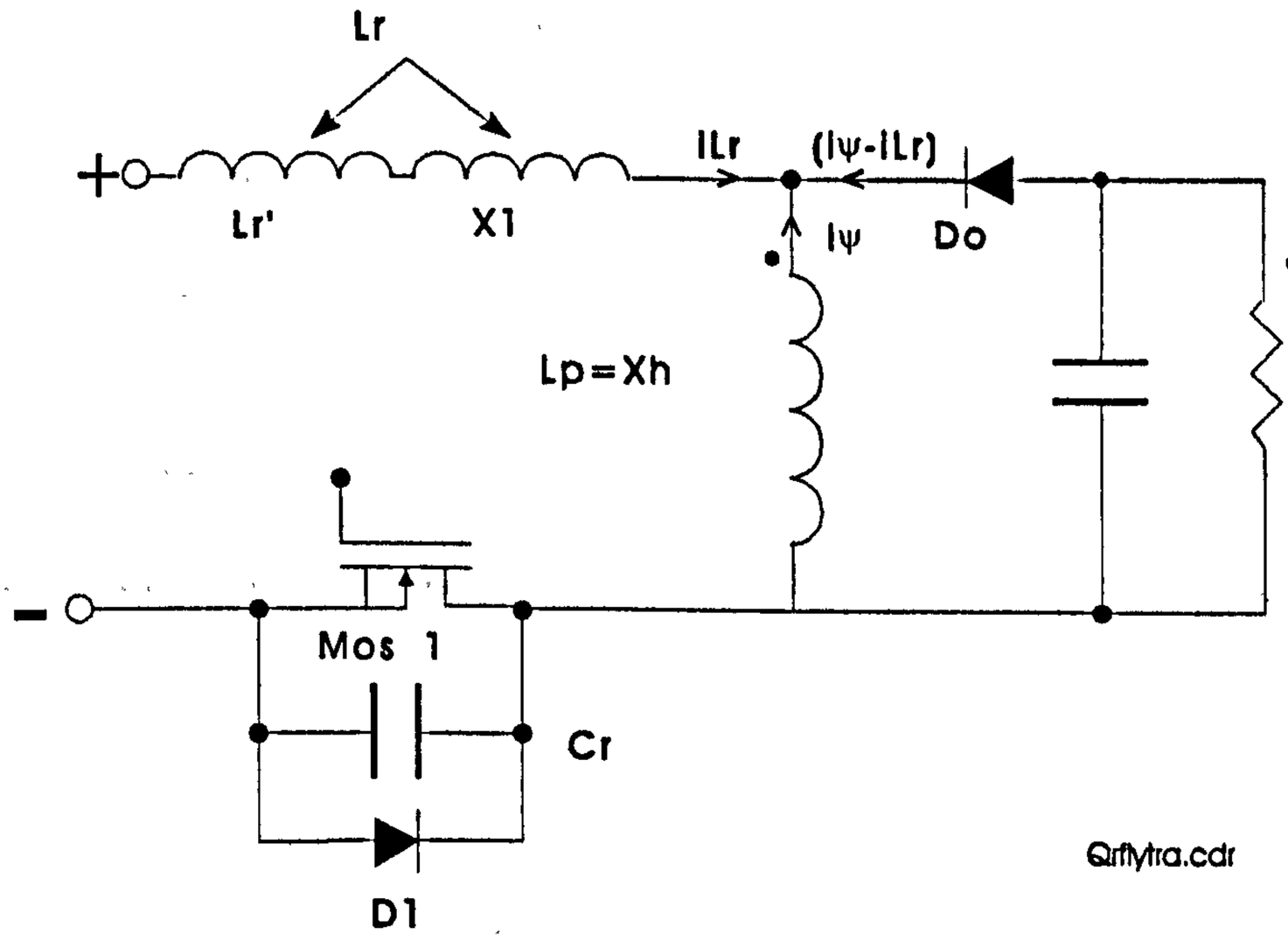

Figure 4.3 ***Quasi-resonant flyback converter including the transformer model***

period	Power switch MOS_1	Diode D_a
t_{01}	off	off
t_{12}	off	on
t_{23}	on	on
t_{34}	on	off

Table 4.1 The switch positions during one cycle of operation

To examine the operation of the proposed converter, each of the four periods shown in table 4.1 is represented by an equivalent circuit (section 4.1.1).

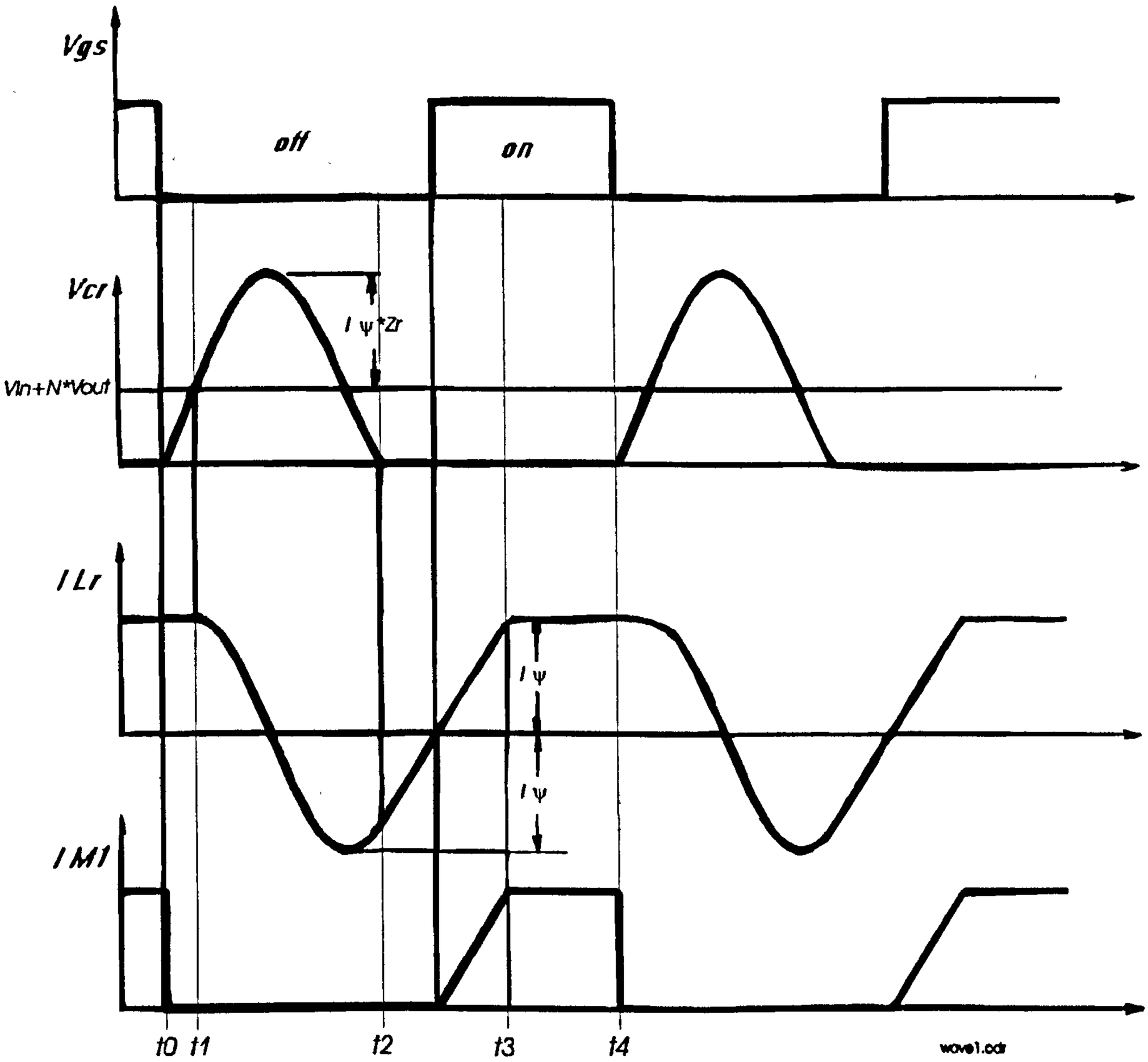

Figure 4.4 ***The wave forms of the examined converter***

V_{gs} ... *Voltage between the gate and the source of the MOSFET*

V_{cr} ... *Voltage across the resonant capacitor (= voltage between drain and source of the MOSFET)*

I_{Lr} ... *current into the resonant inductor*

I_{Ψ} *current through Lp*

I_{M1} ... *drain-current into the MOSFET*

The four operating periods are show in the wave forms in Figure 4.4. Note that the switch does not have to be turned on immediately after V_{Cr} has reached zero.

4.1.1 Equations

The solution of the equations lead to the relation between V_i/V_o and the frequencies f_s/f_r.

Analysis of one cycle under steady state conditions:

For each period of operation an equivalent circuit is given together with a set of equations which are valid for the specific period.

<u>Period 1:</u>

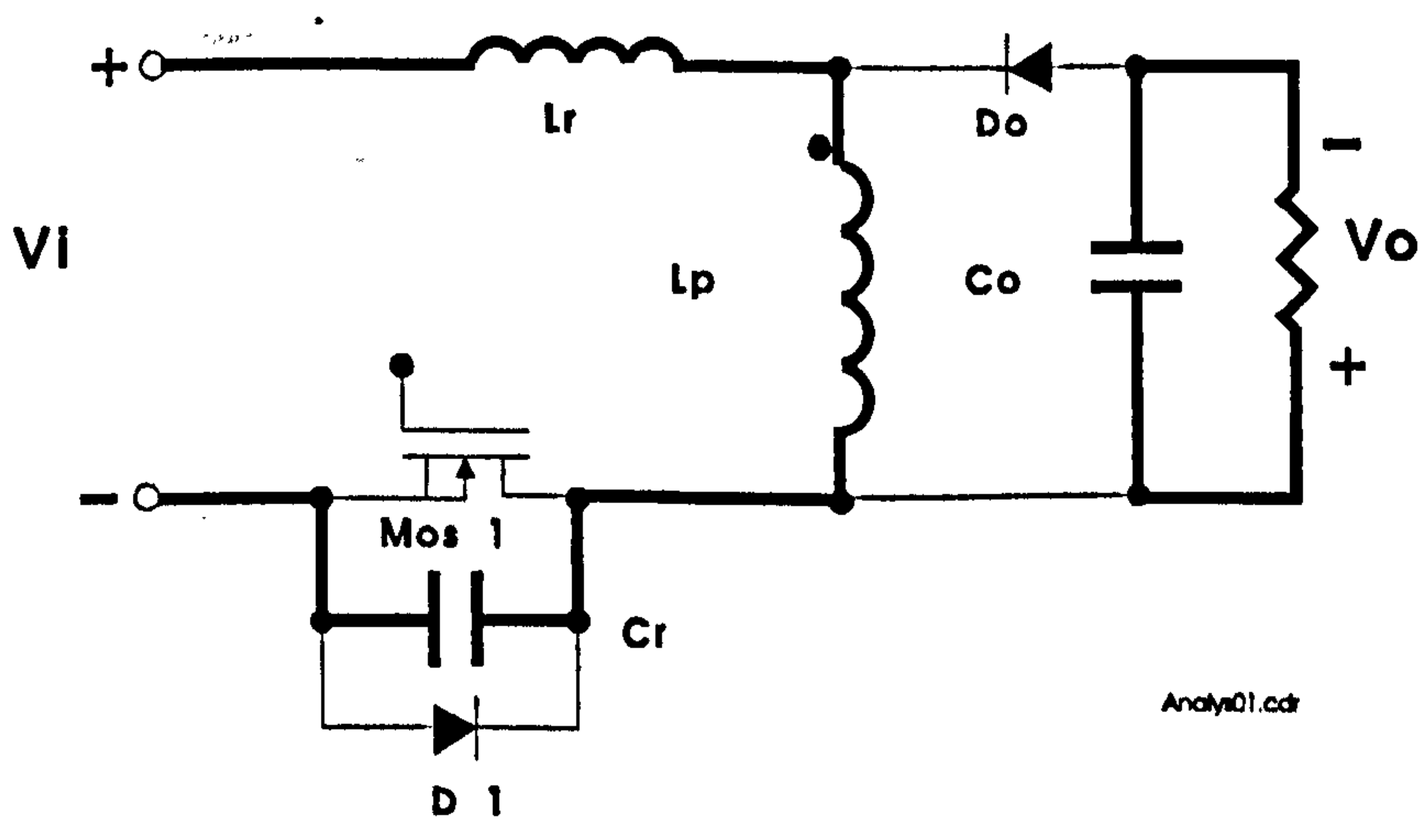

Figure 4.5 Equivalent circuit for period 1

Power switch MOS_1 turn-off

Time period: $t_0 - t_1 = t\overline{01}$

Initial condition: $V_{CR}(t_0) = 0$ (4.10)

State equation: $C_R \cdot \frac{dV_{CR}}{dt} = I_\psi = I_{LR}$ (4.11)

It was assumed that I_ψ is constant and as a result $\frac{dV_{CR}}{dt}$ is constant, which leads to a straight forward time solution. This assumption is valid if L_p is larger when compared to L_R. In this stage the voltage across the resonant capacitor builds up virtually linearly.

Time solution: $t\overline{01} = \frac{C_R \cdot (V_i + V_o \cdot N)}{I_\psi} = \frac{1}{\omega} \cdot \frac{(V_i + V_o \cdot N)}{Z_R \cdot I_\psi}$ (4.12)

Period 2:

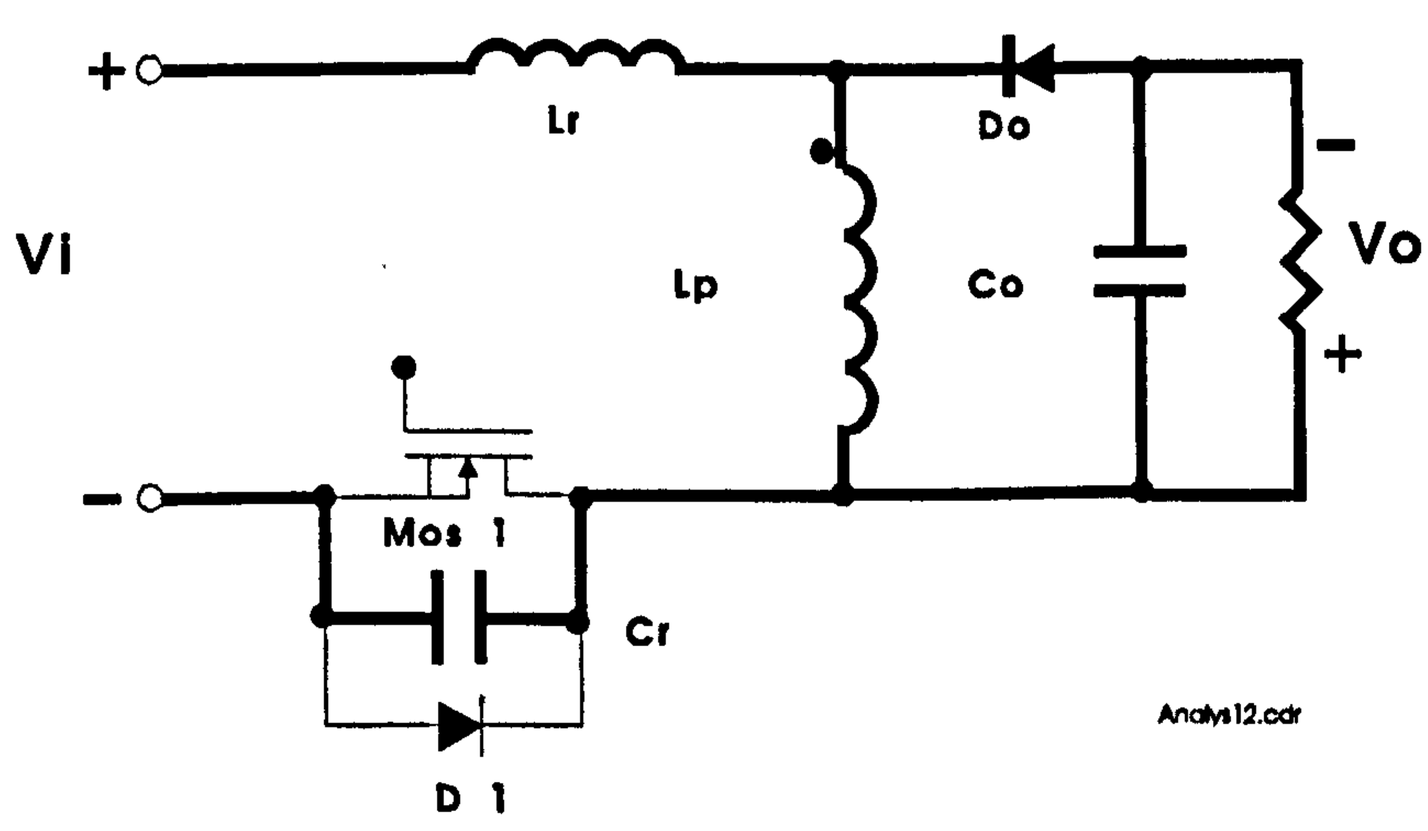

Figure 4.6 *Equivalent circuit for period 2*

V_{Cr} reaches $V_i + V_o \cdot N$ at t_1, D_o conducts.

Time period: $t_1 - t_2 = t\overline{12}$

Initial condition: $I_{LR}(t_1) = I_\psi$ (4.13)

$$V_{CR}(t_1) = V_i + N \cdot V_o \tag{4.14}$$

State equation:

$$C_R \cdot \frac{dV_{CR}}{dt} = I_\psi \tag{4.14b}$$

$$L_R \frac{dI_{LR}}{dt} = V_i + N \cdot V_o - V_{CR} \tag{4.15}$$

The following time solution for this period is determined from the oscillatory circuit (series resonant tank: L_R and C_R) [Her86].

Time solution:

$$I_{LR}(t) = I_\psi \cdot \cos(\omega t) \tag{4.16}$$

$$V_{CR}(t) = V_i + V_o \cdot N + Z_R \cdot I_\psi \cdot \sin(\omega t) \tag{4.17}$$

The voltage across the resonant capacitor naturally reaches zero

where $V_{CR}(t_2) = 0$ (zero-voltage switching) (4.18)

$$\sin(\omega t) = \frac{V_i + N \cdot V_o}{Z_R \cdot I_\psi} \tag{4.19}$$

$$t_{\overline{12}} = \frac{\alpha}{\omega} \tag{4.20}$$

where

$$\alpha = sin^{-1}\left(\frac{-V_i - V_o \cdot N}{Z_R \cdot I_\psi}\right) \equiv \pi + \left|sin^{-1}\left(\frac{-V_i - V_o \cdot N}{Z_R \cdot I_\psi}\right)\right| \tag{4.21}$$

Comment: as the sin^{-1} - function is only defined between $-\pi/2$ and $\pi/2$ the absolute value of the result must be taken and incremented by π.

Period 3:

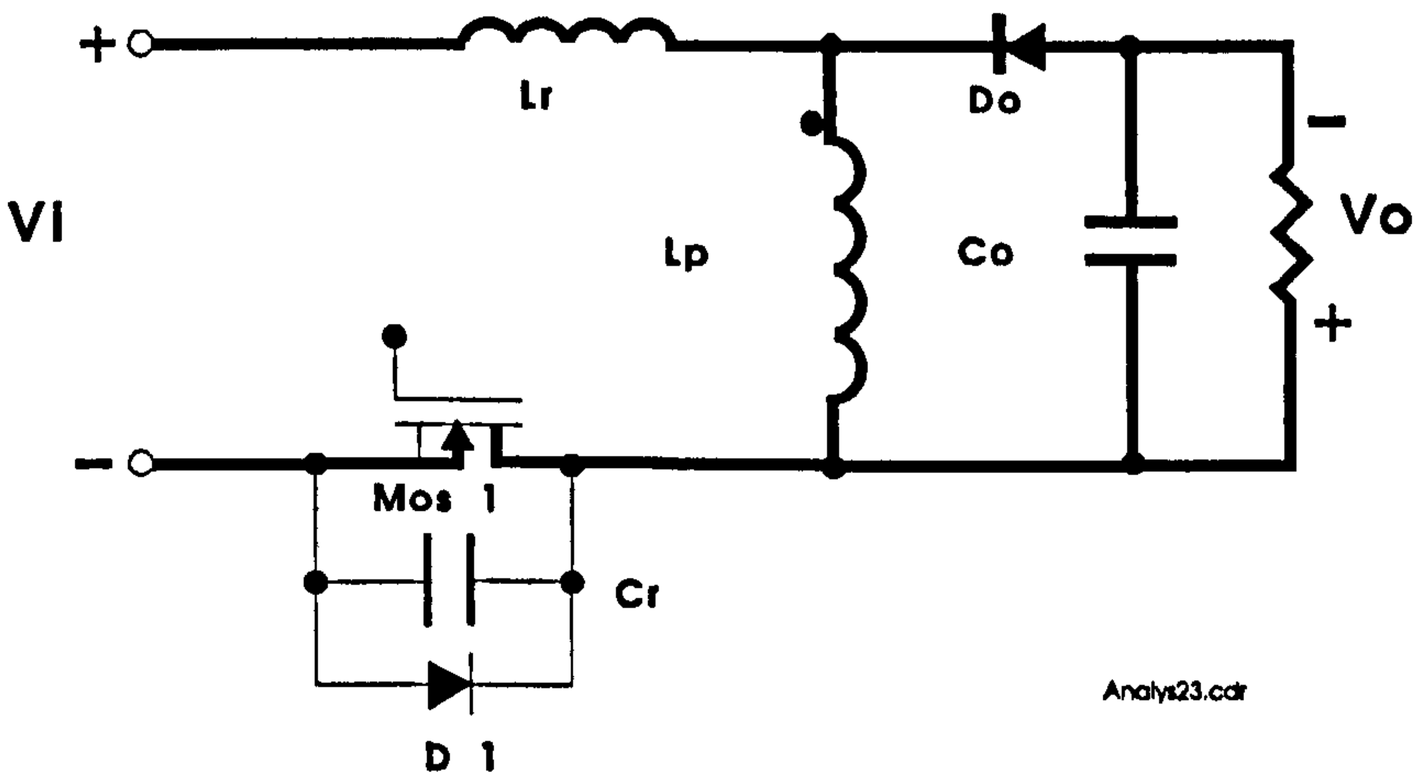

Figure 4.7 Equivalent circuit for period 3

Time period: $t_2 - t_3 = t_{\overline{23}}$

Initial condition: $I_{LR}(t_2) = I_\psi \cdot \cos\alpha$ (4.22)

State equation: $L_R \frac{dI_{LR}}{dt} = V_i + N \cdot V_o$ (4.23)

Time solution: $\frac{L_R \cdot (I_{LR}|^{t3} - I_{LR}|^{t2})}{t_{\overline{23}}} = V_i + N \cdot V_o$ (4.24)

{ where I_{LR} is linear: $I_{LR} = t\frac{(V_i + N \cdot V_o)}{L_R} - I_\psi \cdot \cos\alpha$ } (4.25)

therefore $\frac{L_R \cdot (I_\psi - I_\psi \cos\alpha)}{t_{\overline{23}}} = V_i + V_o \cdot N$ (4.26)

respectively $t_{\overline{23}} = \frac{1}{\omega} \cdot \frac{Z_R \cdot I_\psi}{(V_i + V_o \cdot N)} \cdot (1 - \cos\alpha)$ (4.27)

I_{LR} reaches I_ψ again at t_3

Period 4:

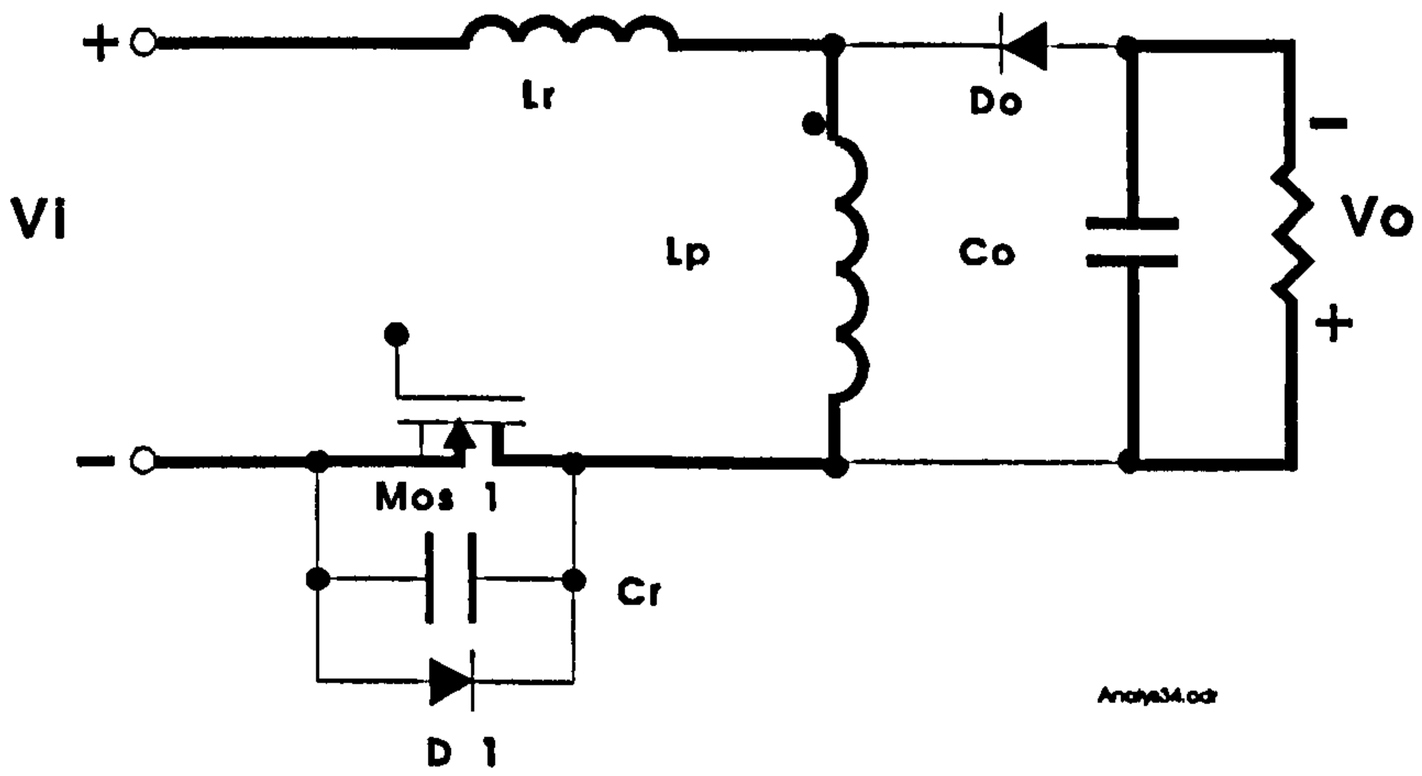

Figure 4.8 *Equivalent circuit for period 4*

I_{Lr} reaches I_ψ at t_3; D_o cuts off.

Time period: $t_3 - t_4 = t_{\overline{34}}$

As can be seen in Figure 4.4 (in the foregoing section) the voltage (V_{Cr}) and the current (I_{Lr}) remain approximately unchanged during this period.

Time solution: $$t_{\overline{34}} = T_s - t_{\overline{01}} - t_{\overline{12}} - t_{\overline{23}} \qquad (4.28)$$

DC voltage conversion ratio:

The conversion rate of the circuit is achieved by assuming that the circuit operates in an ideal fashion. Comparing the output power versus the input power leads to a final equation for which a graphical solution (Figure 4.9 and 4.10) is given after the following equations.

The output power:

$$E_o = \int_{t0}^{t4} V_o \cdot (I_\psi - I_{LR}) \cdot N \cdot dt \qquad (4.29)$$

with $I_\psi - I_{LR} = 0$ between t_3 and t_1 because D_o is not conducting. (The voltage drop across the output diode is neglected.)

Hence:

$$E_o = \int_{t1}^{t3} V_o \cdot (I_\psi - I_{LR}) \cdot N \cdot dt \qquad (4.30)$$

$$\therefore E_o = V_o \cdot N \cdot \int_{t1}^{t3} (I_\psi - I_{LR}) dt = V_o \cdot N \cdot \{I_\psi \cdot t_{\overline{12}} - \int_{t1}^{t2} I_{LR} \cdot dt + I_\psi \cdot t_{\overline{23}} - \int_{t2}^{t3} I_{LR} \cdot dt \qquad (4.31)$$

where the integral was split according to the two time intervals.

The physical interpretation of this equation is simply that the energy is the product of the voltage times the transferred current in the related time periods.

These currents can be determined by:

$$\int_{t1}^{t2} I_{LR} \cdot dt = \int_{t1}^{t2} I_\psi \cdot \cos(\omega t) dt = \frac{I_\psi}{\omega} \sin(\omega t)\Big|^{t_{\overline{12}}} \qquad (4.32)$$

and

$$\int_{t2}^{t3} I_{LR} \cdot dt = \int_{t2}^{t3} \{t \frac{(V_i + N \cdot V_o)}{L_R} - I_\psi \cdot \cos\alpha\} dt = \{t^2 \frac{(V_i + N \cdot V_o)}{L_R \cdot 2} - t \cdot I_\psi \cdot \cos\alpha\}\Big|^{t_{\overline{23}}} \qquad (4.33)$$

which can be express as (using (4.27)):

$$\int_{t2}^{t3} I_{LR} \cdot dt = \frac{Z_R^2 \cdot I_\psi^2 \cdot (1-\cos\alpha)^2}{2 \cdot \omega^2 \cdot L_R \cdot (V_i + V_o \cdot N)} + \frac{Z_R \cdot I_\psi^2 \cdot (1-\cos\alpha) \cdot \cos\alpha}{\omega \cdot (V_i + V_o \cdot N)} \qquad (4.34)$$

$$\therefore \int_{t2}^{t3} I_{LR}\,dt = \frac{Z_R \cdot I_\psi^{\,2}}{2\cdot\omega\cdot(V_i + N\cdot V_o)}\sin^2\alpha \qquad (4.35)$$

Using (4.24) again and (4.31) leads to:

$$E_o = V_o\cdot N\cdot I_\psi\cdot\left\{\frac{\alpha}{\omega} - \frac{\sin\alpha}{\omega} + \frac{I_\psi\cdot Z_R(1-\cos\alpha)^{\,2}}{2\cdot\omega\cdot(V_i + N\cdot V_o)}\right\} = V_o\cdot N\cdot I_\psi\cdot T_o \qquad (4.36)$$

<u>The input power:</u>

$$E_i = \int_{t1}^{t4} I_i\cdot V_i\,dt \qquad (4.37)$$

with $I_i = I_{LR} = I_\psi$ between t_3 and t_1.

$$E_i = V_i\cdot\int_{t1}^{t4} I_\psi\cdot dt = V_i\cdot\{I_\psi(t_{\overline{01}} + t_{\overline{34}}) + \int_{t1}^{t3} I_{LR}\cdot dt\} \qquad (4.38)$$

$$E_i = V_i\cdot I_\psi\left\{\frac{\alpha}{\omega} - \frac{\sin\alpha}{\omega} + \frac{Z_R\cdot I_\psi(1-\cos\alpha)^2}{2\cdot\omega\cdot(V_i + N\cdot V_o)}\right\} = V_i\cdot I_\psi\cdot T_i \qquad (4.39)$$

$$T_i + T_o = T_s \qquad (4.40)$$

$$t_{\overline{01}} + t_{\overline{34}} + \frac{\alpha}{\omega} + \frac{Z_R\cdot I_\psi\cdot\cos\alpha}{\omega\cdot(V_i + V_o\cdot N)} = T_s \qquad (4.41)$$

The transformer is in fact intended to be a two-winding inductor, which has dual functions of providing energy storage as in an inductor and electrical isolation as in a transformer. During the periods t_2-t_4 energy is pumped into the transformer through the primary winding and stored in the magnetic core and the airgap, and during the remaining periods the energy is drawn out from the secondary side. Therefore no flux reset winding is required.

A symbol x is introduced to represent the ratio:

$$x = \frac{V_o \cdot N}{V_i} \tag{4.42}$$

With equation (4.36), (4.39) and (4.40) it can be shown that

$$x = \frac{T_i}{T_o} = \frac{T_s}{T_o} - 1 \tag{4.43}$$

$$x = \frac{T_s}{T_o} - 1 = \frac{V_o \cdot N}{V_i} \tag{4.44}$$

$$T_o = T_s \frac{V_i}{(N \cdot V_o + V_i)} \tag{4.45}$$

also from (4.43),

$$x = \frac{1}{f_s \cdot T_o} - 1 \tag{4.46}$$

substituting T_o in the expression given in (4.36) results in

$$x = \frac{1}{f_s \cdot \left\{ \frac{\alpha}{\omega} - \frac{\sin\alpha}{\omega} + \frac{Z_R \cdot I_\psi \cdot (1-\cos\alpha)^2}{2 \cdot \omega \cdot (V_i + N \cdot V_o)} \right\}} - 1 \tag{4.47}$$

The output power can also be expressed as

$$E_o = \frac{V_o^2 \cdot T_s}{R} \tag{4.48}$$

Equating this expression with the result in (4.36) and furthermore substituting T_o from (4.45) leads to:

$$\frac{V_o^2 \cdot T_s}{R} = V_o \cdot N \cdot I_\psi \cdot \frac{T_s \cdot V_i}{(V_o \cdot N + V_i)} \tag{4.49}$$

$$\frac{V_o}{N \cdot V_i \cdot R} = \frac{I_\psi}{(V_i + N \cdot V_o)} \qquad \text{multiplied by } Z_R \tag{4.50}$$

$$\frac{x}{\beta \cdot N^2} = \left(-\frac{1}{\sin\alpha} \right) = \frac{Z_R \cdot I_\psi}{(V_i + N \cdot V_o)} \tag{4.51}$$

see equation (4.21) and where

$$\beta = \frac{R}{Z_R} \tag{4.52}$$

consequently equation (4.47) can be rewritten as

{using $(1-\cos\alpha)^2 = 2-2\cos\alpha+\sin^2\alpha$ and substituting $-\frac{1}{\sin\alpha}$ from above}

$$x = \frac{1}{\frac{f_s}{\omega}\left[\alpha + \frac{\beta\cdot N^2}{x} + \frac{x\left\{2-2\cos\alpha-\frac{\beta^2 N^4}{x^2}\right\}}{2\cdot\beta\cdot N^2}\right]} - 1 \tag{4.53}$$

$$\therefore x = \frac{1}{\frac{f_s}{\omega}\left\{\alpha - \frac{\beta\cdot N^2}{2x} + \frac{x\cdot(1-\cos\alpha)}{\beta\cdot N^2}\right\}} - 1 \tag{4.54}$$

Finally, with reference to the above equation it can be seen that a voltage ratio between output voltage and input voltage can be determined. The expression α includes x as an factor, hence equation (4.54) is arithmetically unsolveable. Therefore, a graphical solution has to be used. The above equation has been modified according to this:

$$E = \frac{x}{N} \tag{4.55}$$

where E is now the straight forward voltage ratio $\frac{V_o}{V_i}$.

$$E = \frac{1}{\frac{f_s}{\omega}\left[\alpha - \frac{\beta\cdot N}{2\cdot E} + \frac{E\cdot(1-\cos\alpha)}{\beta\cdot N}\right]} - 1 \tag{4.56}$$

referring to (4.51) and the expression for α in equation (4.21)

$$E = \frac{1}{\frac{f_s}{\omega}\left\{\pi + \sin^{-1}\left(\frac{\beta \cdot N}{E}\right) - \frac{\beta \cdot N}{2 \cdot E} + \frac{E \cdot \left[1 - \cos\left\{\pi + \sin^{-1}\left(\frac{\beta \cdot N}{E}\right)\right\}\right]}{\beta \cdot N}\right\}} - 1 \qquad (4.57)$$

In Figure 4.10 and 4.11 the value for the frequency relation can be observed for different combinations of $\beta\left(=\frac{R}{Z_R}\right)$ and the voltage relation $x\left(=\frac{N \cdot V_o}{V_i}\right)$.

The turn ratio N of the transformer is here set to 2 and 0.5 respectively.

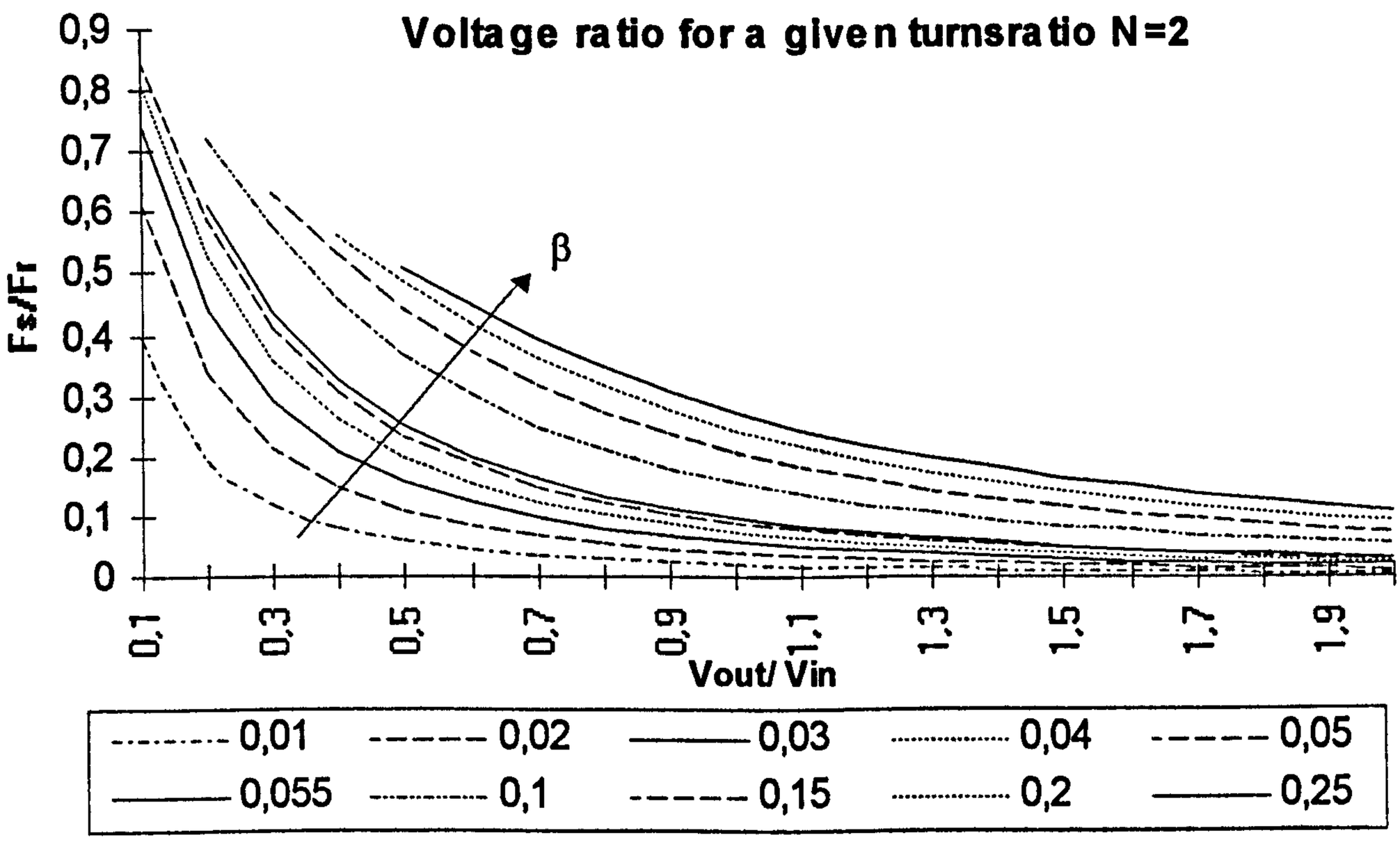

Figure 4.9 Voltage conversion of a QR-flyback converter with turnsratio N=2

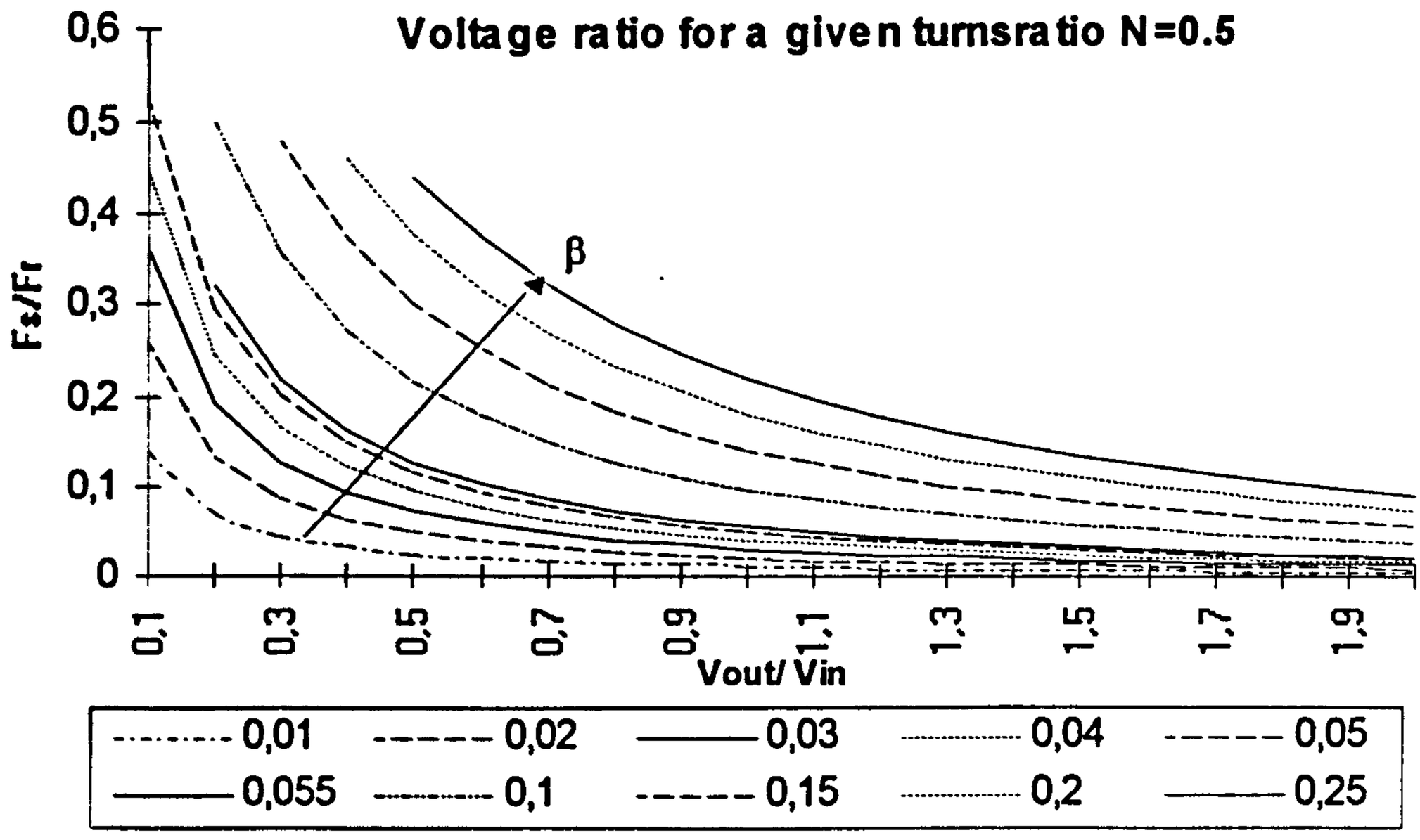

Figure 4.10 Voltage conversion of a QR-flyback converter with turnsratio N=0.5

4.1.2 Determination of the resonance frequency

As shown in the previous section one operating cycle of the quasi-resonant flyback converter can be divided into four periods to enable a mathematical analysis. The second or the resonant period is according to all references[20] determined by the resonant tank consisting of an inductor labelled L_r and a capacitor C_r. Corresponding to these references the resonant frequency of the circuit is given by

$$f_r = \frac{1}{2 \cdot \pi \cdot \sqrt{L_r \cdot C_r}}. \qquad (4.58)$$

[20][Bar90], [Chr89], [Lee86] etc.

Nevertheless, non of the published paper have verified this assertion. Liu states that for a proper analysis of the circuit the assumption that L_o is much larger than L_R is made ($L_o \equiv L_p$) [Liu86]. The influence of the other components seems to be negligible.

In the following analysis the derivation of the resonant frequency is given. By varying the size of the different components their influence on the resonant frequency can be demonstrated which is obviously of great importance for the determination of the circuits parameters. Furthermore, the equivalent circuit was simulated on PSPICE to confirm the theoretical results.

Mathematical confirmation:

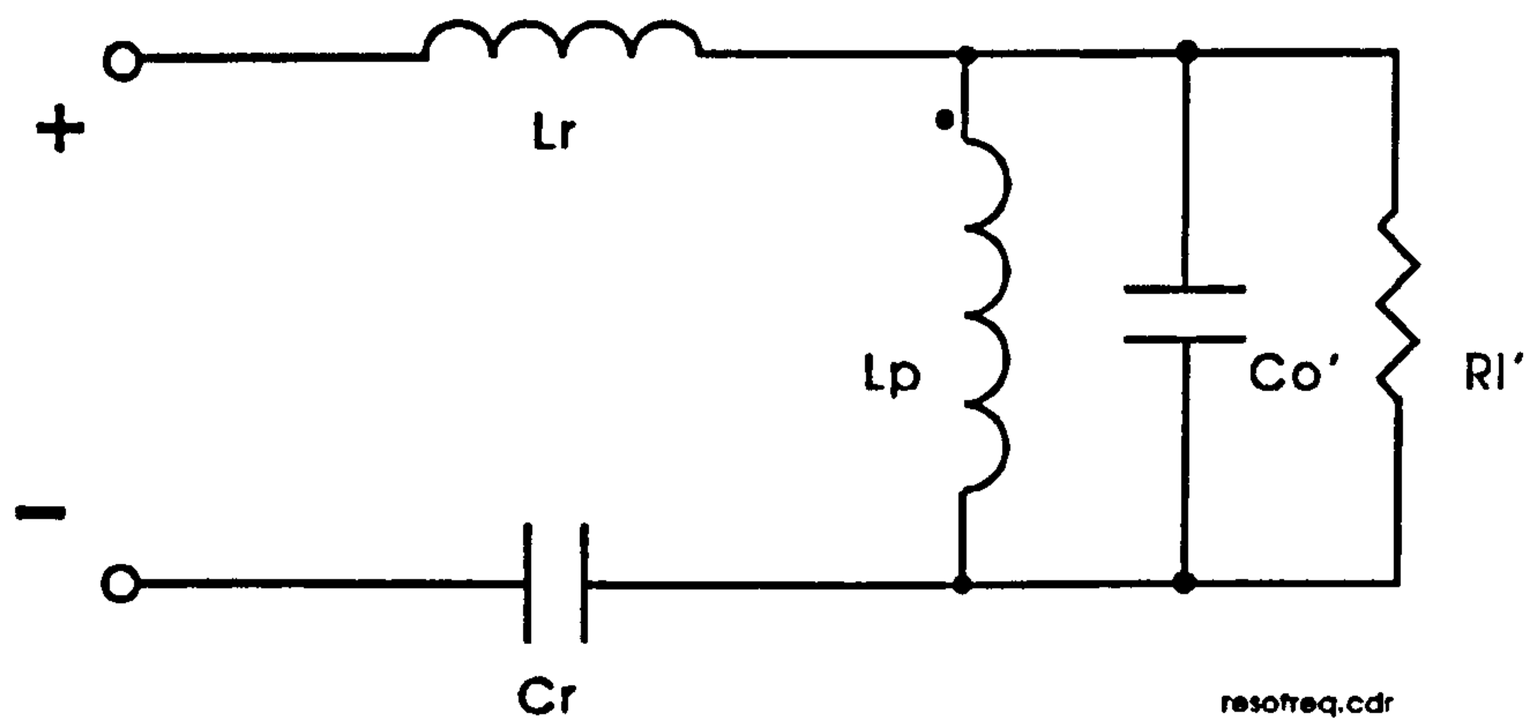

Figure 4.11 The equivalent circuit for the second/resonant period

To find the resonant frequency of any electrical circuit one has to determine the complex impedance Z of it. In the next step the maxima / minima of the of the graph of Z in respect to ω has to be found using the derivation of Z, Z'. Setting this derivation Z' to zero gives these maxima / minima. The equivalent circuit used for the analysis is given in Figure 4.11. It is derived in section 4.1.1.

$$\underline{Z} = \underline{L_r} + \underline{C_r} + \frac{1}{\underline{Y}} \tag{4.59}$$

$$Z = j \cdot \omega \cdot L_r + \frac{1}{j \cdot \omega \cdot C_r} + \frac{1}{Y} \tag{4.59.1}$$

with Y:

$$\underline{Y} = \underline{L_p} + \underline{C_o'} + \underline{Rl} \tag{4.60}$$

$$Y = \frac{1}{j \cdot \omega \cdot L_p} + j \cdot \omega \cdot C_o' + \frac{1}{Rl} \tag{4.60.1}$$

Equation (4.59.1) is inserted into (4.60.1) which leads to the complex impedance:

$$Z = j \cdot \omega \cdot L_r + \frac{1}{j \cdot \omega \cdot C_r} + \frac{1}{\frac{1}{j \cdot \omega \cdot L_p} + j \cdot \omega \cdot C_o' + \frac{1}{Rl}} \tag{4.59.2}$$

$$Z = L_r - \frac{1}{(j \cdot \omega)^2 \cdot C_r} - \frac{1}{\left(\frac{1}{j \cdot \omega \cdot L_{prim}} + j \cdot \omega \cdot C_o' + \frac{1}{Rl}\right)^2} \cdot \left(-\frac{1}{(j \cdot \omega)^2 \cdot L_p} + C_o'\right) \tag{4.61}$$

with

$$\left(\frac{1}{j \cdot \omega \cdot L_p} + j \cdot \omega \cdot C_o' + \frac{1}{Rl}\right)^2 =$$

$$2 \cdot \frac{C_o'}{L_p} + \frac{2}{j \cdot \omega \cdot L_p \cdot Rl} + \frac{2 \cdot j \cdot \omega \cdot C_o'}{Rl} - \frac{1}{\omega^2 \cdot L_p^2} - \omega^2 \cdot C_o'^2 + \frac{1}{Rl^2} = \zeta \tag{4.62}$$

which is set to ζ.

The Equation 4.61 can be rewritten given the common denominator $(\omega^2 \cdot C_r \cdot \zeta)$:

$$Z = \frac{L_r \cdot \omega^2 \cdot C_r \cdot \zeta + \zeta - \left(\frac{1}{\omega^2 \cdot L_p} + C_o'\right) \cdot \omega^2 \cdot C_r}{\omega^2 \cdot C_r \cdot \zeta} \tag{4.61.1}$$

By determining the common denominator of the numerator ($j \cdot \omega^2 \cdot L_p^2 \cdot R'^2$) of this expression one can further simplify this equation in order to find the maxima / minima.

$$Z = \frac{j \cdot \omega^6 \cdot A + \omega^5 \cdot Q + j \cdot \omega^4 \cdot B + \omega^3 \cdot R + j \cdot \omega^2 \cdot C + \omega \cdot S + D}{\text{Denominator}} \quad (4.61.2)$$

The examination of the hereby derived finial numerator leads to the points of the graph where the real part in zero, consequently to the result. The physical interpretation would be that the calculation aims for the frequencies where the impedance of the circuit appears purely inductive or capacitive.

The expressions of the numerator are sorted in respect to their order of ω. The expressions with even orders represent the imaginary part whereas the expressions with odd orders represent the real part.

Even order expressions:

$$\omega^6: \; j \cdot \omega^6 \cdot (-C_r \cdot C_o'^2 \cdot L_r \cdot L_p^2 \cdot R_l'^2)$$
$$\equiv j \cdot \omega^6 \cdot A \quad (4.63)$$

$$\omega^4: j \cdot \omega^4 (2 \cdot C_r \cdot C_o' \cdot L_r \cdot L_p \cdot R_l'^2 + C_r \cdot L_r \cdot L_p^2 - C_o'^2 \cdot L_p^2 \cdot R_l'^2 - C_r \cdot C_o' \cdot L_p^2 \cdot R_l'^2)$$
$$\equiv j \cdot \omega^4 \cdot B \quad (4.64)$$

$$\omega^2: \; j \cdot \omega^2 \cdot (-C_r \cdot L_r \cdot R_l'^2 + 2 \cdot C_o' \cdot L_p \cdot R_l'^2 + L_p^2 - C_r \cdot L_p \cdot R_l'^2)$$
$$\equiv j \cdot \omega^2 \cdot C \quad (4.65)$$

$$\omega^0: \; j \cdot R_l'^2$$
$$\equiv D \quad (4.66)$$

Odd order expressions:

$$\omega^5:\ \omega^5\cdot(-2\cdot C_r\cdot C_o'\cdot L_p^2\cdot R_l') \equiv \omega^5\cdot Q \tag{4.67}$$

$$\omega^3:\ \omega^3\cdot(2\cdot C_r\cdot L_r\cdot L_p\cdot R_l'-2\cdot C_o'\cdot L_p^2\cdot R_l') \equiv \omega^3\cdot R \tag{4.68}$$

$$\omega^1:\ \omega\cdot(2\cdot L_p\cdot R_l') \equiv \omega\cdot S \tag{4.69}$$

Differentiating the numerator with respect to $j\cdot\omega$, the odd exponents (as being constants) become zero and hence are negligible.

To reduce the orders ω^2 was substituted by x and set to zero leading to the following equation:

$$x^3+ax^2+bx+c=0 \tag{4.70}$$

with $a=\frac{B}{A}$; $b=\frac{C}{A}$; $c=\frac{D}{A}$ from the even expressions.

To solve this equation another substitution (Cardanian formula) [Bat90] has been applied:

$$x=y-\frac{a}{3} \tag{4.71}$$

The resulting equation can be seen below:

$$y^3+p\cdot y+q=0 \tag{4.70.1}$$

with
$$p=-\frac{a^2}{3}+b \tag{4.72}$$

and
$$q=2\cdot\frac{a^3}{27}-\frac{a\cdot b}{3}+c \tag{4.73}$$

The first and only non-complex solution is given by

$$y_1 = u + v \tag{4.74}$$

$$\text{with} \quad u = \sqrt[3]{-\frac{q}{2} + \sqrt{\left(\frac{q}{2}\right)^2 + \left(\frac{p}{3}\right)^3}} \tag{4.75}$$

$$\text{and} \quad v = \sqrt[3]{-\frac{q}{2} - \sqrt{\left(\frac{q}{2}\right)^2 + \left(\frac{p}{3}\right)^3}} \tag{4.76}$$

Realistic values were inserted into these equations to compare the result with the established equation to calculate the resonant frequency.

<u>Numerical example:</u>

$C_r =$ 9.2µF

$C_o =$ 470µF

$L_r =$ 6µH

$L_o =$ 32µH

$R_l =$ 2.88Ω

R_l and C_o had to be transferred using the transformer model in section 4.1 to receive R_l' respectively C_o'.

Standard solution:

$$f_r = \frac{1}{2 \cdot \pi \cdot \sqrt{L_r \cdot C_r}} \tag{4.58}^{21}$$

$f_r =$ <u>677kHz</u>

Solution following the above mathematical derivation:

---

[21] recalled from front page of this section

$$y_1 = f_r = \quad \underline{687\text{kHz}}$$

The inaccuracy is less then 2% !

Remark: Variations in the values of L_r and C_r in the EXCEL worksheet[22] has shown that within a realistic rage the inaccuracy remains below this 2%.

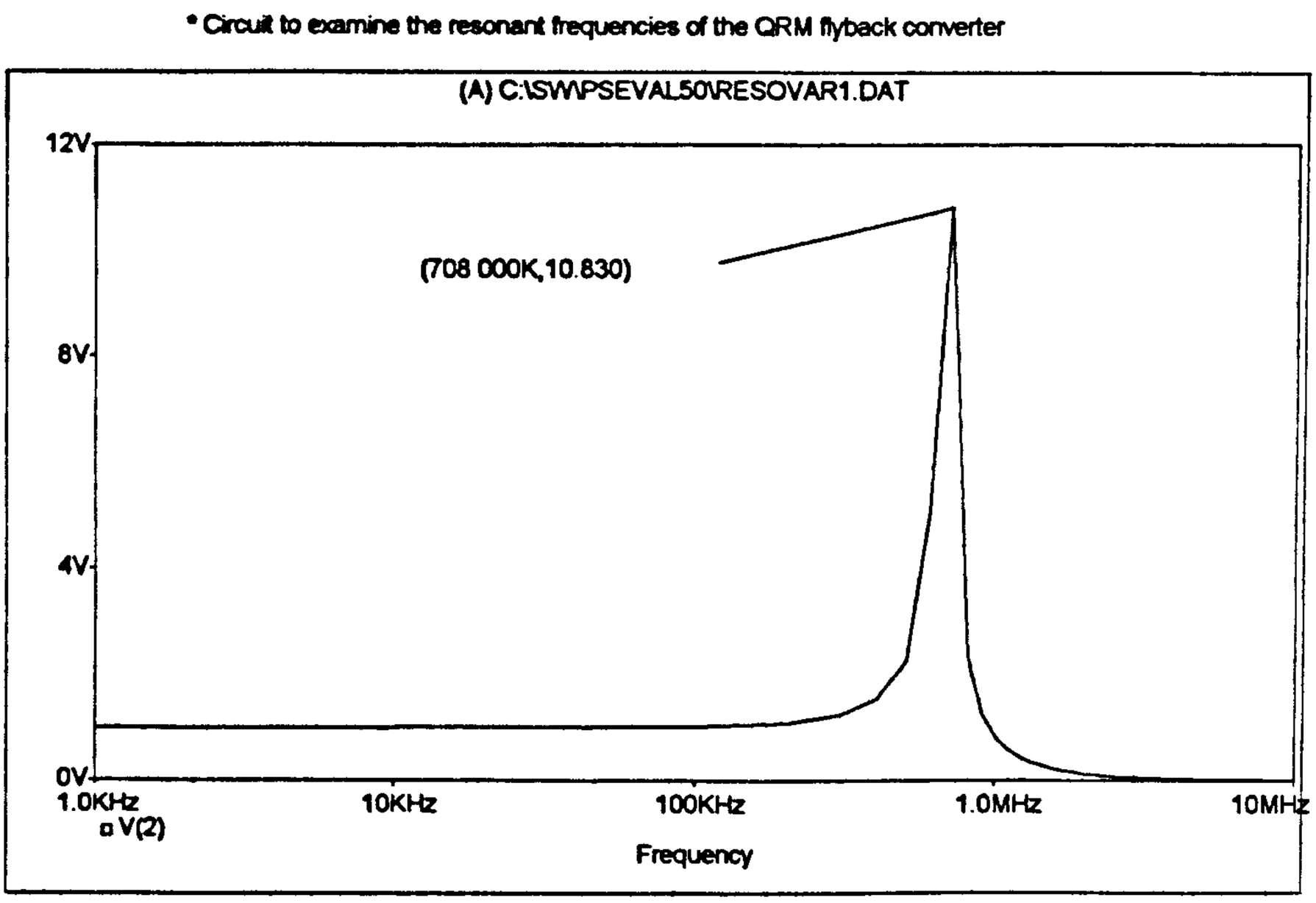

Figure 4.12 Resonant frequency determination with PSpice

A PSPICE simulation of the equivalent circuit was carried out. The result 708kHz (error < 5%) also confirmed the results of the two methods shown above. Hence, it can be said that the shortcut as given in equation (4.58) to determine the resonant frequency in a Quasi-Resonant converter is tolerable.

[22]Appendix D

4.2 Simulation of the Dual converter

The simulation of the *dual converter* was carried out for different reasons. The first reason was that by using simulation the process of designing and developing a new circuit can be radically shortened, as building hardware is not necessary at an early stage. Secondly, mathematical results can be confirmed by simulation. Simplifications that have been applied to mathematical complex problems can be verified by simulation.

Simulation was applied in section 4.1.2 and in the section below where the change-over period of the *dual converter* is examined. Furthermore, the dimensioning of the components of a circuit can be confirmed using simulation. Therefore, a large part of the optimisation of a circuit has been / can be achieved before actually building the circuit.

The circuit was examined by simulation in respect of its electrical as well as its electromagnetic behaviour in following sections. While the use of electrical simulation has become a standard tool during past, magnetic simulation packages are still rather expensive and therefore less frequently applied to design and verification of circuit behaviour.

4.2.1 Electrical Simulation

The practical way to test an electrical circuit is to build it. However, layout and physical effects become more important with high frequency switching technique, so the circuit can not be assembled on a standard board in order to achieve realistic results.

A circuit idea, as presented with the *dual converter* in this paper can be examined before building and even before ordering the parts using simulation. Furthermore, the simulation allows measurements on the circuit which are

- difficult (due to electrical noise),
- inconvenient (special test equipment is unavailable), or
- unwise (the test circuit could destroy itself) [Tui88].

The strategy that was pursued for the simulation of the circuit is similar to the method used for the mathematical analysis. Hence, first of all the two, then independent quasi-resonant flyback converters were simulated. In a second step, the two circuits were combined through the multi-winding transformer to obtain an understanding of the behaviour of the *dual converter* as a whole.

The program which was used required some extra elements in the circuit to enable a proper simulation. Divergence problems would occur without a series resistor in any closed path. Additionally, every node in a circuit has to have an earth connection. Hence, the transformer which normally provides perfect isolation has to be bridged by a large resistor. This does not effect the behaviour of the circuit, but enables a correct analysis.

The circuit is drawn with a CAD tool (pre-processor)[23], that is part of the software package, analysed and finally examined with probe function (post-processor).

---

[23]With this schematic tool it is no longer necessary to insert listings and be concerned about node number etc., the connection list is created by the program itself and not of interest to the designer.

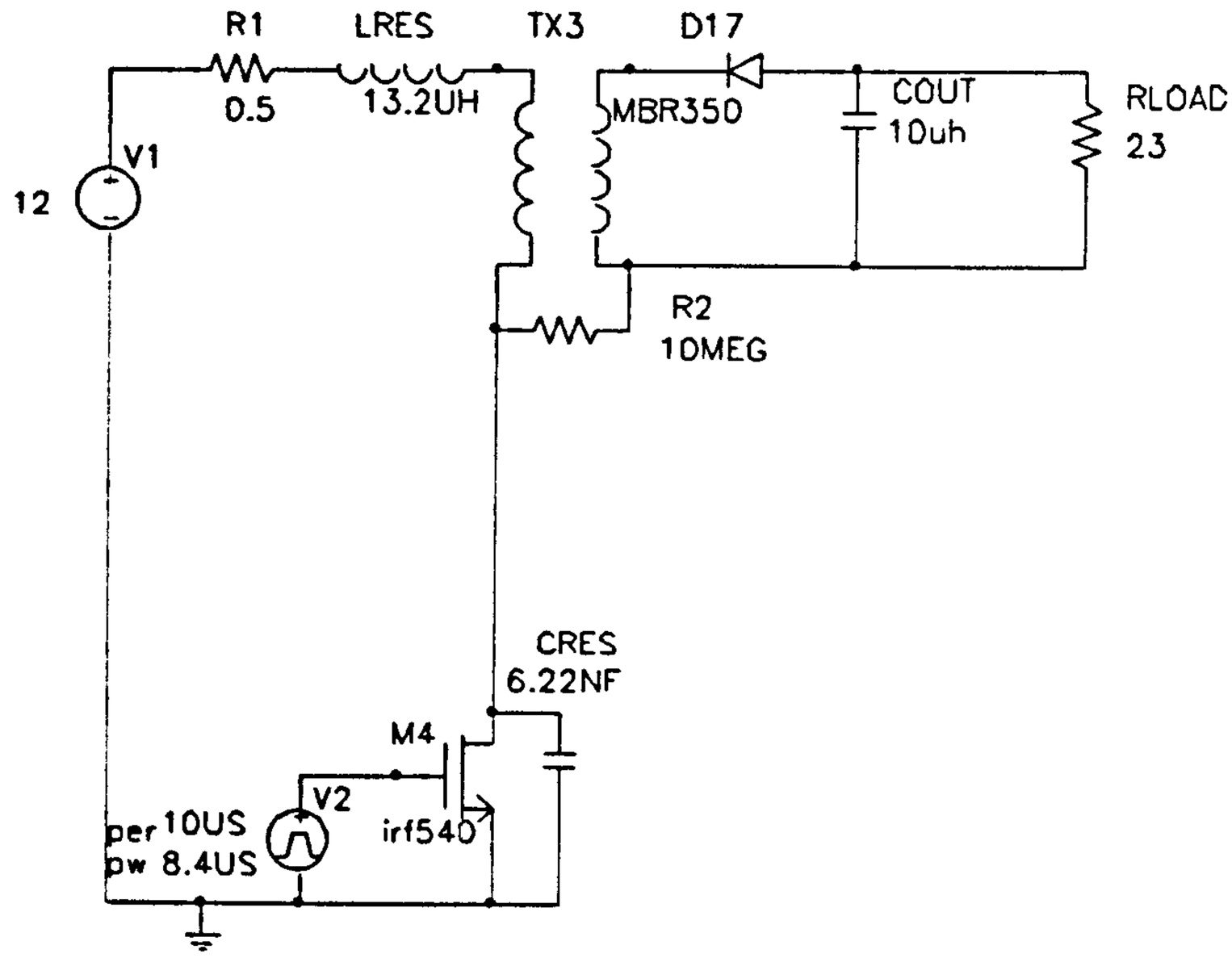

Figure 4.13 Schematic layout of a QR-flyback converter

A copy of the schematic editor is given in Figure 4.13.

The latest option of the package which was used allows to probe at the influence of the board layout of the circuit (it could not be used, due to availability). This is particularly important with high-frequency applications and VLSI circuits.

Simulation results:

In Figure 4.14 the wave forms of the simulation of *dual converter* are given, with the mains input part in operation.

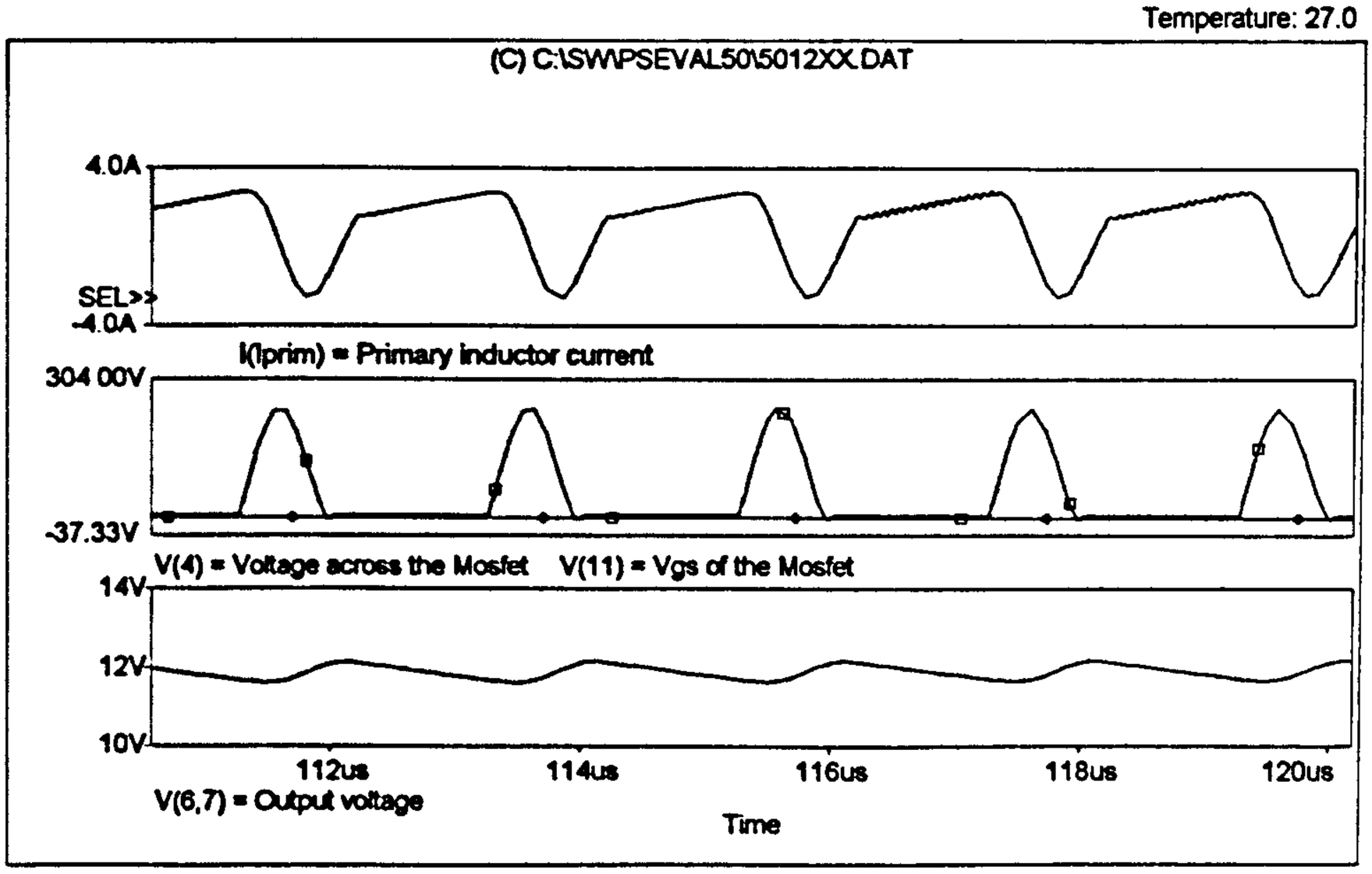

Figure 4.14 Mains input part of the dual converter

The voltage across the MOSFET in the second converter (stand-by source) together with the control voltage that was applied to it can be observed in Figure 4.15. After the MOSFET is turned off the voltage across the MOSFET and the parallel resonant capacitor rises, and peaks at a voltage far higher than the input voltage of the circuit (here: 175.8V peak / 24V input). As soon as the voltage has reached zero the MOSFET can be turned on again with virtually no switching losses.

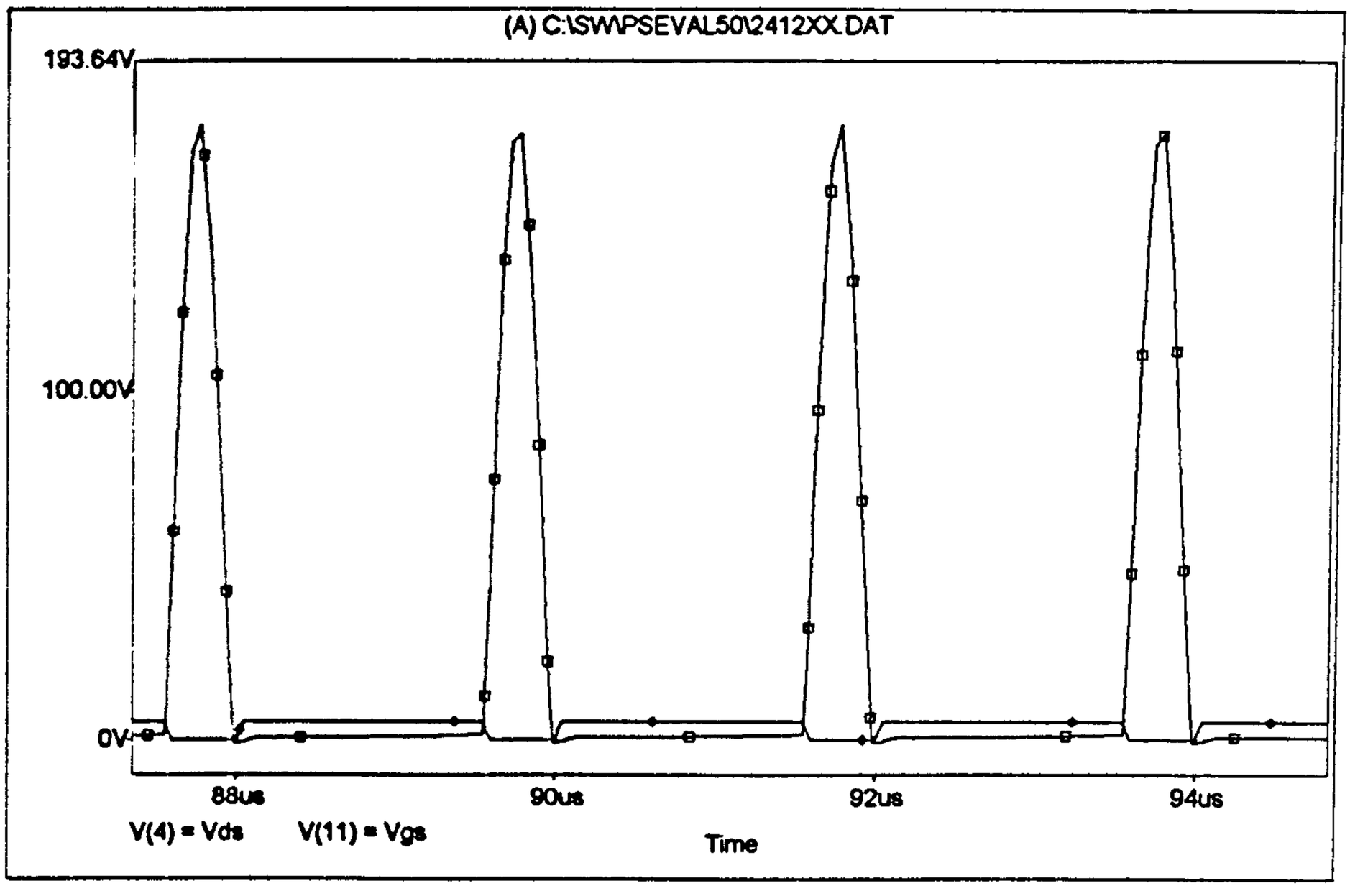

Figure 4.15 Stand-by input with resonant voltage wave form

To verify the principle of the proposed *dual converter* it was necessary to combine the two circuits. The critical period of the operation would obviously be the change-over period from one source to the other. The way in which each circuit would influence its counterpart through the common transformer could not be foreseen. With the simulation it could be shown that the output voltage drops only slightly in case of power failure and no disturbance was observed. The voltage drop is dependent on the pre-set level, at which the stand-by source is activated. It has to be adjusted according to the equipment that the UPS supplies.

Figure 4.16 shows that the output voltage peaks after the stand-by supply has taken over. It then takes a certain period to stabilise at the previous level.

* Simulation of the Dual converter using two independent sources

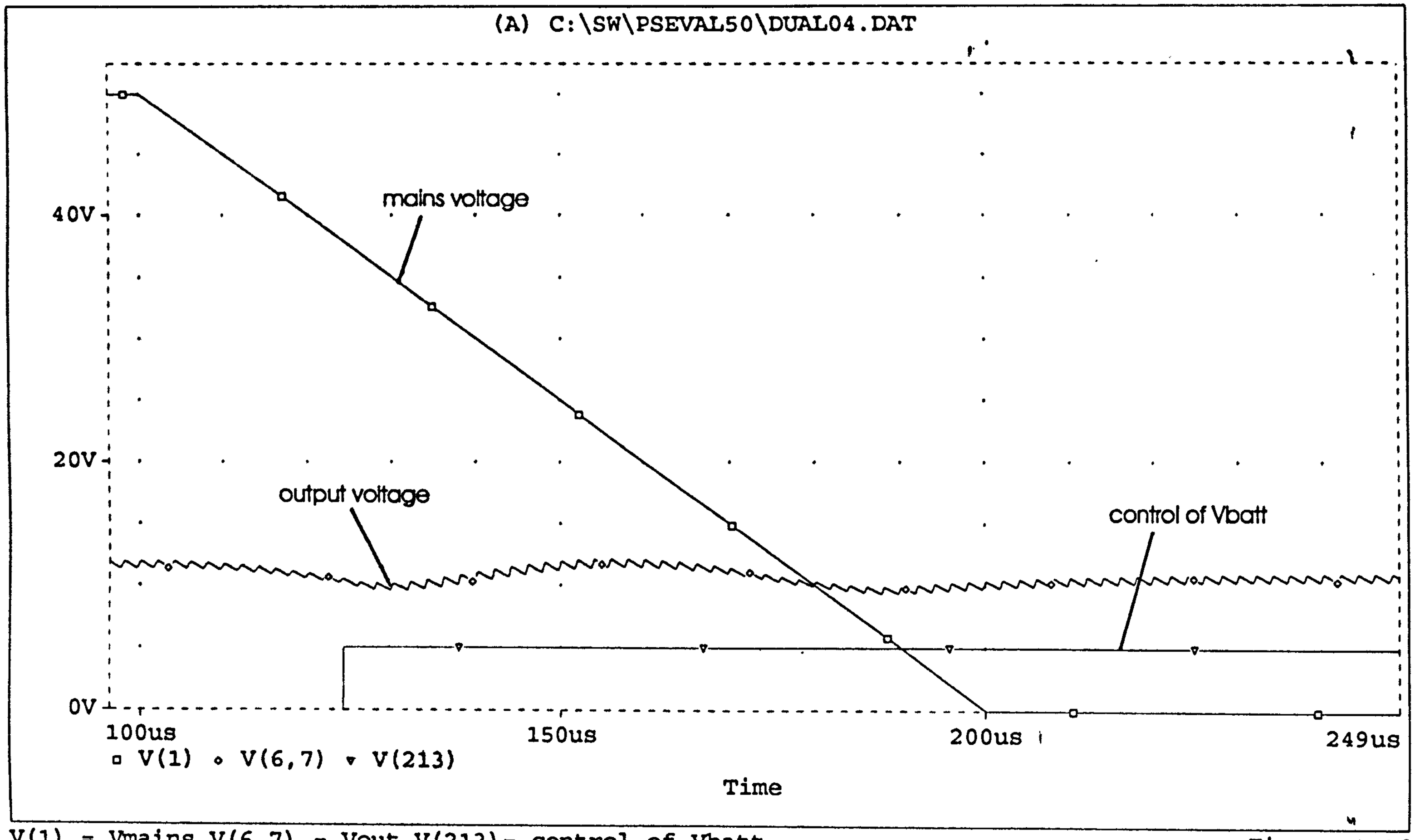

V(1) = Vmains V(6,7) = Vout V(213)= control of Vbatt

Figure 4.16

figure 4.16

4.2.2 Electro Magnetic simulation

There are three main reasons as to why the *dual converter* required an electro magnetic simulation: (a) the inductance of each winding could be verified; (b) the mathematical calculation of the required spacing between the windings of the transformer to achieve the desired leakage inductances can be confirmed by the simulation and (c) the location of the losses (due to hot spots as well as to fringing flux) within the core could be found. Practical experiments fail to illustrate these effects or are less accurate due to measuring errors.

The simulation software

Vector Fields Ltd an Oxford based company developed a package that allows designers to analyse, simulate and design their magnetic circuits or components, such as actuators, sensors, motors etc. The applied program version is PC-based and enables two dimensional FEM (finite element method) analyses. It is used for applications where the third dimension is not a significant factor in the analysis. Examples are axis-symmetrical geometry and design, where stray effects at the end of the part can be disregarded. The shape of the part was inserted in form of geometrical co-ordinates. The program then automatically generated the mesh for the analysis. This mesh can be manually edited in areas where high flux density is expected, such as the area in the vicinity of the airgap. The material specification is edited and applied to the simulation.

Inductances of the single windings:

By applying current to only one of the windings their inductance may be calculated. An area integration over the whole core-half[24] was carried out. The

[24]Only one half of the core was used for simulation because it is axis-symmetric

inductor value can be calculated using the resulting value $E'\left(=BH/_{ds\cdot 2}\right)$ by rearranging the equation for the energy in an inductor ($E=\frac{1}{2}\cdot L\cdot I^2$) and by taking into account that the simulation is only two dimensional for one core half is the result delivered by the simulation. Hence, E' is multiplied by the cores length (third dimension [ds]), by two (for the other half of the core) and divided it by the current that had been applied, the inductance value could be determined.

$$L=\frac{4\cdot E\cdot ds}{I^2} \tag{4.77}$$

Calculation for the primary inductance 1:

$$E=2.934\cdot 10^{-7}\,J/_{mm}$$

$$L=\frac{4\cdot 2.934\cdot 10^{-7}\,J/_{mm}\cdot 17.4mm}{(1A)^2}=20.42\mu H$$

calculation for the primary inductance 2:

$$E=1.274\cdot 10^{-6}\,J/_{mm}$$

$$L=\frac{4\cdot 1.274\cdot 10^{-6}\,J/_{mm}\cdot 17.4mm}{(2.1A)^2}=20.11\mu H$$

calculation for the secondary inductance:

$$E=3.021\cdot 10^{-7}\,J/_{mm}$$

$$L=\frac{4\cdot 3.021\cdot 10^{-7}\,J/_{mm}\cdot 17.4mm}{(4.2A)^2}=1.192\mu H$$

The results justified the practical measurements as given in the Appendix B.

Figure 4.17 shows a section view of one core half of the multi-winding transformer, with the airgap in the middle leg of it. The three windings are drawn as blue rectangles. From the legend it can be observed that the windings have virtually no flux density, whereas the main proportion of the flux is running through the core. Nevertheless the flux density within the core varies from the outer edges (blue areas), where the flux density is very low, to the inner edges, where the core material runs into saturation (red areas). This results in core losses. A reduction could be achieved by having smoother edges at the inner part of the core. Hence, the flux density would change in a more linear fashion towards these edges.

In the second print (Figure 4.18) the flux lines through the core are given in red. It can be seen that some of the lines are "cutting" the windings in the vicinity of the airgap (fringing flux). This flux produces eddy currents in the winding and hence losses. These losses could be lessened by narrowing the airgap. On the other hand the existing dimension of the airgap is required to achieve the necessary energy storage capacity of the transformer.

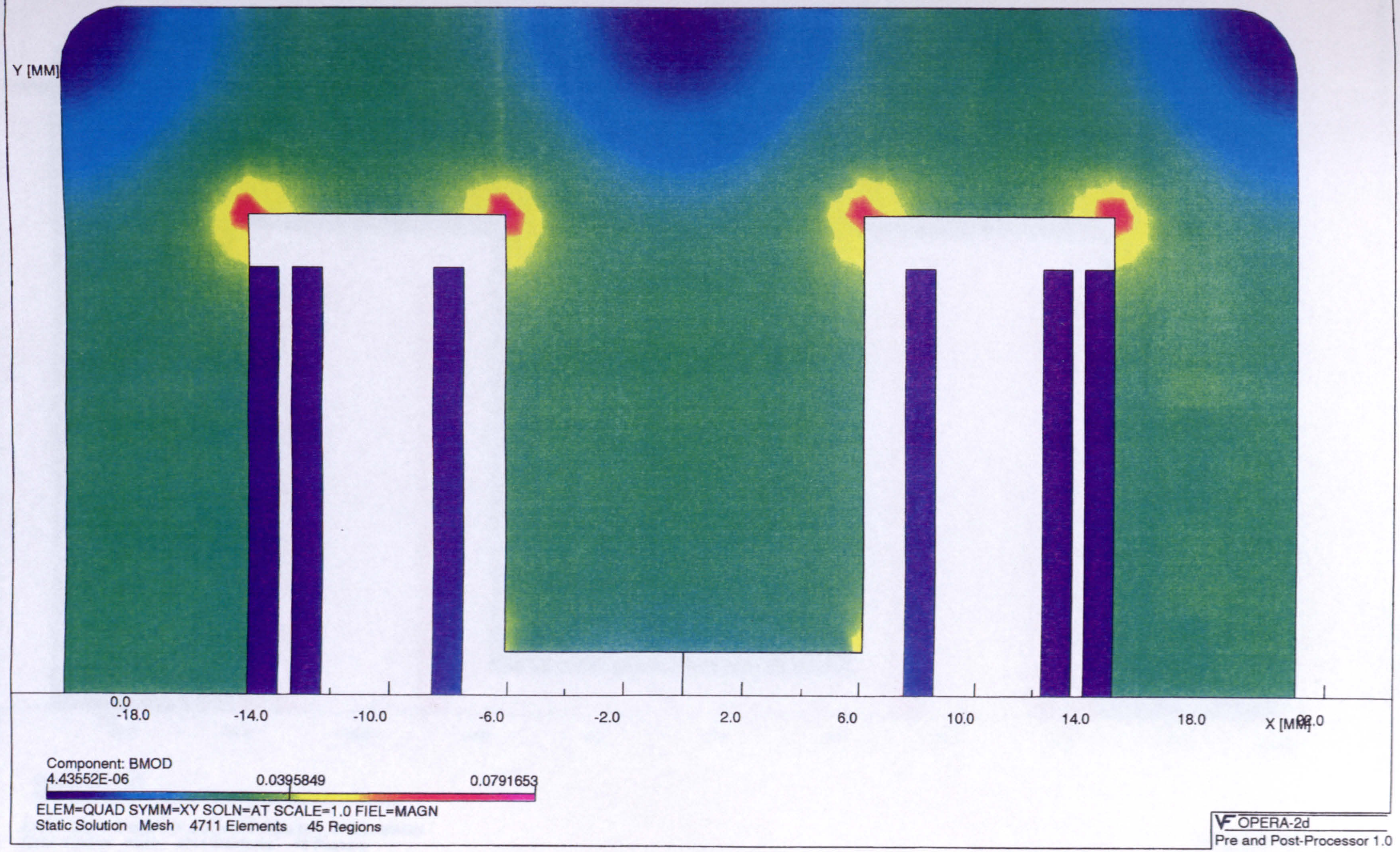

Figure 4.17 Magnetic flux density

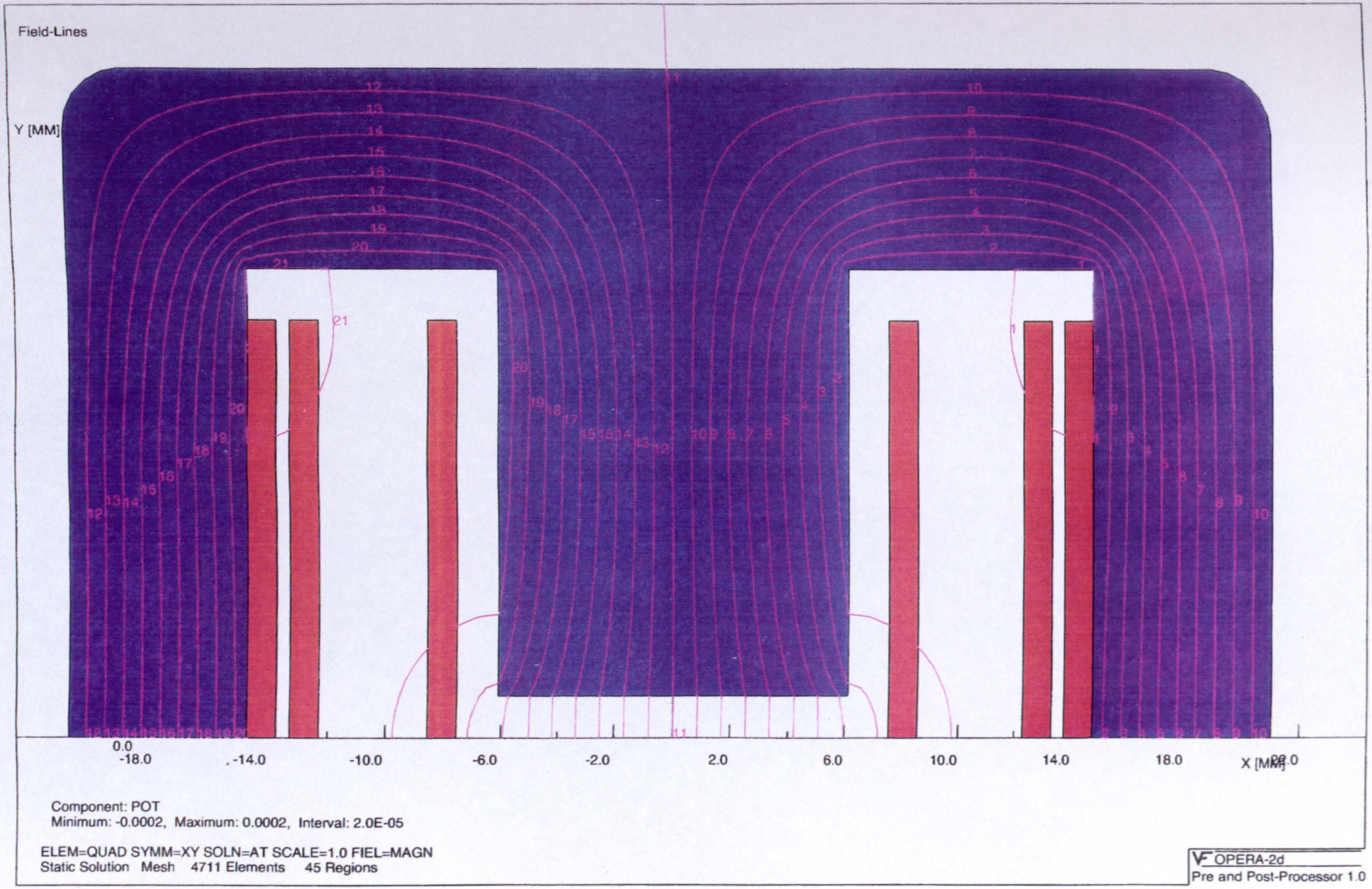

Figure 4.18 Magnetic field-lines

CHAPTER 5

DESIGN AND EXPERIMENTAL RESULTS

The design of a quasi-resonant converter differs in many respects to the design of a pulse-width modulated converter. Due to the high-frequency operation, the position of the components on the circuit board becomes more important. Furthermore the elements have to be chosen to operate within a wide frequency range because these converters are frequency modulated. The design of the *dual converter* is further complicated due to the fact that it uses a multi-winding transformer. Hence, it was necessary to cope with the mutual influence of the windings.

Experiments were undertaken on the basis of the simulation and analytical results obtained in Chapter 4. The choice of the devices to be used, especially the magnetic components which are discussed in Chapter 3, have been reconsidered here. One aim was to verify the theoretical studies of the quasi-resonant converter and the design and analysis tools which have been developed. Even though no hybrid or surface mounted technologies (SMT) were used the practical analysis helped to understand and demonstrate the typical problems related to resonant power supplies. To study the behaviour of high frequency circuits it is necessary to either carry out very complex simulations or, as undertaken in this work, to run additional practical experiments. Influences such as wire material and the quality of mechanical and soldered joints are still very difficult to simulate.

5.1 General

The design procedure of the *dual converter* can be divided into three parts: (a) determination of the circuit parameters of the two quasi-resonant converters including the design of the switches (b) the design of the multi-winding transformer incorporating the two converters and (c) the control aspect.

Several problems arose during the practical work. They can be directly related to the design procedure above. Hence, the determination of the components proved to be difficult because none of the publications in the field of quasi-resonant converters covered the practical aspect in such a way that it would have been of help for the design of the *dual converter.* Therefore a special design routine was developed as illustrated in Figure 5.2 in the following section. The switches have to withstand high voltage stress due to the use of resonant technique. This appeared to be a limiting factor for the design. The multi-winding transformer was manually wound and the exact position of the windings in order to achieve the calculated spacing between them was an exhausting procedure and can never be as accurate as desired. Even though the design was based on the latest experience of the companies which produce special control chips for quasi-resonant converters, the application of the published work to the *dual converter* required additional considerations[25].

A problem that is well known in high frequency applications is the measurement problem. The process of measurement can easily influence the circuits behaviour and therefore produce faulty results or even cause damage to the circuit. Furthermore standard measuring equipment are often not capable of handling the frequencies used. Pins and leads have to be considered in the layout to provide measuring points.

Further problems linked to the location of losses have to be addressed. Simulation (electrical and electro magnetic) was used to find the loss creating components of the circuit. One method that was applied to locate the losses on the circuit board was to measure the temperature of the devices. This method of course is rather inaccurate and difficult to quantify.

---

[25] The author attended several seminars and had direct contact to the design engineers of these companies.

5.1.1 Dimensioning of the Quasi-Resonant Flyback Converter :

Having specified the input and output voltages, the switching frequency and the power rating, the design procedure is aimed at determining the resonant frequency and the voltage rating of the switch to achieve zero-voltage switching.

Figure 5.1 represents a graph of the equation (4.17)

$$V_{CRes}(t) = V_{in} + V_{out} \cdot N + Z_{Res} \cdot I_{\psi} \cdot \sin(\omega t)$$

derived in Chapter 4. The amplitude of the resonant voltage waveform should be such that the voltage across the capacitor/switch should achieve a zero-value as shown, otherwise, as shown by the dotted line the circuit fails to operate in the desired zero-voltage condition. This is mathematically expressed in equation 5.2.

After the selection of the switch there are two alternative approaches to design a quasi-resonant converter as illustrated by Figure 5.2: (1) the design is started by fixing the default switching frequency and thereby the resonant frequency is chosen to be within a range of 1 to 5 times the switching frequency or (2) the design process is started by setting the peak current through the switch.

It become obvious that the amplitude of the voltage across the capacitor should be at least as large as $V_i + N \cdot V_o$ to reach zero again during the oscillating period. In practice Z_R should be chosen at a slightly greater value to operate the transformer with a safe tolerance.

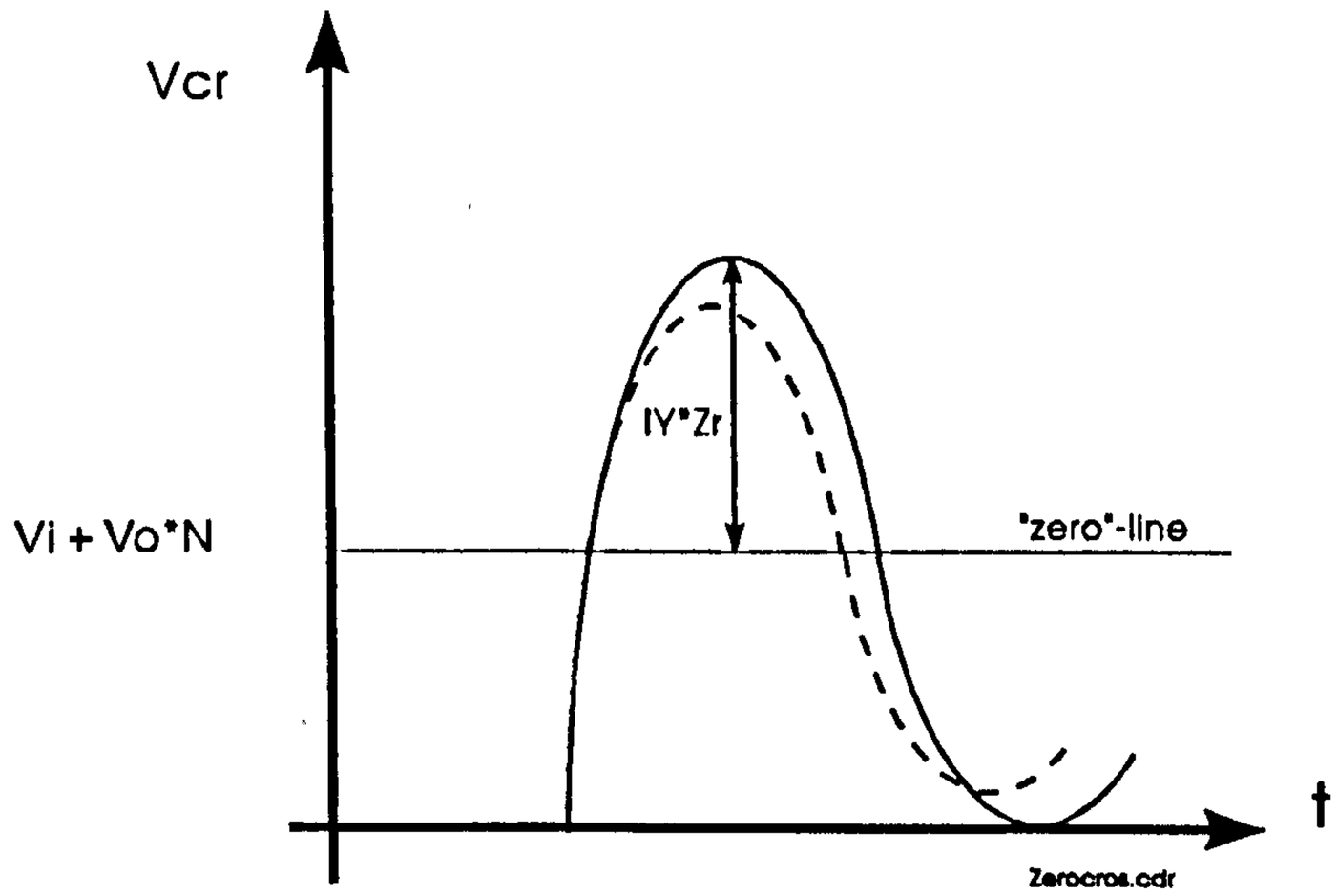

Figure 5.1 Zero-crossing condition

(i) Design procedure via the resonant frequency:

According to the left branch of the flow-chart of the Excel program in Figure 5.2 this procedure starts with the setting of the above mentioned frequency ratio f_s/f_r. Hence, the value of $\beta\left(=R/Z_R\right)$ results from the charts in Figure 4.9 and Figure 4.10 (section 4.1.1). Z_R is therefore determined by

$$Z_R = \frac{R}{\beta} \tag{5.1}$$

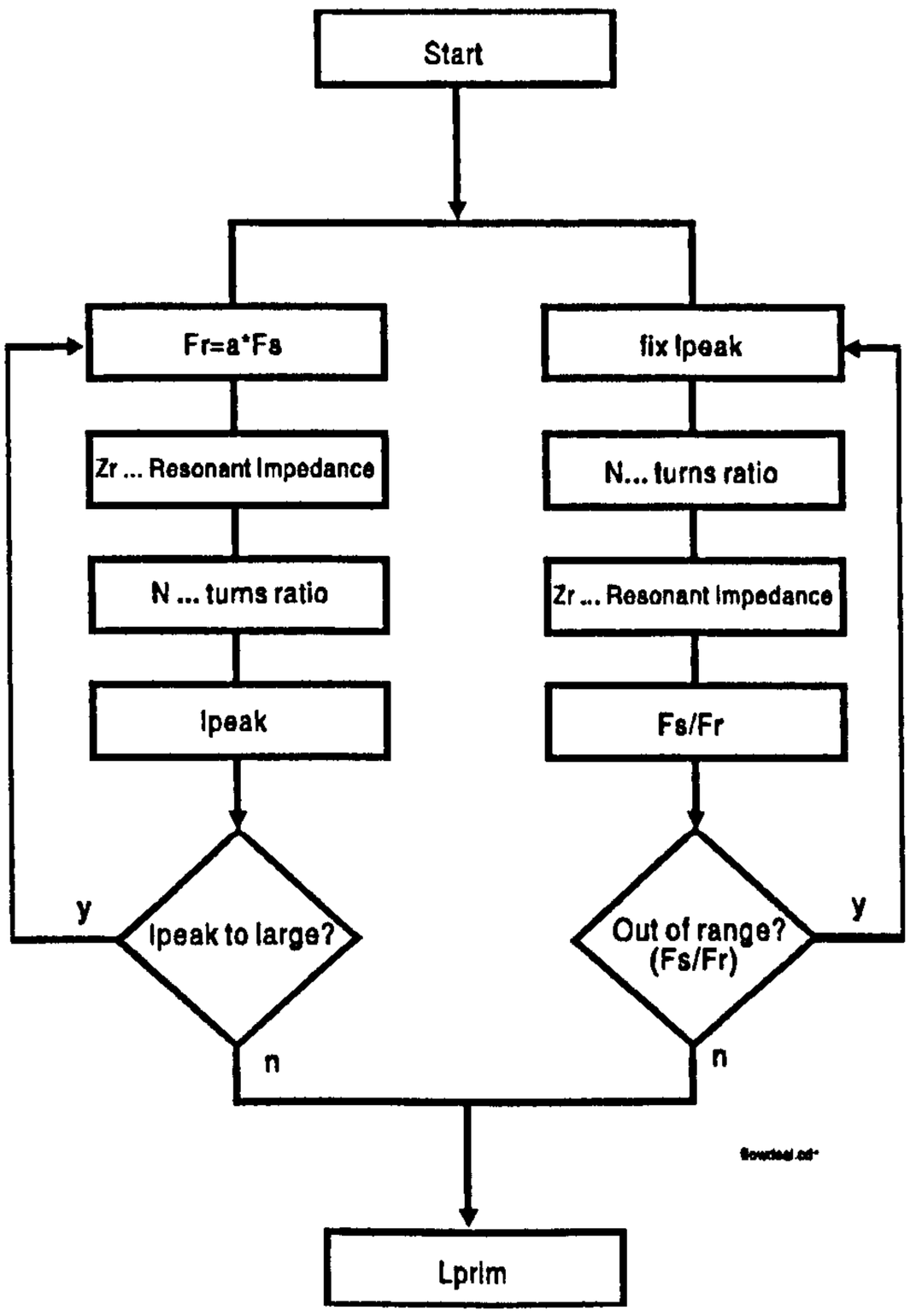

Figure 5.2 Flow-chart of the design program for a quasi-resonant flyback converter

Knowing the resonant impedance the turnsratio of the converter can be calculated. Starting with the zero-crossing condition and rearranging this equation Z_R can be determined.

$$Z_R \cdot I_\psi > (V_{in} + N \cdot V_{out}) \tag{5.2}$$

$$Z_R > \frac{(V_{in} + N \cdot V_{out})}{I_\psi} \tag{5.2.1}$$

Using equation (4.50) $\frac{V_{out}}{N \cdot V_{in} \cdot R} = \frac{I_\psi}{(V_{in} + N \cdot V_{out})}$, I_ψ can be derived as

$$I_{\psi} = \frac{V_{out}(V_{in} + N \cdot V_{out})}{V_{in} \cdot N \cdot R} \tag{5.3}$$

Substituting (5.2) into (5.3) leads to:

$$Z_R > \frac{V_{in} \cdot N \cdot R}{V_{out}} \tag{5.4}$$

Furthermore R can be substituted from:

$$R = \frac{V_{out}^2}{P_{out}} \tag{5.5}$$

leading to:

$$Z_R > \frac{V_{in} \cdot N \cdot V_{out}}{P_{out}} \tag{5.6}$$

Therefore, the turnsratio is given by

$$N < \frac{Z_R \cdot P_o}{V_i \cdot V_o} \tag{5.7}$$

The maximum current can be predicted using an equation derived from (5.3)

$$I_{\psi} = \frac{V_{out}(\frac{1}{N} + \frac{V_{out}}{V_{in}})}{R} \tag{5.8}$$

The resonant tank elements result from the above calculations (see Appendix A).

(ii) Design procedure via the maximum current:

This design method is represented by the branch on the right hand side of Figure 5.2. The maximum current through the primary winding of the transformer and hence through the switch has to be set in the first step of the design. This can be achieved according to the current rating of the selected/available MOSFET. Alternatively, the maximum possible current density can be taken as the limiting parameter. For a given turns ratio N of the transformer the maximum current I_{ψ} in the primary winding can be determined. To ensure a zero-crossing the voltage across the switch and hence switching with no losses a safety margin of 20% is added to the value calculated from equation (5.6). Consequently, β can be determined. The resonant frequency can then be calculated with the rearranged equation (4.56).

$$E = \frac{1}{\frac{f_s}{\omega}\left[\alpha - \frac{\beta \cdot N}{2 \cdot E} + \frac{E \cdot (1 - \cos\alpha)}{\beta \cdot N}\right]} - 1 \qquad (5.9)$$

Thus the elements of the resonant tank can be determined from the following equations.

$$L_R = \frac{Z_R}{2 \cdot \pi \cdot f_R} \qquad (5.10)$$

$$C_R = \frac{1}{2 \cdot \pi \cdot f_R \cdot Z_R} \qquad (5.11)$$

Both approaches were investigated and the results were compared. For both these procedures the aim is to determine the transformer inductances and the size of the airgap.

(iii) Calculation of the transformer inductance:

The value of the primary and the secondary inductance influences the ripple on the output current of the transformer. Where small inductances would allow small transformers, large inductances lead to smooth output currents. Therefore, the determination of the inductance values represents a compromise.

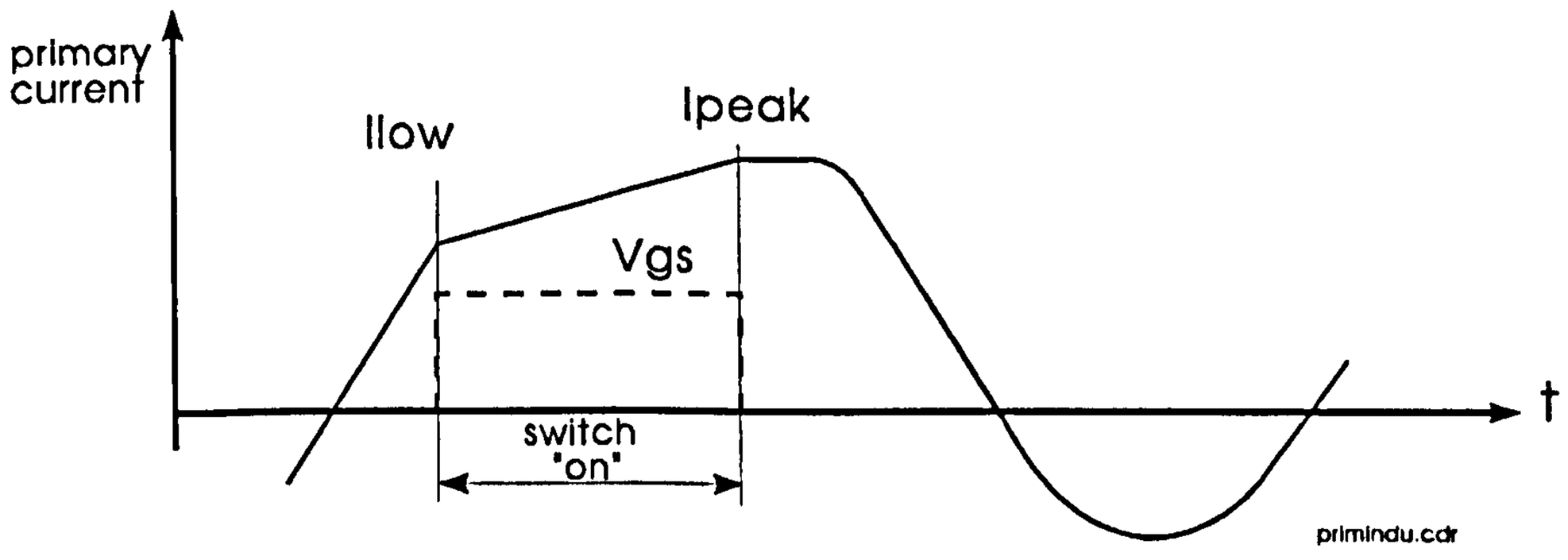

Figure 5.3 Current through the primary inductance

From the general energy equation $E = \frac{1}{2} \cdot L \cdot I^2$ the specific equation to determine the primary inductance can be derived:

$$L_{prim} = \frac{P \cdot 2 \cdot T_s \cdot D}{I_{peak}^2 - I_{low}^2} \qquad (5.12)$$

where the difference between I_{peak} and I_{low} as illustrated in Figure 5.3, is a measurement for the converter quality.

(iv) The airgap:

Additionally, the airgap of the core has to be dimensioned. As it will be shown below the energy is stored in the magnetic core of the transformer and herein mainly in the airgap during the energy transfer from the primary to the secondary side. Hence, it is important to define a suitable airgap. The two limiting factors are that too small an airgap would result in saturation of the magnetic core of the transformer but on the other hand with a too large airgap the stray effects and therefore the losses would increase significantly.

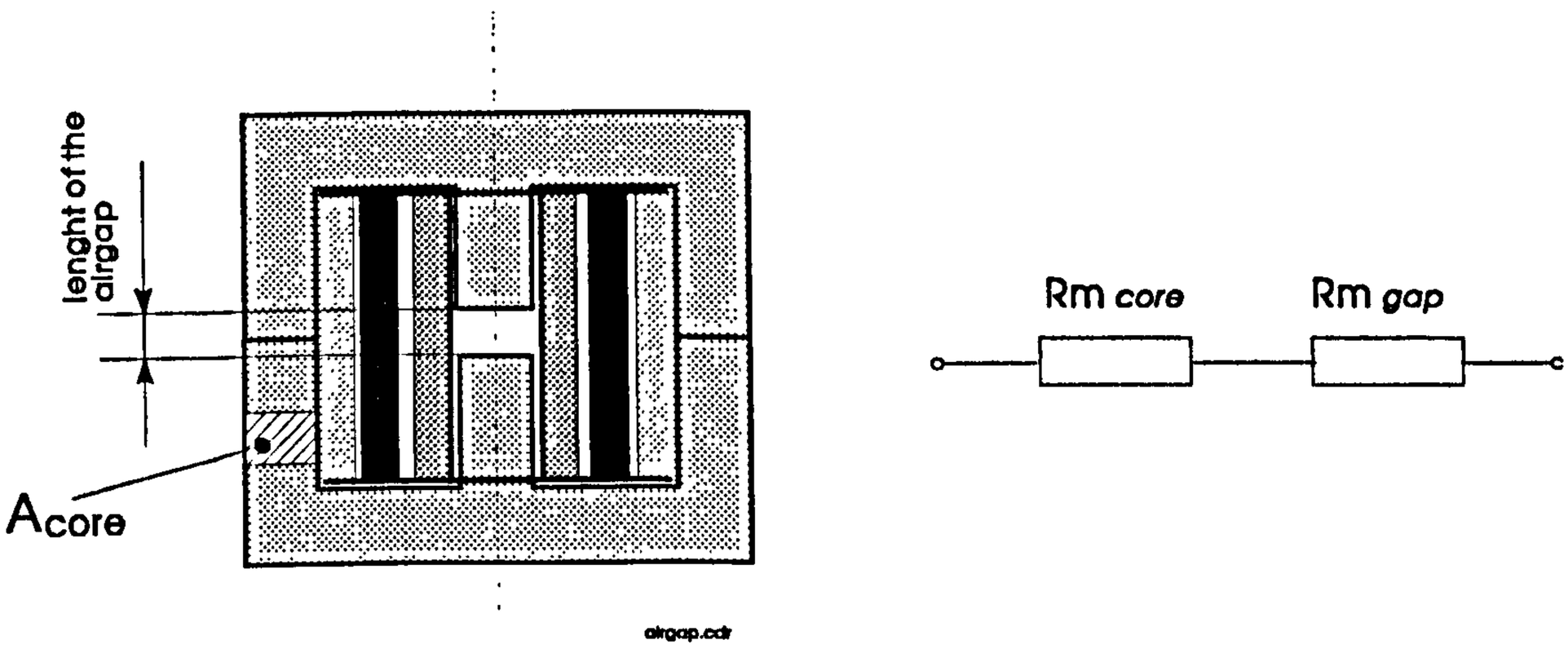

Figure 5.4 *(a) core configuration and (b) related reluctance model*

The reluctance of a the magnetic circuit is represented by a series link of the core's reluctance and the airgap's reluctance in Figure 5.3 (b):

Ferro-magnetic reluctance:

$$R_{Mc} = \frac{l_c}{\mu_R \cdot \mu_0 \cdot A_c} \qquad (5.13)$$

Airgap reluctance:

$$R_{Mg} = \frac{l_{gap}}{\mu_0 \cdot A_c} \text{ (with } \mu_R \cong 1) \tag{5.14}$$

Total reluctance:

$$R_{Mtot} = \frac{l_c}{\mu_R \cdot \mu_0 \cdot A_c} + \frac{l_{gap}}{\mu_0 \cdot A_g} \tag{5.15}$$

With the fundamental equation

$$\Theta = \Phi \cdot R_{Mtot} \tag{5.16}$$

and by replacing R_{Mtot} (equation (5.15)

$$\Theta = \Phi\left(\frac{l_c}{\mu_R \cdot \mu_0 \cdot A_c} + \frac{l_{gap}}{\mu_0 \cdot A_g}\right) \tag{5.17}$$

rearranged and with $A_c \cong A_g \cong A$

$$\Theta = \frac{\Phi \cdot l_{gap}}{\mu_0 \cdot A}\left(\frac{l_c}{\mu_R \cdot l_g} + 1\right) \tag{5.18}$$

By examining the above equation it becomes obvious that for "large" airgaps, hence $\frac{l_c}{l_g} << \mu_R$ [26] equation 5.16 may be written as:

$$\Theta \cong \Phi \cdot R_g = \frac{\Phi \cdot l_{gap}}{\mu_0 \cdot A} \tag{5.19}$$

The energy in the magnetic circuit is generally given by

$$W_{mag} = \int_0^{\Phi} (I \cdot N) d\Phi \tag{5.20}$$

or

$$W_{mag} = \tfrac{1}{2} \cdot I \cdot N \cdot \Phi \tag{5.21}$$

Using equation (5.19) this becomes

---

[26] modern ferromagnetic materials have μ_R value of approximately 2000 up to 3000.

$$W_{mag} = \frac{1}{2} \cdot \frac{I \cdot N \cdot \Theta}{R_{Mg}} \qquad (5.22)$$

This demonstrates that for transformers with "large" airgaps their energy storage capacity is determined by the reluctance of the airgap rather than by the reluctance of the core. The standard equation (5.23) for calculating the primary inductance,

$$L = \mu_0 \cdot \mu_R \cdot A \cdot \frac{N^2}{l_{fe}} \qquad (5.23)$$

can be given as:

$$L = \mu_0 \cdot \mu_R \cdot A \cdot \frac{N^2}{l_{gap}} \qquad (5.23.1)$$

Therefore the airgap length can be determined.

$$l_{gap} = \frac{A \cdot \mu_R \cdot \mu_0 \cdot N^2}{L_{prim}}$$ (μ_R=1 within the airgap).

(v) Leakage inductance used as resonant inductance:

The realisation of the theoretical consideration of section 3.2.3.2 is given below. Equation 3.10 ($L_{Leak} = \frac{\mu_0 \cdot \mu_r \cdot N^2 \cdot (MTL \cdot S)}{W_W}$ section 3.2.3.2) was rearranged to calculate the required spacing between the windings for the desired resonant inductance.

$$S = \frac{L_{Leak} \cdot W_W}{\mu_0 \cdot \mu_r \cdot N^2 \cdot MTL} \qquad (5.24)$$

Therefore, the spacing between the secondary and the primary winding 1 (mains input), as well as the spacing between the secondary and the primary winding 2 (battery input) can be calculated.

$$S_1 = \frac{L_{Leak1} \cdot W_W}{\mu_0 \cdot \mu_r \cdot N_1^2 \cdot MTL_1}$$

$$S_2 = \frac{L_{Leak2} \cdot W_W}{\mu_0 \cdot \mu_r \cdot N_2^2 \cdot MTL_2}$$

with the resonant inductances L_{r1}=7.87 μH and L_{r2}=2.36μH and the data from the core the spacing is determined as follows:

$$S_1 = \frac{7.67\mu H \cdot 0.0296m}{4 \cdot \pi \cdot 10^{-7} \cdot 12^2 \cdot 0.115m} = 0.0109m = 10.9mm$$

$$S_2 = \frac{2.36\mu H \cdot 0.0296m}{4 \cdot \pi \cdot 10^{-7} \cdot 12^2 \cdot 0.09m} = 0.0043m = 4.3mm$$

By relating these data to the core data it can be observed that there is not enough room for the spacing S_1. An alternative would be to use a larger core, hence to gain space for the required winding spacing. This of course, defeats the purpose of reducing the size of the transformer. Therefore, only the spacing S_2 for the stand-by source could be realised in order to replace the resonant inductor.

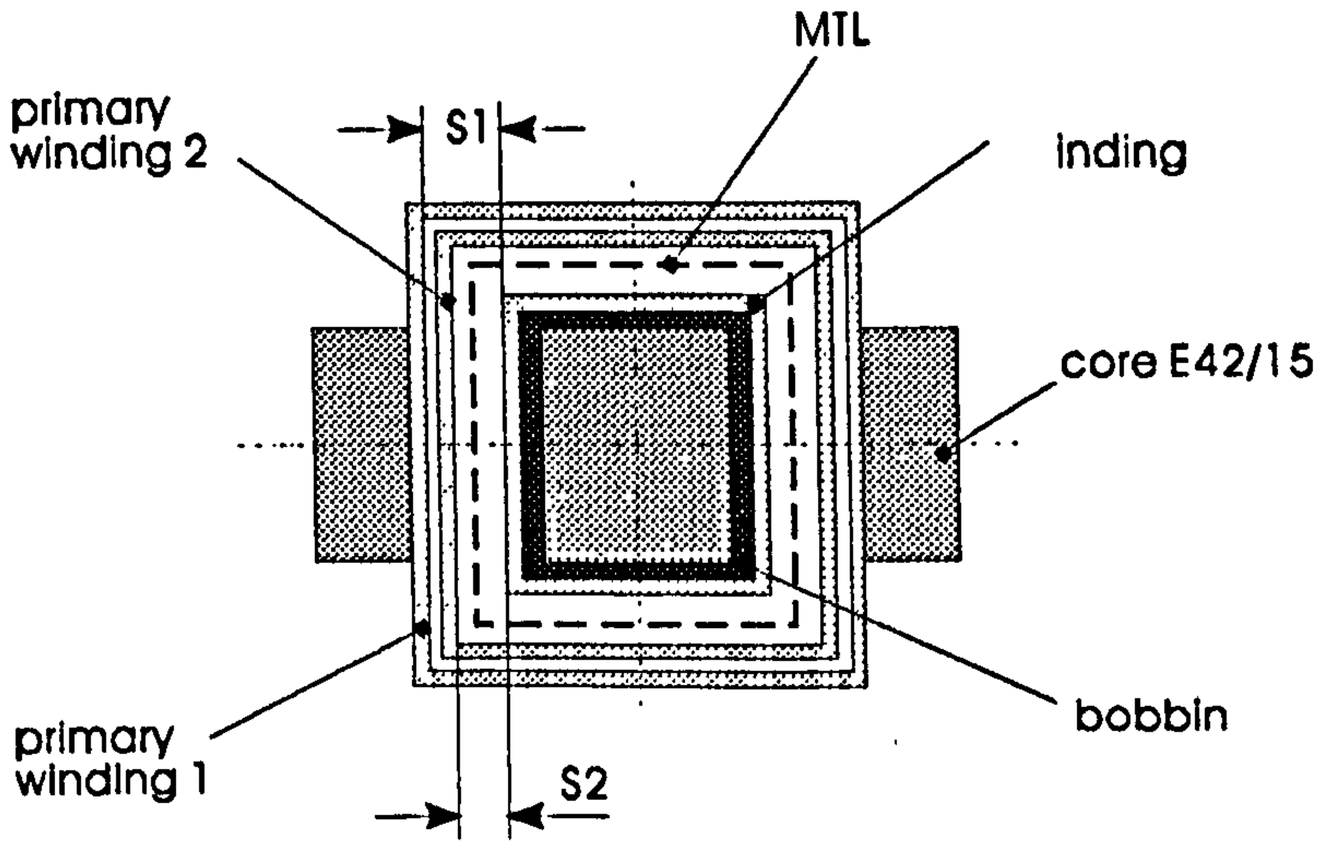

Figure 5.5 *Winding spacing*

The leakage inductance field is a cylindrical area between the windings, which equals the mean length of a turn, *MTL*, multiplied by the separation, *S*, between the windings. The field actually extends into each winding. As an approximation, the effective separation between the windings includes 1/3 of the height of each winding [Dix93]. Hence, S_2 has to be slightly reduced to:

$$S2' = S2 - 2 \cdot (1/3 \cdot 1mm) = 4.3mm - 0.6mm = 3.7mm \qquad (5.25)$$

5.1.2 Snubber

The two MOSFETs of the *dual converter* are operated in a resonant fashion. However, this is not true for the output diode and hence large voltage spikes may lead to the possible destruction of the device.

The leakage inductance L_{leak2} and the junction capacitance C_{junc} of the Schottky rectifier diode D_o in Figure 5.6 form a tuned circuit at turn off.

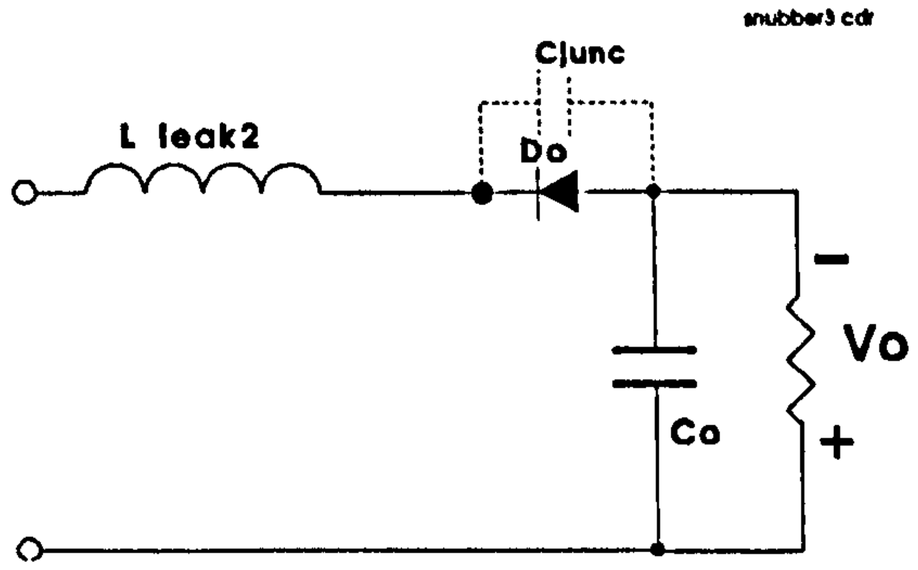

Figure 5.6 Output configuration with resonating circuit

This circuit introduces transient overvoltage ringing as shown in Figure 5.7 (a). The amplitude of this ringing may be high enough to exceed the blocking capability of the Schottky rectifiers, driving them to destruction during the turn-off period of the diode. The addition of RC-snubber networks as shown in Figure 5.8 will suppress this ringing to a safe amplitude (see Figure 5.7 (b)).

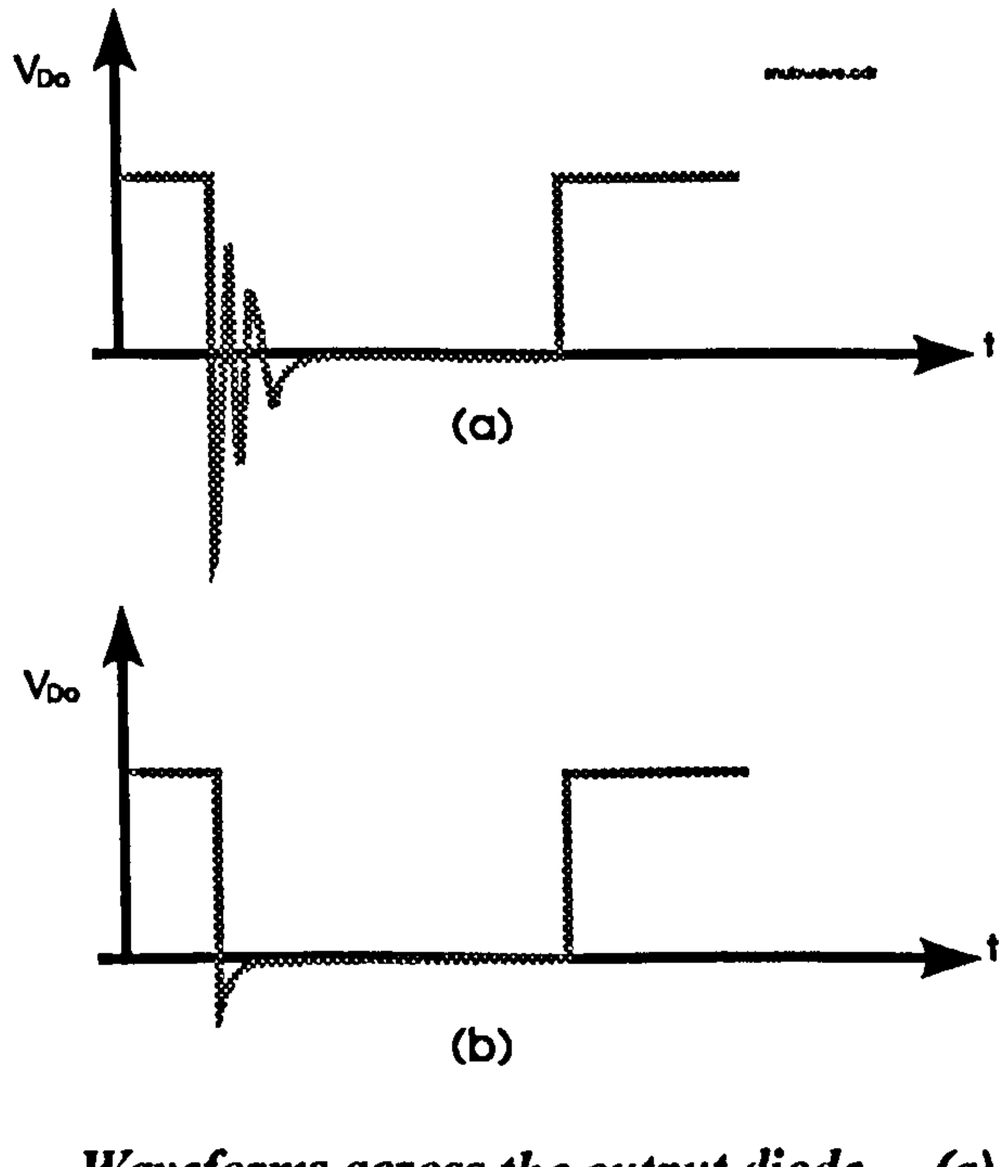

Figure 5.7 Waveforms across the output diode (a) without snubber (b) with snubber

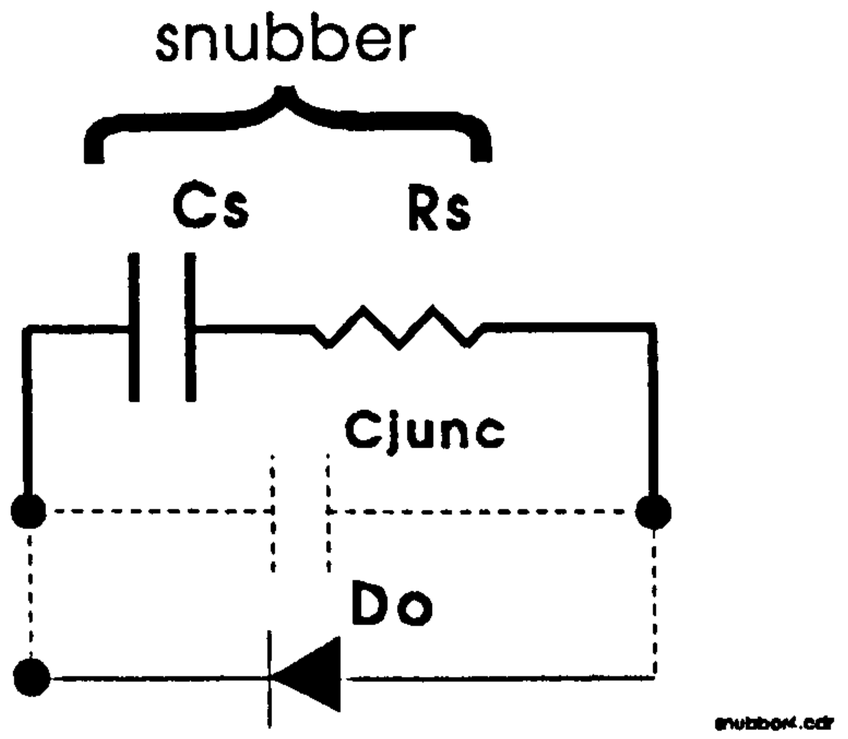

Figure 5.8 RC-snubber circuit

The ringing frequency of the output voltage V_{out} is given by

$$\omega = \frac{1}{\sqrt{L_{leak2} \cdot (C_s + C_{junc})}} \tag{5.26}$$

Hence, it is necessary to chose the capacitor C_s in order to lower the frequency. The resistor R_s is responsible for the damping of the voltage across the diode. A compromise has to be made in order to either keep the power dissipation within the snubber low or to reduce the peak voltage. A low peak voltage requires a larger snubber capacitor. This large snubber capacitor results in higher power dissipation within the snubber resistor.

Experiments were carried out on the output diode of the dual converter to find the optimum values for R_s and C_s.. Table 5.1 shows the results of this test series. Special attention should be given to number 3,4 and 8 (highlighted). It becomes apparent that the output power is influenced by the resistor. The resistor used in number 9 dissipates a large amount of energy. The highest output power level is achieved with the smallest resistor in number 3.

No.	R_s [Ω]	C_s [nF]	V_o [V]	I_o [A]	P_o [W]
1	1	1	8.6	2.8	24.08
2	1.80	2.2	8.8	3	26.4
3	1.8	4.7	9.2	3.2	29.44
4	2.7	4.7	8.9	3.1	27.59
5	1	1	8.5	2.9	24.65
6	-	1	8.6	2.8	24.08
7	0.2	1	-	-	-
8	4.7	1	8.7	2.7	23.49
9	27	1	8.7	2.8	24.36
10	-	-	8.4	2.5	21
11	1	2.2	8.8	3.1	27.28
12	1	4.4	8.55	2.9	24.795

Table 5.1 Test series to determine the optimum snubber configuration

On the other hand the damping of the voltage amplitude is rather poor if a snubber according to no. 3 is used, whereas the damping effect of the snubber in number 9 appears far better.

The oscilloscope curves of the three highlighted snubber combinations of table 5.1 are given in Figure 5.9.

Note that for the first two graphs (no. 3 and 4 of table 5.1) the ringing frequency is almost the same (the same capacitors were used), whereas in the last graph the automatic calculation of a frequency between the two cursors of the oscilloscope failed, because it could not detect any periodic ringing within the first voltage cycle. Furthermore, it becomes obvious how the damping amplitude is influenced by the resistor.

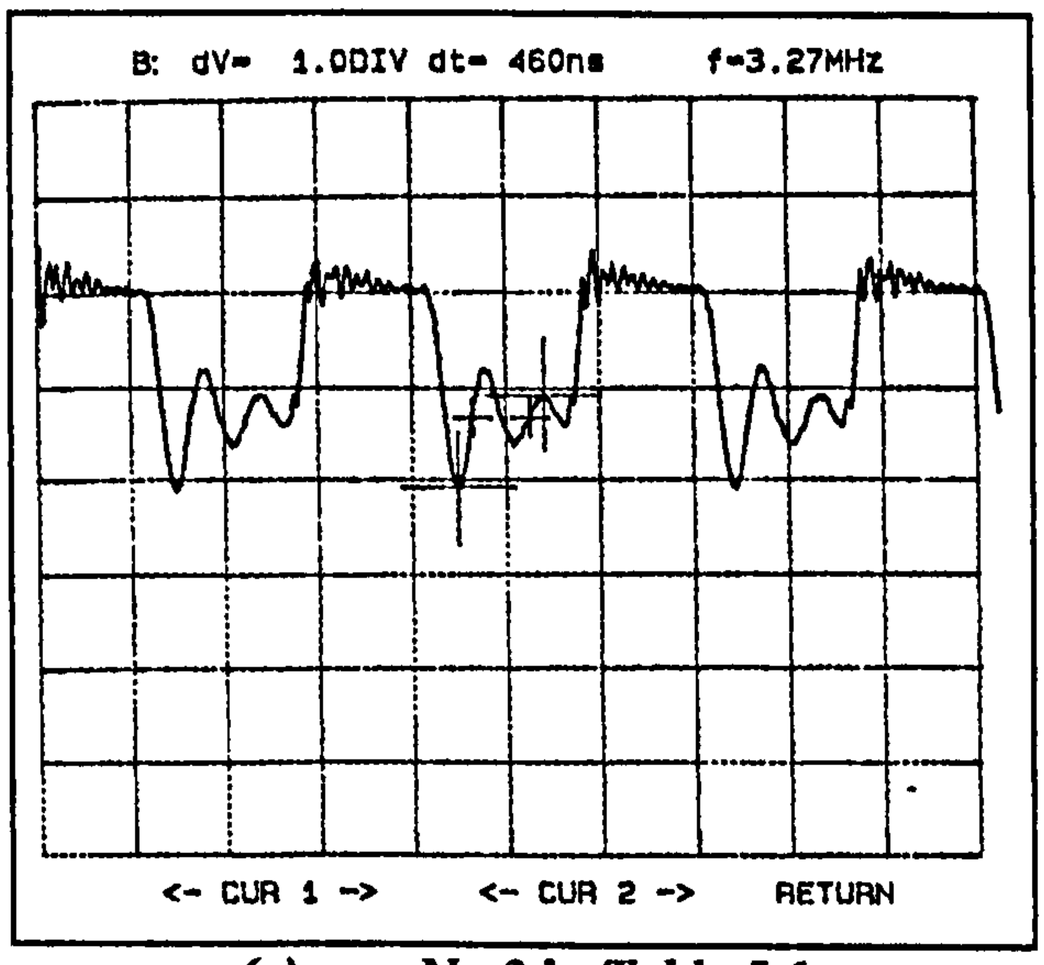

(a) No.3 in Table 5.1

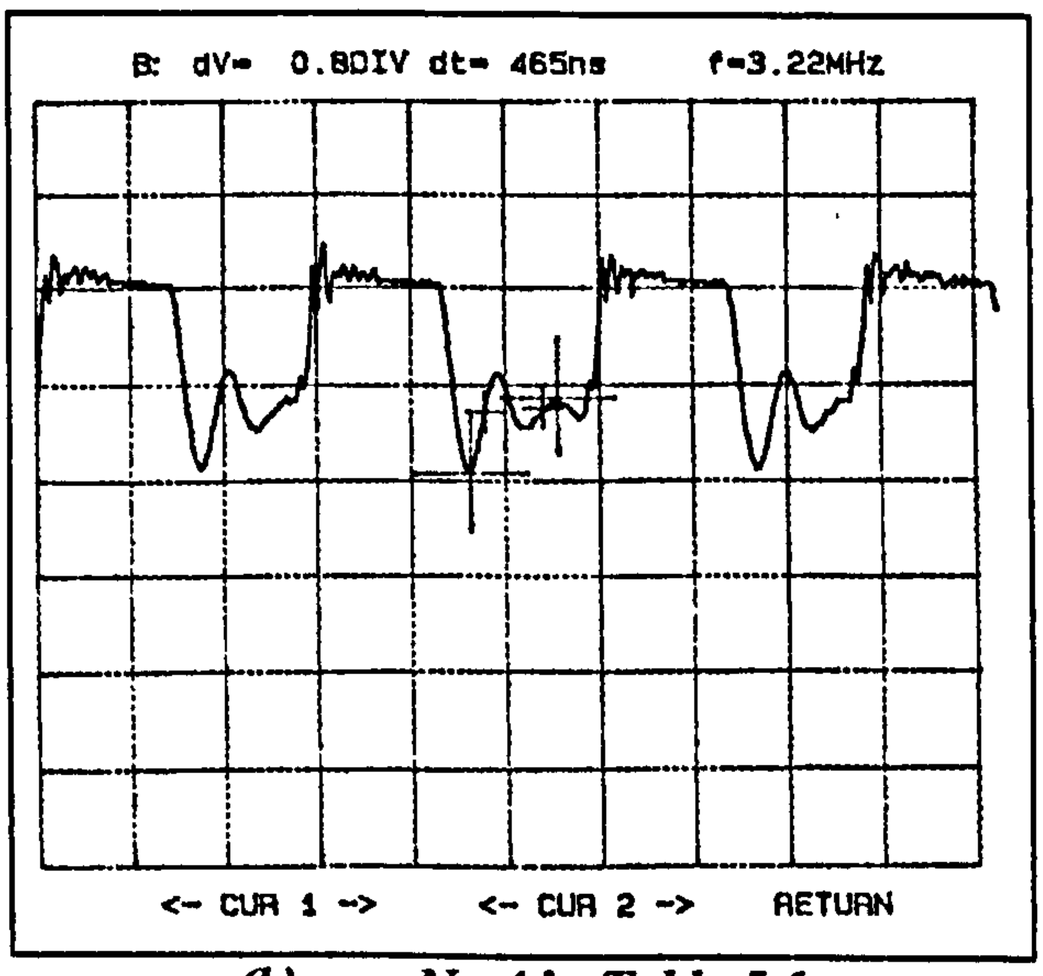

(b) No.4 in Table 5.1

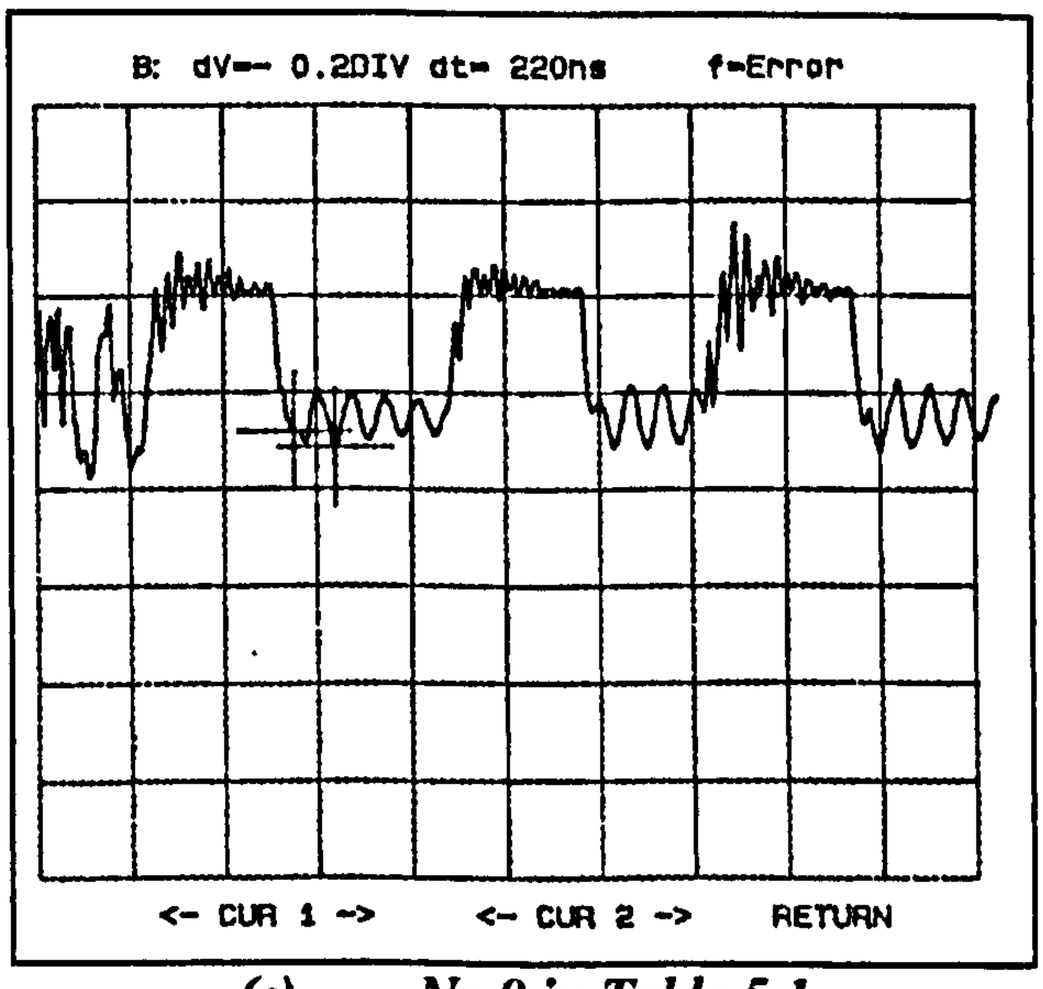

(c) No.9 in Table 5.1

Figure 5.9 voltage wave forms of RC-snubber circuits

5.1.3 The Control Circuit

The most common control methods used for regulation of resonant converters are based on frequency modulation (in contrast to pulse width modulation used for standard converters). This modulation method can be further divided into two groups. The first consists of those converters utilising frequency-modulation with a fixed on-time, also referred to as "off-pulse-density modulation". Converters belonging to the second group use frequency modulation with a fixed off-time ("on-pulse-density modulation")[27].

Some semiconductor manufacturers have now produced integrated controller devices suitable to form the basis for practical realisation of either of the modulation schemes mentioned above [Row90]. Additionally, they provide other functions that conventional integrated pulse-width-modulation controllers also provide, useful in practical converter design, such as integrated error amplifiers and voltage reference sources. In table 5.2 an overview of such controllers is given.

For this project the Controller UC3864 from Unitrode Integrated Circuit Corporation was chosen of which a diagram is given in Figure 5.10. This controllers is optimised for zero-voltage switched quasi-resonant converters as required for the proposed *dual converter*. Each input source of the *dual converter* requires a separate controller (one for the mains input and one for the stand-by battery).

---

[27]see section 3.2.2

Controller	Manufacturer	max. switching frequency	special functions
GP405	Gennum corporation	1MHz	-
CS360	Cherry Semiconductors	1MHz	Programmable min/max frequencies
CS361	Cherry Semiconductors	2MHz	latched over-current protection
MC34066	Motorola Inc.	1MHz	-
UC X860	Unitrode	3MHz	Programmable One shot timer Dual 2A peak totem pole outputs
UCX86X family	Unitrode	1MHz	Zero-crossing terminated one shot timer

Table 5.2 controller overview

The primary control blocks implemented include an error amplifier to compensate the overall system loop and to drive a voltage controlled oscillator (VCO), featuring programmable minimum and maximum frequencies. Triggered by the VCO, the one-shot generates pulses of a programmed maximum width, which can be modulated by the zero detection comparator (Zero pin). The author modified this control method by replacing the fixed resistor with a potentiometer in order to enable a flexible change of the lower switching frequency. This circuit facilitates "true" zero-voltage switching over various line, load, and temperature changes, and is also able to accommodate the resonant components' initial tolerance.

The fault comparator serves normally to detect fault conditions and set a latch while forcing the output drivers low [Uni90a]. This function was utilised in order to control the two inputs. An external operation amplifier (LM311) was applied as a comparator. In case the mains voltage drops under a pre-set level this comparator gives a high signal to the fault pin of the controller of the mains input, hence shuts down its output drivers (OUTA and OUTB in Figure

5.10). At the same time the high signal to the fault pin of the controller of the stand-by source is withdrawn and enables battery to power the load.

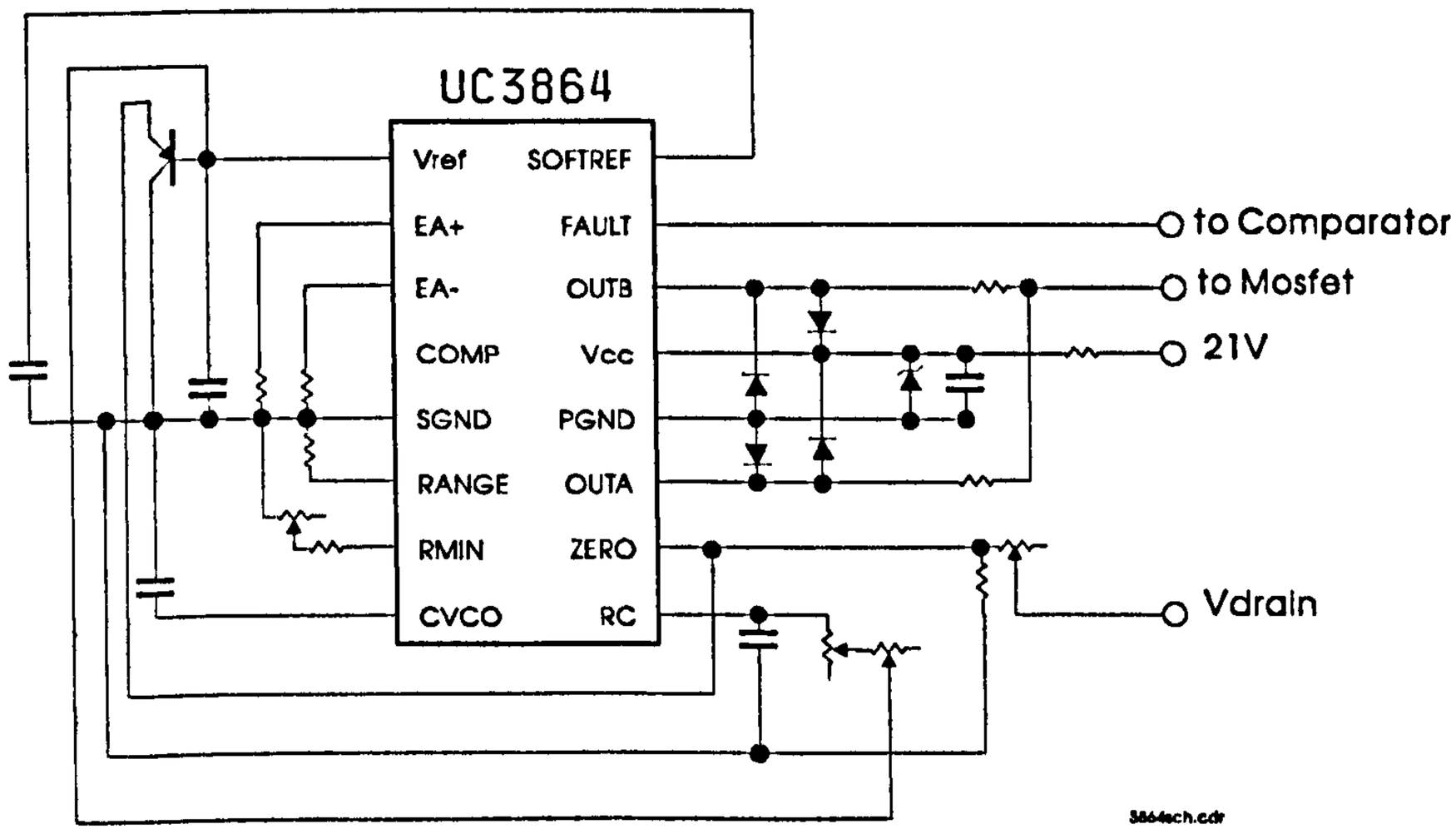

Figure 5.10 Controller UC3864

To avoid a hiccup behaviour an additional function had to be implemented in the control block of the comparator.

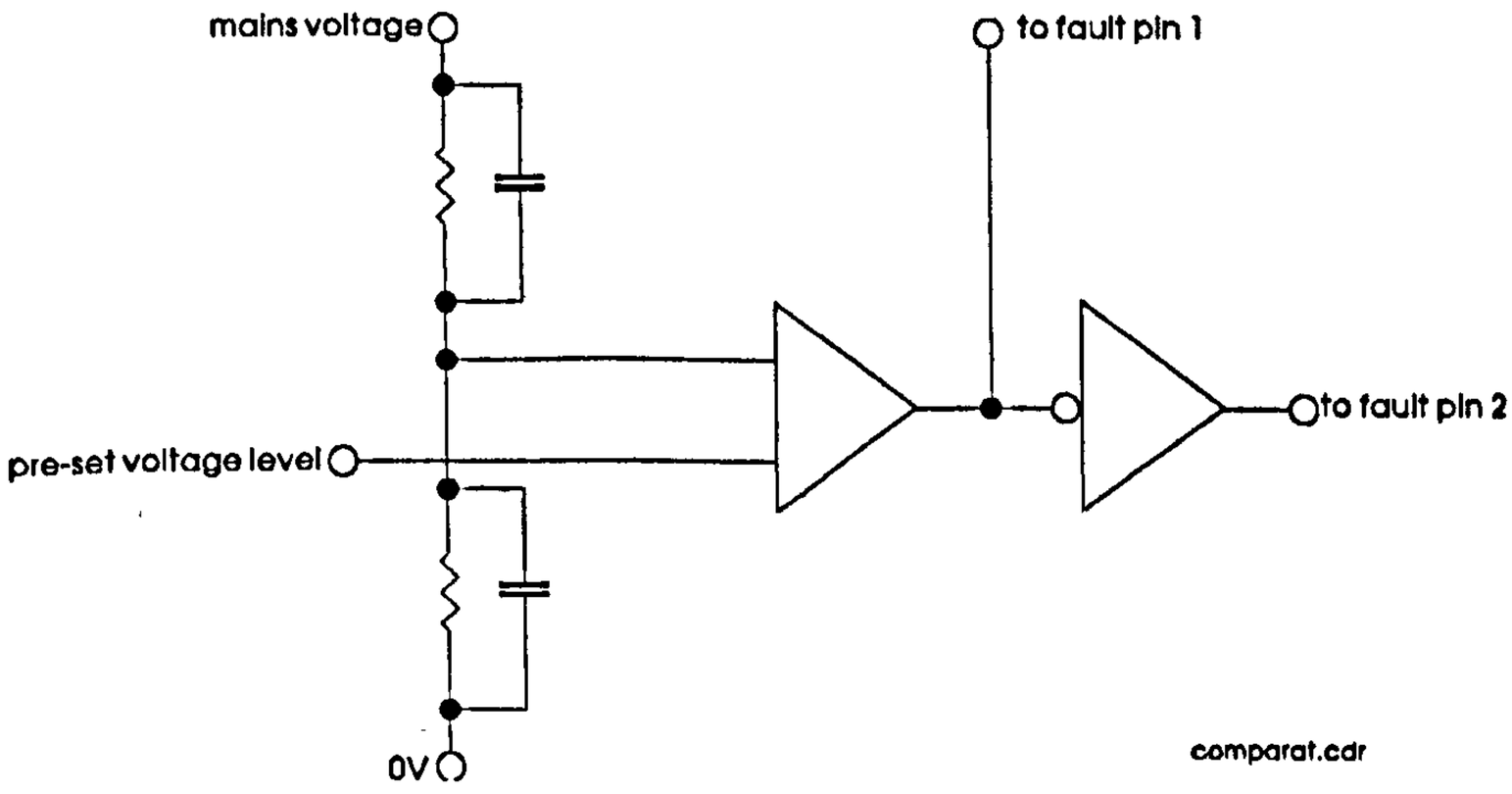

Figure 5.11 functional connection of the comparator

One possibility would have been to use different voltage levels at which the mains voltage is switch on and off, hence introducing a voltage hysteresis. A less complex solution was used for this project. By placing a capacitor in parallel to the resistor (Figure 5.11) a time hysteresis is achieved and the mains voltage appears more stable to the comparator.

5.2 Experimental Results

The ideal technology to build a high frequency resonant converter would be surface mount incorporating flat magnetic components. However, to assess the proposed *dual converter* it was decided to use a printed circuit board approach because of the easy availability of the appropriated facilities at Brunel University and at Fachhochschule Esslingen. Also a printed circuit board approach provides the flexibility necessary to test different layouts easily at very low cost and within a very short time.

The power and voltage levels were selected to be 50 watts and 50 volts respectively. This limitation made it possible to rely on standard components; for example the voltage stress on the Mosfet would not exceed some hundred volts. The effects resulting from these restrictions were carefully examined. With the support of simulation the problems occurring with higher power and higher voltage rating could be estimated. By using higher power ratings, thermal problems would significantly increase.

Serious measurement errors can appear due to the high operating frequencies of up to 1MHz used with the resonant converter through the measuring instrument. Hence, it is necessary to take these errors into account or, if

possible, to compensate for them [Schl93][1]. One type of measurement error originates in the delay and damping caused by the measuring element itself. The currents are usually measured either by a probe-resistor or a Hall-effect current sensor. In the later measurement errors occur due to the magnetic reversal inside the iron core of the sensor. The errors in the digital oscilloscopes however can be neglected. Beside the "static" factors it is necessary to take effects such as temperature, magnetic fields and electric fields into account which can be transferred from the object to be measured to the sensor. It is essential to use shielded cables and to keep them as short as possible.

Concept of the set-up:

Several different set-ups of circuit boards were designed and built in the course of the project. The final set-up consists of three boards: two control boards and one power board. The layout of this set-up configuration is shown in Appendix C and in Appendix E (prints). The power board as given in Figure 5.11 was designed to achieve highest flexibility in respect of exchanging the major components of the circuit such as the transformer, its core, the resonant inductances, the rectifying diode including the snubber. These parts are connected to the printed circuit board via screwed joints rather than soldered joints. Screwed joints could influence the behaviour of the converter and cause distortion. Therefore, the power board was tested and compared to an older version (with soldered joints) using the same components. Thus the effect of the screwed joints could be examined and taken into account.

---

[1]Manfred Schlenk did essential work in this field and published it in his Dr.-Ing. dissertation: "Ein Serienresonanzumrichter in Halbbrückenschaltung mit kombinierter serieller und paralleler Lastauskopplung und mehereen Ausgangskreisen" at the Technische Universität Berlin 1993.

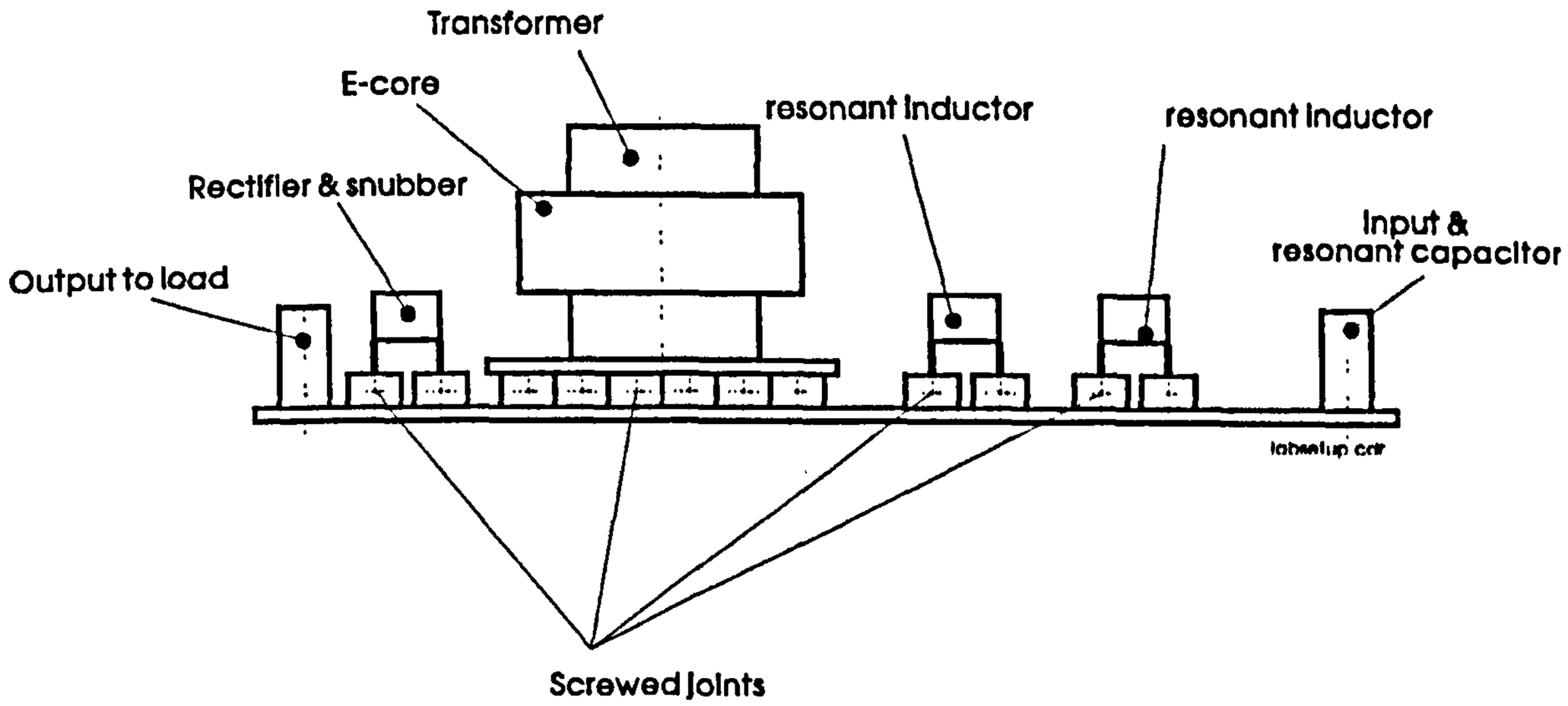

Figure 5.11 Set-up of the experimental board

Transformer:

The transformer as the core part of the *dual converter* was theoretically examined. It was tried to design the spacing between the windings to achieve the desired leakage inductance and hence eliminate the need for an additional physical resonant inductance (see Chapter 3.2.3.2). The difficulties related to the winding and spacing between the windings have already been addressed in the introduction of this Chapter. A number of bobbins were wounded with either Litz-wires or flat copper leads. The spacing between the windings was varied. The bobbins were soldered on special interface boards (see Appendix E) which then could be screwed onto the main board. The different cores with different gap widths were combined with these bobbins. In the tables in Appendix B the various bobbin-core combinations are listed. The third column of these tables gives the configuration of the windings. To lower the leakage inductance some of the windings were split. It is also listed if flat wire material was used. The pin numbers refer to either the bobbin or the interface board

(roman numbers). All the transformers used were examined in respect to their leakage inductance. The results are also listed in the Appendix B.

Capacitor:

To enable an easy adjustment of the resonant capacitor a decade capacitor bank was built. Even though the bank did not show precisely the same behaviour as a single capacitor, due to the leads and several mechanical joints, it allowed a first estimation of the required value. To run the circuit accurately the determined resonant capacitor was inserted as a discrete component.

Test series:

The two converters make up which the *dual converter* were tested separately. The 50V input was linked to one primary winding, while the second (24V) input was kept in the off-position. This process was carried out alternatively to test the other input. The switching frequency and the pulse widths were pre-set to the calculated values and if necessary adjusted to achieve true zero switching conditions. The *most significant* results are demonstrated in the table 5.3 .

No.	V_i	V_a	I_i	I_a	P_i	P_o	$\rho = P_o/P_i$	$V_{R\ max}$	f_s	t_{on}
4	50	7.3	0.6	2.63	30	19.20	0.64	204	709	1.42
13	54	10.38	1.25	5.7	67.5	59.17	0.87	252	526	0.96
14	42	12	1.5	3.8	63	45.6	0.72	236	429	1.42
19	18	7.9	1.7	2.3	30.6	18.17	0.59	135	495	1.52
20	18.37	6.27	1.2	2.26	22.04	14.17	0.64	112	515	1.22
21	21.22	7.09	1.4	2.66	29.7	18.86	0.64	132	487	1.08
22	17.75	6.33	1.5	2.35	26.58	14.88	0.56	130	510	1.2
23	18.29	6.65	1.4	2.49	25.6	16.56	0.67	120	606	1.28
24	17.56	6.29	1.15	2.24	20.19	14.08	0.70	120	529	1.09
25	17.56	6.16	1.1	2.21	19.31	13.61	0.71	122	537	1.05
26	19.56	6.58	1.2	2.36	23.47	15.53	0.62	122	537	0.98
27	11.33	3.5	0.55	1.24	6.25	4.34	0.69	74	704	1.13

Table 5.3 Results of experimental work

The number of the experimental results in the extreme left column refers to the table in Appendix B "leakage inductances". These numbers also appear in the oscilloscope prints below. The efficiency of the different converters is given in the fourth column from the right with the relation between output and input power (ρ). It can also be observed from the table that the switching frequency is not the only parameter to influence this efficiency. Because of the used resonant technique the switching losses on the Mosfet could be reduced. Therefore, the output diode is responible for the largest amount of power losses in the circuit. This influences the output power and hence the efficiency of the converter. Whereas the ringing of the voltage across the output diode could be reduced by a snubber circuit, this helped little to reduce the specific losses.

The upper line in Figure 5.12 shows the typical resonant wave form of the voltage across the MOSFET. This voltage can not fall below 0V due to the internal reverse blocking diode in the switch. After the voltage reaches zero the switch can be turned on with virtually no losses.

The spikes that are overlaid to the wave forms are a reflection of the ringing of the voltage across the output diode D_o.. Related curves are shown in Figure 5.13 to 5.15. The numbers refer to the numbers in table 5.3. A snubber with a low damping factor, hence low power dissipation as described in Chapter 5.1.2, was used which explains the excellent performance of the circuit.

Oscilloscope wave forms:

In Figure 5.13 the 24V input of the *dual converter* is operated below the normal voltage rating. The upper wave form appears almost ideally sinusoidal due to the high damping snubber applied to the output diode. However, as a result of this snubber the output voltage drops significantly beneath the desired value.

In Figure 5.14 the input current was limited which caused the non-ideal wave form across the switch. In this example the measurement problems can be observed. The upper wave form of Channel B is reflected into Channel A.

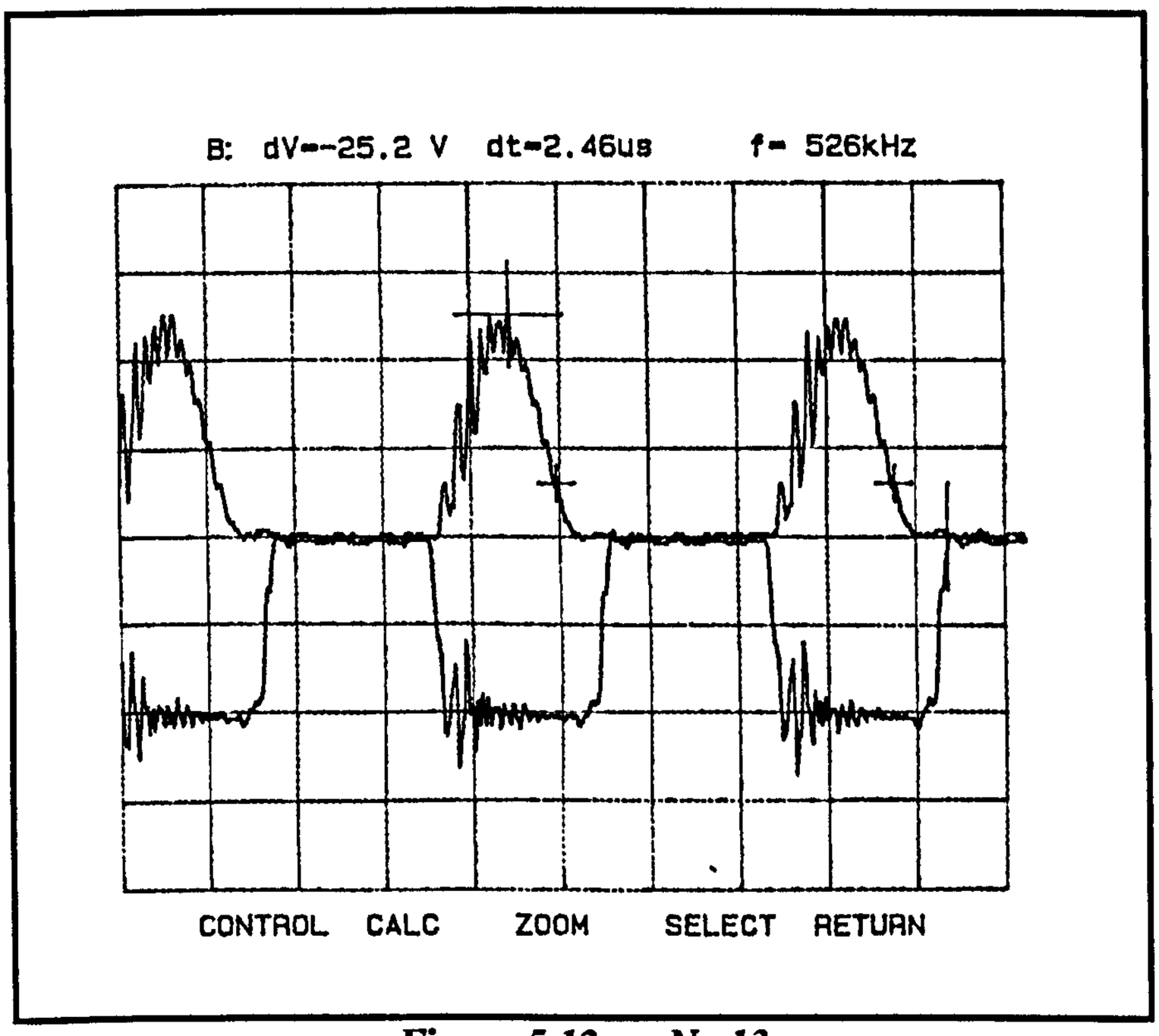

Figure 5.12 No.13

Top: V_{Cr} (100V/div.) Bottom: V_{bais} of MOSFET (5V/div.)

V_i: 54V V_o: 10.38V $\rho = (P_o/P_i)$: 0.87 f_s: 526kHz t_{on}: 0.96 μs

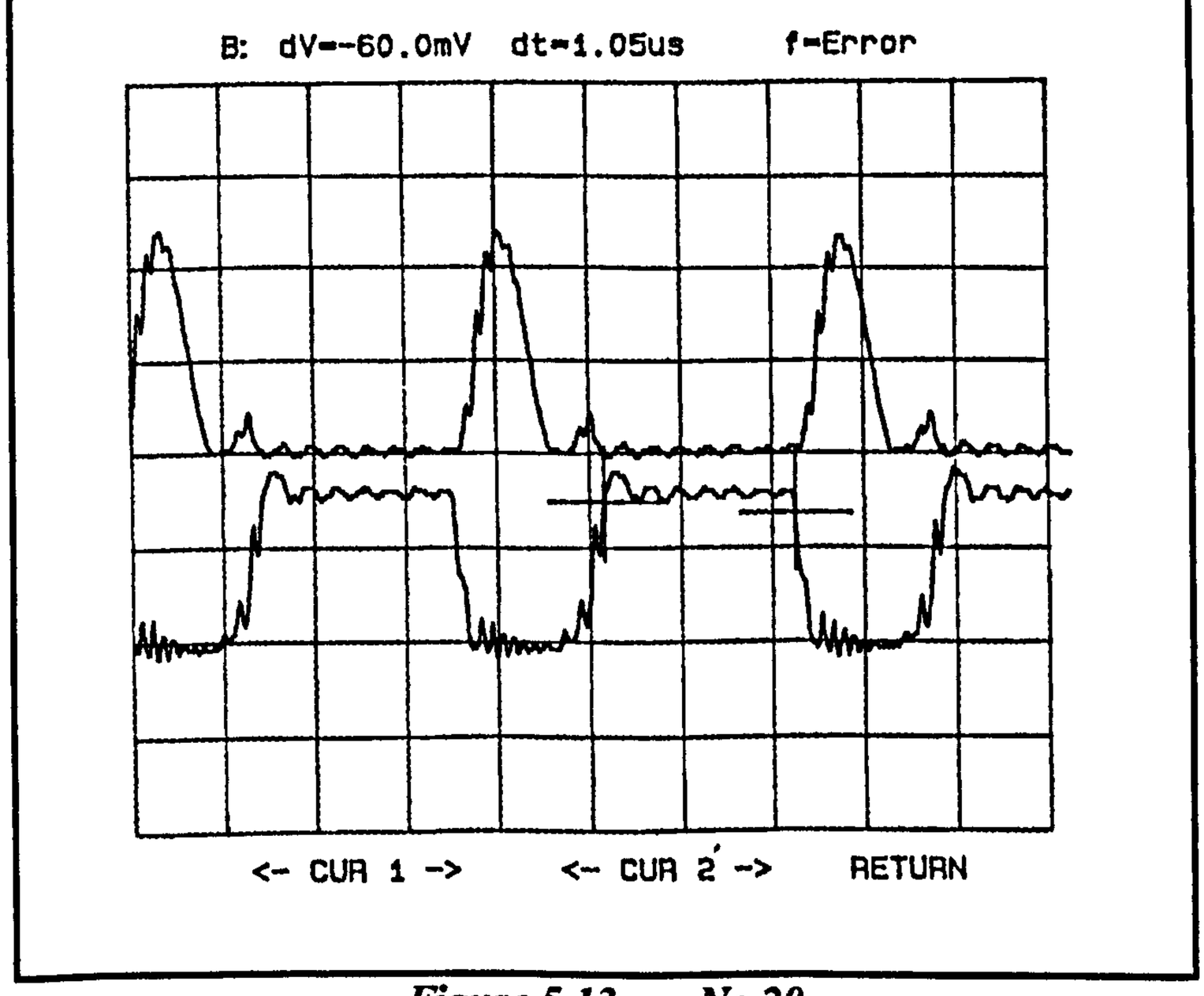

Figure 5.13 No.20

Top: V_{Cr} (50V/div.) Bottom: V_{bais} of MOSFET (5V/div.)

V_i:18.37V V_o: 6.27V ρ (P_o/P_i): 0.64 f_s: 515kHz t_{on}: 1.22μs

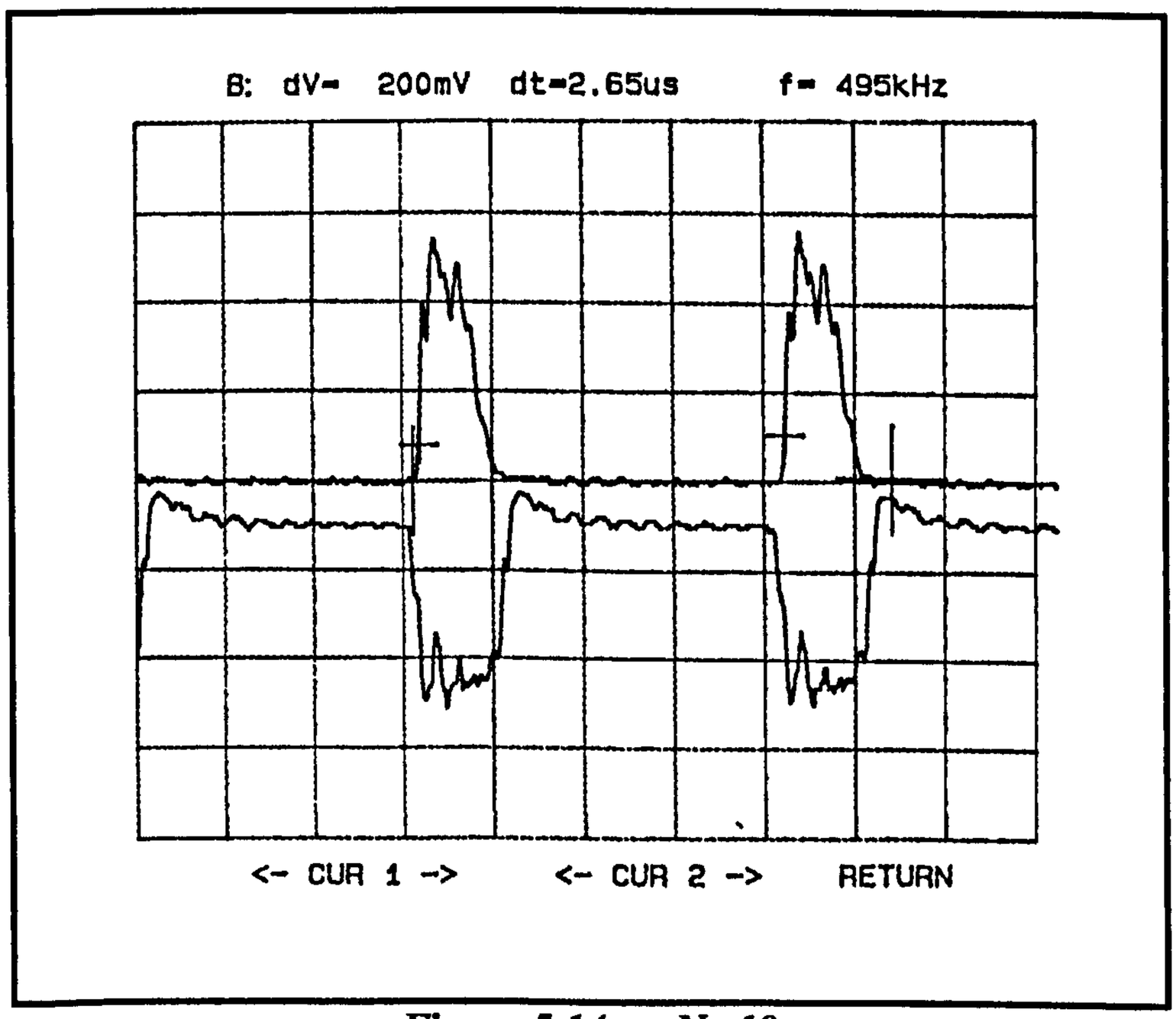

Figure 5.14 No.19
Top: V_{Cr} (50V/div.) Bottom: V_{bais} of MOSFET (5V/div.)
V_i: 18V V_o: 7.9V ρ (P_o/P_i): 0.59 f_s: 495kHz t_{on}: 1.52μs

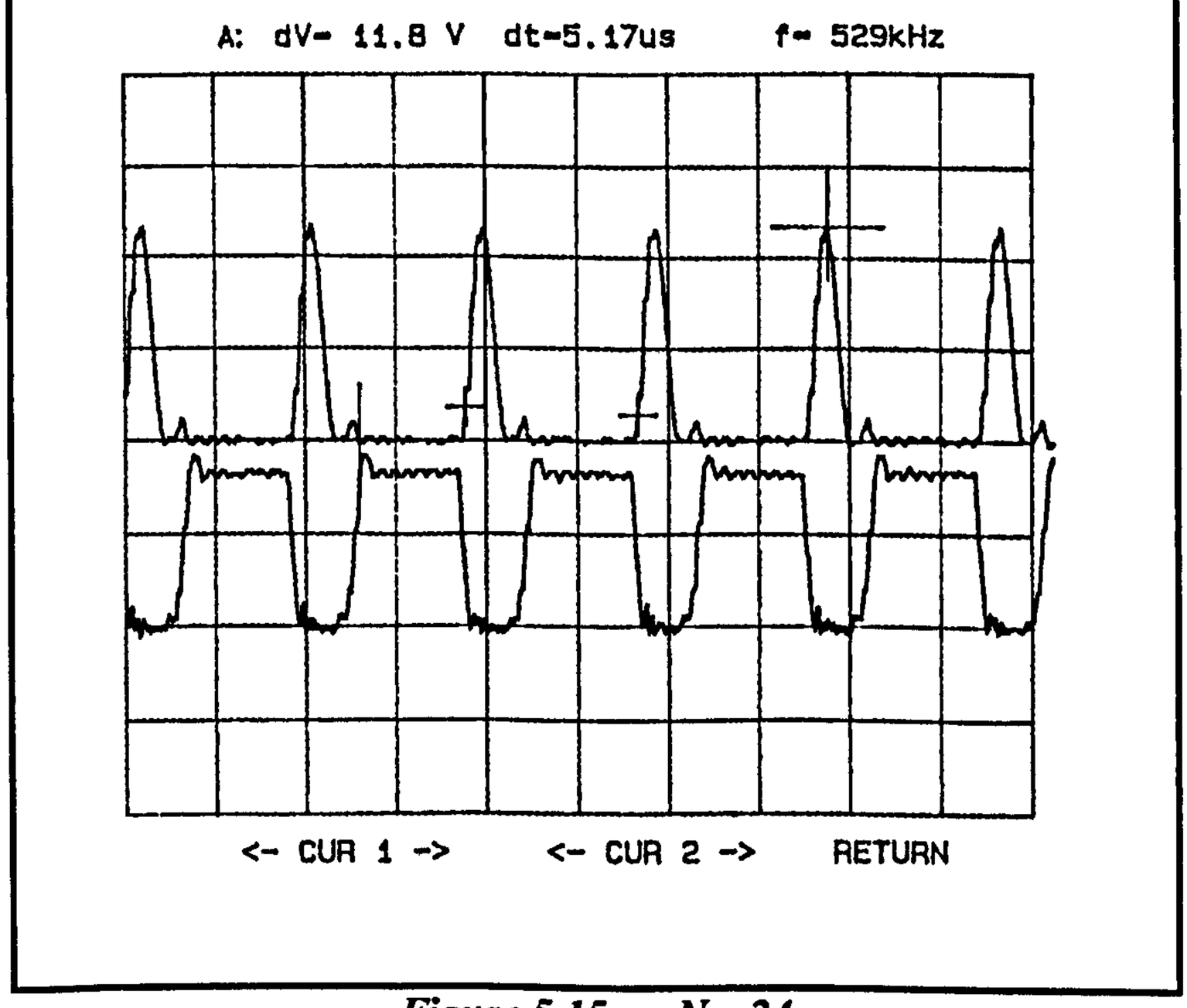

Figure 5.15 No. 24
Top: V_{Cr} (50V/div.) Bottom: V_{bais} of MOSFET (5V/div.)
V_i: 17.56V V_o: 6.29V ρ (P_o/P_i): 0.70 f_s: 529kHz t_{on}: 1.09μs

The almost perfectly sinusoidal wave form in Figure 5.15 coincides with a efficiency of this circuit of 0.7. This is a high value for the 24V voltage part of the *dual converter*, because the voltage drop across the output diode effects this circuit more than its 50V counterpart. Note that the time scale in Figure 5.15 is 1µs/sq whereas it is 0.5µs/sq in the previous Figures (5.12-5.14). This is an additional reason as of why the waveform in Figure 5.15 appears relatively smooth.

Circuit limitations and discussion of risks:

The circuit as it was designed and built is limited in several respects. Short circuit protection was externally achieved via the power supply. Therefore, it would be necessary to reconsider this aspect for a commercial circuit. Furthermore, overvoltage protection and battery failure should be taken into account. As yet there is no protection in case a control unit fails to operate and hereby turns off the MOSFETs. This would lead to a direct drop of the output voltage. The same applies for the output diode. A possible way to overcome this problem would be to include a by-pass into the circuit.

Results:

The practical work in the laboratory confirmed the principle of the *dual converter* that was discussed in Chapter 3. Some detailed points will be addressed as follows: the splitting of the secondary winding had no significant influence on the performance. The use of N87 as core material instead of N27 resulted in higher performance as the operation frequency of the circuit of approximately 500 kHz falls within the specification given by the manufacturer. The current measurement on the circuit elements appeared difficult due to the fact that the leads had to be kept very short in order to

reduce losses, and hence current clamps could only be used at some places. Alternatively a sensing resistor would influence the behaviour of the resonant circuit and may jeopardise the operation of the circuit. The manual winding of the transformer caused slight differences between the bobbins used. New winding material with a squared cross section that came on the market recently would allow a tighter winding set-up, hence the available winding space would be filled more efficiently.

As expected the performance did not reach the excellent values of the most sophisticated circuits mention in the latest publications (e.g. [Jit93]). Reasons for the less efficient operation of the *dual converter* are a) the modular set-up with screwed connection b) the standard printed circuit board design c) the not fully optimised layout of the board in respect of the mutual influence of the components.

The advantages of the circuit lay in its low cost design due to the fact that only standard components were used. An exception is the special winding set-up of the multi-winding transformer. Nevertheless, for mass production the transformer could be wound fully automatically.

The *dual converter* can be used as the core of a UPS system. Such a system particularly suits the protection of low or medium power devices, where the response time is important and hence normally the more expensive on-line system would come into operation. The circuit configuration could also be used wherever there is a demand to operate two alternative power sources. Hence in all stand-by situations such as in solar energy generators or in portable devices the *dual converter* could be used.

CHAPTER 6

CONCLUSION

The IEEE standard No.446 with the title "emergency and stand-by power" gives an exact definition of an Uninterruptible Power Supply: *the system shall be such that a failure of the main power supply leads to a maximum outage of a 1/4 period (4.2 ms for the USA) for a computer.* Shorter outages are covered by the internal capacitor of the computer. The question arises why it is not possible to increase the capacitor to a size to handle longer outage and replace a UPS. The straight answer is that a capacitor that would be able to power a standard PC for ten minutes would consist of 10,000 devices each the size of a Coca-Cola can [APC94].

The increase in demand and the resulting expansion in research and industrial activities made a vast progress of UPS systems in the last two decades possible. These improvements include reduction in weight and size, improvements in efficiency and reliability due to modern semiconductor technology and other improved components. New UPS technologies which can not be classified within the standard groups of on-line and off-line UPS systems, as described in Chapter 2, further supported these improvements and offered new fields of application.

Still, when compared to signal and data processing electronic circuits the UPS systems are protecting, their reduction in weight and size appears far less dramatic. With the advent of very large-scale integrated circuits (VLSI) and high speed integrated circuits, there is an even stronger demand for UPS with very high power density and high reliability.

The new UPS with its inbuilt *dual converter* as presented in this thesis is the result of a systematic examination of the existing configurations used in modern UPS system that was carried out at an early stage of the project. It is a mixture of an on-line and an off-line system. The core of the system is the

multi-winding transformer which was carefully examined in Chapter 3. The application of this multi-winding transformer allowed a reduction in the number of conversion steps. Additionally the conversion that is achieved by this transformer is of high-frequency nature, which effectively reduces the power losses within the device.

With the new concept as shown in Chapter 3 the benefits of the expansive, highly protective on-line UPS systems were combined with the low cost principle of the available off-line systems. The concept suits for multi-output applications and can basically be used with all power ranges, even though it is only demonstrated for a low power range because of the specified reasons. The aforementioned transformer is also responsible for a reduction of the costs due to the fact that less ferrite material is necessary and that the parasitic leakage inductance was used as part of the reactive resonant tank circuit.

The change-over operation can be influenced and hence adapted to the particular need by the dimensioning of this transformer. Electro-magnetic simulation was used to support the design of this transformer after careful pre-considerations were carried out and experts in the field were consulted (company reference list). Furthermore the author attended and published in Seminars and Conferences on subjects related to this paper.

An important result was that no harmful influence between the different windings was found. Therefore, it was possible to apply the advanced quasi-resonant switching technique to the circuit in order to improve efficiency.

This switching technique is not yet established in industry because of two main reasons. One is that it is widely believed that resonant techniques would be more expensive compared with the established pulse-width operation

technique. The opposite is proven by Heribert Schmidt [Sch93]. The other reason is that the complexity of resonant converters, as can be observed in Chapter 4.1 hinders design engineers to use this technique. This problem can be overcome by the usage of the latest computer technology and design tools as described in Chapter 5.1.1 and in the Excel program related to it (Appendix A).

The mathematical examination of the proposed *dual converter*, which represents the core of the UPS system was confirmed both by simulation and by experiments. In addition a mathematical proof of a fundamental equation in resonant circuits was carried out, that is presented in Chapter 4.1.2.

The practical results mainly proved that the concept of applying two input windings to a transformer and operating them alternatively was possible. Even the resonant behaviour of each input part was not effected by the additional winding. This offers new applications apart from the obvious ones. All types of power conversions with more than one source even with bi-directional operation could be derived from this set-up. It was not practically proven if the UPS system as a whole would operate, but the missing parts are considered non critical for the concept.

In relation to this it has to be mentioned that a modern UPS developed into high-tech system with additional features to its core purpose. A modern UPS system consists of modules which are easy to exchange and enable that the system is adjusted to the specific demands of the fast changing equipments to be protected with it. Such a system possesses special cooling devices to transfer the heat that is produced in the system to the environment. It enables the user to monitor the power quality of the mains and even to remote control the system. A safe shut down after previous warning is a standard function. All

these functions have not been addressed in the thesis but are left to further research or are considered to be standard.

The proposed *dual converter* shows yet another way how new technologies can be applied to overcome the limits of established systems. This holds true for efficiency and economical aspects.

References:

References are labelled by using the first three letters of the author in addition to the two digits of the year in which the work was first published.

[APC94]: American Power Conversion Corporate: "The power protection handbook", 1994.

[Bar90]: Ivo Barbi, Julio Bolacell: " Buck Quasi-Resonant Converter Operating at Constant Frequency: Analysis, Design, and Experimentation"; IEEE Transaction on Power Electronics, Vol.5 No.3 July 1990.

[Bat90]: Bartsch: " Taschenbuch Matematischer Formeln"; Verlag Harri Deutsch

[Bog92]: D. Bogaerts (Philips): " HF-Leistungstransformatoren in MID-Technik"; Elektronik Entwicklung 7-8/92

[Che91]: K.W.E. Cheng, P.D.Evans: "A family of extended period circuits for power supply applications, using high conversion frequencies"; EPE Firenze 1991.

[Che92]: D.K.W. Cheng, K.L.Ng: " A new approach to switching mode transformer design with distributive configuration"; IEEE 92

[Chr89]: George Chryssis: "High-Frequency switching power supplies: Theory and Design."

[Chu91]: Y.H.Chung, B.S. Shin, G.H. Cho:"Bilareral series resonant inverter for high frequency link UPS"; IEE Proceedings-B, Vol 138, No.4, July 1991

[Cuk91]: Maksimovic and Slobodan Cuk: "Constant-Frequency Control of Quasi-Resonant converters"; IEEE transaction on Power Electronics, Vol.6 No.1 January 1991.

[Dix93]: Lloyd Dixon: "Coupled Inductor Design"; UNITRODE Power Supply Design Seminar SEM-900 1993.

[Fin93]: Financial Times: "Charged up for battle"; 2th of December 1993

[Füh82]: H.Führer: "Elektrotechik"; Band1

[Gil93]: Gerhard Gilke:"Datenkiller aus der Dose:Markt&Technik Wochenzeitung für Elektrotechnik";Esesix Comp.

[Gri89]: David c.Griffith: "Uninterruptible Power Supplies"; 1989.

[Had89]: K.Al Haddad and V.Rajagopalan: "Novel Method of Power Control of a DC to DC Resonant Converter"; IEEE 1989.

[Her86]: Hering, Martin, Stohrer: "Physik fuer Ingenieure"; VDI Verlag 1986 3.Auflage.

[Ide--]: IDENTA Ausweissysteme GmbH, Villingen-Schwenningen

[Jit93]: Ionel Dan Jitaru: "Seminar 3"; PCIM 1993 Nuremberg

[Jou91]: Gyu B. Joung, Chun T.Rim and Gyu H.Cho: "Integral Cycle Mode Control of the Serie Resonant Converter"; IEEE Transaction on Power Electronics, Vol.4 No.1 July 1989.

[Jon87]: J.Jongsma: "Transformer winding design"; Philips 3C85 Handbook: First in ferrites 1987

[Lee86]: F.C.Lee and K.H. Liu: "Zero-Voltage Switching Techniques in DC-DC converter circuits." IEEE PESC 1986.

[Lee89]: F.C.Lee:"High-frequency resonant, quasi-resonant, and multi-resonant converters"; Volume 1 of the Virginia power electronics center publication series

[Leh73]: Lehmann, Geisweid: "Elektrotechnik und Elektrische Antriebe"; Springer Verlag Siebente Auflage 1973.

[Liu86]: Kwang-Hwa Liu: " High-frequency quasi-resonant converter techniques"; PhD dissertation Oct.86.

[Mak91]: Dragan Maksimovic, Slobodan Cuk: "Constant-Frequency control of Quasi-Resonant converters."

[MCP93]: MC:"Power-PC"; Nov. 93, page 38

[Mea86]: L.G.Meares: "New techniques using SPICE." IEEE 1986.

[Meh90]: Dr.P.Mehta and Dr.M.Darwish : "High-Frequency Uninterruptible Power Supply systems." ERA Report 90-0699

[Mer93]: Nikolaos Merianos: "Ferrites - Briefly explained"; Siemens Matsushita Components GmbH & Co. KG, Edition 1993

[Moh89]: Mohan, Undeland, Robbins: "Power electronics: converters, applications and design."; John Wileys & Sons

[Mol84]: B.Molnar: "Basic limitation on Waveforms achievable in single-ended switching-mode tuned (E-class) power amplifiers", IEEE J. solid-state circuits, vol. SC-19, no.1, February 1984

[Nek93]: Neckarwerke Aktuell:"Mehr Licht, weniger Strom"; 9/93 page 11

[Neu92]: K. Neumann: "Bewertung und Zukunftsaussichten der Leistungshalbleiter"; ETG Fachbericht No.39, 1992

[Ngo87]: K.D.T. Ngo: "Generalisation of Resonant Switches and Quasi-Resonant DC-DC converters." IEEE PESC 1987

[Ray92]: Biswajit Ray: "Bi-directional DC-DC power conversion using quasi-resonant topology"; IEEE 1992

[Rößß90]: E.Röß: "Der Spule Kern"; Ferrite und Zubehör, Fachaufsätze, Siemens 1990

[Row90]: Anna Rowley: "A new zero-voltage-mode resonant converter"; PhD dissertation Brunel University Oct.1990

[Sch87]: M.F.Schlecht and L.F.Casey: "Comparison of the Square-Wave and Quasi-Resonant Topologies"; Second Annual Applied Power Electronics Conference, San Diego, CA. USA.

[Sch93]: Heribert Schmidt, Christoph Siedle:"The charge equaliser"; PCIM 93 page 461

[Sch94]: Uwe Schmidt:"Uninterruptible power supply systems using a quasi-resonant technique in a dual converter mode"; PEVD-conference 1994

[Scl93]: Manfred Schlenk, "Ein Serienresonanzumrichter in Halbbrückenschaltung mit kombinierter serieller und paralleler Lastauskopplung und mehereen Ausgangskreisen"; Disseration TU Berlin 1993

[See92]: Anton Seelig: "Strom im Luftspalt"; Technische Rundschau No.51 1992

[Sky89]: Federik E. Skyes Gennum corp.: " Resonant-mode power supplies: a primer"; IEEE Spectrum May 1989 pp.36-39

[Spi94]: Der Spiegel: “Revolution in der Energiespeicherung“, 2/94

[Stu93]: Stuttgarter Zeitung: "Kurzschluß in Abspannwerk"; 9.10.93

[Stt93]: Stuttgarter Zeitung: "Stromausfall in Feuerbach"; 12.10.93

[Tem93]: V.Temple, D.Burke, F.Lokuta, B.Arlt:"MCT and the future"; PCIM '93

[Tie86]: Tietze, Schenk: "Halbleiter Schaltungstechnik" 1986 8.Auflage"

[Tok95]: Tokyo University of Agriculture and technology Japan, fon: 42383 4719 fax: 42384 3804, 1995

[Tui88]: Paul W.Tuinenga:"Spice- A Guide to Circuit Simulation & Analysis Using PSpice"; page XV;1988

[Uni89]: Unitrode: "Semiconductor databook and application notes"; DB600 1989.

[Uni90a]: Unitrode: "Switching Regulated Power Supply Design Seminar Manual"; SEM-700 1990.

[Uni90b]: Unitrode: "Linear Integrated circuits data and applications book"; IC600 1990.

[Vic91]: Vicor, 23 Fromtage Road, Andover, MA 01810 USA

[Vin83]: P.Viniarelli: "Forward Converter Switching at Zero Current." U.S. Patent #4,415,959 Nov 1983.

[Was90]: Wasinger,P.: "Stromnetz sabotiert Computer-Einsatz"; ETZ 111, 1990, No. 20 pages 1070-1074 1990

[Wei65]: P.E.Weiss 1865-1940

[Wei88]: A.H.Weinberg, P.Rueda Boldo: "A High-Power, High Frequency DC-DC converter for space application."

[Wol85]: H.Wolf: "Lineare Systeme und Netzwerke" 1985 2.Auflage

APPENDIX A

Worksheet to a systematic design of a Quasi-Resonant Flyback converter

Author: Uwe Schmidt Date: 10th of march 1993
Institutes: Brunel University West London & Fachhochschule für Technik Esslingen

This sheet should be regarded as a tool for designers who are familiar with QRC
or they should be in possess of the related PhD thesis by the author.
The author also refers to this source for drawing, waveforms and
the circuits layout.

Table of necessary data

Input Voltage	Vin=	**50 V**	
Output Voltage	Vout=	**12 V**	
Power	P=	**50 W**	
Switching frequency:	Fs=	**500 kHz**	
Hence the load is given:	R=	**2,88 Ohm**	R=Vout^2/P

Comment: Choose the switching frequency in regard to the
Mosfet and more important in regard to the controller

Starting with these data two design procedures can be used:

1. The resonant frequency can be fixed to a defined relation to the switching frequency

2. The max. peak current of the primary side can be fixed.

The following flowchart should clearify both way.

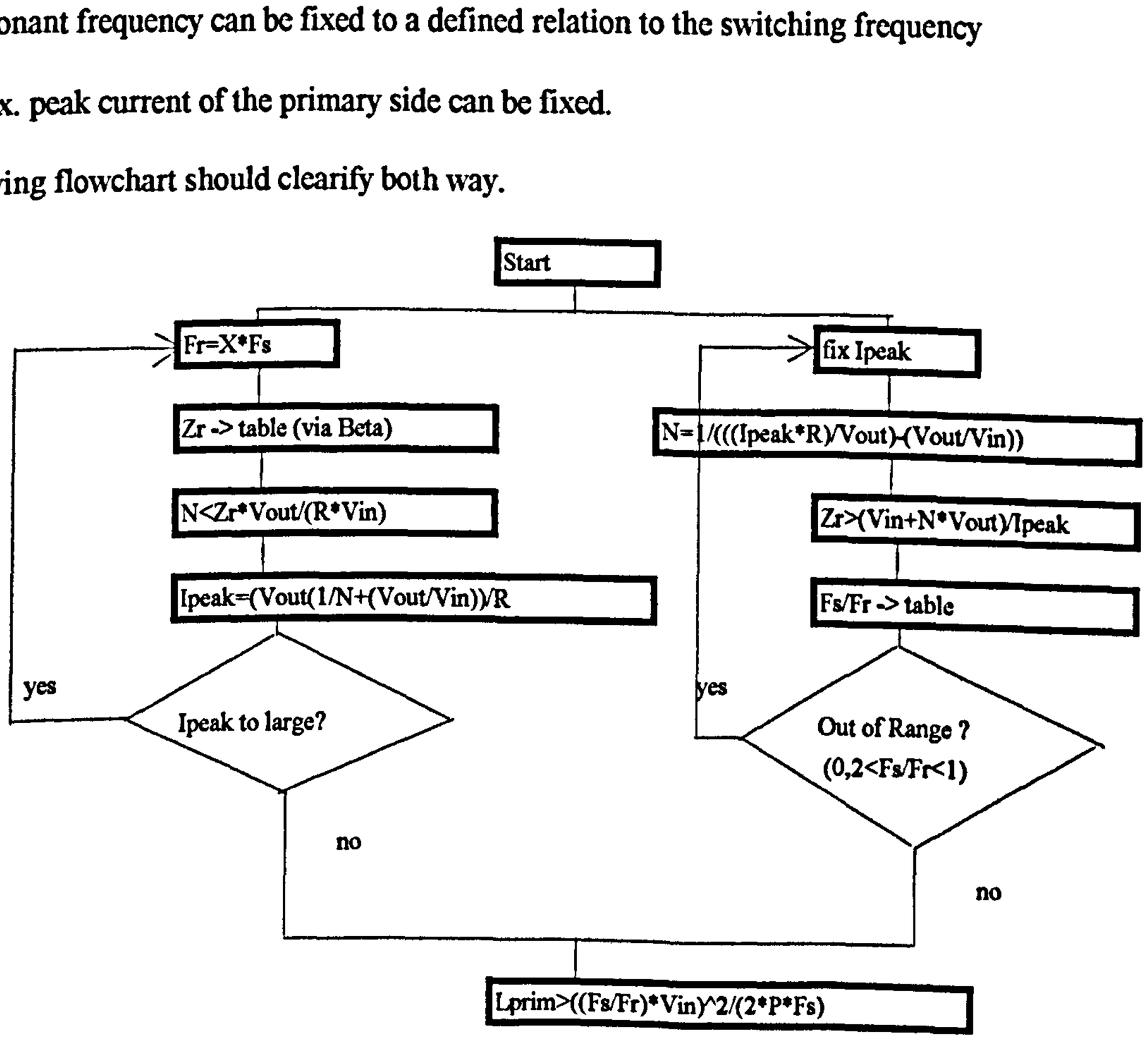

****

APPENDIX A

1. Design starting with Fr (Resonant Frequency):

a fix Fs/Fr= *0,4* (approximately 0.5)

Fr= **1250** Khz w= **7853,9816** Khz

b **look up the value of Beta=R/Zr in the table below !**

Beta= *0,045 to achieve good results take a fairly high Beta*

hence the impedance of the resonant circuit can be given as:

Zr= **64** Zr=R/Beta

c The turnsratio should be smaller than:

N< 5,3333333 N<Zr*Pout/(Vout*Vin)

N= **4** turns

d Ipeak= **2,042** A Ipeak=(Vout(1/N+Vout/Vin))/R

e The resonant tank device are dimesioned as:

Lr= **8,15** uH

Cr= **1,99** nF

****

Timing for 1. Design:

Period 1: t01= **95,504407** nsec t01=Cr*(Vin+Vout*N)/Ipeak

Period 2: t12= **507,95505** nsec t12=Alpha/w

Alpha= 3,9894697 Alpha=PI+Abs(arcsin((-Vin-Vout*N)/(Zr*Ipeak)))

Period 3: t23= **282,12406** nsec t23=Zr*Ipeak*(1-cos(Alpha)/(w*(Vin+Vout*N)

Period 4: t34= **1114,4165** nsec t34=Ts-t03

t03= 885,58352 nsec Ts= **2000** nsec

ton= ***1242,924*** nsec *1% safty margin added! at 10.03.94*

toff= ***757,0763*** nsec

****

The values for Lr and Cr must be new calculated for the second version

2. Design starting by fixing Ipeak

a. fix Ipeak to a reasonable value

Ipeak= *2,00* A

b. Setting the turnsratio to:

N= 4

c. The resonat impedance can be fixed:

Zr> 49 *to ensure Zero Voltage switching a safety factor is used.*

Zr= 58,8

d. The relation between the two charataristic frequencies is given from the table below via Beta

Beta= 0,045 ***insert below***

Fs/Fr= *0,403099* **automaticlly inserted !!!**

Fr= 1240,3905 KHz w= 7793,6031 KHz

Timing for 2 Design:

Period 1: t01= **97,51** nsec t01=Cr*(Vin+Vout*N)/Ipeak

Period 2: t12= **525,4282** nsec t12=Alpha/w

Alpha= 4,1267034 Alpha=PI+Abs(arcsin((-Vin-Vout*N)/(Zr*Ipeak)))

Period 3: t23= **237,2459** nsec t23=Zr*Ipeak*(1-cos(Alpha)/(w*(Vin+Vout*N)

Period 4: t34= **1139,8159** nsec t34=Ts-t03

t03= 860,1841 nsec Ts= **2000** nsec

ton= **1252,1467** nsec *0,5 % safty margin added at 10.03.94*

toff= 757,07628 nsec

Resonant Elements:

Lr= 7,544649 uH

Cr= 2,1821489 nF

****

3.

APPENDIX A

a.

Insert the chosen Beta value above !

E=Vout/Vir	0,24
E*=(3V+Vc	0,3

Beta=R/Zr

0,045	Fs/Fr=	0,4030989	**The straight forward result for design procedure 2**
0,01	Fs/Fr=	0,1562785	
0,012	Fs/Fr=	0,1807389	
0,015	Fs/Fr=	0,2140615	
0,019	Fs/Fr=	0,2529587	
0,02	Fs/Fr=	0,2618	
0,03	Fs/Fr=	0,3342533	
0,032	Fs/Fr=	0,3457959	
0,034	Fs/Fr=	0,3565162	
0,036	Fs/Fr=	0,3664714	
0,038	Fs/Fr=	0,3757134	
0,04	Fs/Fr=	0,3842901	
0,042	Fs/Fr=	0,3922451	
0,046	Fs/Fr=	0,4064473	
0,05	Fs/Fr=	0,4186024	
0,06	Fs/Fr=	0,4414968	
0,07	Fs/Fr=	0,4556517	
0,08	Fs/Fr=	#ZAHL!	**... out of range**

Results of experimental work:

No. (as table leakage)	V_{in}	V_{out}	I_{in}	I_{out}	P_{in}	P_{out}	$\rho P_{out}/P_{in}$	V_{Reseak}	f_s	t_{on}
4	50	7.3	0.6	2.63	30	19.20	0.64	204	709	1.42
13	54	10.38	1.25	5.7	67.5	59.17	0.87	252	526	0.96
14	42	12	1.5	3.8	63	45.6	0.72	236	429	1.42
19	18	7.9	1.7	2.3	30.6	18.17	0.59	135	495	1.52
20	18.37	6.27	1.2	2.26	22.04	14.17	0.64	112	515	1.22
21	21.22	7.09	1.4	2.66	29.7	18.86	0.64	132	487	1.08
22	17.75	6.33	1.5	2.35	26.58	14.88	0.56	130	510	1.2
23	18.29	6.65	1.4	2.49	25.6	16.56	0.67	120	606	1.28
24	17.56	6.29	1.15	2.24	20.19	14.08	0.70	120	529	1.09
25	17.56	6.16	1.1	2.21	19.31	13.61	0.71	122	537	1.05
26	19.56	6.58	1.2	2.36	23.47	15.53	0.62	122	537	0.98
27	11.33	3.5	0.55	1.24	6.25	4.34	0.69	74	704	1.13

Leakage inductance:

No.	V_{in} [V]	N	L_{Res} [µH] calculated	Trafo No. a-=1,3 b-g =1	Board No.	L_{Lead}[µH] transformer	L_{Res} discret No.	C_{Res} [nF]	F_{Res} calc. [MHz]	$t_{Res}/2$ meas. [µsec]	F_{Res} meas [MHz]	V_{out}*N+V_{in} [V]
1	50	4	13.16	1	1	1.9	2	9.2	0.84	0.526	0.95	78
2	50	4	8.15	3a	1	4.9	6	1.8	1.14	0.47	1.06	80
3	50	4	8.15	4a	1	5.0	6	2.0	1.07	0.49	1.02	86
4	50	4	8.15	5a	2	4.2	1	1.9	1.60	0.42	1.19	80
13	50	4	8.15	5b	2	3.9	1	2.39	1.47	0.475	1.05	95
14	50	4	8.15	5b	2	3.9	1	2.39	1.47	0.43	1.12	90
19	24	4	2.38	7a	2	2.7	0	2.5	1.94	0.315	1.59	46
20	24	4	2.38	7a	2	2.7	0	3.2	1.71	0.340	1.47	43
21	24	4	2.38	7b	2	2.6	0	3.2	1.75	0.370	1.35	50
22	24	4	2.38	5a	2	4.2	0	2.2	1.66	0.315	1.59	43
23	24	4	2.38	8a	2	2.6	0	3.2	1.75	0.365	1.37	45
24	24	4	2.38	8b	2	2.5	0	2.0	2.25	0.295	1.69	50
25	24	4	2.38	8b	2	2.5	0	2.2	2.15	0.295	1.69	50
26	24	4	2.38	8b	2	2.5	0	2.2	2.15	0.31	1.61	50
27	24	4	2.38	8b	2	2.5	0	3.2	1.78	0.395	1.27	25

Core / bobbin configuration:

g=2mm Coretype E 42/15 Siemens:

bobbin no.	board no.	configuration inner to outer winding	core material	L_{prim1}	Pin	L_{prim2}	Pin	L_{sec}	Pin	L_{leak1} L_{sec} S/C	L_{leak2} L_{sec} S/C	L_{leak3} $L_{p1}+L_{p2}$ S/C
1[1]	1	L_{seca},L_{prim2}, L_{secb},L_{prim1}	N27	*not used*	4-7 (6=9)	-	2-11	-	1-12	-	-	-
2[1]	1	L_{seca},L_{prim2}, L_{secb},L_{prim1} , all flat copper winding	N27	*not used*	4-7 (6=9)	-	2-11	-	1-12	-	-	-
3	1	L_{sec}, L_{prim2}, L_{prim1}	N87	*not used*	IV-VI	-	I-X	-	II-IX	-	-	-
4	1	L_{sec}, L_{prim2}, L_{prim1}	N87	*not used*	IV-VI	-	I-X	-	II-IX	-	-	-
5	2	L_{sec}, L_{prim2}, L_{prim1}	N87	25.6µH 12 win.	IV-VI	25µH 12 win.	II-IX	2.2µH 3 win.	I-X	2.7µH	2.7µH	0.8µH
6	2	L_{prim2a}, L_{sec}, L_{prim2b}, L_{prim1}	N87	24.6µH	IV-VI	24.6µH 6+6 win.	II-IX (III= VIII)	2.2µH 3 win.	I-X	3.4µH	2.7µH	0.8µH
7	2	L_{sec}(flat copper), L_{prim2}, L_{prim1}	N87	26.9µH	IV-VI	25.9µH	II-IX	2.2µH 3 win.	I-X	3.4µH	2.6µH	0.8µH
8		L_{sec} (gap 2mm), L_{prim2}, L_{prim1}	N87	25.9µH	IV-VI	24.7µH	II-IX	2.2µH 3 win.	I-X	2.8µH	2.5µH	0.8µH

[1]airgap g=1.16mm

Core / bobbin configuration:
g= 2.6mm Coretype E 42/15 Siemens:

bobbin no	board no.	configuration inner to outer winding	core material	L_{prim1}	Pin	L_{prim2}	Pin	L_{sec}	Pin	L_{sec}, L_{prim1} S/C	L_{sec}, L_{prim2} S/C
1[1]	1	L_{seca},L_{prim2}, L_{secb},L_{prim1}	N27	31.9µH	4-7 (6=9)	8.8µH	2-11	2.9µH	1-12	1.9µH	790µH
2[1]	1	L_{seca},L_{prim2}, L_{secb},L_{prim1}, all flat copper winding	N27	35.4µH	4-7 (6=9)	9.6µH	2-11	3.1µH	1-12	2.2µH	1.1µH
3	1	L_{sec}, L_{prim2}, L_{prim1}	N87	23µH 12 win.	IV-VI	20.5µH 12 win.	I-X	2.1µH 3 win.	II-IX	4.9µH	3.7µH
4	1	L_{sec}, L_{prim2}, L_{prim1}	N87	22.4µH 12 win.	IV-VI	20.8µH	I-X	1.9µH 3 win.	II-IX	5.0µH	2.5µH
5	2	L_{sec}, L_{prim2}, L_{prim1}	N87	22µH 12 win.	IV-VI	20.5µH 12 win.	II-IX	1.8µH 3 win.	I-X	4.2µH	2.5µH
6	2	L_{prim2a}, L_{sec}, L_{prim2b}, L_{prim1}	N87	21.7µH 12 win.	IV-VI	20.1µH 6+6 win.	II-IX (III= VIII)	1.9µH 3 win.	I-X	3.7µH	2.9µH
7	2	L_{sec}(flat copper), L_{prim2}, L_{prim1}	N87	22.3µH 12 win.	IV-VI	21.4µH	II-IX	2.2µH	I-X	3.7µH	2.8µH
8	2	L_{sec}, (gap 2mm), L_{prim2}, L_{prim1}	N87	21.7µH 12 win.	IV-VI	20.5µH	II-IX	2.0µH	I-X	2.9	2.7
9	2	L_{prim2a}, L_{sec}, L_{prim2b}, L_{prim1}	N27 /N87	41.3µH 12 win.	IV-VI	39.8µH	II-IX (III= VIII)	3.2µH	I-X	2.9	2.4

General comment: The measuring of the leakage inductance was carried out by short curcuiting the secondary and the second primary winding.

[1]airgap g=1.16mm

APPENDIX C

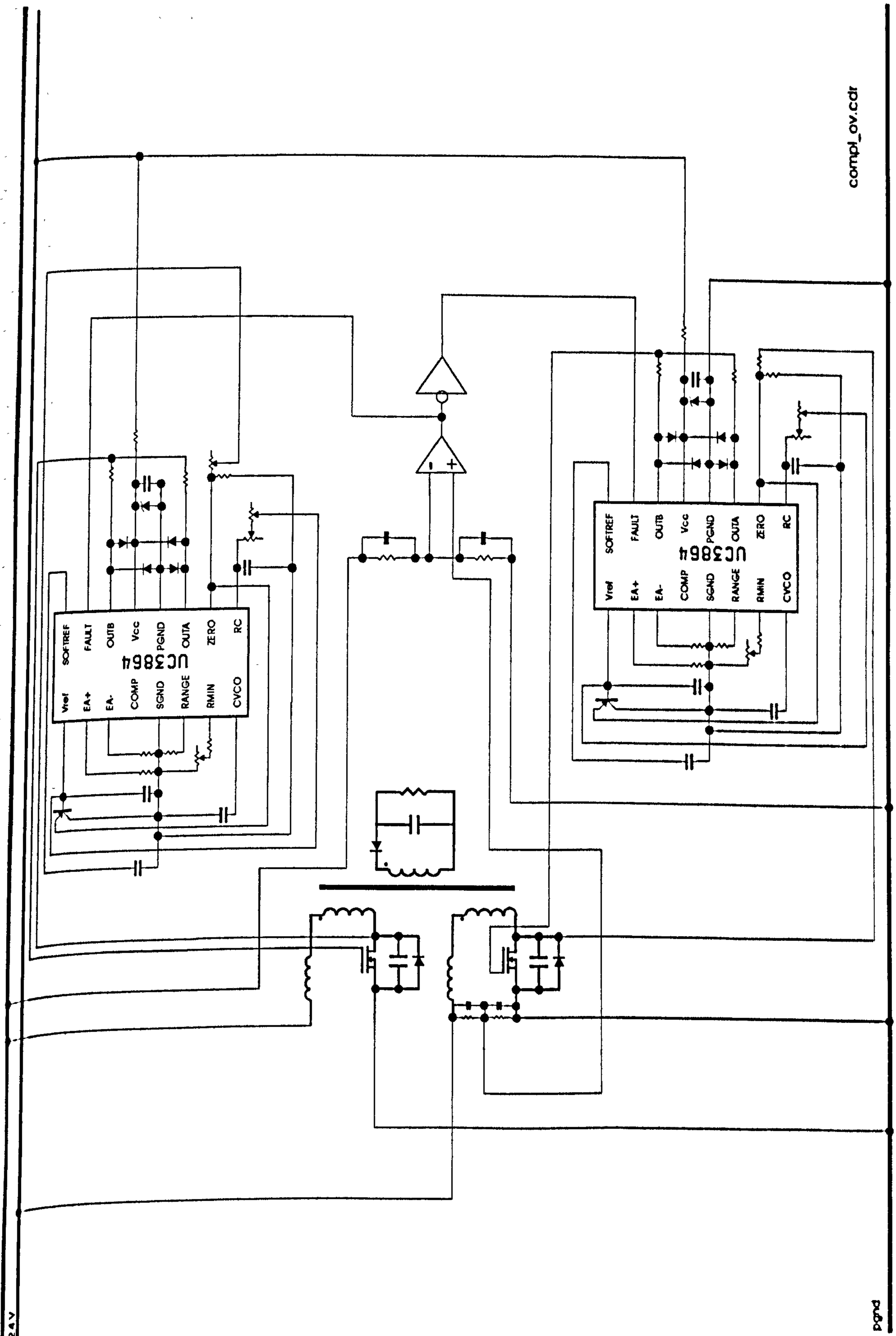
compl_ov.cdr
SOFTREF
FAULT
OUTB
Vcc
PGND
OUTA
ZERO
RC
UC3864
Vref
EA+
EA-
COMP
SGND
RANGE
RMIN
CVCO
50V
24V
pgnd

APPENDIX C

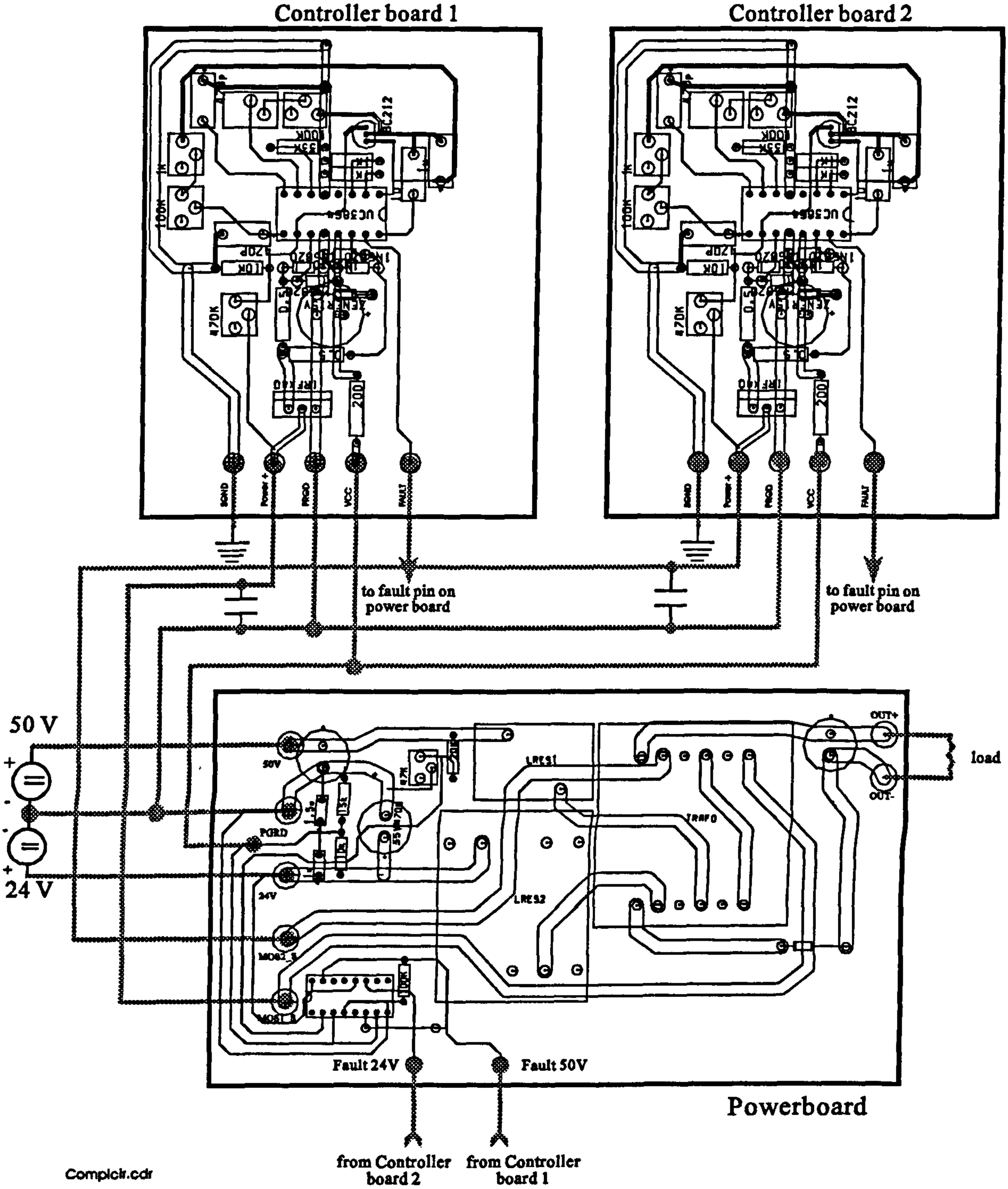

Complclr.cdr

Setup of the experimental circuit

APPENDIX C

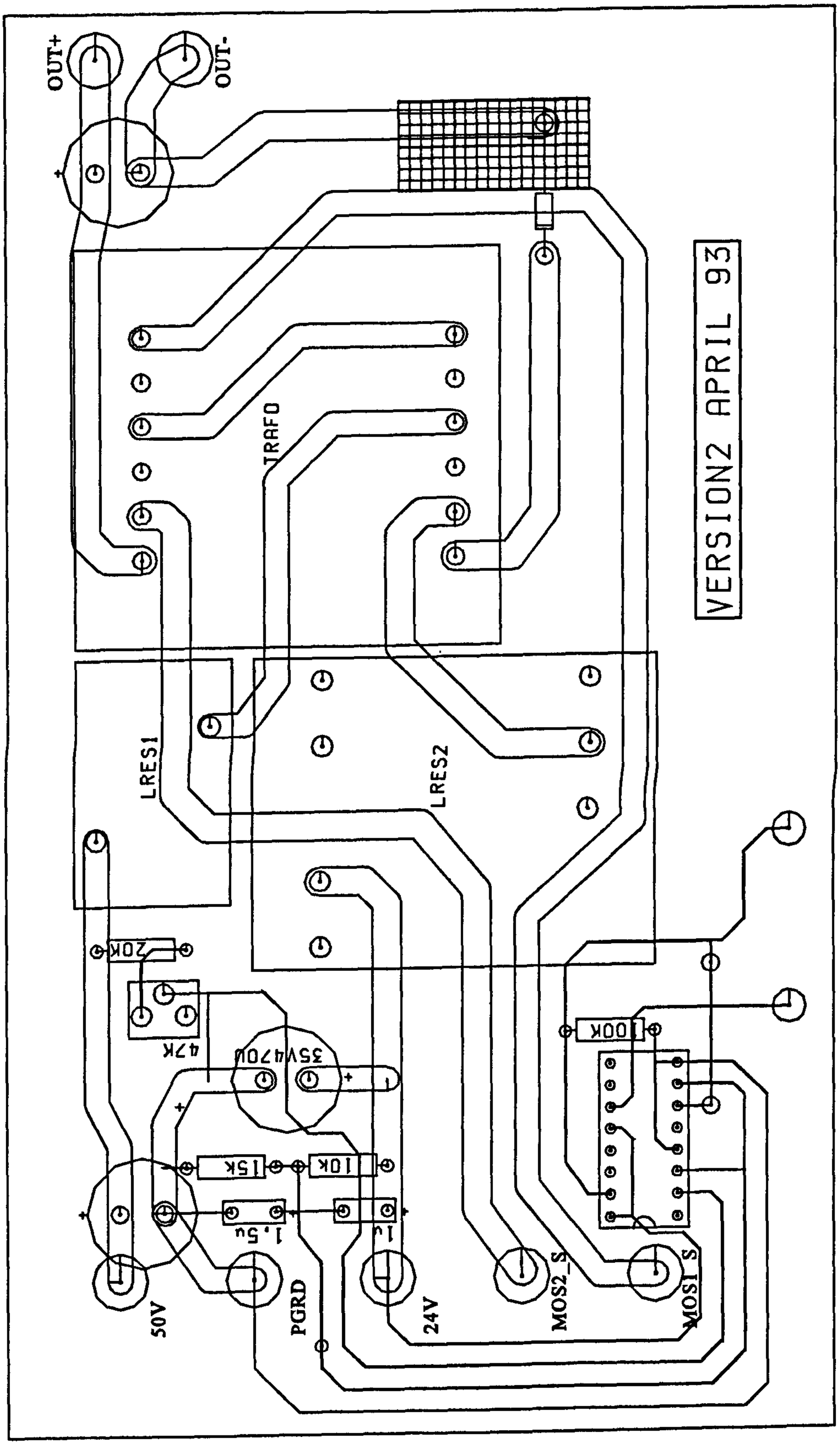
OUT+
OUT-
JRAFO
LRES1
LRES2
20K
4,7K
35V470U
15K
10K
1,5u
1u
100K
50V
PGRD
24V
MOS2_S
MOS1_S
93
VERSION2 APRIL
Trafo2.cdr
Trafo2

APPENDIX C

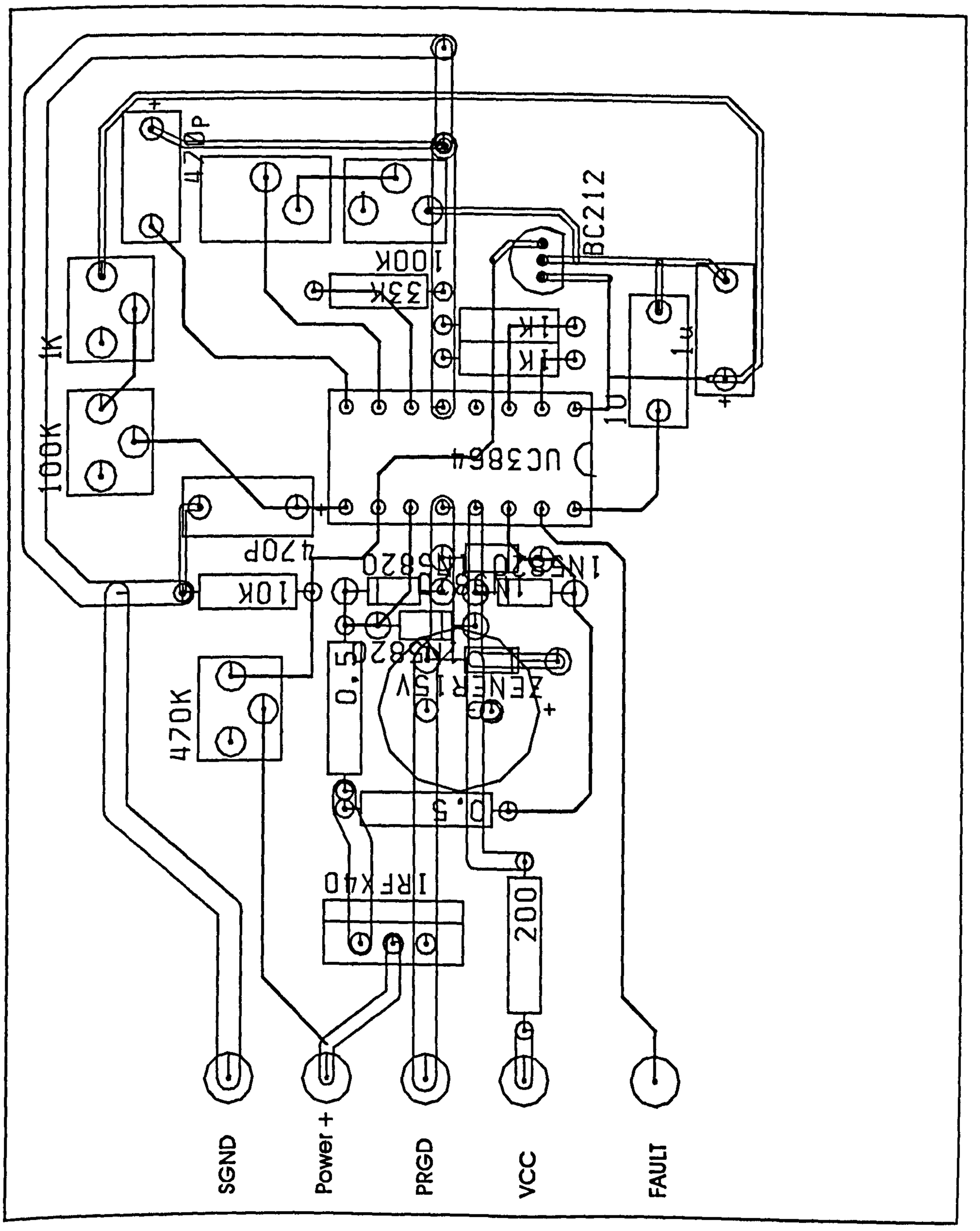
3864.CDR
Controller UC3864
+
47
100K
33K
BC212
1K
1K
1µ
1K
100K
UC3864
470P
10K
1N5820
1N5820
1N5820
0.5
ZENER 15V
470K
0.5
IRFX40
200
SGND
Power +
PRGD
VCC
FAULT

APPENDIX C

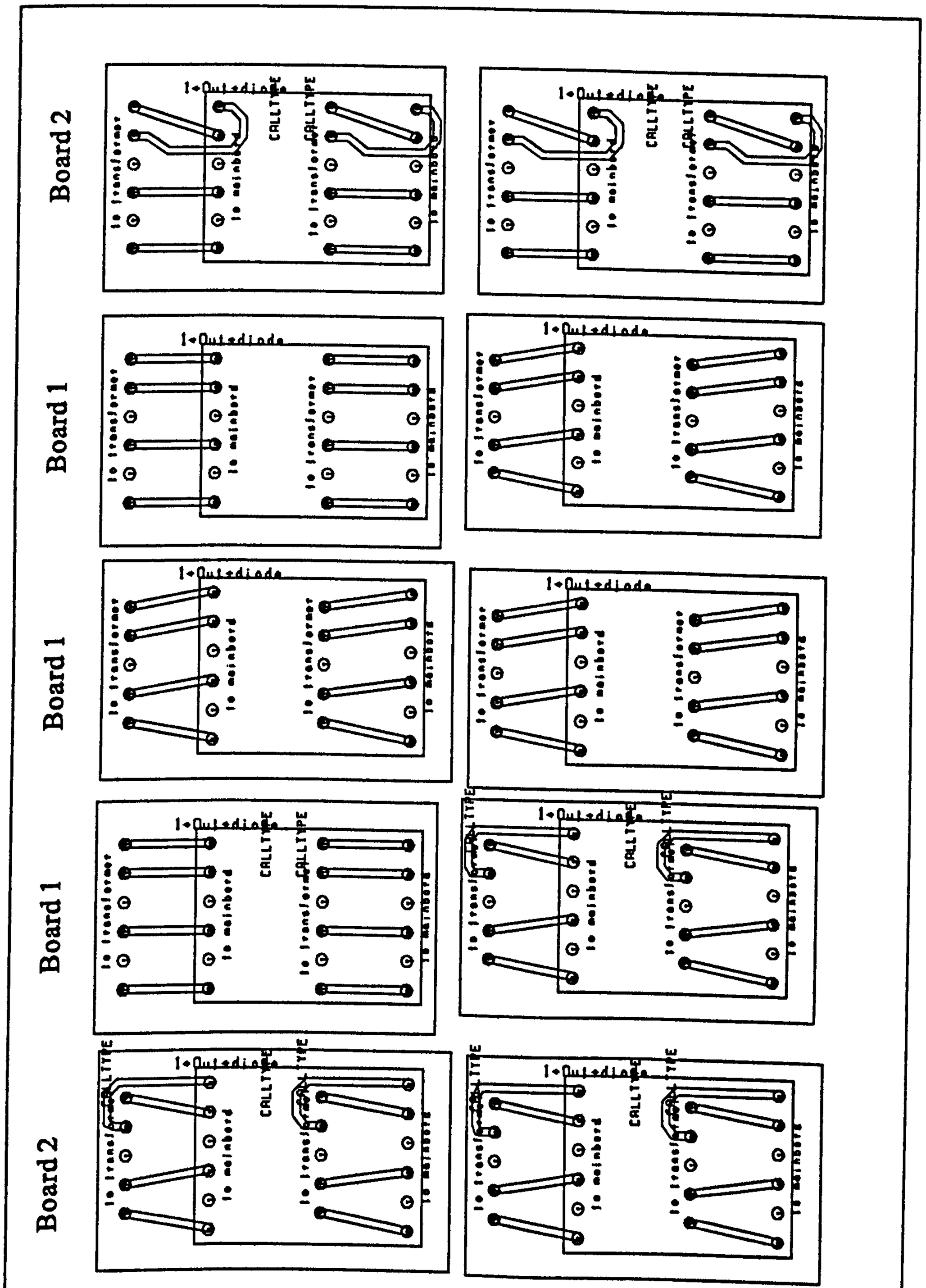
Transformer Interface Boards
Board 2
Board 1
Board 1
Board 1
Board 1
Board 2
1-Outedioda
CALLTYPE
to transformer
to mainbord
interfac.cdr

APPENDIX D

Determination of resonance frequency

This calculation table is related to Chapter 4.1.2 and helps to determine the resonant frequency for different parameters of the main components

A*w^6+B*w^4+C*w^2+D=0

Parameters:

C1=	9,2E-09	6,89E-21
C2=	4,70E-04	
L1=	6,00E-06	
L2=	3,20E-05	
R=	2,88E+00	

Ax^3*Bx^2+Cx+D=0

A=-C1*C2^2*L1*L2^2*R^2		A=	-1,04E-28
B=2*C1*C2*L1*L2*R^2+C1*L1*L2^2+C2^2*L2^		B=	-1,88E-15
C=-C1*L1*R^2+2*C2*L2*R^2+L2^2-C1*L2*R^2		C=	1,26E-07
D=R^2		D=	8,29E+00

x^3+ax^2+bx+c

a=B/A	1,81E+13		
b=C/A	-1,21E+21		
c=D/A	-8,01E+28		

x=y-a/3

y^3+py+q=0

p=-a^2/3+b	1,09E+26		
q=2*(a^3)/27-b*a/3+c	4,40E+38	q/2=	3,30E+38
D=(q/2)^2+(p/3)^3	9,70E+76		

D 1

Solutions:

y1= u+v	y1=	1,26E+13
u=	4,50E+12	
v=	8,10E+12	

Back-substitution:

x1=	y1+ a/3	x1= 1,86407E+13
ω1= x1^(1/2)		ω1= 4,32E+06
f1=	687 kHz	

APPENDIX E

Photos of experimental circuits 1

Circuit board

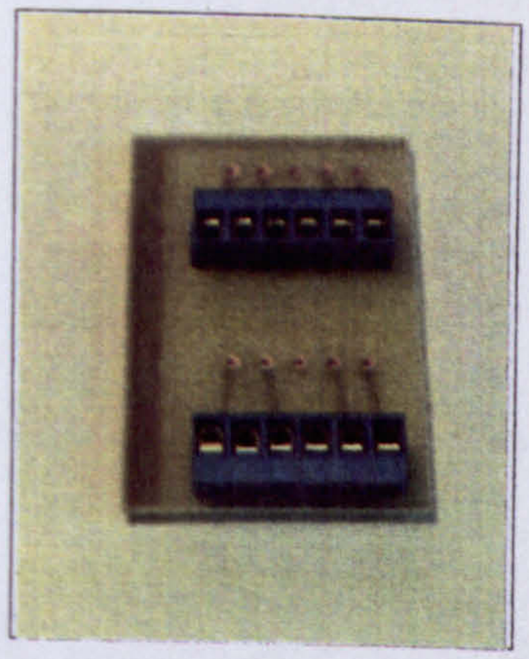

... with screw connection

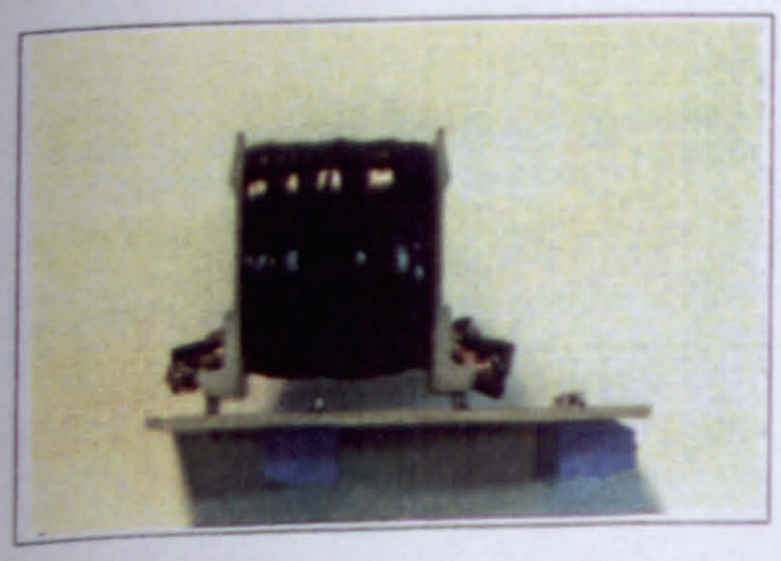

... with bobbin

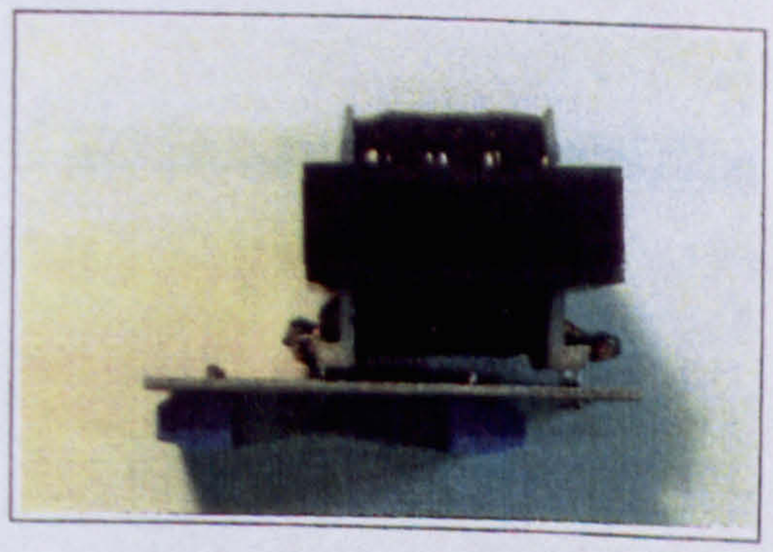

... with ferrit-core

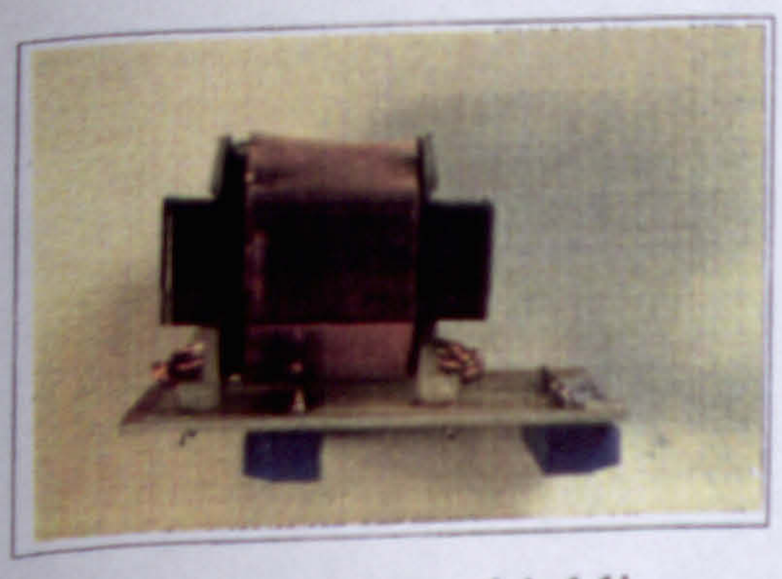

... with copper shielding

APPENDIX E

Photos of experimental circuits 2

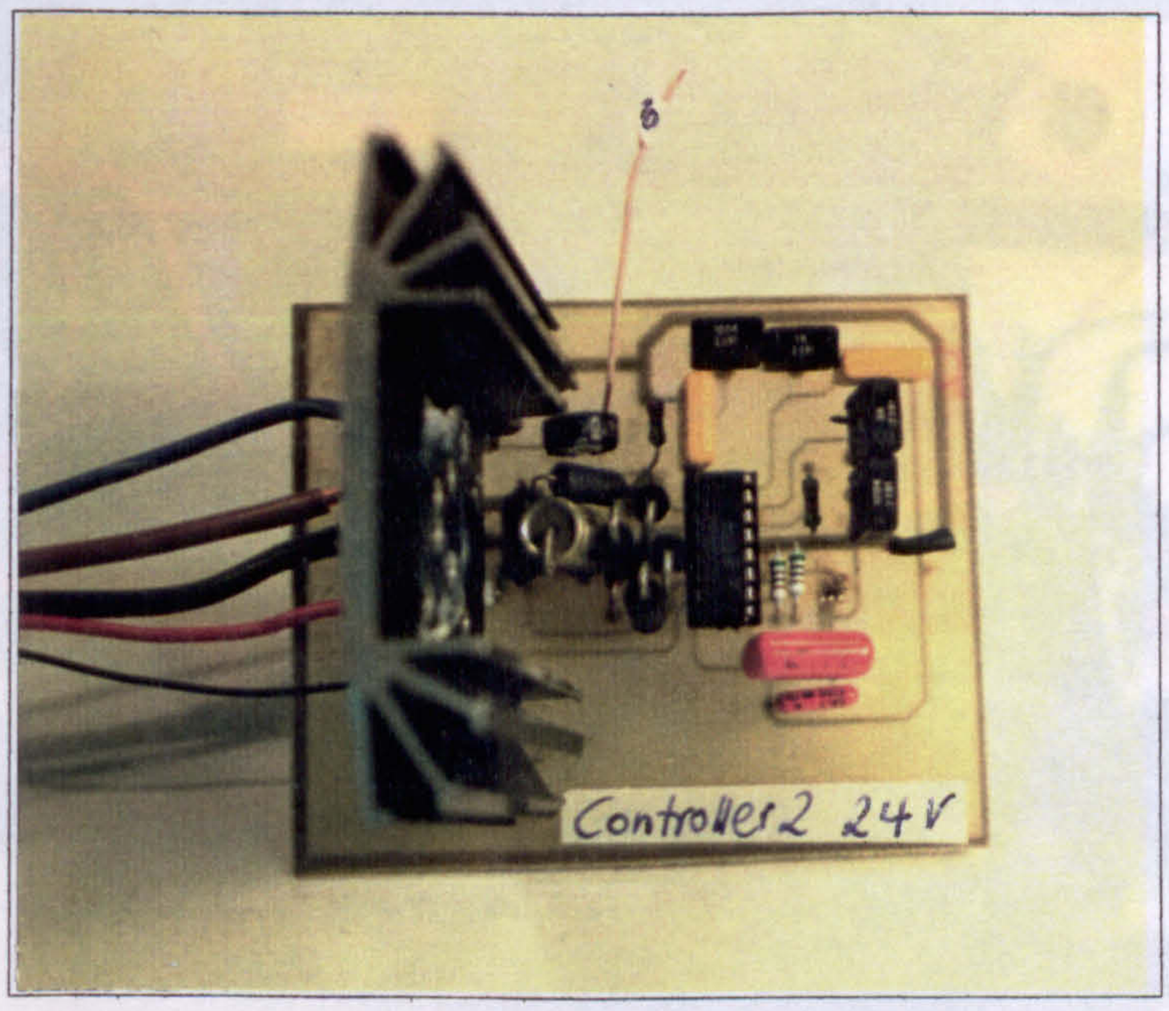

controller

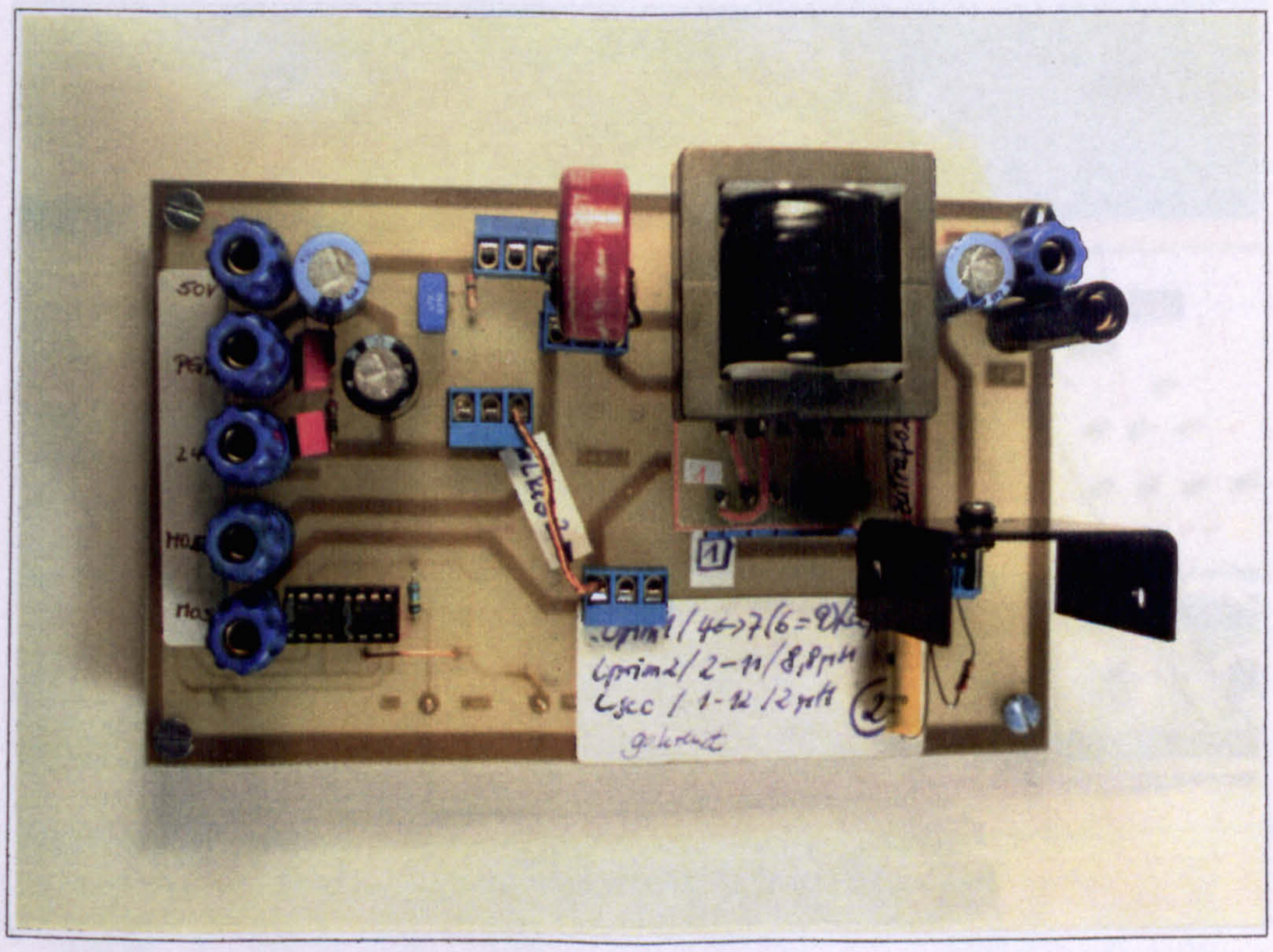

power board

APPENDIX E

Photos of experimental circuits 3

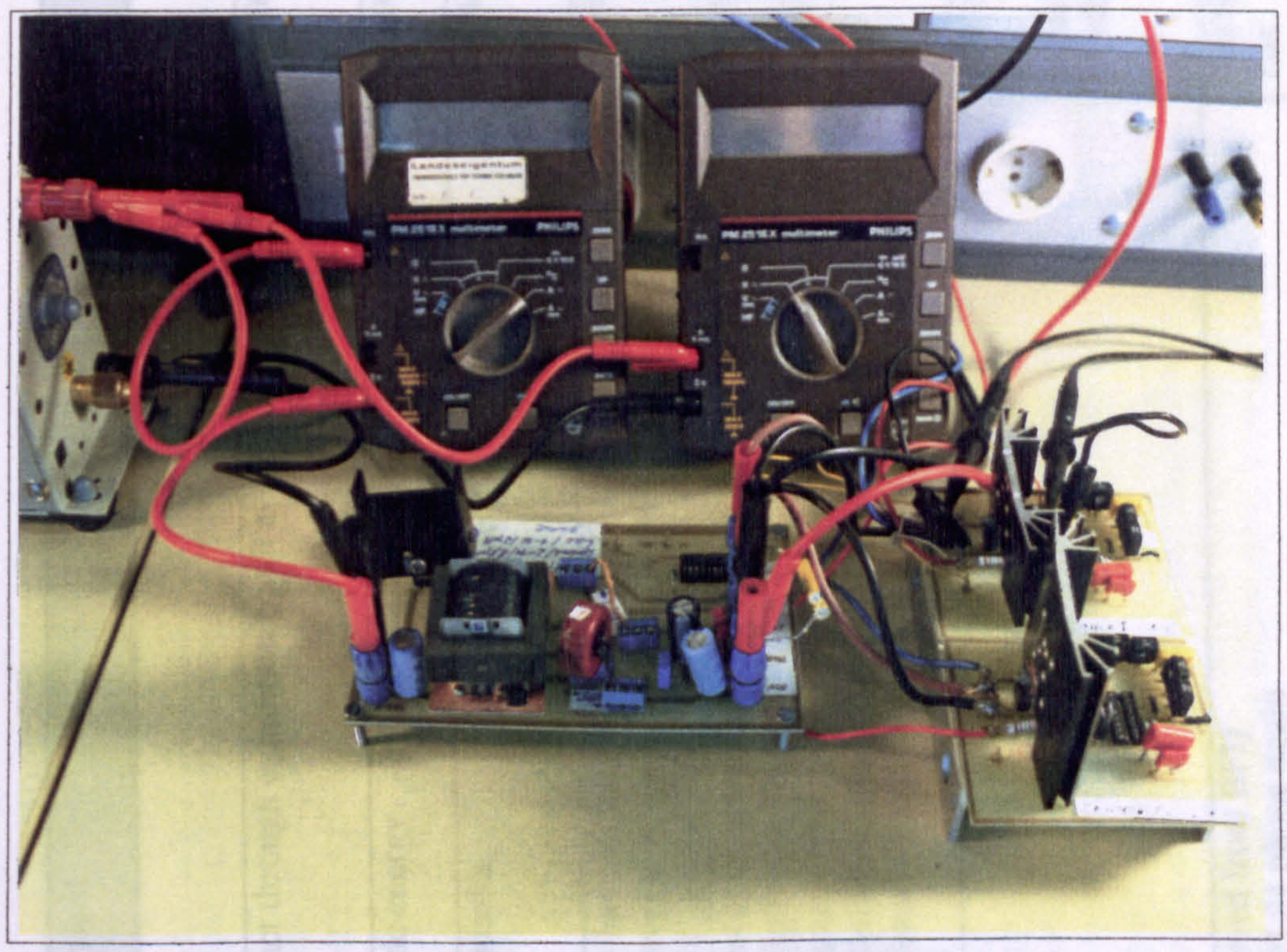

set-up 1

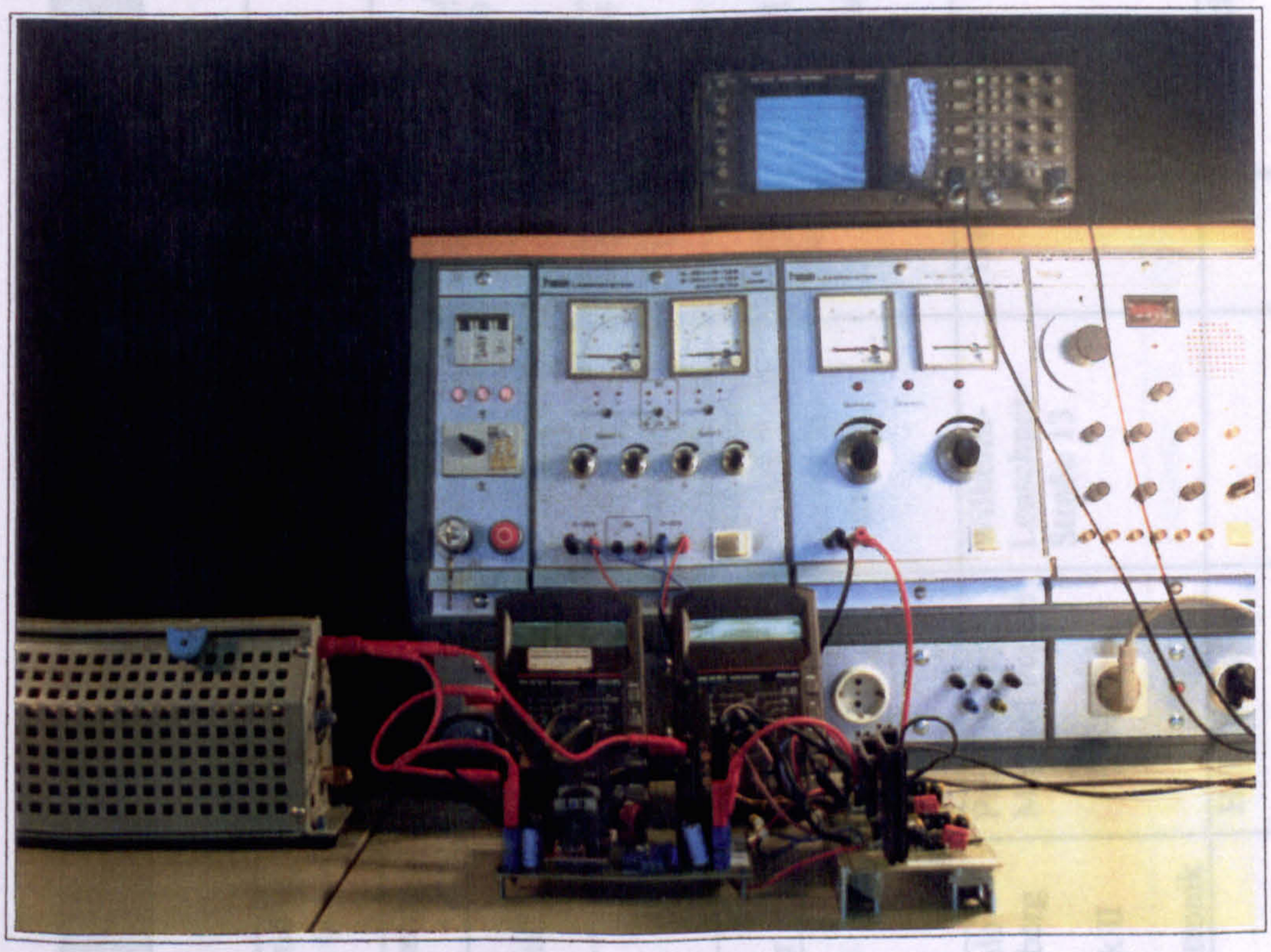

set-up 2

APPENDIX F
Company-list

Company	Contact person	Street	Post code	Town	Comment	Tel /Fax
Alcatel R&D and Factory Centre de Lannion	Talmont	4, rue de Broglie	22301	Lannion Cedex France	contact through exhibition booth at PCIM conference 93	Fax: 0033/96483148
Argonne National Laboritory		9700 S.Cass Ave.	60439	Argonne Illinois USA	kinetic energy	Fax: 001/708972/2206
BFI Eletronics PQ Kernformen Hochformat				Ditzenbach	-> Haluska	06074/40980
Blinzinger Elektronik GmbH	Blinzinger	Ohrnberger Straße 24	74670	Sindringen	They have already built a AC-DC resonant converter. However it was not accepted by the market. 8.2.94: second call -> information material	07948/2526 /2527
Cherry Semiconductor		2000 South County Trail	RI 02818	East Greenwich	Producer of controllers. Contact at the "Electronica" Exhibition in Munich 92.	001/401/885-3600 Fax: -5786
ELFI S.A Electronic Feasibility Investigations	Dr. Richard Redl	Derrey-la-Cabuche	1756	Onnens Switzerland	Program Committee member of the IEEE Power Electronics Specialists Conference 1989 - 93. Chairman at PCIM conference Nuremberg 93; several interesting papers in the area	0041/37/302-483 Fax: -379
Fachhochschule Giessen Friedberg Fachbereich Elektrotechnik II Fachgebiet Leistungselektronik	Prof.Dr.-Ing. Michael Peppel	Wilhelm-Leuschner-Straße 13	61169	Friedberg		06031/604-276 Fax: -198 E-mail: peppel @ prfhfb.fh-friedberg.de
Haluska	H. Haluska			Ditzenbach	(derived from BFI) 17.02.94 phone again 20.02.94 offer to be send	06074/66281 Fax: /66283

APPENDIX F
Company-list

Company	Contact person	Street	Post code	Town	Comment	Tel /Fax
Heinzinger	Franck		83022	Rosenheim	has done his PhD in the area -Technical University München. Recommends amorph metal cores for the transformer and to use ferrites for resonant inductors. "All converters are derived from the buck-converter in respect to dimensioning"	Fax: 08031/440444
Megapin	Pöhlmann	Kampenwand weg 4	85617	Aßling	high frequency DC-DC converters	08092/32360 Fax: /32360
Philips Components Coperate Innovation Materials	Steef A. Mulder			Eidhoven Netherland	papers on high frequency transformer design (low profile)	0031/40/722-128 Fax: -542
Philips	Bogaerts		1301	Wavre/ Belguim	16.03.94: Will send a paper on the subject of MID	0032 / 10 / 438-211 (-383) Fax: -212
Syko	Hopf	Jahnstraße 2	63533	Mainhausen	good economical situation. Report in "Markt & Technik" Dez.93 9Mio. DM turnover increase of 15%	06182/26079
Siemens Nixdorf	Manfred Schlenk			Augsburg	recommends forward-converter instead of flyback because of transformer capacity. Expert in the monitor field. Multi-layer boards as transformer windings possible, however they have to be etched rather then milled. Dissertation: "Ein Serien Resonanzumrichter mit Halbbrückenschaltung mit kominierter serieller/paraller Lastauskopplung und mehreren Ausgangskreisen" 93 Technical University Berlin Fachbibiliotek	0821 / 804-0 -2896
Siemens AG Passive Bauelemente	Maurizio Esquerra Vissing	Balanstr. 73	81541	München	Samples of different ferrite cores (latest material N87). Information material: general about ferrites, MOSFETs and power diodes. Special informations about magnetic properties of deliveries samples	089/4144 -5356 -2508 Fax: -2198/ -8384

APPENDIX F
Company-list

Company	Contact person	Street	Post code	Town	Comment	Tel /Fax
Siemens AG ASI 1 SWE T 243	Fischer	G.-Scharowsky-Str.1	8520	Erlangen	Contact on PCIM 93 and exchange of several papers	09131/7-31646 Fax: -32148
TDK	Apple			Düsseldorf	Information to measure the transformer 25-50 µm isolation-foil between the windings recommends to glue the cores together in the final stage Orders parts directly from Japan	0211/9077-0 Fax: -104
Thomatronik Herbert M. Müller GmbH	Dr. Lu	Brückenstr.1	83022	Rosenheim	Vektorfields demonstration package. Agent for VF in Germany and for PSpice First visit: 8.3 14.03 Information faxed Second visit: 30.5	08031/2175-22 -> Dr.Lu ***VF*** -13 Bursian -> ***PSpice*** Fax: -30
Ulmer					no expert in the field ... refers to VOGT	07031/652081
Unitrode Intergarted Circuits	George Georgalis			USA	information about the simulation of the control Chip 3864 forwarded. No precious Spice data available of this chip	001/603/429-8522 Fax: /424-3460 (4354)
Universität Stuttgart	Köhler				diploma thesis about leakage inductance. His brother is an external reader at FHTE.	0711/121-3677
Vakuum Schmelze Hanau	H.Keinert			Hanau	sends leaflets and calls back recommends ferrites	06181/38 -2022 -2636 (Jansen)
Vector Fields ltd.	Simon Taylor	24 Bankside	OX5 1JE	Kindlington Oxford	additional support for VF. Exchange of Core data and results.	0044/865/370 -151 Fax: - 277 Email:100144.3073@compuserve.com

UNINTERRUPTIBLE POWER SUPPLY SYSTEMS USING A QUASI-RESONANT TECHNIQUE IN A DUAL CONVERTER MODE

File: T_220494.DOC

U Schmidt, P Mehta, F Seutter

Brunel University - England

Fachhochschule für Technik Esslingen - Germany

ABSTRACTS

This paper investigates the application of resonant techniques for building Uninterruptiple Power Supply (UPS) systems incorporating a dual converter. The magnetic circuit of the dual converter consists of a high frequency transformer with two primary and one secondary windings. The two primary windings are supplied from the mains and a stand-by power source. The major contribution of the proposed approach is that all the windings operate at high frequency in a quasi-resonant mode; parasitic leakage inductance being used as part of the resonant circuits.

The paper outlines the basic principle of a 700 kHz system together with the analysis design and experimental results including simulation results obtained using PSpice.

INTRODUCTION

The rapid widespread use of electronic devices in almost every field of industry as well as medicine and domestic sector has led to increasing dependence on power supply systems. Survey of electronic equipment has shown that 80% of all break downs of computer systems are caused by power disturbances or voltage irregularities (*1*).

Hence, Uninterruptible Power Supplies become a necessity. Modern electronic equipment has to be reliable and often incorporate Uninterruptible Power Supply system. This adds to the overall weight and volume of the equipment and therefore there is a considerable demand to improve the power to weight ratio of the UPS system.

Resonant switching techniques help to overcome the limits of PWM switching techniques, by increasing the switching frequency into the MHz range. The components for the resonant-tank circuits require inductors and capacitors which add to the overall weight and volume of the UPS systems. The proposed approach uses a single transformer with three windings and the leakage inductances are used as part of the resonant circuit.

THE DUAL CONVERTER

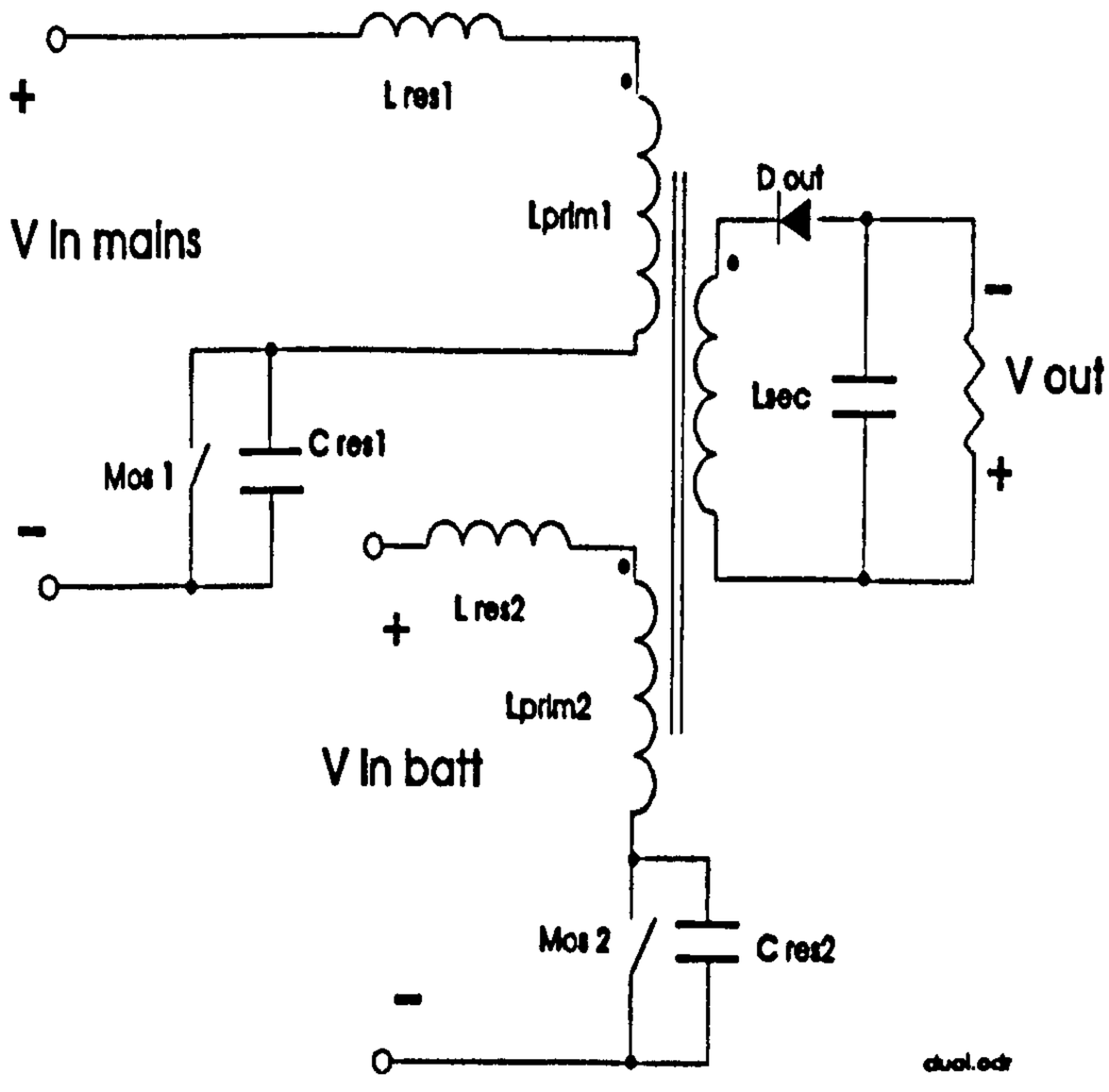

Figure 1: *The Dual Converter*

The simplified circuit diagram in Figure 1 illustrates the basic principle of the dual-mode quasi-resonant flyback converter which represents the core of the proposed UPS system.

One of the primary windings is connected to the mains and the other one to the stand-by battery. The third winding provides the output (a fourth winding can be added for charging the battery).

The transformer in a flyback converter is in fact intended to be a two winding inductor, which has dual functions of providing electrical isolation and energy storage by including an air-gap. The energy storage facility is utilised to overcome the inherent delay in bringing the off-line UPS in operation after power failure. A comparator monitors the mains voltage and when the mains fails the stand-by battery takes over at pre-set value of the output voltage. As the voltage increases again the stand-by source is turned off.

When operating in a zero-voltage mode the quasi-resonant circuit uses the parasitic elements, C_{oss} of the Mosfet and L_{Leak} of the transformer, as resonant components, thus eliminating the need for external inductors. The leakage inductance can be adjusted by proper design of the transformer by including a suitable spacing S between the windings.

Using the reluctance modelling and duality to translate the physical structure of a magnetic device into its equivalent inductance values and their locations, as Dixon (*2*) demonstrated, the authors were able to determine the leakage inductors for the dual converter. Figure 2 (a) shows the winding arrangement and Figure 2 (b) and 2 (c) show the equivalent reluctance model and the electrical circuit respectively of the arrangement.

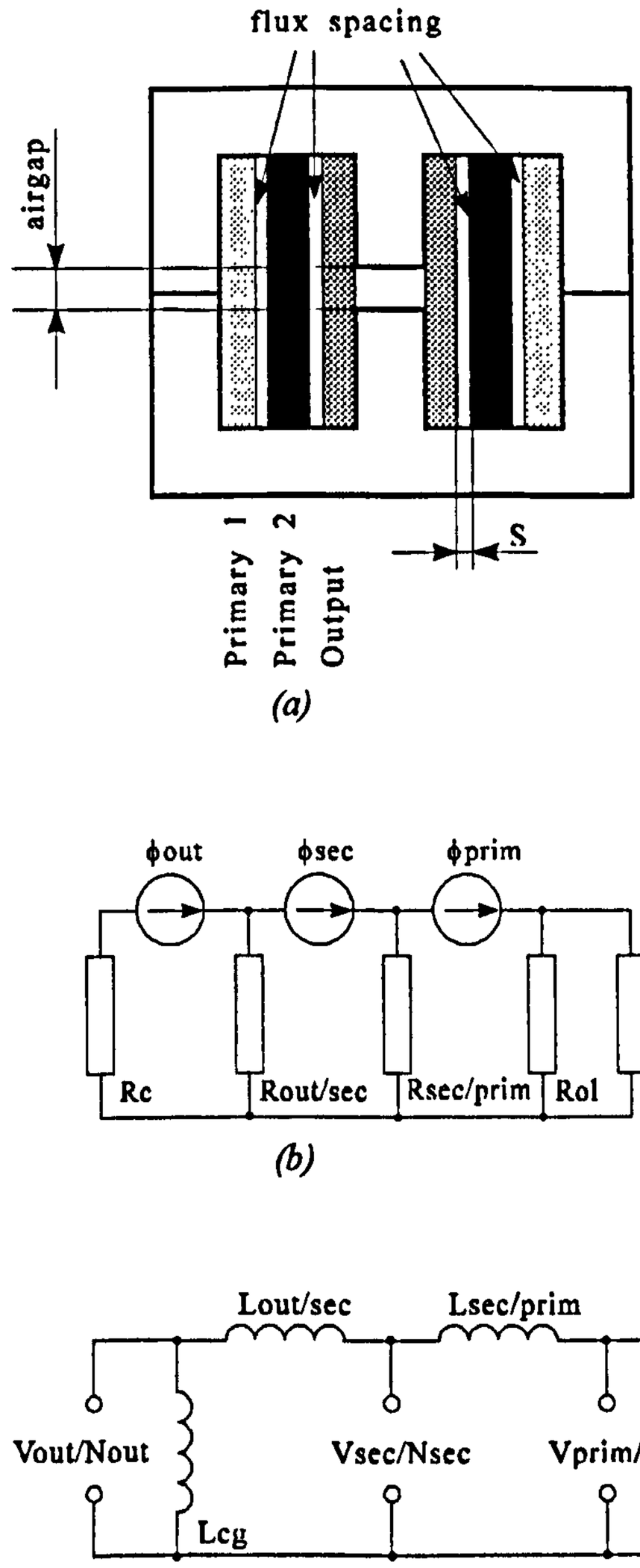

Figure 2 a: *Physical model of the transformer*
b: *Reluctance Model of the coupled inductors*
c: *Electrical equivalent circuit of the coupled inductors*

The leakage flux lies between the windings and the outer leg of the core. The path through the centre leg of the core has significantly higher magnetic resistance due to the air-gap.

The equation below gives the values of the leakage inductance between L_{prim1} and L_{sec1} respectively L_{prim2} and L_{sec2}, as labelled in Figure 1.

$$L_{Leak} = \frac{\mu_0 \cdot \mu_r \cdot N^2 \cdot (MTL \cdot S)}{W_w} \cdot 10^{-2} cm \quad [1]$$

MTL ... mean length of a turn

S ... spacing between the windings

W_W ... Window width

The aim of the procedure was to adjust the leakage inductance so that it equals the required resonant inductance value $L_{Leak} \equiv L_{res}$, hence making an additional physical element unnecessary. In other words the leakage inductance was designed to be greater than that for a conventional transformer to achieve the value of L_{res1} and L_{res2}.

Apart from the reduction of costs which can be achieved using this configuration, another drawback can be eliminated: The disadvantageous voltage divider that results between the discrete resonant inductor and the transformer, as Schlenk (*3*) showed in his dissertation.

ANALYSIS AND EXPERIMENTAL RESULTS

Mathematical analysis

The mathematical analysis was carried out by considering the operation over four distinct periods (t_0-t_4) (*4*). For each period energy consideration was determined and summed up for the input and output part of the circuit respectively.

Input power:

$$E_{in} = \int_{t0}^{t4} I_{in} \cdot V_{in}\, dt \quad [2]$$

$$E_{in} = V_{in} \cdot I_{\psi} \cdot \left((t_{01} + t_{34}) + \frac{\sin\alpha}{\omega} + \frac{Z_R \cdot I_{\psi} \cdot \sin^2\alpha}{2 \cdot \omega \cdot (V_{in} + V_{out} \cdot N)} \right) \quad [3]$$

Output power:

$$E_{out} = \int_{t0}^{t4} V_{out} \cdot (I_y - I_{Lr}) \cdot N \cdot dt \quad [4]$$

$$E_{out} = V_{out} \cdot N \cdot I_{\psi} \cdot \left(\frac{\alpha}{\omega} - \frac{\sin\alpha}{\omega} + \frac{Z_R \cdot I_{\psi} \cdot (1-\cos\alpha)^2}{2 \cdot \omega \cdot (V_{in} + N \cdot V_{out})} \right) \quad [5]$$

Using the law of energy conservation the relationship between the input and the output voltage is given by the following expression:

$$\frac{V_{out} \cdot N}{V_{in}} = \frac{1}{f_s \cdot \left(\frac{\alpha}{\omega} - \frac{\sin\alpha}{\omega} + \frac{Z_R \cdot I_{\psi} \cdot (1-\cos\alpha)^2}{2 \cdot \omega \cdot (V_{in} + N \cdot V_{out})} \right)} - 1 \quad [6]$$

$\frac{\alpha}{\omega}$ ... *Resonant period*

Z_R ... *Resonant tank impedance*

N ... *Transformer turns ratio*

I_{ψ} ... *Transformer current*

The resulting non-linear equation is than solved to determine the magnitude of the circuit parameter from which the transformer design is derived. This is carried out using Figure 3, where for a desired voltage-ratio and a predetermined turns-ratio (here N=4) the required resonant frequency for a given switching frequency can be obtained.

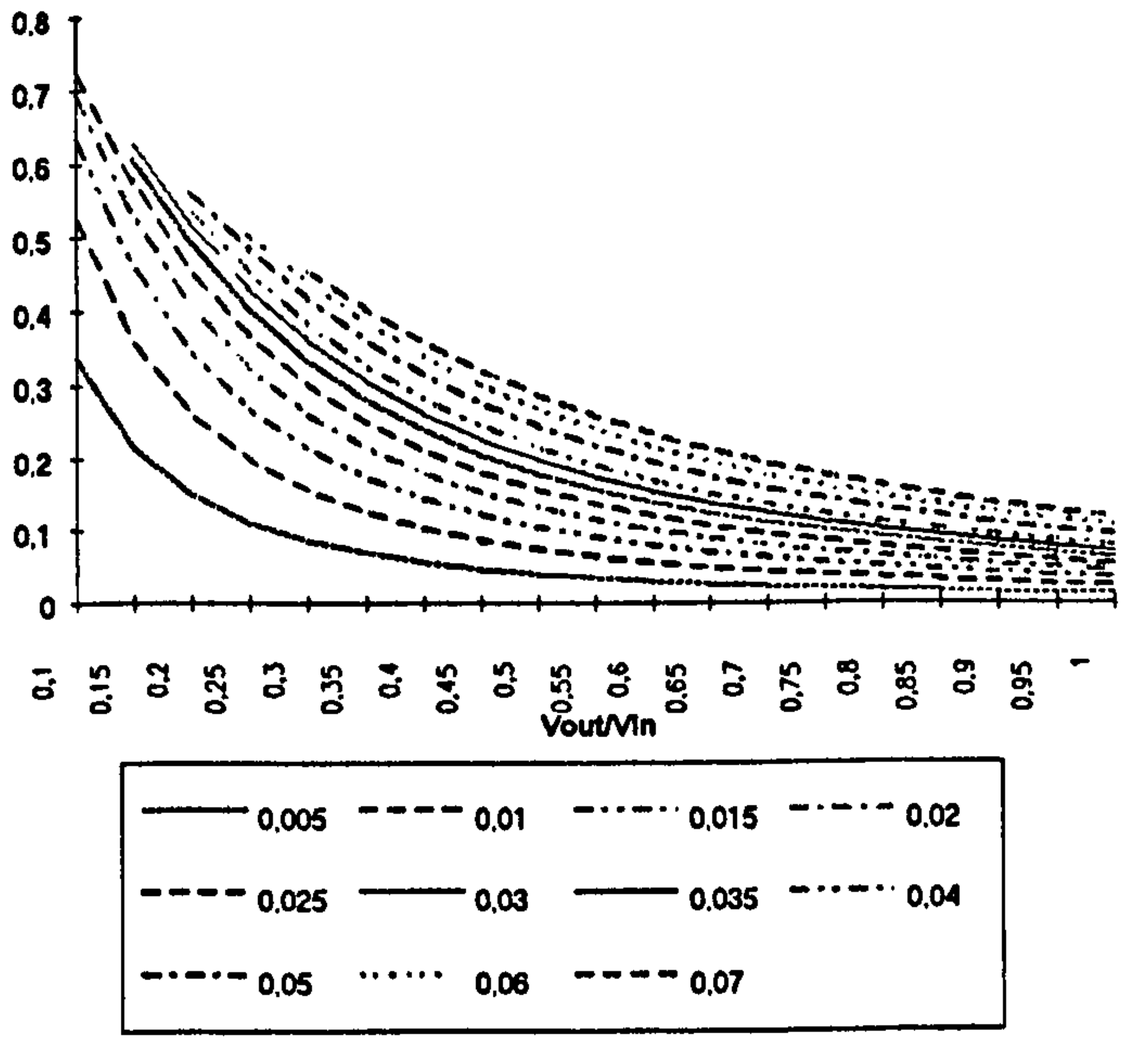

Figure 3: *Voltage conversion versus requency relation for different loads R_{load}/Z_{res} (turnsratio N=4)*

Simulation

Before building the converter the design was verified on PSpice (electric circuit simulation) and Vector Field (magnetic circuit simulation). Both tools proved to be very helpful in the attempt to reduce development time and increase the efficiency. Especially, the change over period from on source to the other, which was not determined by the mathematical analysis could be investigated and showed satisfying results.

Design Program

To optimise the design of the converter a special program was developed based on an Excel spreadsheet of which the flowchart is shown in Figure 4. It gives the designer the option of either starting with the selection of the resonant frequency ($0 < f_r / f_s < 1$) or the peak current, depending on the facts as either switching frequencies of the available Mosfet or per-selected winding material.

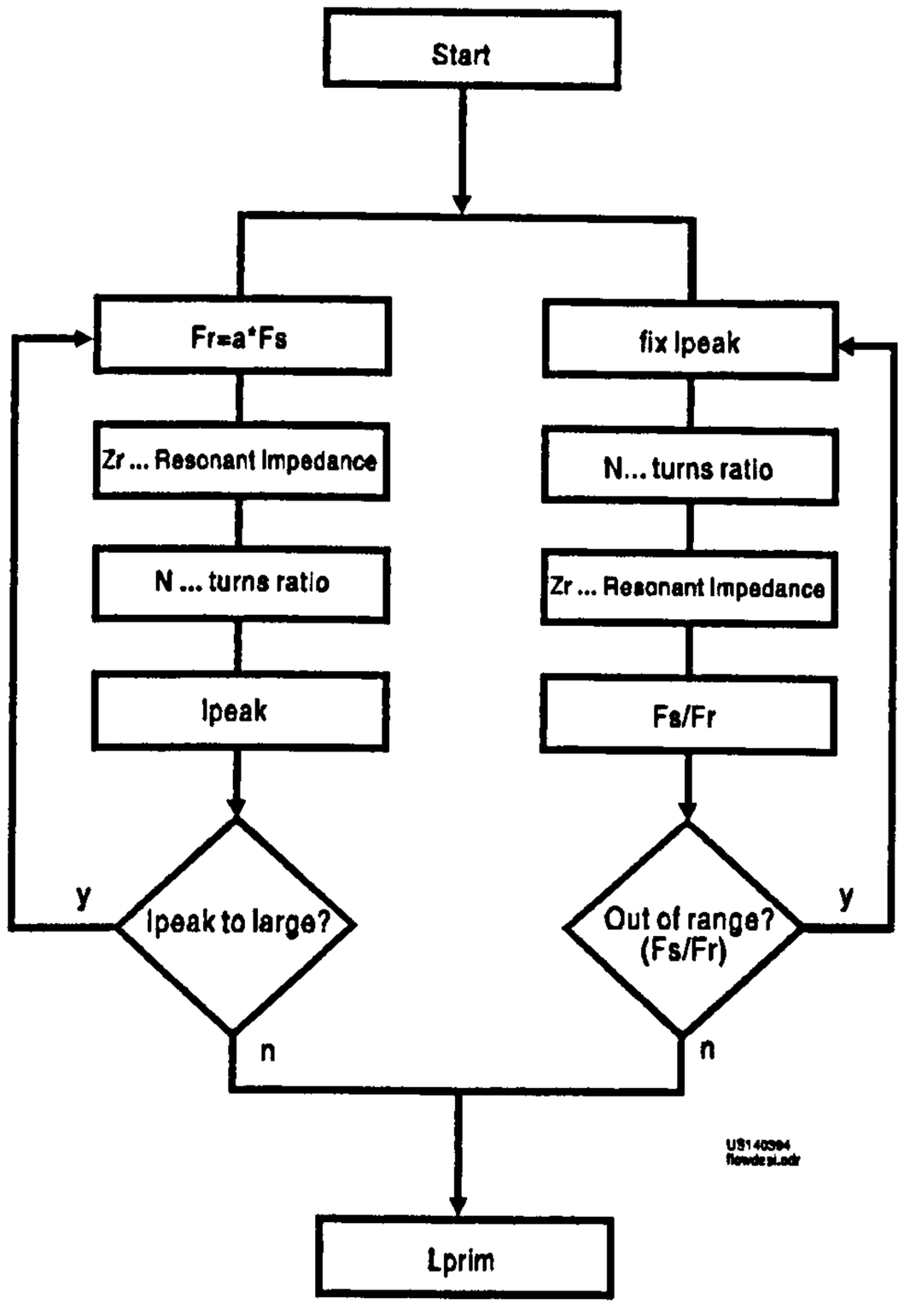

Figure 4: *Flowchart of the design program*

Control

The same controllers were used for both mains and stand-by input parts of the circuit. These control IC's (UC3864) are specially designed for quasi-resonant zero voltage mode switching. They embody zero voltage crossing detection to ensure "true" zero voltage switching. The minimum and the maximum frequency (f_{smin} / f_{smax}) can be adjusted through an external R-C circuit connected to the chip.

Using the fault pin. The fault pin of the controllers are used for two functions: First, as recommended by the producer, to detect fault conditions and set a latch while forcing the output drivers low (5) and second as input from the comparator, which monitors the mains voltage *(see Figure 5)*. During normal operation fault pin 1 of the controller 1 is set "low". Hence, the Mosfet 1 in the mains circuit is driven by the controller 1.

The comparator sets the fault pin 1 to "high", as soon as an undervoltage condition occurs. Meanwhile the controller 2, of the battery circuit, is activated by the negative signal of the comparator which is passed on to the fault pin 2. The output drivers of the controller 2 are pulsing the Mosfet 2 to supply power from the battery, via the transformer.

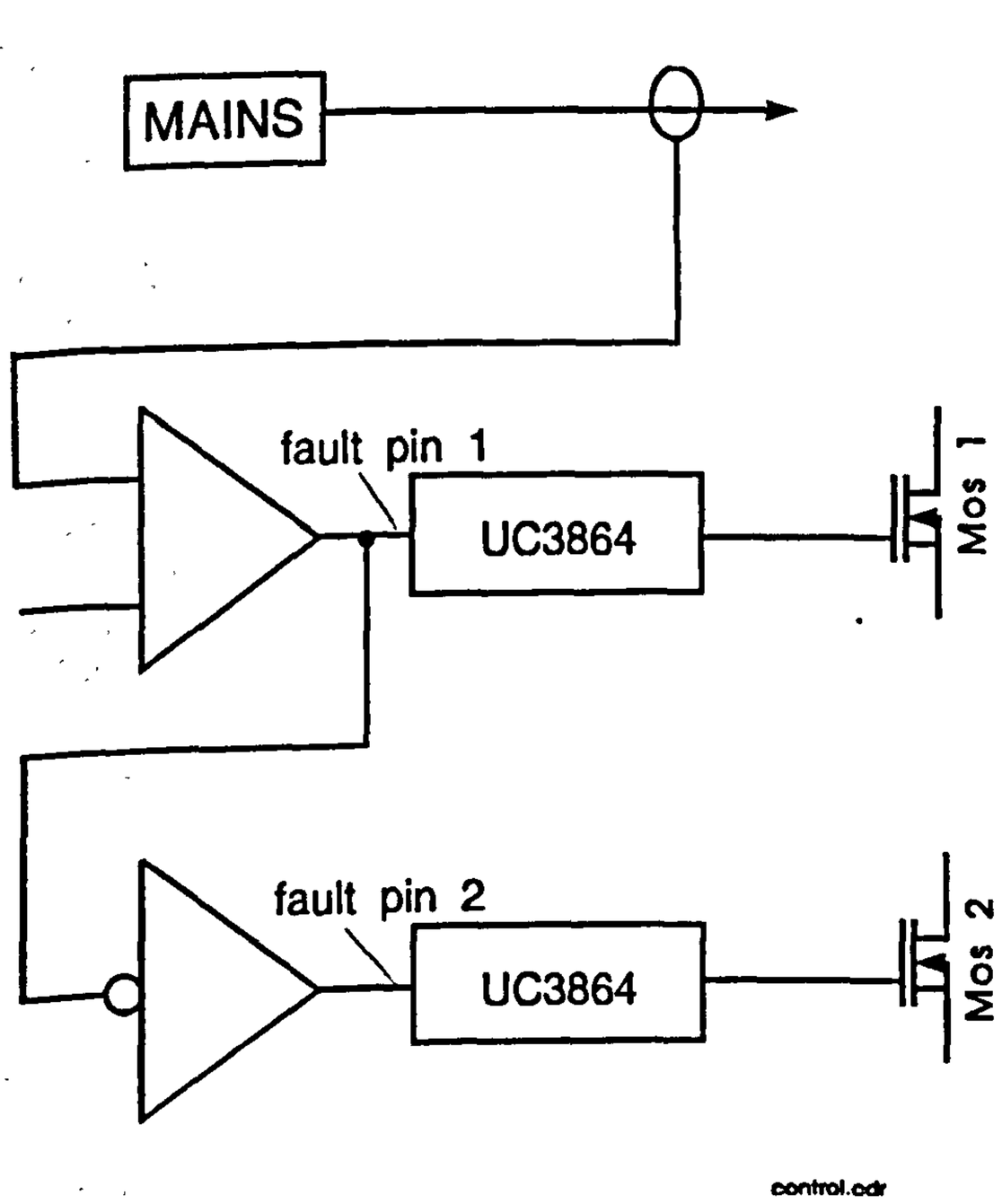

Figure 5: *A simplified part of the control circuit*

Experimental results:

The prototype was rated at 50 Watts, and 720 kHz and operated at 75% efficiency. It was build on a special type of board, used at FHT Esslingen to develop prototypes, where no lithographic processes are involved. Although the use of this technology is limited to prototyping and small scale production, it provides a very environment friendly production. Further, improvement in efficiency of the converter would be gained, by using surface mount techniques (SMT), to reduce the distances between components, and hence the voltage drops and stray effects.

The waveforms of the first prototype are given below, after the references, Figure 6.

CONCLUSION

While results of the investigated circuit were quite satisfying the efficiency figure does not confirm to favourable the ones obtained with resonant techniques (6). It is anticipated that this figure would be significantly increased if SMT is utilised. This of course would also allow a higher switching frequency, hence a further reduction in volume.

References:

1. AT&T and IBM: Research on computer breakdowns in the Bell Labs, 1990

2. Dixon L.1993. "Coupled Inductor Design", UNITRODE Power Supply Design Seminar SEM-900, 8-1-4

3. Schlenk, M., "Ein Serienresonanzumrichter in Halbbrückenschaltung mit kominierter serieller und paralleler Lastauskopplung und mehreren Ausgangskreisen.", Dr.-Ing. Dissertation,

4. Liu, K.-H. "High-frequency Quasi-Resonant converter techniques", PhD dissertation

5. Vektor Fields, Thomatronik Rosenheim.

6. Lee, F.C. and Liu, K-H.: "Zero-Voltage Switching Techniques in DC-DC converter circuits." IEEE PESC 1986.